Structuro-Kinetic Studies of the Crystallisation of Straight Chain Surfactants and Homologues Mixtures

Richard N.M.R. van Gelder

Department of Pure and Applied Chemistry
University of Strathclyde

Degree of Doctor of Philosophy
1998

The copyright of this thesis belongs to the author under the terms of the United Kingdom Copyright Acts as qualified by University of Strathclyde Regulations 3.49. Due acknowledgement must always be made of the use of any material contained in, or derived from, this thesis.

Signature:

Date: 6 October 1998

Acknowledgements

I would like to thank my supervisor Professor Kevin J Roberts for his constant support throughout this project and Professor RA Pethrick for officially taking over my supervision, after the group's move from the University of Strathclyde (in Glasgow) to Heriot-Watt University (in Edinburgh) and for his continuous interest in the project's progress. Professor JN Sherwood generously gave me the opportunity to use and modify a zone refiner for the purification of fatty acids. Evelyn Shepard is thanked for helping me to use this zone refiner and for teaching me the basics of the art of glass blowing.

This PhD was carried out in collaboration with Unilever Research Port Sunlight Laboratory, whom I am grateful for the financial support as well as the advice and discussions with my industrial supervisors Dr Terry Instone and Dr John Chambers. I would also like to thank Professor Gordon Tiddy for very useful discussions on liquid crystalline phases. The following people at Unilever are thanked for helping me with experimental techniques and providing background information on surfactant manufacture: Ian Tucker, Dorothy Paterson, Ralph Calvert, Bryan Joy and Geoff Irlam.

I gratefully acknowledge the research institutes whose facilities I have been using throughout this PhD: The Department of Pure and Applied Chemistry at the University of Strathclyde, The Centre for Molecular and Interface Engineering in the Department of Chemical and Mechanical Engineering at Heriot-Watt University, Unilever Research Port Sunlight Laboratory, the Synchrotron Radiation Source at CLRC Daresbury Laboratory in Warrington (UK) and the National Synchrotron Light Source at Brookhaven National Laboratory in New York (USA).

Realisation of all the equipment vital to this project was only possible with the enthusiastic help of the staff at the electronic and mechanical workshops of the above mentioned research institutes.

At Daresbury Laboratory special thanks go to Manolis Pantos for help with the *xotoko* software and showing interest in the project, and to Liz Towns-Andrews, Ernie Komancheck, Sue Slawson and Anthony Gleesom for providing excellent support in using the experimental stations.

Malcolm Capel, station scientist at X12B at the NSLS is acknowledged for providing excellent software for the analysis of small angle X-ray scattering data.

The EPSRC is thanked for supporting this project through the soft solids initiative (grants GR/K/42820 and GR/K/80488), thus providing additional financial support enabling me to travel to the synchrotron sources which have proved to be essential for this project.

Two students whom I supervised are gratefully acknowledged: Paul van Lamsweerde carried out the measurements for the purification of fatty acids. The crash cool experiments were carried out by Gavin Palmer. JM Sasaki and Charles Kerr are thanked for helping out with the experiments at the synchrotron sources. Special thanks go to Rob Hammond for always finding time for useful discussions and Deri Jones for helping with the three-dimensional drawings of the intermediate liquid crystalline phases.

All the people from the group are thanked for creating an inspiring atmosphere especially: Alison Hennessy, Ann Blyth, Xiaojun Lai, Carol Peacock, and Susan Girdwood.

Personal thanks go to Amaia Montaya-Goñi, Ceasar Agra, Emil Vogels, John Andrésen, Kay Lederer, Merche Maroto-Valer, Moira Stemp and Suchada Chareanpunsirikul, who helped me in enjoying and exploring Scotland.

Karina is thanked for sharing with me her unspoiled views on physical chemistry and crystallography. She as well as my family are thanked for unfailing moral support.

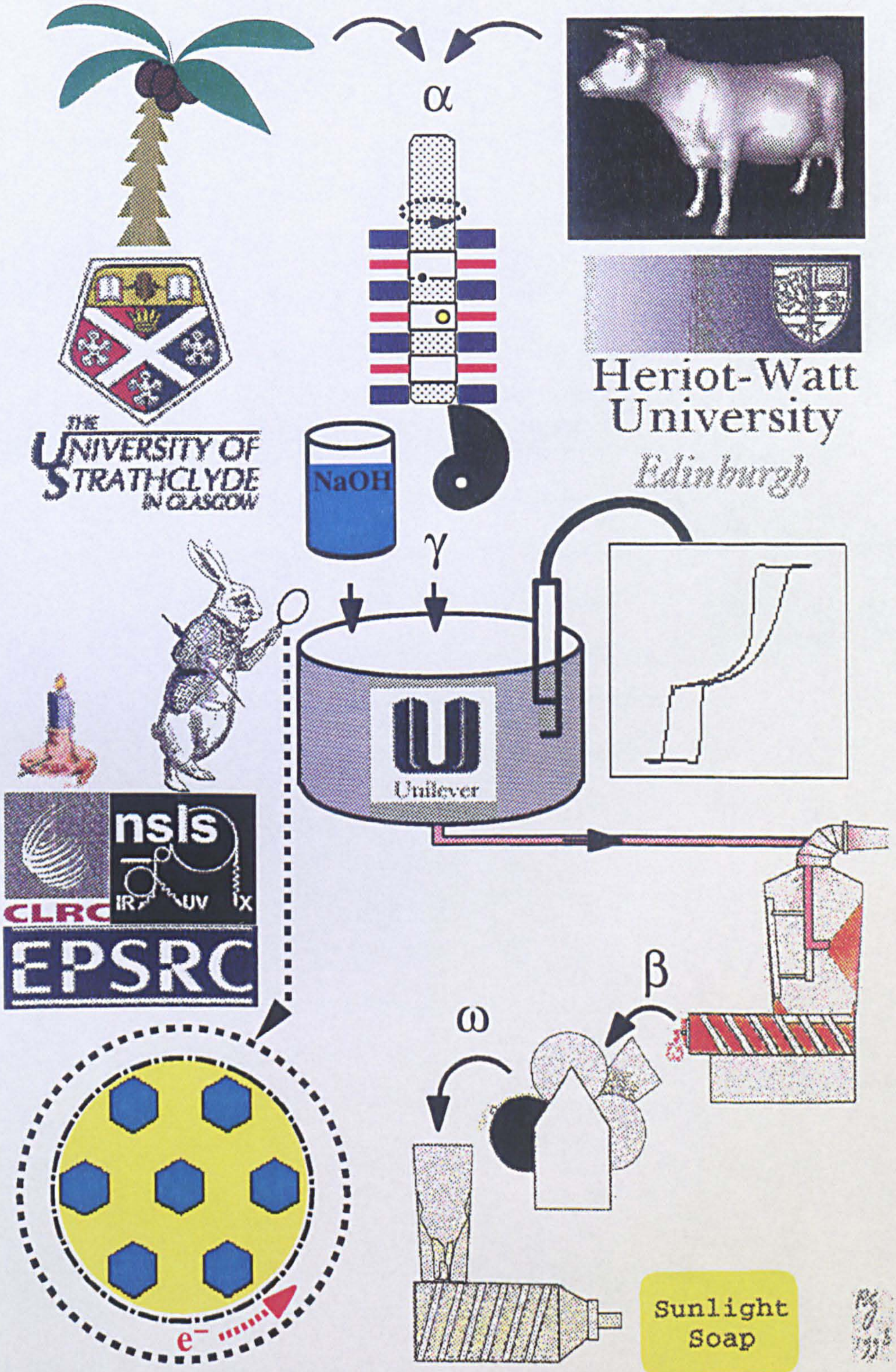
α
Heriot-Watt
University
Edinburgh
THE
UNIVERSITY OF
STRATHCLYDE
IN GLASGOW
NaOH
γ
Unilever
nsls
IR
UV
X
CLRC
EPSRC
β
ω
e⁻
Sunlight
Soap

Graphical summary, the candle is the old logo of the National Synchrotron Light Source at Brookhaven National Laboratory (USA); the White Rabbit was taken from *Alice in Wonderland*, the author of which (Lewis Carol) was born in Daresbury, location of Britain's Synchrotron Radiation Source. The rest should become apparent after reading this thesis

Abstract

An investigation was undertaken into the crystallisation process of the natural surfactants sodium laurate, myristate and palmitate.

A multi-pass zone refiner was modified for purification of fatty acids, the starting materials in soap manufacture. It was found that purified lauric and myristic acid transform spontaneously in the solid state over a period of days from the C ($=\alpha$) form to the A-super ($=\gamma$) form, which was previously unknown. Low levels of impurities were found to inhibit this phase transformation. This was explained in terms of molecular rearrangement necessary for this transition.

The nucleation behaviour from the isotropic micellar phase of single and mixed surfactant systems was studied using a specially developed turbidity probe. A two step nucleation and dissolution process was found to occur for some surfactant mixtures. Since this was not observed during static *in-situ* XRD experiments, it was postulated that during crystallisation above a certain degree of agitation segregation occurs of the two surfactants present in the mixture. Based on induction time measurements the size of the critical nucleus was estimated. The results indicated that the shorter the chainlength the more molecules are required to form a stable nucleus.

The crystallisation process of single and mixed surfactant systems from the isotropic micellar phase, the hexagonal and the lamellar liquid crystalline phases was investigated by *in-situ* XRD using synchrotron radiation. A detailed transformation mechanism for the crystallisation process from the liquid crystalline phases was proposed based on epitaxial relations between all ordered phases of the following sequence: lamellar, tetragonal mesh, hexagonal mesh, (deformed hexagonal for surfactant mixtures with a chainlength difference of two CH_2 groups), hexagonal, isotropic micellar, solid phase. Crystallisation of soap from ethanol-water mixtures revealed the ethanol to be incorporated into the micelles and to affect the resulting solid state structure above a certain ethanol content.

Table of contents:

Chapter 1 Historical and industrial perspective to surfactant manufacture 1

1.1 Introduction 2

1.2 History 2

1.3 Natural sources for soap production 4

1.4 Soap manufacture 4

1.5 Thesis outline 11

1.6 References used in this chapter 12

Chapter 2 Background theory 14

2.1 Introduction 15

2.2 The influence of supersaturation on the crystallisation process 15

2.3 The Van 't Hoff equation 18

2.4 The nucleation process 20

- 2.4.1 The formation of a nucleus in the metastable zone 21
- 2.4.2 An empirical description of nucleation kinetics 27

2.5 The internal structure of crystalline substances 29

- 2.5.1 Lattice planes 33

2.6 Crystal growth mechanisms 35

- 2.6.1 Diffusion 35
- 2.6.2 The creation of growth sites 36
- 2.6.3 Rate limiting factors in the crystal growth process 38
- 2.6.4 Factors affecting the crystal morphology 39

2.7 Purification through crystallisation 41

- 2.7.1 Zone refining 42

2.8 Principles of X-ray diffraction 47

- 2.8.1 The Bragg law 47
- 2.8.2 The production of X-rays 50
- 2.8.3 The detection of X-rays 53

2.9 Summary 54

2.10 References used in this chapter 55

Chapter 3 Surfactant phase behaviour 59
3.1 Introduction 60
3.2 Binary Phase Diagram 62
    3.2.1 The T_c and the T_i curve 65
3.3 Phases below the T_c-line: gels and coagels 66
3.4 Phases between the T_c and the T_i line 69
3.5 The aqueous mesophases 70
    3.5.1 Dilute isotropic soap phases 72
    3.5.2 The hexagonal liquid crystalline phase 74
    3.5.3 The lamellar phase 76
    3.5.4 The reversed hexagonal phase 79
3.6 The intermediate phases 82
    3.6.1 The intermediate phases of sodium soaps 83
    3.6.2 Intermediate phases observed for other surfactant systems 86
3.7 Trends in surfactant intermediate aqueous phase behaviour 103
3.8 Thermotropic mesophases 106
    3.8.1 Thermotropic liquid crystalline soap phases 107
3.9 Crystalline soap phases 111
3.10 Summary of surfactant phase behaviour 124
3.11 References used in this chapter 128

Chapter 4 Experimental procedures and equipment 134
4.1 Introduction 135
4.2 Soap preparation 135
4.3 Procedures and equipment used for purification and characterisation of fatty acids 136
    4.3.1 Multi-pass zone refiner used for purification of fatty acids 137
    4.3.2 GC analysis 142
    4.3.3 Differential scanning calorimetry 143

4.3.4 X-ray diffraction 143
4.4 Procedures and equipment used for nucleation studies of soaps 144
4.4.1 Turbidity meter 144
4.4.2 Slow cool apparatus 145
4.4.3 Crash cool apparatus 149
4.5 Equipment used for *in-situ* XRD studies of the crystallisation process of soaps 152
4.5.1 X-ray cells for *in-situ* crystallisation experiments 152
4.5.2 Facilities used at synchrotron sources 155
4.6 References used in this chapter 158

Chapter 5. Purification of fatty acids, the first step in obtaining purified soaps 159
5.1 Introduction 160
5.2 General observations 160
5.3 Gas chromatography (GC) results 161
5.3.1 GC results for lauric acid 163
5.3.2 GC results for myristic acid 170
5.4 Differential scanning calorimetry (DSC) results 178
5.4.1 DSC results for lauric acid 178
5.4.2 DSC results for myristic acid 179
5.5 X-ray diffraction (XRD) results 179
5.5.1 XRD results for lauric acid 181
5.5.2 XRD results for myristic acid 181
5.6 Discussion 182
5.6.1 Trends in the GC results 182
5.6.1.1 Lauric acid 186
5.6.1.2 Myristic acid 188
5.6.2 DSC discussion 189
5.6.3 General discussion 190
5.7 Conclusions 197

5.8 Suggestions for future work 199
5.9 References used in this chapter 200

Chapter 6 Nucleation of single and mixed straight chain surfactants from dilute aqueous solutions 202
6.1 Introduction 203
6.2 Slow cool experiments 203
6.2.1 Results and discussion: single surfactants 204
6.2.2 Results and discussion: surfactant mixtures 208
6.2.2.1 The NaL/NaM mixtures 209
6.2.2.2 The NaL/NaP mixtures 210
6.2.2.3 The NaM/NaP mixtures 210
6.2.2.4 Discussion 216
6.3 Crash cool experiments 218
6.3.1 Crash cool results and discussion 219
6.4 Conclusions of slow and crash cool experiments 226
6.4.1 Slow cool experiments 226
6.4.2 Crash cool experiments 228
6.5 Recommendations for future work 229
6.6 References used in this chapter 229

Chapter 7 An *in-situ* XRD investigation into the crystallisation process of soaps from liquid crystalline phases 230
7.1 Introduction 231
7.2 Calculation of the surfactant volume fraction 233
7.3 Single and mixed coagel systems 235
7.4 Dissolution and crystallisation of 20 and 40wt% surfactant systems 242
7.4.1 The dissolution process of the 20 and 40wt% surfactant samples 242
7.4.2 Crystallisation from the hexagonal liquid crystalline phase 253
7.5 Dissolution and crystallisation of 70wt% surfactant systems 253
7.5.1 The formation of the lamellar phase from a coagel 253

7.5.1.1 The transformation from the hexagonal to the first intermediate phase 255
7.5.1.2 The structure of the first intermediate phase 260
7.5.1.3 The transformation from the second intermediate phase to the lamellar phase 266
7.5.1.4 The structure of the second intermediate phase 269
7.5.1.5 The lamellar phase 273
7.5.2 Crystallisation from the lamellar liquid crystalline phase 273
7.6 Texture revealing epitaxial growth 277
7.7 Crash cool experiments 281
7.8 Samples exhibiting additional phases 284
7.9 Micellar behaviour of samples containing ethanol 288
7.10 Discussion 291
7.10.1 Coagels 291
7.10.1.1 Single surfactant coagels 291
7.10.1.2 Mixed surfactant coagels 292
7.10.1.3 Solid soap crystallised from ethanol-water mixtures 293
7.10.2 The 20 and 40wt% surfactant samples 294
7.10.2.1 The isotropic micellar phase 294
7.10.2.2 The hexagonal phase 295
7.10.3 The transformation process between the lamellar and the solid phase 295
7.10.3.1 Assumptions made in the proposed models 296
7.10.3.1.1 The hexagonal mesh phase 297
7.10.3.1.2 The tetragonal mesh phase 298
7.10.3.1.3 Comparison of the size of the water holes in the mesh phases 301
7.10.3.1.4 The deformed hexagonal phase and the defected lamellar phase 302
7.10.3.2 Epitaxial relations during the overall transformation process 303

7.10.3.2.1. Orientation of the hexagonal phase 304

7.10.3.2.2 The deformed hexagonal phase 308

7.10.3.2.3 The hexagonal mesh phase 308

7.10.3.2.4 The tetragonal mesh phase 310

7.10.3.2.5 The lamellar phase 311

7.10.3.3 Generic model for the structural transformation processes between the lamellar and the solid phase 311

7.10.3.4 Phase transformations during rapid cooling 313

7.10.4 Micellar phase behaviour of samples containing ethanol 318

7.11 Conclusions 318

7.11.1 Mixed structures 318

7.11.2 Coagels 318

7.11.3 The aqueous mesophases 320

7.11.4 Generic process 322

7.12 Recommendations for future work 322

7.13 References used in this chapter 323

Chapter 8 Conclusions 325

8.1 Introduction 326

8.2 Overall conclusions from this work 326

8.3 Future perspective 331

8.4 References used in this chapter 335

Appendix A: Calculation of the available area per polar head group 336

A1 Introduction 337

A2 Spheres with radius r_{sphere} 337

A3 Cylinders with radius r_{cyl} and length l 338

A4 Surfactant lamellae with thickness d_s 338

A5 A comparison between the different aggregate structures 339

A6 References used in the appendix 340

Appendix B: Peak positions and transition temperatures from chapter 7 341

Chapter 1

Historical and industrial perspective to surfactant manufacture

Chapter 1 Historical and industrial perspective to surfactant manufacture

1.1 Introduction

Soaps are the alkali salts of fatty acids and are the best known examples of a wide variety of products, called surfactants (surface active agents). These substances work by lowering the surface tension at the interface between water and the surface to be cleaned, thus improving the wetting ability of the surfactant solution and thereby allowing an even distribution of it across the relevant surface, whilst still retaining most of the properties of the water (*e.g.* [1]). In this chapter a brief historical and industrial perspective is given as a background to this thesis and in order to illustrate some of the problems encountered during soap production. More details on soap manufacture can be found in [2-5]. At the end if this chapter the scope of this thesis is outlined.

1.2 History

People have been using soap for more than 4500 years [3]. Different explanations exist for the origin of the word soap. It might be derived from the sacrificial *Mount Sapo* of Roman legend. The animal fats of the animals burned there, reacted with potassium carbonate in the wood ashes to form soap according to:

$$2CH_3(CH_2)_nCOOH + K_2CO_3 \rightarrow 2CH_3(CH_2)_nCOOK + H_2O + CO_2$$

This was washed downstream by rainwater to form a clay deposit on the banks of the river Tiber, which the Romans used to wash their clothes. Others believe that the word soap originates from the word *saipo*, the name given by the Celts to soap produced from animal fats and plant ashes [2]. Through the middle ages soap making was carried out in a number of cities in Italy, France and England. The soap produced at that time was extremely expensive. It was not until the nineteenth century when the *LeBlanc* process for caustic soda was developed that soap became much cheaper and therefore became a common product.

Nowadays soap can be made from either synthetic (petrochemical) sources or from natural sources (animal and vegetable fats). Up until the second world war all surfactants were still made from natural sources. As most animal and vegetable fats are edible, fat shortages during the war led to the development of synthetic surfactants. Another reason for the demand for an alternative to natural soaps was their poor performance in hard water, *i.e.* water containing relatively high concentrations of calcium and magnesium ions. The soaps reacted with these ions to form the calcium and magnesium salts of the fatty acids. As these salts are insoluble, this results in an insoluble "scum". Thus more soap has to be added to the water to give a satisfactory lather and cleaning performance. This caused the need for substances such as phosphates to be used in surfactants to control the water hardness. Huge developments in synthetic detergents since the 1950s led to the gradual replacement of natural soaps by synthetic ones in most cleaning applications, except the toilet soap bar. Unlike natural surfactants, branched-chain synthetic surfactants, are poorly biodegradable. As a result, some of these surfactants (*e.g.* alkyl benzene sulphonate, ABS, the most commonly used synthetic surfactant in the 1960s) caused huge environmental problems, in some cases froth was even present in the water coming from the taps. For these reasons alternatives to branched chain surfactants, had to be developed that had to be more environmentally friendly. This was not a simple task as the performance had to be at least equal to that of branched chain detergents. At the present moment several incentives exist for soap industry to look for ways to use natural soaps again for more applications than just toilet soap bars. Apart from environmental reasons natural soaps have the long-term advantage that they are made from renewable sources. On top of that, even though nowadays highly biodegradable synthetic surfactants have been developed, the increasingly environmentally conscious customer causes a large demand for natural products. In addition, through the use of natural sources surfactant industry would become less dependent on the oil price.

1.3 Natural sources for soap production

The basic raw materials for the manufacture of natural soap are triglycerides and free fatty acids. Fatty acids from natural sources contain even numbered, straight-chain hydrocarbons. These fatty acids can be either saturated or unsaturated. The best type of fat for soap-making is a hard fat, which has a high degree of saturation. Unsaturated hydrocarbons cause rancidity in soaps as they are oxidised in air. High costs of animal fats, have led to other starting materials such as palm oil, palm kernel oil, hydrogenated rice bran oil and coconut oil being used as substitutes for tallow. Palm and coconut oil have actually proved to be excellent sources for soap-manufacture as they contain a high proportion of saturated fats, as can be seen from table 1.1. There are however far more sources of natural fats such as various vegetable oils (*e.g.* sunflower and castor seed oil [6]) and only a few decades ago even whale oil was still used in soap production [3]. For soap manufacture often a blend of a variety of fats is used in order to obtain soap with the desired properties. In some countries, however, for example India, the use of certain animal fats (here: tallow from oxen) is prohibited for religious reasons, so that industry needs to ensure animal fat free formulations for these markets.

1.4 Soap manufacture

The main steps in soap production are (see figure 1.1):

1. *saponification*, this involves the reaction of fats (triglycerides), or free fatty acids with *lye* (a strong alkaline solution) to form soap and, in the case of triglycerides glycerine (also called glycerol) according to:
   $C_3H_5(O_2CR)_3 + 3NaOH \rightarrow 3RCO_2Na + C_3H_5(OH)_3$ (figure 1.1a). During this step most of the triglycerides are converted to soap but a rest sometimes remains.
2. The next step is called *graining out* or *salting out* of the soap. A two phase system is created through washing of the reaction mixture with brine in order to recover the glycerine (figure 1.1b and 1.1c), a valuable by-product of the saponification process.

3. In some cases the soap is subsequently boiled with an excess of alkali to complete saponification, this is called *the strong change*. After this, the soap is grained out further.
4. The soap is then *fitted* or *finished*, which means separation of the useful *neat soap* (a liquid crystalline phase) which is further processed for the final product, and *nigre*, an isotropic aqueous solution of soap and impurities from the fats. This phase separation results from the addition of water and subsequent settling of the two phases (see figure 1.1d and 1.1e).

Palm oil Obtained from the outside fibrous layer of palm fruit Contains a high proportion of free fatty acids as well as tripalmitin and triolein Very high degree of saturation
Coconut oil Obtained from the copra (dried coconut meat) Contains lauric, myristic and palmitic acids and their triglycerides High degree of saturation
Palm kernel oil Obtained from the hard kernel of some palm fruit; is very similar to coconut oil Contains fewer short-chain fatty acids than coconut oil Lower degree of saturation than coconut oil
Tallow Obtained from body fats of sheep and oxen Contains large quantities of stearic and palmitic acids. Also present are high quantities of saturated triglycerides, principally tristearin, tripalmitin and triolein. Medium degree of saturation
Lard Obtained from body fats of pigs Contains palmitic, stearic and myristic acid Low degree of saturation
Fish oils Obtained from fish Contain glycerides of oleic and stearic acids as well as a high proportion of unsaturated fatty acids Very low degree of saturation

Table 1.1. Various natural sources for soap-production

In the early part of this century soap was made in a batch process, known as the *kettle process*. Measured amounts of oils and fats were poured into large kettles and boiled up with alkali until a clear liquid was produced. This was then separated in a soap and a glycerol solution. The kettle process had many disadvantages, not only was it very labour-intensive and took very long production times (nearly a week per batch), but it was also very dangerous as the kettles often overflowed during the boiling process. These problems were resolved by the development of continuous processes, mainly in Germany and Italy where many kettle houses had been destroyed during the war. In modern industry, there are three principal chemical reactions which can be used to produce soap on an industrial scale [*e.g.* 6]:

1. Direct saponification of the triglycerides

   This involves the direct reaction between the triglycerides and an alkali, usually potassium or sodium hydroxide. A problem here is that triglycerides are not very miscible with the alkali and thus the reaction will only succeed if the reaction mixture is vigorously stirred. However, once the reaction is initiated, as soap is a surface active substance, the formation of the soap helps to emulsify the triglycerides and the alkali, leading to auto-catalysis of the reaction and to an increased rate of production. Complex procedures of salting out and washing are required before the soap is obtained.

2. Neutralisation of fatty acids

   Soaps can be made in a more controlled manner by first splitting the triglycerides into free fatty acids. This is generally done by using high pressure steam to break the triglycerides down into fatty acids and glycerine. After this the fatty acids are neutralised with alkali to form soap. Advantages of this process are that the reaction is faster and that no washing or salting out processes are needed to separate the soap from the reaction mixture. Glycerol recovery is also easier.

3. Saponification of fatty methyl esters

This is the most modern method used for soap production. In this process both the triglycerides and the free fatty acids present react with methanol to produce fatty acid methyl-esters and glycerol. The reason for this esterification is that fatty acids can inhibit the catalytic action in later stages of the process. Another reason is that the methyl-esters can also be used to make other derivatives apart from soap. For soap-making however, the final step is the saponification of the methyl-esters with alkali to form soap.

These processes all yield a *neat soap*, *i.e.* a liquid crystalline phase with approximately 30% moisture content. During the saponification process, electrolytes are added (in the form of an excess of alkali and strong brine) to prevent *bunching*. This is the formation of *middle phase*, an extremely viscous liquid crystalline phase, much feared by soapmakers as it makes further processing of the soap impossible because of its high viscosity. When too much salt is added however, the soap is salted out which is unwanted at this stage. The addition of too much water also results in the formation of middle phase, but if on the other hand not enough water is used in the process, *soap curd* will form, a heterogeneous mixture of soap fibers and water. It is therefore essential to stay within very narrow limits with the amounts of salt and water used. Until the 1970s one of the main ways to judge whether the concentrations of salt and water were right was by tasting samples of the reaction mixture, to test for the degree of alkalinity by a "bite on the tongue" [3]. Since the phase boundaries depend on the fats used, a considerable amount of experience was needed for soap manufacture. Although nowadays analytical methods are used soap making is still largely an empirical process, the exact processes taking place during soap boiling are still not fully understood.

After saponification the moisture content is reduced to approximately 15% by spray drying (see figure 1.2). Additives such as builders, perfumes, antioxidants and colouring agents are then mixed with the soap in mixers and mills. A mill consists of a number of metal rolls, which rotate at different speeds, in order to subject the soap to an intensive shearing action (see figure 1.3). This is necessary to obtain a certain

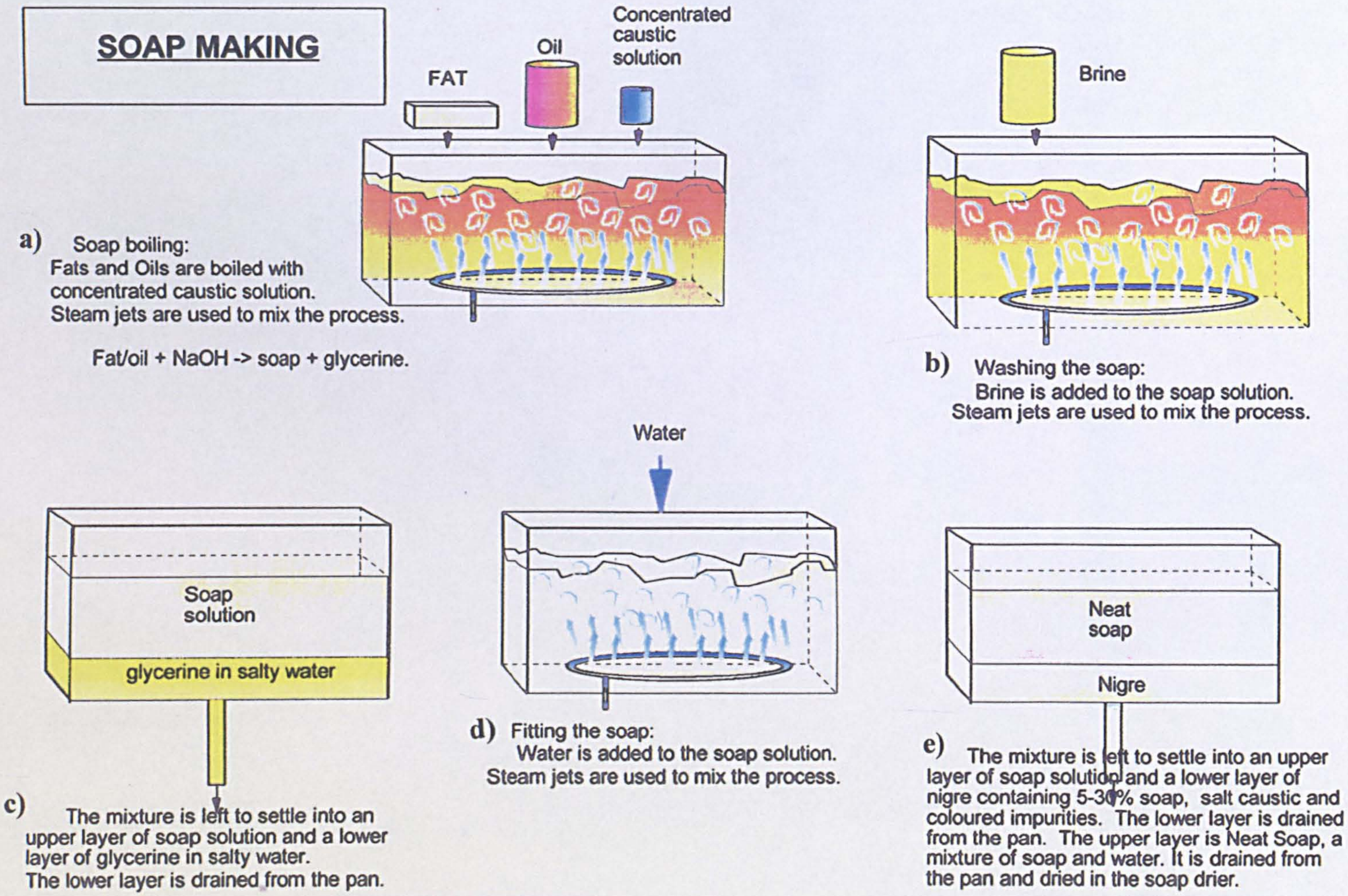
SOAP MAKING
FAT
Oil
Concentrated caustic solution
Brine
Water
Soap solution
glycerine in salty water
Neat soap
Nigre

a) Soap boiling:
Fats and Oils are boiled with concentrated caustic solution.
Steam jets are used to mix the process.

Fat/oil + NaOH -> soap + glycerine.

b) Washing the soap:
Brine is added to the soap solution.
Steam jets are used to mix the process.

c) The mixture is left to settle into an upper layer of soap solution and a lower layer of glycerine in salty water.
The lower layer is drained from the pan.

d) Fitting the soap:
Water is added to the soap solution.
Steam jets are used to mix the process.

e) The mixture is left to settle into an upper layer of soap solution and a lower layer of nigre containing 5-30% soap, salt caustic and coloured impurities. The lower layer is drained from the pan. The upper layer is Neat Soap, a mixture of soap and water. It is drained from the pan and dried in the soap drier.

Figure 1.1 The different steps in the soap making process (figure generously provided by Unilever Research Port Sunlight Laboratory)

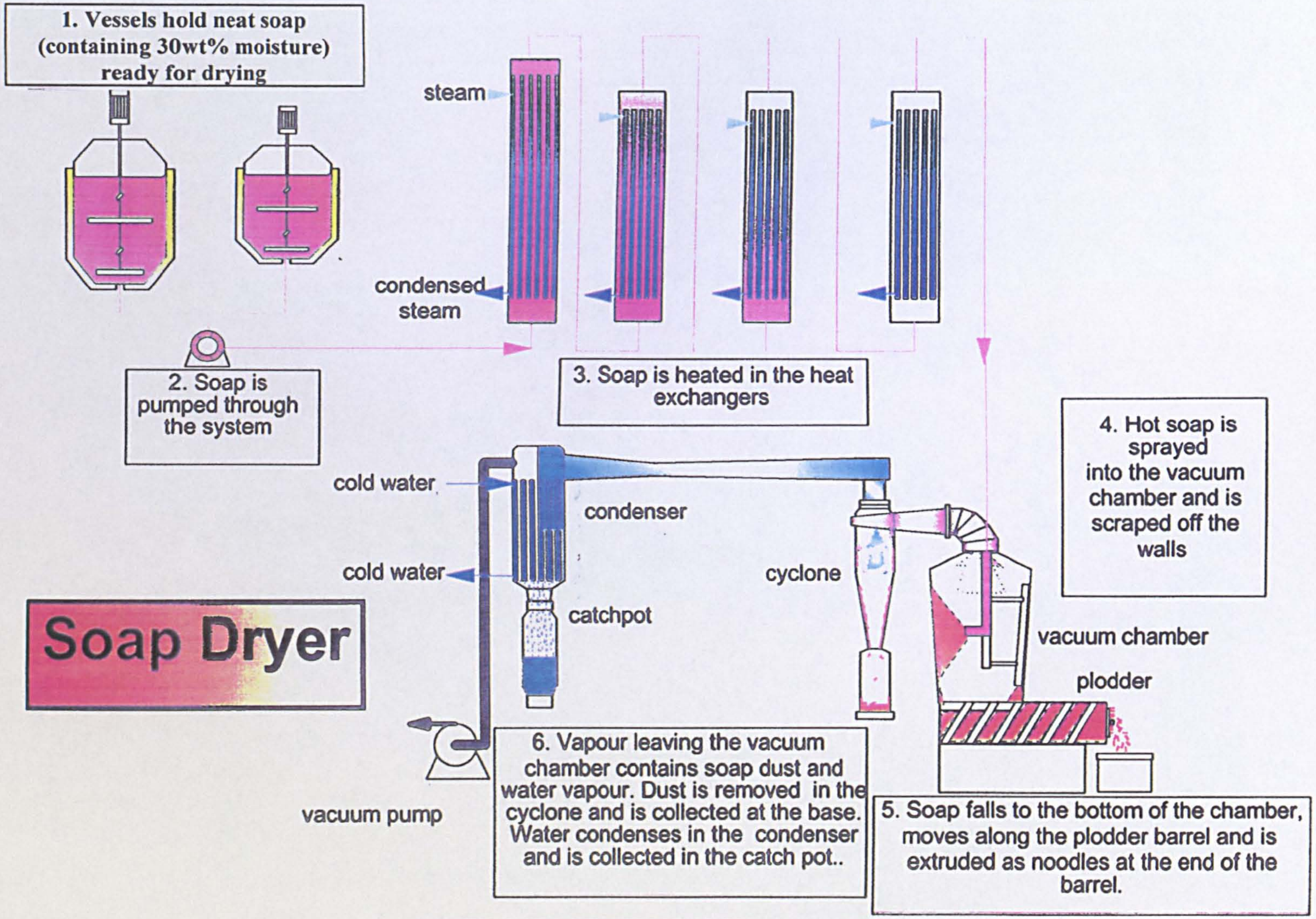
1. Vessels hold neat soap (containing 30wt% moisture) ready for drying
steam
condensed steam
2. Soap is pumped through the system
3. Soap is heated in the heat exchangers
4. Hot soap is sprayed into the vacuum chamber and is scraped off the walls
cold water
condenser
cold water
catchpot
cyclone
vacuum chamber
plodder
Soap Dryer
vacuum pump
6. Vapour leaving the vacuum chamber contains soap dust and water vapour. Dust is removed in the cyclone and is collected at the base. Water condenses in the condenser and is collected in the catch pot..
5. Soap falls to the bottom of the chamber, moves along the plodder barrel and is extruded as noodles at the end of the barrel.

Figure 1.2 Drying of the soap in a spray dryer (figure generously provided by Unilever Research Port Sunlight Laboratory)

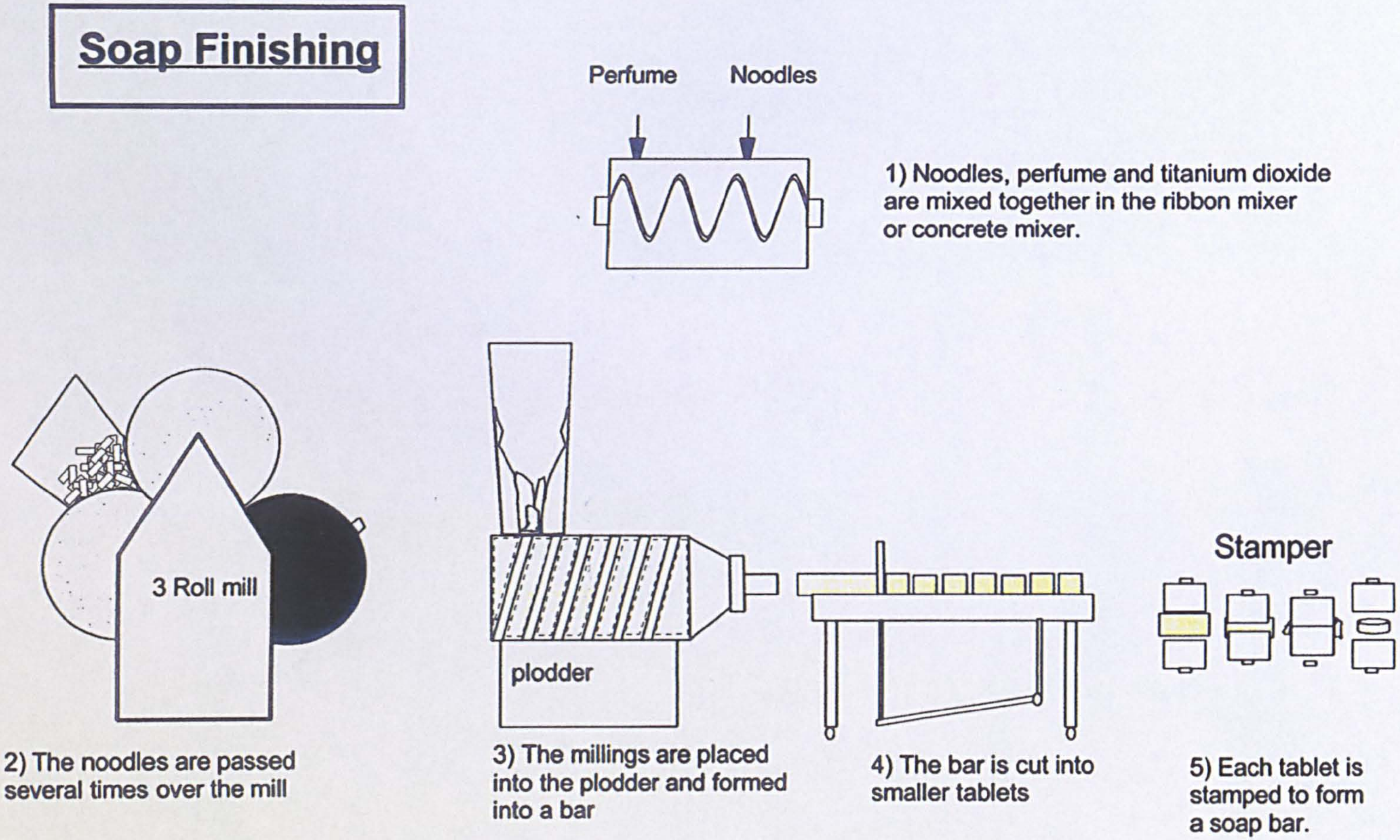
Soap Finishing
Perfume
Noodles
1) Noodles, perfume and titanium dioxide are mixed together in the ribbon mixer or concrete mixer.
3 Roll mill
plodder
Stamper
2) The noodles are passed several times over the mill
3) The millings are placed into the plodder and formed into a bar
4) The bar is cut into smaller tablets
5) Each tablet is stamped to form a soap bar.

Figure 1.3 The final processing steps in soap production (figure generously provided by Unilever Research Port Sunlight Laboratory)

degree of orientation of the crystalline soap fibres, which contributes to the distinctive physical properties of the product. The next stage takes place in the plodder, a machine that is not unlike an ordinary sausage grinder, where the milled soap is compressed into a dense coherent form. The soap mass is extruded from the plodder under high pressure through an opening where it comes out in the form of a continuous soap bar. This is then cut and stamped into soap bars, which are then ready for wrapping.

1.5 Thesis Outline

From the above it is clear that although the chemistry of soap making has been known for a very long time, control of the physical changes taking place during soap processing is still largely empirical. Although control of the liquid crystalline phases is essential in order to prevent the formation of the viscous middle phase, the phase transitions occurring during crystallisation of the soaps from the liquid crystalline neat phase are not fully understood. Mechanical actions such as milling and extrusion during subsequent processing are used in order to obtain soap with the desired physical properties, as mechanical shearing can alter the crystal structure, size and orientation. However, exactly which transformations occur during processing are not known. As the fat components used as feedstock depend on their availability and price, the composition of the raw material is far from constant. Soaps however have the ability to form numerous different crystalline and liquid crystalline forms depending on composition, temperature and mechanical shearing. It is then surprising to find that although soap is such a common product there is little molecular scale understanding of the processes (such as structural phase transformations) taking place during soap manufacture. Phase diagrams of individual soaps are known, but very little information exists on the influence of surfactant chainlength mixing on the phase behaviour of mixed soap systems. This information is essential however for assessing the influence of different chainlengths fatty acids on the crystallisation process and the properties of the resulting soaps. Aim of this PhD was therefore to improve this situation and to obtain a better insight into the processes that take place during soap crystallisation from liquid crystalline phases.

The thesis is presented in the following way: in the following chapter (chapter 2) a concise theoretical background is provided on crystallisation, a mechanism by which solids can be formed and purified. A section on X-ray diffraction, a very powerful technique which provides information on the structural nature of substances, is included. In chapter 3 an overview is given on the complex phase behaviour of surfactants. The equipment and experimental procedures used are described in chapter 4. Much of the equipment used was especially developed for this PhD. This included the re-design of an existing zone refiner, which was used for the purification of fatty acids, in order to investigate the influence of very low concentrations of impurities on the crystal structure and physical properties of the fatty acids. The findings of this are given in chapter 5. The nucleation process of soaps from aqueous solutions has been investigated using automated nucleation rigs. The results of these studies are given in chapter 6. The main experimental method used for structural analysis in this PhD involved the use of synchrotron radiation for *in-situ* crystallisation studies of single soaps and soap mixtures from liquid crystalline phases in order to investigate the phase changes taking place during this process and to assess the effect of chainlength on the crystallisation process. The resulting findings are given in chapter 7. At the end of each chapter the main conclusions derived from the experiments are given. In the last chapter of this thesis (chapter 8) the conclusions of all the chapters are drawn together and some recommendations for future work are highlighted.

1.6 References used in this chapter

1. *Surface activity, a Unilever educational booklet* (1969)
2. Davidsohn J, Better EJ, Davidsohn A, *Soap Manufacture* **vol 1** (1953), Interscience Publishers inc New York

3. Swern D (ed.), *Bailey's industrial oil and fat products* **vol 1 4th ed.** (1979), J Wiley and Sons Inc. USA
4. Woollatt E, *The manufacture of soaps, other detergents and glycerine*, Ellis Horwood Ltd (1985) Chichester
5. Whalley GR, *Manufacturing Chemist* (1990) **61**, 5, 41-47
6. *Vegetable oils and fats, a Unilever educational booklet, revised ordinary series* **no 2** (1975)

Chapter 2

Background Theory

Chapter 2 Background theory

2.1 Introduction

In this chapter a concise background is provided on the aspects of nucleation, crystallisation and crystallography relevant to the work presented here. In section 2.2 the effect of supersaturation on the crystallisation process is discussed, followed by section 2.3 where it is explained how the degree of supersaturation can be calculated with the aid of the Van 't Hoff equation. In section 2.4 a descriptive model of the nucleation process (the process taking place prior to crystal growth) is given. More insight is provided into the internal structure of crystals in section 2.5, followed by a brief discussion on crystal growth mechanisms in section 2.6. The purifying nature of the crystallisation process is briefly explained in section 2.7. This is followed by section 2.8 where the use of X-ray diffraction for the study of crystalline substances is discussed as this is one of the key techniques used for the work presented here, for investigating the crystallisation process of soaps from liquid crystalline phases. The chapter is concluded with a summary in section 2.9.

2.2 The influence of supersaturation on the crystallisation process

Crystallisation is an important unit operation used for the formation and purification of a wide range of substances. A good introduction to crystallisation processes was given by Price [1], more details can be found in text books such as [2-5]. Crystallisation can take place from the gas phase, from a melt or from solution. Most of the theory in this chapter will be based on crystallisation from solutions although zone refining (a technique used for purification through crystallisation) in section 2.7 is explained in terms of crystallisation from the melt.

When a substance is dissolved in a solvent, there is a maximum to the amount of material that be can be dissolved. The solution is then said to be *saturated.* The concentration at which this occurs is called the *equilibrium concentration,* or *saturation concentration* which is dependent on the temperature; in general the higher the temperature the more solid can be dissolved. When the equilibrium concentration is reached and more solid is added this will not dissolve and a suspension is formed. The *saturation temperature* of a solution is defined as the temperature at which dissolution occurs whilst heating the solution at an infinitely slow rate. It can thus be obtained experimentally by extrapolation to zero heating rate of a graph of the dissolution temperature versus heating rate. Many solutions can be *undercooled.* This means that they can be cooled to a temperature below the saturation temperature without crystallisation taking place. The concentration of solute is then higher than the equilibrium concentration and the solution is said to be *supersaturated.* Supersaturation can be defined as the ratio of the actual concentration of the substance at a certain temperature and the equilibrium concentration of that substance at that temperature:

$$\sigma = \frac{c}{c^*} \qquad (2.1)$$

where σ is the supersaturation, c is the concentration of the solution at a certain temperature and c^* is the equilibrium concentration corresponding with that temperature. Supersaturation is the driving force for crystallisation; through the formation of the solid phase the solute concentration decreases so that supersaturation is relieved. Crystallisation cannot occur if the solution is not supersaturated.

The solubility behaviour of a solute in a solvent can be graphically represented in a so called *solubility diagram* where the solubility is given as a function of temperature (see figure 2.1). In this diagram three regions can be distinguished:

1. A *stable* (unsaturated) *zone* where crystallisation of the solute is impossible as the solute concentration is lower than the equilibrium concentration at that temperature.
2. The *metastable zone*. In this zone a certain degree of supersaturation exists. Spontaneous crystallisation of the solute is improbable but crystal growth will occur if a crystal seed would be placed in the solution.

3. The *labile zone* where the supersaturation is higher than in the metastable zone; spontaneous crystallisation of the solute is highly probable.

In figure 2.1 the lower curve is the solubility curve which can experimentally precisely be determined by preparing a sample of a certain concentration and observing at which temperature dissolution occurs whilst heating the solution at a very low rate. The broken curve is the supersolubility curve. In solutions at the temperatures and concentrations given by this curve, bulk nucleation and spontaneous crystal growth will almost certainly occur on cooling of the sample. The position of this curve cannot be as precisely defined as that of the solubility curve. Its position in the diagram depends *e.g.* on the rate by which supersaturation is generated and the intensity of agitation.

Supersaturation can be induced in several ways. The distinction is made between a *precipitation process* and a *crystallisation process*, depending upon which way supersaturation is created. If supersaturation is created by cooling of the solution, evaporation of the solvent (thus increasing the solute concentration), or by a combination of the two, the process is called crystallisation. When supersaturation is created by a chemical reaction (by which a less soluble product is formed) or by the addition of an anti-solvent (a liquid which is miscible with the solvent, so that a mixture is created in which the solute has a reduced solubility) the process is called precipitation.

The condition of supersaturation alone is not a sufficient cause for the system to begin to crystallise. Before crystals can grow there must exist in the solution a large number of minute solid bodies, known as clusters or nuclei. Supersaturation is the driving force for the molecules in solution to aggregate together and form these clusters. Crystallisation can thus be divided into two processes: nucleation and crystal growth. Nucleation is the creation of a new phase within a homogeneous phase, which can only be achieved when a certain degree of supersaturation exists within the system. Once a nucleus of a certain critical size has been created, crystal growth can take place. The formation of a nucleus is a three-dimensional process, through local temperature and concentration fluctuations, molecules can aggregate together and form clusters (mechanisms for this process are discussed in more detail in section 2.4). Crystal growth is a two-dimensional process, where well defined faces of the crystal grow at certain rates. As supersaturation is the driving force for both nucleation and growth, these are thus are thus two competing mechanisms by which supersaturation can be relieved. When crystallisation takes place at high supersaturation, the nucleation rate dominates over the crystal growth rate, resulting in a product consisting of small particles. At low supersaturations the nucleation rate is low in comparison to the crystal growth rate so that larger crystals can be obtained.

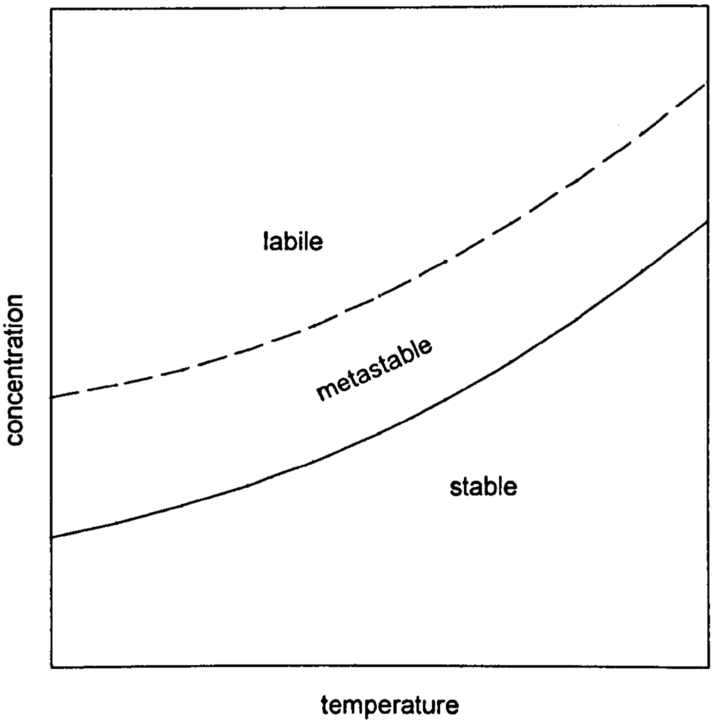

Figure 2.1 The solubility-supersolubility diagram showing the stable, metastable and labile zones

2.3 The Van 't Hoff equation

Since the final particle size distribution of a crystallisation process depends on the degree of supersaturation, knowledge of the equilibrium solubility curve, which describes the equilibrium concentration of solute as a function of temperature, is thus of great importance in designing and controlling such processes. In addition, knowledge of the metastable zone aids to predict which degree of supersaturation is needed before crystallisation will occur. If crystallisation at a lower supersaturation is required this can be accomplished by techniques such as seeding of the solution or the use of ultrasonic sound *e.g.* [6].

For ideal solutions the dissolution behaviour can be described by the *Van 't Hoff* equation:

$$\ln(x) = \frac{\Delta S_d}{R} - \frac{\Delta H_d}{RT_{sat}} \tag{2.2}$$

where x is the mole fraction of solute in solution, T_{sat} (in K) is the saturation temperature, R is the gas constant (=8.31Jmol^{-1}K^{-1}) and ΔS_d (Jmol^{-1}K^{-1}) respectively ΔH_d (J/mol) are the entropy and enthalpy of dissolution. When the saturation temperatures for a series of solute concentrations are known, the Van 't Hoff equation can be used to calculate the entropy and enthalpy of dissolution. This equation assumes ideal solution behaviour. An ideal solution is a solution in which the interactions between all molecules are identical, *i.e.* the interactions between solute and solvent molecules are identical with those between the solute and the solvent molecules themselves.

Once the entropy and enthalpy of dissolution have been obtained experimentally the Van 't Hoff equation can be used to calculate the degree of supersaturation of a solution at a given temperature T_p in the following way. Supersaturation is induced in a solution of concentration x, by cooling it below its saturation temperature, T_{sat}, to a temperature T_p (the precipitation temperature). If given enough time, a certain amount of the solute will precipitate at this temperature in order to relieve supersaturation. This amount can be found from: $\Delta x = x - x_e$, where x_e is the equilibrium mole fraction at temperature T_p. However, until the solution starts to precipitate the concentration will remain constant. In order to determine the degree of supersaturation of the solution at T_p, it needs to be known what the equilibrium mole fraction, x_e, is at this temperature. This can be calculated from the Van 't Hoff equation because T_p, ΔS_d and ΔH_d are known:

$$\ln x_e = \frac{\Delta S_d}{R} - \frac{\Delta H_d}{RT_p} \qquad (2.3)$$

The saturation temperature T_{sat} (which is higher than T_p) of the solution under consideration can also be calculated from the Van 't Hoff equation because the mole fraction of solute in the solution is known (as well as ΔS_d and ΔH_d):

$$\ln x = \frac{\Delta S_d}{R} - \frac{\Delta H_d}{RT_{sat}} \qquad (2.4)$$

The degree of supersaturation of the solution of concentration x at temperature T_p can then be found by combining equations 2.3 and 2.4, which results in:

$$\ln x - \ln x_e = \ln \frac{x}{x_e} = \ln \sigma = \frac{\Delta H_d}{R}\left(\frac{1}{T_p} - \frac{1}{T_{sat}}\right) \qquad (2.5)$$

This equation illustrates that the more a solution is undercooled (cooled below its saturation temperature) the greater the supersaturation of the solution becomes.

2.4 The nucleation process

Nucleation can take place according to the following three mechanisms: primary homogeneous nucleation, primary heterogeneous nucleation and secondary nucleation. *Primary homogeneous nucleation* is spontaneous nucleation, taking place in systems free from either dissolved or solid impurities. *Primary heterogeneous nucleation* occurs when nuclei form around impurity sites such as foreign particles (hetero-nuclei) or the vessel walls. Heterogeneous nucleation will almost always play a role in the nucleation process as it is virtually impossible to prepare a solution without impurities, such as atmospheric dust which contains hetero-nuclei (and sometimes even particles of the product itself). In addition there are always the container walls and a free surface. When impurities are present crystallisation will occur at a lower supersaturation than for a pure solution. *Secondary nucleation* differs from primary nucleation in that it is induced by crystals already present in the sample. These can form new nuclei by attrition, fracture or by crystalline dust being swept of them. For these reasons secondary nucleation usually increases with increased agitation of the solution (Mullin [3]). An increase in agitation does not always lead to increased nucleation rate however (Mullin and Raven [7,8]). A possible explanation for this is that agitation could lead to disruption of the subnuclei (nuclei smaller than the critical size, see next section) in the solution.

2.4.1 The formation of a nucleus in the metastable zone

A good historic overview on nucleation theory can be found in Zettlemoyer [9]. Classical nucleation theory originates from the thermodynamic approach of Gibbs [10] which was further developed by Volmer and Weber [11], Farkas [12], Kaischew and Stranski [13] and by Becker and Döring [14]. Classical nucleation theory was mainly developed for the nucleation process of condensation of vapours. This is however analogous to the nucleation of solids from solutions.

Nucleation, the formation of a new phase within an existing homogeneous phase, is associated with a change in the Gibbs free energy, ΔG, of the system (*i.e.* the change in energy occurring at constant pressure). For a process to occur spontaneously ΔG has to be negative. For most substances the solubility increases with increasing temperature. At high undercooling crystallisation is energetically favourable. At intermediate undercooling, within the metastable zone, first an energy barrier must be overcome before a nucleus becomes stable. This is illustrated by the following model. In developing a descriptive theory for the formation of nuclei from a mother phase (solution or melt), a certain shape of the nucleus has to be assumed. The supposition is made here that for surfactant systems the nucleus will be cylindrical. Reason for this presumption is that surfactants are long molecules, which in the solid phase are likely to be packed parallel to each other, orientated tail to tail (see chapter 3). Two parameters: the radius, r, and the height, h, are needed to describe a cylinder. The following model however only allows for evaluation of one parameter that characterises the size of the nucleus. For this reason the height is assumed to be constant and equal to the height of the unit cell (see section 2.5). The radius of the cylinder can then be calculated using the following model. An analogous model can be derived if a different geometry of the nucleus is assumed (see *e.g.* [2] for a spherical shape).

The change in Gibbs free energy for the formation of a nucleus is due to two opposing effects:

1. An interface has to be created between the forming solid phase and the remaining solution. This is an energetically unfavourable process. The change in the Gibbs free energy associated with this will thus be positive and will be proportional to the size of the interface that is created (when the molecules are dissolved there is no interface as there is only one phase present). The constant of proportionality is called the interfacial tension, γ. This is the interfacial tension between the solution and a forming nucleus and must not be confused with the solution's interfacial tension (which is the interfacial tension between a liquid surface and air saturated with the relevant vapour). If for simplicity the forming nucleus is assumed to be cylindrical, then the change in interfacial Gibbs free energy, ΔG_s, of this forming nucleus is equal to:

   $$\Delta G_s = (2\pi rh + 2\pi r^2)\gamma \qquad (2.6)$$

   where r is the radius of the forming nucleus, h the height of the cylindrical nucleus and γ is the interfacial energy between the solution and the forming nucleus.
2. The creation of "bulk" solid phase (with the term "bulk solid" is meant here all material in the solid phase that does not contribute to the interface) from a solution or melt, is energetically favourable. The change in Gibbs free energy associated with this will thus be negative and will be proportional to the volume of solid phase created. Therefore if a cylindrical nucleus is assumed, then the change in the Gibbs free energy due to the creation of bulk solid phase is given by:

   $$\Delta G_b = \pi r^2 h \Delta G_{b,v} \qquad (2.7)$$

   where ΔG_b is the change in Gibbs free energy for the bulk solid phase and $\Delta G_{b,v}$ is the change in Gibbs free energy of the bulk solid phase per unit volume ($\Delta G_{b,v}$

must not be confused with the *total change* in Gibbs free energy per volume, *i.e.* $\Delta G_{b,v} \neq \frac{\Delta G}{V_m}$, where V_m is the molar volume).

The total change in Gibbs free energy due to the formation of a nucleus from a solution or melt is given by the sum of equations 2.6 and 2.7:

$$\Delta G = \Delta G_s + \Delta G_b = (2\pi rh + 2\pi r^2)\gamma + \pi r^2 h \Delta G_{b,v} \qquad (2.8)$$

In figure 2.2 a qualitative graph is shown for equations 2.6-8. The figure illustrates that for a nucleus to become stable, first an energy barrier must be overcome, corresponding to the maximum in the total change in Gibbs free energy.

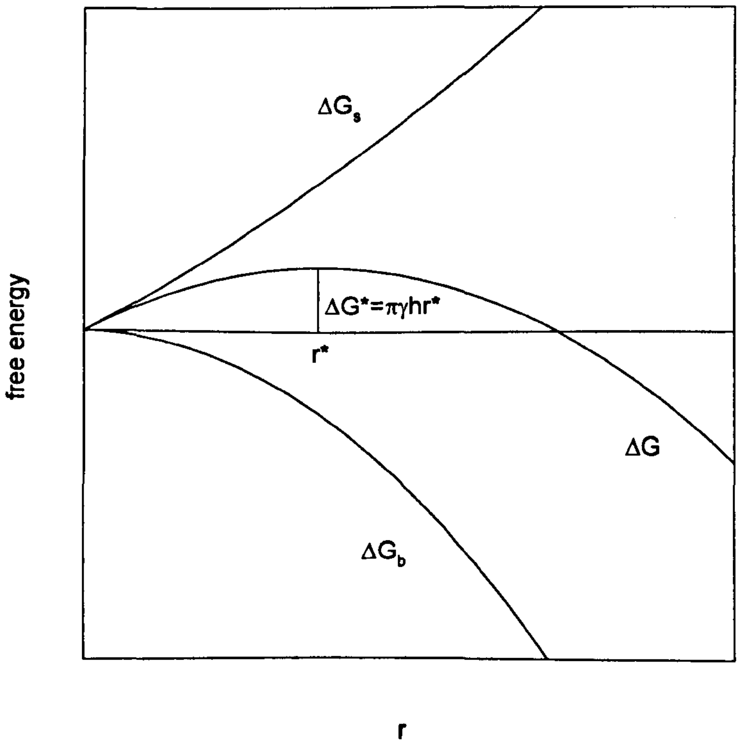

Figure 2.2 showing the different contributions to the Gibbs free energy for the formation of a nucleus

A cluster will always try to minimise its total excess free energy. From figure 2.2 it can be seen that if $r<r^*$ it can only minimise its excess free energy by re-dissolving and that only if $r>r^*$ it can accomplish this by growing. A nucleus is thus unstable if its radius is smaller than r^*, which is called the *critical radius*. Once a nucleus has achieved a size given by r^* or larger, the total change in Gibbs free energy is reduced by growth of the nucleus. The nucleus has thus become stable and will grow further. Clusters can only reach the critical size due to local temperature and concentration fluctuations in the solution. Experimental evidence for the formation of clusters is given by *e.g.* Larson and Garside [15]. Clusters below the critical size have been called *subnuclei* and clusters above the critical size *supernuclei* (Kaschiev [16]). It is not known whether the critical nucleus is a tiny crystal or that it is an amorphous body with no clearly defined surface. Once the critical size has been reached the cluster will grow as long as the solution remains supersaturated.

The point where ΔG becomes negative signifies the lower limit of the metastable zone. From this point onwards the formation of a nucleus is energetically favourable since no energy barrier has to be overcome anymore, thus enabling spontaneous nucleation. The critical radius and the maximum in the total change in Gibbs free energy can be found by taking the derivative of ΔG with respect to r and equating this to zero:

$$\frac{\partial \Delta G}{\partial r} = (2\pi h + 4\pi r)\gamma + 2\pi r h \Delta G_{b,v} = 0 \qquad (2.9)$$

Therefore :

$$r^* = \frac{-h\gamma}{2\gamma + h\Delta G_{b,v}} \Rightarrow \Delta G_{b,v} = \frac{-h\gamma - 2\gamma r^*}{hr^*} \qquad (2.10)$$

Substitution of $\Delta G_{b,v}$ in equation 2.8 leads to:

$$\Delta G^* = \pi\gamma h r^* \qquad (2.11)$$

The classical approach is then to use the Gibbs-Thomson equation to relate the size of the critical nucleus to the supersaturation:

$$\ln\sigma = \frac{2\gamma v_m}{kTr} \Rightarrow r = \frac{2\gamma v_m}{kT\ln\sigma} \qquad (2.12)$$

where k is the Boltzmann constant ($=1.38\text{x}10^{-23}$ J/K), v_m is the molecular volume and T is the temperature at which the nucleus is formed. The weak point of the classical description of the nucleation process is that bulk thermodynamic properties such as the interfacial tension and the volume free energy are being ascribed to small molecular clusters. There is little unambiguous experimental evidence confirming the applicability of the Gibbs-Thomson equation to small clusters [4]. It is however still widely used as it links physical size and solubility of the particles (Walton [17]). Equation 2.12 illustrates that for smaller supersaturation the critical radius of a nucleus must be larger. Substitution of equation 2.12 in 2.11 results in:

$$\Delta G^* = \frac{2\pi\gamma^2 v_m h}{kT\ln\sigma} \tag{2.13}$$

This equation illustrates that in the limiting situation, as $\sigma \downarrow 1$ the energy barrier for the formation of a nucleus becomes infinitely large (and so does the critical radius see equation 2.12), which shows that nucleation becomes impossible if the solution is not supersaturated. If on the other hand the supersaturation is increased, this will lead to a reduction of the energy barrier that needs to be overcome for the formation of a critical nucleus (and will decrease the size of a critical nucleus, see equation 2.12).

Thermodynamics can only make predictions about the likelihood of a process to occur, in terms of stability. It does not make predictions about the rate at which a process takes place. The link between thermodynamics and the kinetics of nucleation is made here by assuming that the nucleation rate, J (rate of formation of new clusters of critical size per unit volume of the solution), can be expressed by an Arrhenius type relation, where ΔG^* is the activation energy:

$$J = A\exp\left(\frac{-\Delta G^*}{kT}\right) \tag{2.14}$$

T is the temperature (in Kelvin), at which the nucleus is formed (the precipitation temperature), A is a pre-exponential factor (sometimes called the collision factor, Mullin [3]) and k is the Boltzmann constant ($1.38\text{x}10^{-23}$ JK^{-1}). This equation is based on the assumption in classical nucleation theory, that nuclei are not formed by a simultaneous collision of a number of molecules but by an addition mechanism:

$m + m = m_2$

$m_2 + m = m_3$

$m_{c-n} + m = m_c$

where m_i represents a nucleus consisting of i molecules. Molecules are added to the forming nucleus until it has reached its critical size. Whether the spatial ordering of the molecules (as in the crystalline state) is already present in the critical nucleus or that re-ordering of the molecules occurs after the formation of the critical nucleus is not known.

To obtain J as a function of the parameters controlling the nucleation process is one of the central problems in nucleation theory and experiment. When a solution is cooled to a temperature within the metastable zone, nucleation will only occur after a certain time, as it takes some time before critical nuclei are formed. This time is called the *induction time*. This time can be obtained experimentally by cooling a solution extremely fast to a temperature within the metastable zone and measuring the time it takes before nucleation occurs. The drawback is that since nuclei have to grow to a detectable size the measured induction time will depend on the sensitivity of the method used. This error will be negligible if the time it takes for the nuclei to reach the critical size is much larger than the subsequent period that it takes before they have reached a detectable size. The induction time, τ, can be taken to be inversely proportional to the nucleation rate (*e.g.* Mullin [3]):

$$\tau \propto \frac{1}{J} \tag{2.15}$$

therefore:

$$\ln\left(\frac{1}{\tau}\right) = \ln A' - \frac{2\pi\gamma^2 v_m h}{k^2 T^2 \ln\sigma} \tag{2.16}$$

The interfacial tension between the solution and the forming nucleus, γ, can thus be determined from the slope of a plot of $\ln(1/\tau)$ versus $\frac{1}{T^2 \ln\sigma}$. When γ is known, the size of the critical nucleus can be evaluated at a given supersaturation from equation 2.12.

Equation 2.16 predicts an exponential dependence of the nucleation rate on the supersaturation. In practise however the nucleation rate first increases, but then decreases with further increasing supersaturation. Turnbull and Fisher [18] tried to account for this by including a correction term for the viscosity in equation 2.13. The idea behind this is that a correction term is needed as the increase in viscosity of the solution during cooling might prevent the solute molecules to aggregate and form clusters. A review on nucleation mechanisms can be found in *e.g.* Zettlemoyer [9] or more recently by Kaschiev [13]. To experimentally test a quantitative nucleation mechanism for homogenous nucleation is extremely difficult since it is virtually impossible to prepare impurity-free solutions. In addition the results depend strongly on the technique used and the criteria for judging when nucleation has occurred. Due to the discrepancies between nucleation theory and experimental data, in many cases an empirical description of the nucleation process is favoured; this will be discussed in the next section.

2.4.2 An empirical description of nucleation kinetics

Since the homogeneous nucleation theory is very hard to verify experimentally, an empirical description of the nucleation process has been developed (see *e.g.* Nyvlt [19]). Further justification for the use of an empirical model is that nucleation taking place in most industrial processes is likely to be heterogeneous or caused by secondary nucleation. An empirical way to express the nucleation rate J at the metastable zone limit is:

$$J = k_n(\Delta c_{\max})^m \qquad (2.17)$$

where k_n is the nucleation rate constant, m is the apparent order of nucleation and $\Delta c_{\max}$ is the maximum possible supersaturation (defined as $\left(c - c^*\right)_{\max}$, where c is the solution concentration and c^* is the equilibrium saturation concentration at a given temperature). The constant m has no fundamental mechanistic significance unless correctly matched against a mathematical mechanistic model of the process under consideration. It does not give an indication of the number of elementary species involved in the nucleation process. The maximum possible supersaturation $\Delta c_{\max}$ can be written as a function of the maximum possible undercooling of the system as follows:

$$\Delta c_{\max} = \left(\frac{dc^*}{dT}\right)\Delta T_{\max} \tag{2.18}$$

where: $\Delta T_{\max} = T_{dissolution} - T_{precipitation}$ (the value of $\Delta T_{\max}$ at equilibrium (zero cooling rate) corresponds to the metastable zone width). The nucleation rate can also be written in terms of the rate at which supersaturation is created by cooling, this is proportional to the product of the slope of the solubility curve $\left(\frac{dc^*}{dT}\right)$ and the rate at which the solution is cooled $\left(\frac{-dT}{dt}\right)$:

$$J = \varepsilon\left(\frac{dc^*}{dT}\right)\left(\frac{-dT}{dt}\right) \tag{2.19}$$

ε is a correction factor for the change in concentration, in case the species under consideration is being hydrated, c^* is the equilibrium saturation concentration at a given temperature, T is the temperature, t is the time. Combining equations 2.17 and 2.19 and subsequent substitution of 2.18 leads to:

$$\varepsilon\left(\frac{dc^*}{dT}\right)b = k_n\left[\left(\frac{dc^*}{dT}\right)\Delta T_{\max}\right]^m \tag{2.20}$$

where: $b = -\frac{dT}{dt}$ is the rate at which the solution is cooled. Taking the logarithms of both sides of equation 2.20 and some rearranging results in:

$$\log(b) = (m-1)\log\left(\frac{dc^*}{dT}\right) - \log(\varepsilon) + \log(k_n) + m\log(\Delta T_{\max}) \tag{2.21}$$

This equation was derived by Nyvlt [19] and shows that a plot of log(b) versus log($\Delta T_{\max}$) should result in a straight line with slope m. The above analysis contains an over-simplification however. Expression 2.17 assumes that changes in supersaturation within a system are due only to nucleation, although in practice changing supersaturation is due to both nucleation and growth of already existing nuclei. Further, in practical measurements the nuclei have to grow to a certain size before they can be detected, therefore such measurements are not dependent only on nucleation, but also on the subsequent crystal growth process. Due to this, the obtained value for m depends on the sensitivity of the experimental method used.

2.5 The internal structure of crystalline substances

Although it is often not realised, most solids including soaps are at least to some degree crystalline. This means that there are at least regions in the solid where the molecules are ordered on a regular three-dimensional lattice. Every atom of each molecule takes up a specific place within this lattice. Some substances, like surfactants can also form so called *liquid crystals* in which the order (at least in one dimension) is constituted by large groups of molecules; there is no short range order, *i.e.* the atoms of the molecules have no specific positions, there is only long range order. In polar liquids such as water there is only short range order: in small groups the molecules are orientated with respect to each other due to dipole-dipole interactions, there is no long range order however. The terms short and long range order are used here in relation to the distances between the molecules. The different kinds of order found in liquid crystals and the liquid crystalline structures formed by surfactants are explained in chapter 3.

When there is no order in the packing of the molecules of a solid it is said to be *amorphous*. Some substances have the ability to pack their molecules in different ways on a three-dimensional lattice. This phenomenon is called *polymorphism* or *allotropy*; a good review on polymorphism in organic compounds is given by Threlfall [20]. A special case of polymorphism is that in which a substance can form different *solvates*, or *hydrates* when the solvent used is water. This means that a specific number of solvent molecules occupies certain positions in the crystal lattice. This phenomenon is sometimes called *pseudo-polymorphism*, as the crystalline substance is chemically different in the different polymorphic forms, since there are a different number of solvent molecules present. Soaps are thought to form a number of different hydrates, as is discussed in more detail in chapter 3. The various polymorphs that a substance can form are often named according to the order in which they have been discovered, or in the order of increasing melting point and are usually labelled with Greek letters. The material of the different polymorphic structures is identical from a chemical point of view (apart from hydrates), but can have different physical properties, such as solubility (important for pharmaceuticals as this determines the bio-availability), melting point, hardness, colour (many pigments exhibit polymorphism), particle shape and size. It is therefore of significant industrial importance to know if a substance has the ability to form different polymorphic structures and under which circumstances they are formed. Often phase transformations between different polymorphs can be induced by external influences such as temperature, the rate at which the substance is cooled during crystallisation or grinding of the material. If a conversion between two polymorphic forms takes place at a definite temperature this is called *enantiotropy* (Greek for change into opposite). Sometimes seed crystals with a certain polymorphic form, used during crystallisation, can act as template, inducing the material to crystallise in the polymorphic form of the seed crystals. Ostwald's step rule (Ostwald [21, 22] says that in any process the state which is initially obtained is not the *most* stable state but the *least* stable state, that is closest in terms of free energy change to the original state. For a crystallisation process this means that a substance can crystallise in a certain polymorphic form, which is not necessarily the most stable state at that temperature. This polymorphic form is therefore metastable at the temperature at which it has been obtained, which can lead to conversions into successively more stable polymorphic forms until the most stable form at those conditions has been reached. The kinetics of this transformation process might be very slow however. Since the resulting polymorphic form depends strongly on its conditions of preparation, it is best to investigate the material *in-situ*, as for instance temperature changes or grinding of the material can lead to changes in the crystal structure. Sometimes it is extremely hard to reproduce material with a certain polymorphic form (*e.g.* Dunitz and Bernstein [23]).

In a crystal the molecules can be thought to be ordered on a three-dimensional lattice, the lattice points representing one or more molecules. Each lattice point in the lattice has identical surroundings. The smallest repeating unit within the lattice is called the *unit cell.* The unit cell contains a certain number of lattice points, and can be thought of as the building block with which the lattice can be formed by a three-dimensional repetition. To fill space throughout by the repetition of a unit is only possible with seven geometrical shapes of this unit (see table 2.1). These seven different shapes of the unit cell distinguish the seven *crystal systems.* In each case the unit cell is characterised by six parameters, called the *cell parameters*: the length of its three axes, called a, b and c and the three angles between them, α, β and γ; where α is the angle between the b and the c axis, β is the angle between the a and the c axis and γ is the angle between the a and b axis. The constraints imposed on the unit cell parameters by the seven crystal systems are summarised in table 2.1. In some crystal systems different types of unit cells are possible, which differ in the number of lattice points that they contain. A *primitive* unit cell (symbol P) for instance contains one lattice point, one at each corner of the unit cell that is shared with eight other unit cells. Other types are the *body-centred* (symbol I from the German *innenzentriert*) and the *face centred* unit cell of which there are different types depending upon which faces are centred: symbol A (face defined by the b and the c axis), B (face defined by the a and the c axis), C (face defined by the a and the b axis), or F (all faces centred). This differentiation leads to a total of 14 different crystal lattices, called the 14 *Bravais lattices*, which are also given in table 2.1 and are shown in figure 2.3. A further differentiation can be made between the different lattices on the basis of the symmetry operations that are possible in the real lattice, this depends on the shape of the molecules and how they are arranged in the unit cell. If only the symmetry operations rotation, reflection, inversion or rotation-inversion are considered the 14 Bravais lattices can be divided into the 32 *point groups* (which are called point groups because all the symmetry operations considered here leave at least one point in the same position). These can be further sub-divided into the 230 *space groups*, when in combination with the previous symmetry operations translation is considered which can then give rise to screw axes and glide planes. All

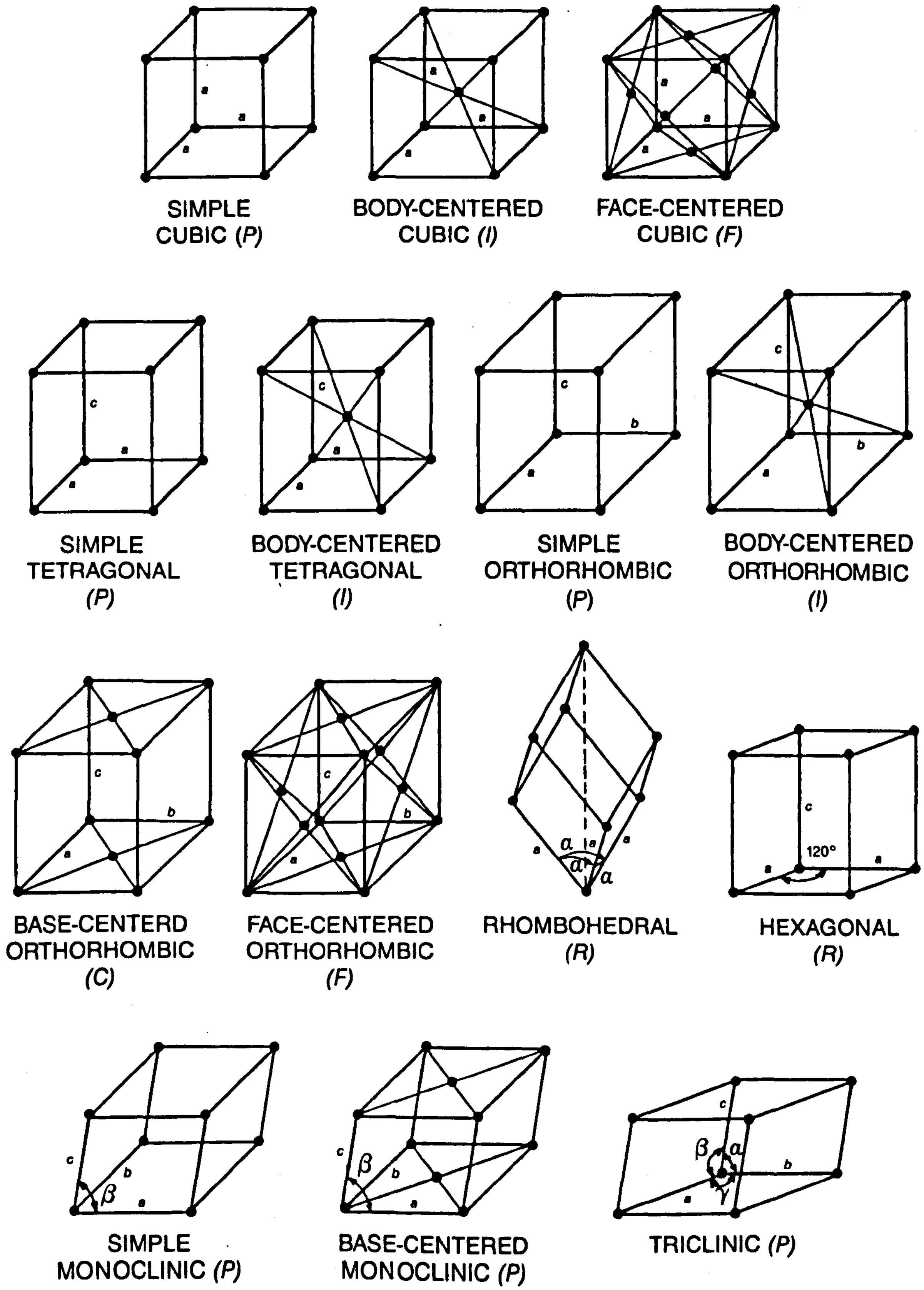
SIMPLE CUBIC (P)
BODY-CENTERED CUBIC (I)
FACE-CENTERED CUBIC (F)
SIMPLE TETRAGONAL (P)
BODY-CENTERED TETRAGONAL (I)
SIMPLE ORTHORHOMBIC (P)
BODY-CENTERED ORTHORHOMBIC (I)
BASE-CENTERD ORTHORHOMBIC (C)
FACE-CENTERED ORTHORHOMBIC (F)
RHOMBOHEDRAL (R)
HEXAGONAL (R)
SIMPLE MONOCLINIC (P)
BASE-CENTERED MONOCLINIC (P)
TRICLINIC (P)
a
b
c
α
β
γ
120°

Figure 2.3 The seven crystal systems and the 14 Bravais lattices (from [2])

crystal system	definition	Bravais lattice
cubic	$a=b=c$, $\alpha=\beta=\gamma=90°$	primitive body-centred face centred
tetragonal	$a=b\neq c$, $\alpha=\beta=\gamma=90°$	primitive body-centred
orthorhombic (also called rhombic)	$a\neq b\neq c$, $\alpha=\beta=\gamma=90°$	primitive body-centred base-centred face centred
hexagonal	$a=b\neq c$, $\alpha=\beta=90°$, $\gamma=120°$	primitive
trigonal (also called rhombohedral)	$a=b=c$, $\alpha=\beta=\gamma\neq 90°$	primitive
monoclinic	$a\neq b\neq c$, $\alpha=\gamma=90°\neq\beta$	primitive base centred
triclinic	$a\neq b\neq c$, $\alpha\neq\beta\neq\gamma\neq 90°$	primitive

Table 2.1 The seven crystal systems and 14 Bravais lattices.

possible crystal structures can thus be categorised into the 230 space groups (see [24]). More details on crystallography can be found in textbooks such as [25-27]. Due to symmetry elements present, certain atoms and molecules *within* the unit cell are related to each other. The unique part of the unit cell is called the *asymmetric unit*, this can contain several atoms or molecules. Operation of all the symmetry elements of the space group on the asymmetric unit generates the full crystal structure.

2.5.1 Lattice planes

Each two-dimensional plane in the crystal lattice can be represented by three integers (*hkl*), which are called the *Miller indices*. These parameters are defined as the reciprocals of the intercepts of the plane with the axes of the unit cell. If the plane is parallel to one of the cell parameters the corresponding index is zero. The Miller indices do not just refer to one plane but to a set of parallel planes. The faces which are present on a crystal are always parallel to specific lattice planes and can thus also be described by the Miller indices. On the basis of the geometry of the lattice, equations can be derived, which relate the spacing (the so called *d-spacing*) between successive (parallel) lattice planes to the cell parameters (see table 2.2). With the use of these equations the crystal system can be determined and the unit cell parameters solved with the use of X-ray diffraction, by finding the equation that is consistent with the experimental data.

crystal system	$1/d^2_{hkl}=$
cubic	$\frac{(h^2+k^2+l^2)}{a^2}$
tetragonal	$\frac{(h^2+k^2)}{a^2}+\frac{l^2}{c^2}$
orthorhombic	$\frac{h^2}{a^2}+\frac{k^2}{b^2}+\frac{l^2}{c^2}$
hexagonal	$\frac{4}{3}\left(\frac{h^2+k^2+hk}{a^2}\right)+\frac{l^2}{c^2}$
trigonal	$\frac{1}{a^2}\frac{(h^2+k^2+l^2)\sin^2\alpha+2(hk+hl+kl)(\cos^2\alpha-\cos\alpha)}{1+2\cos^3\alpha-3\cos^2\alpha}$
monoclinic	$\frac{h^2}{a^2\sin^2\beta}+\frac{k^2}{b^2}+\frac{l^2}{c^2\sin^2\beta}-\frac{2hl\cos\beta}{ac\sin^2\beta}$
triclinic	$(1-\cos^2\alpha-\cos^2\beta-\cos^2\gamma+2\cos\alpha\cos\beta\cos\gamma)^{-1}\left[\frac{h^2}{a^2}\sin^2\alpha+\right.$ $\frac{k^2}{b^2}\sin^2\beta+\frac{l^2}{c^2}\sin^2\gamma+\frac{2kl}{bc}(\cos\beta\cos\gamma-\cos\alpha)+$ $\left.\frac{2lh}{ca}(\cos\gamma\cos\alpha-\cos\beta)+\frac{2hk}{ab}(\cos\alpha\cos\beta-\cos\gamma)\right]$

Table 2.2 Expressions for d_{hkl} for the different crystal systems

2.6 Crystal growth mechanisms

After a stable nucleus has been formed in a supersaturated solution, crystal growth will take place. Nucleation is a three-dimensional process, solute molecules come together to form a three-dimensional cluster. Crystal growth however is a two-dimensional process, taking place by the addition of (two-dimensional) layers of molecules on the different faces of the crystal. A crystal thus grows in directions perpendicular to the crystal faces. This process is explained in some more detail in the following sections.

2.6.1 Diffusion

For a crystal to grow transport is required of solute molecules from the bulk solution to the crystal surface. There the molecules move across the surface and become desolvated (dehydrated in the case of water). When the molecules have reached an energetically favourable growth site (this is explained in the following section) they are incorporated into the crystal lattice. On the face of the crystal there thus exists a layer of adsorbed molecules, called the *adsorption layer*, where two-dimensional or *surface diffusion* of molecules takes place.

The solute molecule has to fit into the lattice, sterically and energetically. In general foreign particles do not fit into the lattice as well as the host molecules, which causes them to be rejected. The incorporation step into the crystal lattice is thus based on *molecular recognition.* In general, the greater the differences in the molecular structures of the impurity molecules and the molecules of the host material are, the less likely it is that the impurity molecules are built into the crystal lattice.

As the solute molecules of the host material are being built into the growing crystal and impurity molecules are rejected at the surface, concentration gradients build up. The concentration of impurities becomes highest at the crystal surface and the concentration of host molecules in solution becomes lowest at the interface.

Therefore a *diffusion layer* is formed around the crystal. The impurity molecules diffuse from the crystal surface to the bulk solution, whereas at the same time transport of host molecules in solution occurs in the opposite direction. This demonstrates two important points: firstly, agitation can aid in improving the purity of the crystallising material, as it will reduce the diffusion layer. Secondly, the slower the crystal is grown the more time the impurities have to diffuse away from the crystal surface. If the crystal grows at a higher rate than the impurities can be transported away from the surface, the crystal will become less pure. In addition, at high supersaturation macroscopic solvent *inclusions* can occur, which further reduce the crystal's purity.

2.6.2 The creation of growth sites

As explained above, when a solute molecule has approached the crystal surface it will move across the surface until it has reached a site where it is energetically favourable to become incorporated into the crystal lattice. It is energetically most favourable when the molecule has as many nearest neighbour molecules as possible. On the basis of this, the following sites on a crystal surface can be distinguished: flat surfaces, steps, kinks, edge vacancies and surface vacancies, some of these are shown in figure 2.4. The surface and edge vacancies are most easily occupied by incoming molecules and then the kinks and edges. This will cause the surface and edge vacancies to disappear, and the kinks and edges to move until the crystal face is completely covered. Then a new energetically favourable growth site has to be created.

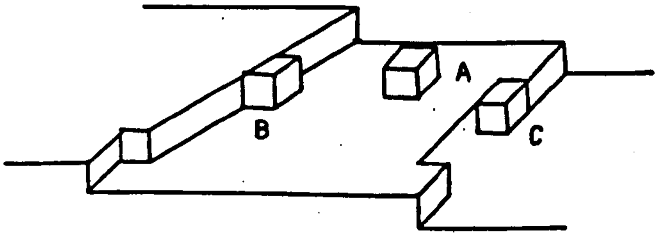

Figure 2.4 Showing the different growth sites on a crystal surface, A=flat surfaces, B=steps, C=kinks (from Ohara and Reid [28])

One of the first mechanisms suggested for the formation of steps and kinks was through a process called *two-dimensional nucleation* or *surface nucleation.* Two-dimensional nucleation is the process by which a nucleus is formed on the crystal surface. This is a dynamic process, where at the crystal surface adsorption and dissolution of molecules takes place until a critical size nucleus has been formed. Two-dimensional nucleation theory is analogous to the theory for homogeneous nucleation given in section 2.4.1. For the shape of a two-dimensional nucleus normally a circular disc is assumed. This is of course a three-dimensional object, but the growth mechanism is called two-dimensional nucleation because in the first instance growth initiated from it will only occur in the two-dimensional plane defined by the crystal surface. For the formation of the two-dimensional nucleus less interfacial area needs to be created than for a three-dimensional nucleus, since the bottom of the two-dimensional nucleus is in contact with the crystal and not with the mother liquor. It can be shown theoretically that because of this, the energy barrier for the formation of a two-dimensional nucleus is lower than for a three-dimensional nucleus (*e.g.* Mullin [3]). Different growth models have been developed based on two-dimensional nucleation. The *mononuclear* model assumes that once one two-dimensional nucleus has formed it will spread until the face is completely covered. The *polynuclear* model assumes that the two-dimensional nucleus does not grow after its formation but that instead a layer is formed by a large number of nuclei. A combination of these two models is formed by the *birth and spread* model (*e.g.* Ohara and Reid [28] and van der Eerden *et al.* [29]), which assumes that a number of two-dimensional nuclei is created, which all grow at finite constant rates. However, especially at low supersaturations, crystal growth rates predicted by surface nucleation theories alone were found to be much lower than observed experimentally.

In 1949 Frank [30] postulated that a certain type of dislocation in the crystal lattice, called a *screw dislocation* could be an important source of growth sites on a crystal face. Once a screw dislocation has been created, spiral staircases form, which do not disappear but provide the crystal with perpetual growth sites, see figure 2.5. Therefore for this growth mechanism no surface nucleation is required. On each crystal face many screw dislocations can occur at the same time. The growth spirals formed by these will overlap during growth of the crystal. This model for crystal growth is now known as the BCF (Burton, Cabrera and Frank [31]) theory and is the basis of modern crystal growth models. Since in the BCF model no surface nucleation is required, growth rates predicted with this model at low supersaturations were found to be much more realistic than those predicted on the basis of surface nucleation theories.

In general, at low supersaturation crystal faces grow by a spiral growth mechanism; with increasing supersaturation two-dimensional nucleation becomes dominant. At even higher supersaturations a transition can occur to a different growth mechanism called *kinetic surface roughening*, (*e.g.* Jackson [32] and Bennema [33]). Due to the high level of supersaturation the size of the critical two-dimensional nucleus has been reduced to one molecule. There is thus no need anymore for layer growth so that the surface roughens. The interface between the growing crystal and the mother liquor becomes poorly defined and faces that grow by this mechanism loose their crystallographic orientation. If impurities are present in the mother liquor, kinetic surface roughening usually leads to a reduced purity of the resulting crystals.

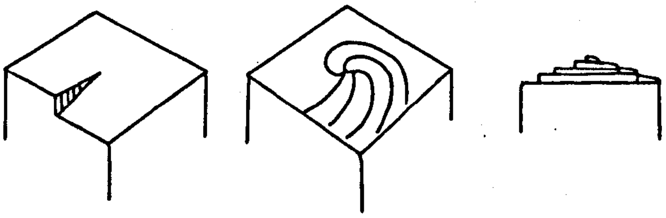

Figure 2.5 Development of a growth spiral starting from a screw dislocation (from Mullin [3])

2.6.3 Rate limiting factors in the crystal growth process

From the previous sections it is clear that at least three steps can be differentiated in the crystal growth process:

1. diffusion of solute molecules from the bulk solution through the diffusion layer to the crystal surface

2. desolvation of the solute molecules
3. integration of the solute molecules into the crystal lattice through surface diffusion and molecular recognition

In principle each of these steps can be the rate limiting factor in the overall crystal growth process. Most crystal growth theories however only consider the first and the third step. If the first step is rate determining the process is said to be *diffusion controlled*, whereas if the incorporation of the solute molecules into the crystal lattice is the slowest step the crystal growth process is said to be *surface integration controlled* (*e.g.* Garside and Tavare [34])

2.6.4 Factors affecting the crystal morphology

The external appearance of a crystal (*i.e.* the relative sizes of the developed faces of the crystal) is called the *morphology* or *habit* of the crystal and is closely related to its internal crystal structure but also depends strongly on the conditions under which the crystal was grown (*e.g.* solvent, impurities present or degree of supersaturation). This can be explained in the following way: since in general a crystal is anisotropic, crystallographically different faces can be distinguished on its external appearance. Due to this, different faces can grow at different rates by different mechanisms, *i.e.* for some faces two-dimensional nucleation may be dominating while other faces may contain more screw dislocations and therefore grow by the BCF mechanism. In general different faces grow at different rates and it is the relative growth rates of the faces which determine the habit of the resulting crystal.

Which growth mechanism is dominating on a certain face is dependent on growth conditions, such as the level of supersaturation, type of solvent, degree of agitation, the presence of impurities etc. The relative growth rates of the different faces can thus be affected by changing the growth conditions. It is thus possible to modify the external appearance of a crystal, *e.g.* by varying the degree of supersaturation.

The morphology of a crystal can have vast consequences for processing and handling of the material (*e.g.* [35]). The crystal morphology affects for example flow properties during pneumatic transport, fluidisation of the material in fluidised beds or the ease at which a material can be obtained from a suspension through filtration. When a material exhibits a plate-like morphology this can lead to caking of the material during storage as the platelets stick together. In some cases the morphology of the material is affected by small concentrations of impurities, the molecules of which are very similar to those of the host crystal, so that they fit into the crystal lattice and are preferentially incorporated into particular faces of the crystal during its growth phase. The impurities thereby change the relative growth rates of the different faces and thus affect the crystal habit. When such impurities are added on purpose in a crystallisation process with the aim of manipulating the morphology of the particles, these substances are called *tailor made additives,* as their molecular structure is tailored to fit into the crystal lattice of the host material. In this way it is sometimes possible to manipulate the crystal's morphology by the addition of impurities at the parts per million level. A technique by which (unwanted) impurities can be removed is discussed in section 2.7.

Due to the anisotropy of (most) crystals, the different faces of the crystal may exhibit different properties. For some purposes a specific crystal face can be desired, for example for semiconductor devices. One way of attempting to grow crystals where the dominating faces are the required ones, is through manipulation of the growth conditions as outlined above. Another way by which growth of large (relative to the other faces) required faces can be achieved is through *epitaxial growth.* Epitaxial growth is the process by which a crystal is grown on a substrate in such a way that specific lattice planes of the growing crystal correspond to specific lattice planes of the material that serves as a substrate. Epitaxial growth can be homogeneous when the substrate consists of the same material as the growing crystal, or it can be heterogeneous when the substrate consists of different material from the growing crystal. Some examples of epitaxial growth during phase transitions between liquid crystals are given in chapter 3.

2.7 Purification through crystallisation

The crystallisation process has a dual nature, it is the process of particle formation and purification. The use of crystallisation rather than distillation for purifying substances has two advantages: firstly crystallisation is energetically favourable compared to distillation because the enthalpy of melting is usually considerably lower than the enthalpy of evaporation. Secondly, lower temperatures are required for crystallisation, thus enabling purification of materials which are not chemically stable at higher temperatures. The purifying nature of crystallisation is a consequence of the ordering of the molecules within the structure. A crystal grows by molecular recognition as was explained in the previous section. Growth at high supersaturations however can lead to a reduced purity of the product due to a build-up of impurities in the diffusion layer, kinetic surface roughening and inclusions of mother liquor. This will result in crystals of poor quality in terms of purity and hardness. To use the purifying nature of the crystallisation process most effectively, it must therefore be ensured that the rate limiting step in the crystal growth process is the incorporation of the molecules into the crystal surface. This can be achieved by limiting the degree of supersaturation (the driving force for crystallisation) and by providing good mass transfer from the melt or solution to the growing crystal surface. The two functions of the crystallisation process, particle formation and purification are thus of conflicting nature. In general, the faster the product is formed (as is especially important in industrial crystallisation processes) the less pure the product will be. Therefore in industrial crystallisation a compromise has to be made between production rates and purity of the product, depending on desired product specifications.

In some cases even very low levels of impurities are intolerable, either from a chemical point of view (*e.g.* in pharmaceutical products), or because they affect the crystal structure or external morphology and thus the physical properties of the material. In the production of semi-conductors for instance, very low levels of impurities have a dramatic effect on the desired properties of the material. The only way to be able to assess the influence of impurities on the physical properties that a substance exhibits, is to purify the material to ultra-high purity. Through comparison of the unpurified material with the purified material it can then be determined if the physical properties of the material are affected by the impurities. Through controlled mixing in of impurities it can be determined how the properties of the material vary with its composition.

Some substances form *solid solutions*. This means that a mixture of these substances does not fully segregate on crystallisation but a homogeneous solid mixture of the two materials is formed. These substances are usually *isomorphous*, meaning that they have the same crystal structure (they are *isostructural*) and in addition have very similar unit cell parameters. The unit cell parameters of the solid solution vary with the composition of the mixture. It can be very difficult to obtain one of the components of the solid solution by purification through a single crystallisation step. For purifying materials to a very high purity a technique called *zone refining*, or *zone melting* has been developed by Pfann [36,37]. An incentive for the development of this technique was the need for high purity materials by the semi-conductor industry for the production of transistors and diodes. In principle however, zone refining can be used for any crystalline substance which does not degrade on melting, provided that the impurities show a preference either for the molten or for the solid phase of the host substance. This technique is explained in the following section, more details on zone refining can be found in *e.g.* [36-39].

2.7.1 Zone refining

Zone refining is a general technique used to purify solid materials to a very high purity. Essentially zone refining is a process which conveniently permits a large number of successive re-crystallisations from the melt. In this process a narrow molten zone is passed through the material to be purified, which can be accomplished either by slowly moving a heater along a tube filled with the solid material or by moving this tube through a heating zone. At the end of the tube the material is frozen. The movement of the zone through the material from one end to the other is called a *pass*. When the exchange of impurities between the melt and the solid phase is in equilibrium, an equilibrium *distribution* or *segregation coefficient*, k_{eq} of an impurity can be defined:

$$k_{eq} = \frac{\text{concentration of the impurity in the solid phase}}{\text{concentration of the impurity in the liquid phase}} \tag{2.22}$$

This is a measure for the expected efficiency of the purification process. The more k_{eq} differs from unity, the more efficient purification will be by zone refining. If the impurity is rejected by the growing solid phase and thus piles up in the liquid close to the solid-liquid interface k_{eq} will be smaller than one (such impurities lower the melting point of the mixture). If on the other hand the impurity is preferentially incorporated into the solid, leaving the interfacial region of the liquid depleted k_{eq} will be larger than unity (such impurities raise the melting point of the mixture). If k_{eq}=1 purification by zone refining is impossible. The value of k_{eq} is not constant for all concentrations. This can be demonstrated theoretically in the following way (*e.g.* Pfann [36] or Matz [40]): $k_{12,eq}$ is the segregation coefficient of impurity 1 in host substance 2. Similarly $k_{21,eq}$ is the segregation coefficient of impurity 2 in host substance 1. If for simplicity a binary mixture of components 1 and 2 is considered then:

$$k_{12,eq} = \frac{x_{1,s}}{x_{1,l}} \tag{2.23}$$

$$k_{21,eq} = \frac{x_{2,s}}{x_{2,l}} = \frac{1 - x_{1,s}}{1 - x_{1,l}} \tag{2.24}$$

where $x_{i,s}$ is the mole fraction of component i in the solid phase and $x_{i,l}$ is the mole fraction of component i in the liquid phase. Combination of these equations leads to:

$$x_{1,l} = \frac{k_{21,eq} - 1}{k_{21,eq} - k_{12,eq}} \tag{2.25}$$

This should hold for all values of $x_{1,l}$. From this equation it can be seen that if the mole fraction of component 1 in the liquid phase becomes very small $\left(x_{1,l} \downarrow 0\right)$ then $k_{21,eq} \to 1$ and similarly if the mole fraction of component 2 in the liquid phase becomes very small $\left(x_{1,l} \uparrow 1\right)$ then $k_{12,eq} \rightarrow 1$. For most practical purposes however the value of k_{eq} is taken to be constant.

For zone refining, the observed segregation coefficient is called the *effective segregation coefficient*, k, which is related to the equilibrium segregation coefficient by the following equation (Burton *et al.* [41]):

$$k = \frac{k_{eq}}{k_{eq} + (1 - k_{eq}) \exp\left(\frac{-f\delta}{D}\right)} \tag{2.26}$$

where f is the rate at which the melt is solidified (in cm/s), D is the diffusion coefficient of the impurity in the melt (in cm^2/s) and δ is the thickness of the diffusion layer (in cm) (see section 2.6.2). From equation 2.26 it can be seen that when f is very small the value of k approximates that of k_{eq} (the assumption is made here that solid-state diffusion is negligible). A reduction of the thickness of the diffusion layer has the same effect. When f is very large k approaches unity and purification becomes impossible. The rate at which the melt is solidified and the thickness of the diffusion layer should therefore be kept to a minimum. In practice these conditions are met by moving the molten zone very slowly through the material and by agitation of the melt, thus minimising a concentration gradient of impurities in the liquid phase. The distribution of an impurity after one pass is given by (*e.g.* Mersmann [5] or McArdle [42]):

$$\frac{c(x)}{c_0} = 1 - (1 - k) \exp\left(-k \frac{x}{l}\right) \tag{2.27}$$

where $c(x)$ is the concentration of the impurity at a distance x measured along the ingot, c_0 is the initial uniform concentration of the impurity and l is the length of a molten zone. This equation is not valid for the last zone as the impurities are compressed into a small volume by passage of the zone through the end of the ingot. Impurities for which k<1 tend to be rejected by the growing solid and will thus move down in the tube (if the tube is vertical). For impurities with a distribution coefficient greater than unity the solid material will be less pure than the molten zone, therefore these impurities will accumulate at the top end of the tube. After several passes the material in the middle of the tube becomes purified as the impurities move toward the ends. The more k differs more from unity the fewer passes will be needed to obtain material of a the required purity. Zone refining is not effective for cases in which $k \approx 1$.

The distribution of impurities after n passes can be calculated by an iterative procedure [43-45]. The mathematical description of the process is complicated because the concentration of impurities in the liquid zone is increased by an influx of impurities from the melting end of the zone. Further redistribution of the impurities becomes less with each successive pass. After a certain number of passes the distribution of impurities does not change any further, this is called the *ultimate distribution.* When this is reached the flux of impurities rejected by the solidifying interface into the molten zone is balanced by the influx of impurities, entering the melt from the other side of the molten zone. The equation to describe the ultimate distribution can be derived as follows (Pfann [36]): let the ultimate distribution of an impurity as a function of the distance along the ingot, x, be $c(x)$. When this distribution has been reached it will not be altered when a molten zone of length l is passed through the material so that the concentration at each point x is remains equal to $c(x)$. The concentration of impurities in the molten zone, $c_L(x)$ is given by:

$$c_L(x) = \frac{c(x)}{k} \tag{2.28}$$

The concentration of impurities in the liquid zone is also equal to the sum of the impurities present in the zone divided by the volume of the zone. If a unit cross section is assumed this results in:

$$c_L(x) = \frac{1}{l} \int_x^{x+l} c(x) \mathrm{d}x \tag{2.29}$$

Combination of 2.28 and 2.29 leads to:

$$c(x) = \frac{k}{l} \int_x^{x+l} c(x) \mathrm{d}x \tag{2.30}$$

The solution of this equation is given by:

$$c(x) = Ae^{Bx} \tag{2.31}$$

where A and B are constants. B can be determined from substitution of 2.31 in 2.30 and subsequent integration, which results in

$$k = \frac{Bl}{e^{Bl} - 1} \tag{2.32}$$

The constant A can be found by realising that the sum of all the impurities in the material divided by the volume of the material must be equal to the initial impurity concentration c_0, thus (assuming again unit cross section):

$$c_0 = \frac{1}{L}\int_0^L c(x)\mathrm{d}x = \frac{1}{L}\int_0^L Ae^{Bx}\mathrm{d}x \tag{2.33}$$

where L is the length of the ingot. Integration results in:

$$A = \frac{c_0 BL}{e^{BL} - 1} \tag{2.34}$$

When the ultimate distribution is reached, the value for the segregation coefficient of an impurity can thus be calculated from equation 2.32 when B is known. The value of B can be obtained as the slope of a graph of the logarithm of the concentration of the impurity versus the distance along the ingot, since from equation 2.31:

$$\ln c(x) = \ln A + B \ln x \tag{2.35}$$

A way to evaluate the validity of assuming an ultimate distribution is to calculate the value of c_0 with equation 2.34 and compare this with the measured value.

The time-efficiency of zone refining can be increased in the following way: segregation of the impurities only takes place at the interface between the solid and the liquid phase; the rate at which this interface is passed through the material to purify is limited, as higher rates result in poorer purification. The time-efficiency of the purification process can therefore only be increased by the creation of a larger interface. This can be accomplished by moving a series of alternating heating and cooling units along the ingot. The material is molten by the first heater, solidifies and is then molten by the second heater etc. In this way a number of molten zones move simultaneously through the material to purify. This technique is called *multizone* or *multi-pass zone refining* (*e.g.* McArdle and Sherwood [42]). Agitation of the liquid zones is very important to enable mass transfer between the "bulk" liquid zone and the growth interface, this can be accomplished by rotation of the tube. In addition, the higher the temperature at which the heaters are operated at, the more convective currents in the melt are created *e.g.* [46]. A detailed description of the zone refiner used for the present study is provided in chapter 4.

2.8 Principles of X-ray diffraction

A very important tool for crystal phase identification and structure determination is the use of X-ray diffraction (XRD). X-rays are electromagnetic radiation like ordinary light, but with a much shorter wavelength (between 0.1-10Å), which is comparable to the distances between atoms and molecules. It is this property that allows X-rays to be diffracted by the regular distances present in crystal lattices. The X-ray diffraction pattern is therefore the result of the regular crystal lattice of the material. This makes XRD a very powerful method for phase identification (an XRD pattern can be seen as the fingerprint of a substance in a certain phase), to elucidate phase transformations and for unravelling the spatial arrangements of the atoms through the determination of crystal structures. The basic principles of XRD are explained in the following sections, more details can be found in *e.g.* [26 and 47-49]. In section 2.8.1 the Bragg equation which is the basis for structure-determination using XRD is briefly explained, followed by a concise discussion on the different ways X-rays can be produced in section 2.8.2 and detected in section 2.8.3.

2.8.1 The Bragg law

The use of XRD as a technique for structure determination is based on the (electromagnetic) wave character of X-rays. Electrons in the path of these waves are excited to periodic vibrations by the changing field and will thus emit electromagnetic waves of the same wavelength as the incident beam. The thus scattered waves from the several electrons in an atom combine so that each atom may be considered as a point source of scattered X-rays. When the atoms in the sample under consideration are regularly spaced, a characteristic interference pattern will result. Consider for example the atomic planes shown in figure 2.6. The spacing between the planes is *d*. For constructive interference to occur between layer p and p_1, the difference in pathlength between the wavelet from A to C and the one from A' to C has to be a whole number of wavelengths. Thus:

$$B'C - BC = n\lambda \tag{2.36}$$

Trigonometry shows that

$$B'C = \frac{d}{\sin\theta} \tag{2.37}$$

and

$$BC = B'C\cos 2\theta = \frac{d\cos 2\theta}{\sin\theta} \tag{2.38}$$

Substituting 2.37 and 2.38 in 2.36 results in the *Bragg equation*:

$$n\lambda = 2d\sin\theta \tag{2.39}$$

where *n* is an integer which is zero for the zeroth order reflection, one for the first order reflection etc., θ is the angle between the atomic planes and the reflected beam and *d* is the spacing between the planes. This equation is known as the Bragg equation or the Bragg law. This equation defines all the values of θ where a reflection can occur for lattice planes in a crystal with spacing *d* and X-ray wavelength λ. At all other angles no reflected beam will occur because of destructive interference.

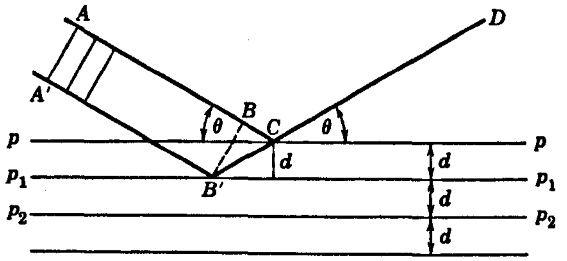

Figure 2.6 Diffraction from lattice planes (from Klug and Alexander [47])

When a crystal is built up of more complicated molecules than just single atoms, the diffraction pattern will still be the result of the interplanar spacings of the crystal lattice. The diffraction pattern for a large enough (minimal size approximately 0.2mm) *single crystal*, a crystal in which the unit cell orientation is the same throughout the crystal, results in a large number of peaks. For many materials however it can be very difficult to grow large enough single crystals. Such materials are *polycrystalline*, *i.e.* consists of a large number of randomly oriented crystallites. For such samples (as well as for non-oriented liquid crystals) many diffraction peaks of the individual crystallites merge. This leads to the effect that the diffracted X-rays emerge from the sample in three dimensions as concentric cones of radiation with apex in the sample (see figure 2.7). The complete observed intensity distribution is the sum of the contributions from the individual fragments.

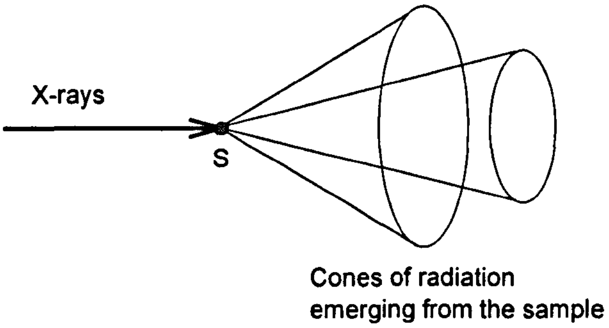

Figure 2.7 The formation of the diffraction pattern from a polycrystalline material (S indicates the sample position)

With the Bragg equation the lattice spacings can be calculated by measuring the angles under which diffraction occurs using a known wavelength and rewriting equation 2.39 in terms of the Miller indices *hkl*:

$$d_{hkl} = \frac{\lambda}{2\sin\theta_{hkl}} \tag{2.40}$$

Other parameters which are used often used in X-ray scattering are Q (or q) and s. These can be defined in the following way: $Q = \frac{2\pi}{d}$ and $s = \frac{1}{d}$.

The crystal system is determined by finding an equation with which all the observed lattice spacings agree (see table 2.2) and from this the dimensions of the unit cell can be calculated. However, specific peaks (*e.g.* all ($0k0$) peaks when k is odd) which would have been expected on the basis of the equations given in table 2.2, can have zero intensity due to certain symmetry elements. These “missing peaks” are called *systematic absences*. Knowledge of these is needed for space group determination. If the X-ray diffraction data is of sufficient quality (*i.e.* enough sharp peaks) the crystal structure can in principle be solved from the peak intensities (which depend on the density of the atoms present in the lattice planes) and with the aid of molecular modelling techniques. It is much easier to determine the structure of a sample if the material is a single crystal than when the material is polycrystalline, as a single crystal gives rise to far more individual peaks, see *e.g.* Clegg [50]. Often however, X-ray diffraction is only used to identify a substance or a polymorphic form of a substance by using XRD patterns as a fingerprint of the material.

2.8.2 The production of X-rays

The high energy photons in X-rays can be produced with the use of *X-ray tubes* or with *synchrotron radiation sources*. An X-ray tube mainly consists of two electrodes, a cathode which is usually a tungsten wire spiral and an anode which is covered with the target material *e.g.* copper. The space between the cathode and the anode is evacuated. The cathode is heated using a current of 1.5 to 5A at 4 to 12V. A potential gradient of typically 40kV produced by the *generator* (a high voltage transformer) accelerates the thus produced thermal electrons towards the anode where they hit the target material. Here X-rays are produced by two processes. Firstly a high speed electron may displace a tightly bound electron in one of the inner shells, thereby ionising the atom. As a result of this, an electron from a higher shell may fall into the vacant place whereby it emits an X-ray characteristic for that transition. This process results in sharp peaks in the X-ray spectrum which are characteristic for each element *e.g.* the copper K_α line at 1.54Å (called “K” because an electron from the K shell is ejected from the atom and “α“ because this vacancy is filled by an electron from one shell further). Secondly a high speed electron may be slowed down in passing through the strong electric field of the nucleus without colliding with one of the atom's electrons. The decrease in energy of the high speed electron is emitted as an X-ray photon. The latter process produces a continuous spectrum, which is called *Compton radiation.* In X-ray diffraction experiments, the radiation has to be essentially monochromatic as the diffraction pattern produced depends on the wavelength used. Non-monochromatic radiation would consequently result in a spectrum which is the sum of a series of overlapping spectra. It is therefore necessary to use a filter to obtain radiation of the required wavelength. A filter is made of a material that absorbs most of the unwanted radiation while only slightly absorbing radiation of the desired wavelength. This is accomplished by choosing a filter material of which the absorption edge is just below the required wavelength. Radiation with a wavelength just below the absorption edge is absorbed strongly as this radiation has sufficient energy to eject an electron from the K orbital of an atom of the filter material, so that absorption of energy increases dramatically. X-rays with a wavelength slightly larger than the absorption edge are less absorbed. A nickel filter is usually used with copper radiation. If strict monochromatisation is required a crystal monochromator can be used. The principle of a crystal monochromator is that the angle under which X-rays are diffracted by a crystal depends on the wavelength of the incident radiation (as can be seen from the Bragg law). Therefore, selecting a certain diffraction angle for the radiation to be used, is equivalent to choosing a particular wavelength out of the spectrum of the incident radiation on the crystal monochromator.

The intensity of the X-ray beam produced with X-ray tubes is limited due to the fact that most of the collision energy (≈98% [47]) of the high speed electrons is being converted into heat. Therefore the anode has to be cooled with water in order to be able to use the X-ray tube at a higher power. A way to further increase the intensity of the X-ray beam is to use a rotating target so that constantly relatively cool metal is hit by the electron beam, thus enabling high a power density. With these so called *rotating anode sources* the intensity can be tens of times higher than for a tube with a stationary anode [47]. However, even with these very powerful X-ray tubes the intensity can still be too low for studying certain processes which take place on a very short time-scale, such as structural phase transitions. For such investigations long exposure times or counting times are unacceptable. *Synchrotron radiation* can be used for investigating such processes. Synchrotron radiation is the name given to the electromagnetic radiation produced when electrons or positrons moving at relativistic energies are constrained to follow a circular path, which is defined by dipole magnets. The principle of synchrotron radiation is that charged particles under the influence of an accelerating field emit electromagnetic radiation. If the velocity of the particles is high enough (approaching the speed of light) the wavelength of this radiation is in the X-ray range. The main part of a synchrotron source is the storage ring in which the electrons are made to follow a circular trajectory. The storage ring has to be kept under high-vacuum because else particles would be lost by collisions with the molecules present in air. Beam lines tangential to the storage ring lead the radiation to experimental stations. As synchrotron sources are extremely expensive only few exist world-wide; their number is growing however. A brief description of the experimental stations used is given in chapter 4. The main advantages of synchrotron radiation over conventional laboratory X-ray sources are firstly its superior intensity (10^5-10^{10} times the intensity of a rotating anode [26]), which permits very short data acquisition times, thus enabling X-ray diffraction measurements to be carried out on a real-time basis. The dynamics of processes taking place during crystallisation can thus be observed *in-situ*. Secondly the beam divergence is extremely low, thus enabling high-resolution powder diffraction data to be collected for use in structure determination. A third advantage is that synchrotron radiation is so called *white radiation*, meaning that a continuous spectrum of electromagnetic radiation is emitted. The wavelength can be chosen by the use of crystal monochromators. In addition synchrotron radiation is highly polarised.

2.8.3 The detection of X-rays

X-rays are detected with either photographic film or with detectors. There are different types of detectors serving different purposes *e.g.* [48]. The principle of most detectors however is based on the ionising character of the X-ray photons. When they enter a detector they ionise a gas, which is held between two electrodes over which a high potential difference is applied. This induces an avalanche of ions between the electrodes, which results in a current which can be amplified and electronically registered. In conventional detectors, such as proportional counters this principle is used to measure the intensity at one point in space. This type of detector can be used for example for high-resolution powder diffraction, where the detector scans around the sample, thus collecting the angle dependent diffraction data. The electrical current from the detector is registered for a certain amount of time at each angle. This is called the *counting time*. As this procedure requires a considerable amount of time it is not suited for time-resolved XRD studies. For those purposes *position sensitive counters* are used such as one-dimensional (linear) or two-dimensional (area) detectors. These enable simultaneous data collection over a wide angular range, thus enormously reducing the required counting time. An *area detector* is a multi-wire detector: an anode consisting of parallel wires is sandwiched between two cathodes which also consist of parallel wires, perpendicular to the anode wires. The detector is filled with gas and the detection principle is identical to that described above for more conventional detectors, with the difference that here the position of the incoming X-ray photon can be electronically calculated in two dimensions from the orthogonal coordinate system provided by the anode and cathode wires.

A different type of two-dimensional position sensitive detector is the *image plate*. In an image plate the energy of the incoming X-ray photons is stored by $\mathrm{Ba\,F\,Br\,Eu^{2+}}$ crystals. Some of the Eu^{2+} ions in this material are further ionised by the X-ray photons to Eu^{3+}, the freed electrons are stored in Br vacancies. The energy can be released as luminescence when the material is exposed to laser light of the right wavelength. For this the image plate is put on an *image reader* which collects the radiation emitted from the image plate as it is exposed to laser light and converts it into an electrical signal. The image plate can be used repeatedly, since the light from the laser restores the material to its original state.

The diffraction pattern recorded with a two-dimensional position sensitive detector is the result of the intersection of concentric cones of radiation coming from the sample (if the sample is polycrystalline, see figure 2.7) and the plane of the detector which is perpendicular to these cones and thus results in *diffraction rings*. Two-dimensional detectors have several advantages over proportional counters and linear (one-dimensional detectors), apart from the fact that data collection times are reduced by their use. When preferred orientation is present in the sample, this results in *texture* of the diffraction rings; certain parts of the rings are of higher intensity than other parts. In the study of liquid crystals structural information can sometimes be deduced from these effects. In addition, texture in the diffraction rings of different liquid crystalline phases can reveal epitaxial growth relations between different liquid crystalline phases *e.g.* [51]. When the diffraction rings are *isotropic* (the same intensity throughout the rings) a two-dimensional detector is still favoured over a one-dimensional detector since the latter only collects a fraction of the scattered radiation of the two-dimensional detector. The two-dimensional diffraction pattern consisting of isotropic diffraction rings can be integrated circularly, to produce a one-dimensional diffraction pattern. This will then have a superior signal to noise ratio to one that would have been obtained with a one-dimensional detector (using the same counting time).

2.9 Summary

Crystallisation is an important process by which solids can be formed and purified. The process can be divided into nucleation and subsequent crystal growth. It has been shown that the saturation temperature, the metastable zone width and the induction time are important parameters in a crystallisation process. Crystal size, shape and purity may be controlled through knowledge of those parameters as these properties are affected by the degree of supersaturation and the rate at which supersaturation is induced by *e.g.* cooling. The Van 't Hoff equation can be used to calculate the degree of supersaturation.

In the crystalline state the molecules are ordered on a regular crystal lattice. Many materials can exist in different polymorphic forms, in which the material is chemically identical but exhibits different physical properties (*e.g.* solubility). The external morphology of the crystal is determined by its internal structure and growth conditions. Small concentrations of impurities can have dramatic effects on the physical properties of substances and can effect changes in crystal structure and morphology. It can therefore be very important to determine the influence of impurities on the properties of the material by purifying it to ultra high purity. For many substances this can be achieved by zone refining. X-ray diffraction is a very powerful tool for recognition of polymorphic and liquid crystalline structures and for structure determination.

2.10 References used in this chapter

1. Price CJ, *Chemical Engineering Progress* **93**, 34 (1998)
2. Myerson AS (ed), *Handbook of industrial crystallization*, Butterworth-Heinemann (1993)
3. Mullin JW, *Crystallization,* third ed, Butterworth Heinemann Ltd (1992)
4. Söhnel O and Garside J, *Precipitation, basic principles and industrial applications*, Butterworth Heinemann Ltd (1992)
5. Mersmann A, *Crystallisation technology handbook*, Marcel Dekker Inc, New York Basel Hong Kong (1995)
6. Cains PW, Martin PD, Price CJ, *Org Process Res Dev* **2 (1)**, 34 (1998)
7. Mullin JW and Raven KD, *Nature* **190**, 251 (1961)
8. Mullin JW and Raven KD, *Nature* **195**, 35-38 (1962)
9. Zettlemoyer AC (ed), *Nucleation*, Dekker Inc, New York (1969)
10. Gibbs JW, Collected works, **vol. 1**, *Thermodynamics*, Yale University Press, New Haven (1948)

11.Volmer M and Weber A, *Zeitschrift für physikalische Chemie A* **119**, 277-301 (1926)

12.Farkas L, *Zeitschrift für physikalische Chemie A* **125**, 236-242 (1927)

13.Kaischew R and Stranski IN, *Zeitschrift für physikalische Chemie B* **26**, 317-326 (1934)

14.Becker R and Döring W, *Annalen der Physik* **5, 24**, 719-752 (1935)

15.Larson MA and Garside J, *Chemical Engineering Science* **41**, 1285-1289 (1986)

16.Kaschiev D, *Science and Technology of Crystal Growth (Lectures given at the Ninth Summer School on Crystal Growth)*, pgs 53-66, van der Eerden JP and Bruinsma OSL (Eds.), Kluwer (1995)

17.Walton AG, *Dispersion of Powders in liquids (with special reference to pigments)*, sec ed., chapter 5, Parfitt GD (ed.), Applied Science Publishers Ltd, London (1973)

18.Turnbull D and Fisher JC, *Journal of Chemical Physics*, **17**, 71-73 (1949)

19.Nyvlt J, *Journal of Crystal Growth* **3, 4**, 377-382 (1968)

20.Threlfall TL, *Analyst* **120**, 2435 (1995)

21.Ostwald W, *Lehrbuch der allgemeinen Chemie* **2**, p. 444, Englemann, Leipzig (1896)

22.Ostwald W, *Zeitschrift für physikalische Chemie* **22**, 289 (1897)

23.Dunitz JD and Bernstein J, *Acc Chem Res* **28**, 193-200 (1995)

24.Hahn T (ed.), *The International Tables for Crystallography*, Kluwer Academic Publishers (1989)

25.Windle A, *A first course in crystallography*, G Bell and Sons, London(1977)

26.Giacovazzo C (ed.), *Fundamentals of Crystallography*, Oxford University Press Inc. New York (1994)

27.Kleber W, *Einführung in die Kristallographie*, VEB Verlag Technik, Berlin (1956)

28.Ohara M and Reid RC, *Modelling Crystal Growth Rates from Solution*, Prentice Hall, Englewood Cliffs, NJ (1973)

29.van der Eerden JP, Bennema P and Cherepanova TA, *Progress in Crystal Growth and Characterisation* **1**, 219 (1978)

30.Frank FC, *Discussions of the Faraday Society* **5**, 48 (1949)

31.Burton WK, Cabrera N and Frank FC, *Philosophical Transactions* **A243**, 299 (1951)

32.Jackson KA, *Mechanism of Growth, in Liquid Metals and Solidification*, American Society for Metals, Cleveland (1958)

33.Bennema P, *Growth and Morphology of Crystals, in Handbook of Crystal Growth* **1**, edited by Hurle DTJ, Elsevier (1993)

34.Garside J and Tavare NS, *Chemical Engineering Science* **36**, 863 (1981)

35.Telfer GB, Roberts KJ, Jackson RA and Wilde PJ, *Characterization of Crystal Structure/Morphology Relationships, World Congress of Chem Eng July 14th-18th 1996*, hosted by AICHE (1996)

36.Pfann, WG, *Zone Melting*, Wiley, New York (1958)

37.Pfann WG, "On recent advances in the theory and application of zone melting", *Zonenschmelzen und Kolonnenkristallisieren Symposium*, Karlsruhe (1963)

38.Schildknecht H, *Zone Melting*, Academic Press, New York (1966)

39.Parr NL, *Zone refining and allied techniques*, George Newnes Ltd, London (1960)

40.Matz G, *Kristallisation, Grundlagen und Technik*, Springer Verlag, Berlin Heidelberg New York (1969)

41.Burton JA, Prim RC and Slichter WP, *J Chem Physics* **21**, 1987 (1953)

42.McArdle BJ and Sherwood JN, *Chemistry and Industry* **8**, 268-274 (1985)

43.Lord NW, *Journal of Metals*, 1531(Nov 1953)

44.Braun I and Marshall S, *British Journal of Applied Physics*, **8**, 157 (1957)

45.Schreiber G and Schubert R, *Zeitschrift für physikalische Chemie* (Leipzig) **206 1-2**, 102 (1957)

46.Maire J, Moritz JC, Kieffer R, L'institut de Chimie de Strasbourg, *Zonenschmelzen und Kolonnenkristallisieren Symposium*, Karlsruhe (1963)

47.Klug HP and Alexander LE, *X-ray Diffraction Procedures for Polycrystalline and Amorphous Materials*, J. Wiley & Sons, New York, 2nd edition (1974)

48.Glatter O and Kratky O, *Small Angle X-ray Scattering*, Academic Press (1982)

49.Hukins DWL, *X-ray Diffraction by Disordered and Ordered Systems*, Pergamon Press, Oxford (1981)

50.Clegg W, *Crystal Structure Determination*, Oxford Science Publications (1998)

51.Rançon Y and Charlovin J, *J Phys Chem* **92**, 2646 (1988)

Chapter 3

Surfactant phase behaviour

Chapter 3 Surfactant phase behaviour

3.1 Introduction

In this chapter an overview is given of the literature concerning phase behaviour of soap systems relevant to this thesis. Soaps are the alkali salts of natural fatty acids and are part of the much bigger group of surfactants, which are also called lipids (this term is usually used when the amphiphile can also be found in living organisms), detergents or emulsifiers. The soaps under consideration are summarised in table 3.1 together with their usual abbreviations and trivial names. These soaps were chosen as they represent typical examples of surfactants which can be made of natural sources. The sodium soaps of saturated fatty acids are *anionic surfactants*, *i.e.* surfactants of which the active part is a negative ion (in this case the carboxyl ion) with a positive counter ion (in this case the sodium ion). Surfactants are *amphiphiles*, having a hydrophilic (polar) head group and a lipophilic (apolar) hydrocarbon chain. For the amphiphiles under consideration the polar head group is the COO^- group.

systematic name	trivial name	abbreviation	chemical formula
sodium 1-dodecanoate	sodium laurate	NaC_{12}, NaL, NaDD	$CH_3(CH_2)_{10}COONa$
sodium 1-tetradecanoate	sodium myristate	NaC_{14}, NaM, NaTD	$CH_3(CH_2)_{12}COONa$
sodium 1-hexadecanoate	sodium palmitate	NaC_{16}, NaP, NaHD	$CH_3(CH_2)_{14}COONa$

Table 3.1 Names and abbreviations of sodium soaps

Apart from exhibiting polymorphism in the solid state, amphiphiles are well known to have the ability to form several liquid crystalline phases or mesophases, due to their dual nature. A *liquid crystal* is a substance that flows like a liquid but has some order in the arrangement of its molecules. It is thus a *mesophase* (intermediate phase) between the highly ordered solid and the isotropic melt, or between the highly ordered solid and an isotropic solution. In general, phases which are organised in one or two dimensions are called mesophases in contrast with crystalline phases which have three-dimensional order (Chapman [1]); some liquid crystal structures however exhibit three-dimensional order. The main difference between the solid state and the liquid crystalline state is that in the solid (crystalline) state there is both short and long range order in three dimensions, whereas in the liquid crystalline state there is only long range order, which can be in one- two- or three-dimensions (nematic liquid crystals are an exception to this as they only exhibit orientational order and no long range order). Amphiphiles show both *thermotropic* and *lyotropic* mesomorphism. Thermotropic mesomorphism means that the mesophase formed is dependent on the temperature. When a substance is lyotropic, the phase formed does not only depend on the temperature but also on the addition of solvent (see figure 3.1).

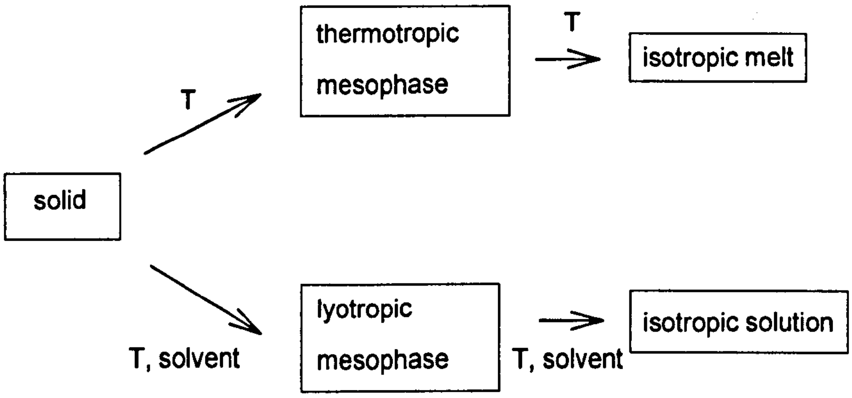

Figure 3.1 Thermotropic and lyotropic mesophases

Lyotropic liquid crystals are frequently encountered in everyday life, although their presence is not normally recognised. They occur during the dissolution of soaps and detergents and some products are even sold in a liquid crystalline form (Tiddy [2]). In this chapter an overview is given of the known liquid crystalline (both lyotropic and thermotropic) and crystalline phases of sodium soaps. No data was found on phase behaviour of ternary mixtures consisting of two sodium soaps and water. Ternary systems of soap, water and hydrocarbons (*e.g.* alcohols or fatty acids) are outside the scope of this review and will not be discussed here. In section 3.2 a typical surfactant phase diagram is explained. In the following sections the various phases are discussed: the gels and coagels in section 3.3, the lyotropic liquid crystalline phases of which the structures have been well established in section 3.4 and 3.5, followed by the less well known intermediate lyotropic phases in section 3.6. In section 3.7 an overview is given of the trends in aqueous phase behaviour. Although the work presented here is mainly focused on the aqueous mesophases, a section on the thermotropic mesophases (section 3.8) as well as a section on the different crystalline forms of soaps is included (section 3.9) in order to provide a complete overview of the variety of phases formed by surfactants. At the end of the chapter a summary of surfactant phase behaviour is provided in section 3.10.

3.2 Binary phase diagrams

Amphiphiles are well known to form a large number of crystalline and liquid crystalline structures. In these different forms the soaps constantly display changing properties, such as hardness, viscosity and solubility, and are able to perform widely differing functions (Davidson *et al.* [3]). A *binary phase diagram* graphically summarises all these different phases as a function of concentration and temperature. In figure 3.2 an example is given of a typical phase diagram for a soap-water system, to illustrate the manifold of phases formed by soaps. In assessing the likelihood of a proposed liquid crystalline structure it is necessary to construct phase diagrams to obtain a reliable concept of the different structures of the phases, rather than considering *e.g.* X-ray data on one phase in isolation. There should always be a logical progression in the structures of the aggregates of the successive phases.

The determination of phase diagrams and the recognition of the various phases can be accomplished by a variety of techniques *e.g.* X-ray diffraction, measurements of vapour pressure, NMR (nuclear magnetic resonance), dilatometry, thermal analysis techniques such as DSC (differential scanning calorimetry) (*e.g.* Reiss-Husson *et al.* [4]) and DTA (differential thermal analysis), and polarised light microscopy. The latter can be used to study the optical properties of mesophases (with the use of a hot-stage) as a function of temperature and concentration. The sign of the birefringence or double refraction can be determined and the characteristic interference pattern produced by a mesophase can be studied with the polarisers on the microscope (*e.g.* Hartshorne [5]). A much used microscopy method is the so called penetration technique: some solid surfactant is placed between microscope slide and cover slip and is slowly hydrated by putting water around it. The capillary forces draw the water in between the slide and the cover slip so that a concentration gradient is created, the surfactant concentration being the highest in the centre. The phases can then be identified by the characteristic texture they exhibit between crossed polarisers. Cubic liquid crystalline phases are optically isotropic but can be identified by their high viscosity. From such microscopy studies, information about the orientation of the aggregates in the liquid crystalline phases can be deduced, possibly in combination with evidence from X-ray analysis. Phase diagrams for other surfactant systems than the ones under consideration here, have recently successfully been determined with the use of measurements of the speed of sound waves (Glatter [6,7]). However, the description of the phases in terms of structure calls upon the use of X-ray diffraction (Reiss-Husson and Luzzati [4]), although often evidence from other techniques is necessary to elucidate structure and phase behaviour.

Amongst the first to systematically study phase diagrams for sodium and potassium soaps were McBain *et al.* ([8] for NaL up to NaS; [9] for KL up to KS). McBain *et al.* [8,9] measured vapour pressures and used data from previous studies, obtained from various techniques to determine phase diagrams for these soaps. However, these diagrams are incomplete in some regions, while in other regions the boundaries have only been tentatively placed and hence are indicated by dashed lines or left blank [9,10]. The phase diagrams for KL, KM, KP, KS are quite incomplete between 90 and 100% soap (McBain [9]). Phase diagrams of soaps have further extensively been studied by Luzzati *et al.*, *e.g.* [11] for KM. Later detailed the phase diagram studies were undertaken by Madelmont and Perron [12-18] of NaL, NaM, NaP and NaS. This is discussed in more detail in section 3.6. First in the following sections the aqueous soap phases are explained of which the structures have been well established.

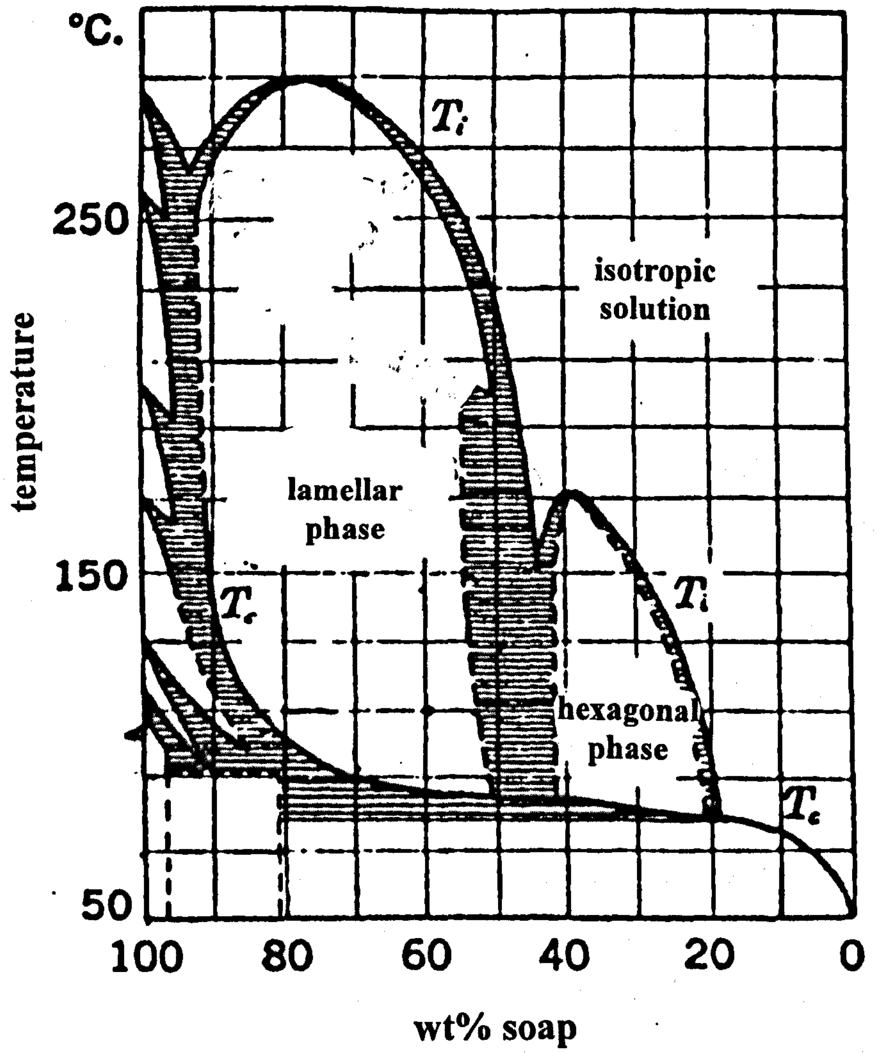

Figure 3.2 Schematic of a typical sodium soap-water phase diagram (from McBain *et al.* [8])

3.2.1 The T_c and the T_i curve

The two main curves in the phase diagram are the T_c and the T_i curve. The T_c curve (c for crystalline) shows above which temperature at a certain concentration the *short range* crystalline order breaks down. The T_i curve (i for isotropic) signifies above which temperature at a certain concentration the *long range* liquid crystalline order breaks down and an isotropic solution is formed. The two curves separate the numerous surfactant phases into three groups:

1. The solid phases: gels and coagels, these are found at temperatures below the T_c curve and will be discussed in section 3.3. More details about the different crystalline forms (anhydrous and hydrated) of soaps are given in section 3.9.
2. The lyotropic and thermotropic mesophases, these exist at temperatures in between the T_c and the T_i curve. The nature of these phases is explained in sections 3.5 and 3.6 for the lyotropic mesophases and section 3.7 for thermotropic mesophases.
3. Isotropic liquid; at temperatures above the T_i curve all order breaks down and an isotropic liquid is formed.

A good review about the all these phases is given by Tiddy [2], about the gels, coagels and aqueous mesophases by Winsor [19] and more recently by Tiddy [20] and Bleasdale and Tiddy [21]. The aqueous mesophases and the crystalline forms of soaps are also discussed by Gray and Winsor [22]. A useful reference is further *The Lipid Handbook* [23]. All the phases will be discussed here, starting with the gels and coagels in section 3.3, followed by the other phases in order of increasing surfactant concentration, from the isotropic micellar solution in section 3.5.1 to the polymorphic crystalline forms in section 3.9. There has always been considerable confusion concerning the nomenclature of the different forms of soaps. Apart from that the term *phase map* might also cause confusion. *Phase maps* have been published by *e.g.* Buerger *et al.* [24,25], who used X-ray diffraction [25] to investigate what they called the "descendant phases" of aqueous sodium myristate systems. A descendent phase is obtained by quenching a sample of a certain composition and temperature. The resulting sample is not necessarily composed of the same phases which were present at elevated temperature, but it is composed of phases which are descendants of the original phases. These phases can be summarised in a *phase map* which is thus not necessarily identical to a phase diagram. Phase maps are not further discussed here.

3.3 Phases below the T_c-line: gels and coagels

The T_c-line separates two areas in the phase diagram (*e.g.* Winsor [19]). For compositions at temperatures higher than indicated by this line the system is in a liquid or liquid crystalline state, below the T_c-line the system is in a solid phase (gel or coagel). At high water concentration the T_c-line often flattens out into a plateau, the temperature of this plateau is called the *Krafft point* (*e.g.* Reiss-Husson and Luzzati [4]). This is the temperature at which a soap becomes soluble. The longer the hydrocarbon chain, the higher the Krafft point. This temperature is labelled the *genotypic point* when a phase transition occurs in the crystalline state of the soap (*e.g.* Thiessen and Stauff [26,27]).

The T_c-line can be considered as the melting point of the hydrocarbon chains of the soap molecules as a function of the concentration, (*e.g.* Luzzati and Husson [28]). If a soap-water sample is cooled below the T_c-line, either a homogenous and translucent precipitation, the *gel*, is obtained or a mixture of two phases, the *coagel*. The word "gel" is used ambiguously in literature, where it is sometimes used to denote all aqueous liquid crystalline phases such as the hexagonal and lamellar phase. In the present study however the following will be meant with the terms gel and coagel. A *coagel* is characterised as a dispersion of hydrated solid soap (Winsor [19]), a heterogeneous mixture of water and soap crystals (Thiessen [26]) in which the soap fibers form a capillary system containing the water. The coagel used to be described with the term "soap curd" (*e.g.* McBain *et al.* [29]); its structure is independent of the water content of the system. The structure of the *gel does* depend upon temperature and concentration. A gel can transform into a coagel at low temperatures (Chapman [1], Vincent and Skoulios [30]) and is therefore said to be unstable in contrast to the coagel which is stable, Thiessen [26]. The differentiation between gel and coagel is easily made by their optical appearance; if the material is translucent it is a gel, if it is opaque it is a coagel (Thiessen [26] and Vincent and Skoulios [30]). These phases are very important to the detergent industry as those are often found in soap products. Vincent and Skoulios used X-ray diffraction and optical microscopy to investigate the structure of gel phases, of KS [30]; KM, KP and KP/KS mixtures [31] and mixtures of KS and octadecanol [32]. The following characteristics for the X-ray patterns of these phases [30] were found: the X-ray patterns of the coagel contain five or six sharp peaks, the positions and intensities of these do *not* depend upon the concentration. The X-ray pattern for the gel phase contains a series of equidistant spacings (ratio 1:2:3:4:5). However, for the gel the spacings *do* vary with concentration. The gel phase further shows a diffuse band around 3Å, indicating liquid water present in the system and a single sharp peak at 4.1Å. The common feature of the X-ray diffraction diagrams of the gel and coagel is the presence of sharp reflections at spacings smaller than 5Å and the absence of the diffuse 4.5Å band found for micellar systems (see later) (Chapman [1] and Luzzati and Husson [28]). The wide angle region can be used to differentiate between gel, coagel, and aqueous mesophase: if this region contains a number of sharp peaks the system is a coagel, if it contains one sharp peak the system is a gel phase and if it contains no sharp peaks the system is in an aqueous mesophase, (Vincent and Skoulios [30]).

On the basis of their results Vincent and Skoulios [30] suggested the gel phase of KS to have a structure made up of regularly alternating planar and parallel layers of water and soap. The soap molecules are perpendicular to these lamellar planes and ordered in a two-dimensional hexagonal array; the direction of the soap molecules alternates with position (see figure 3.3). The thickness of the water layer varies with concentration while the thickness of the soap leaflet remains constant (Reiss-Husson and Luzzati [4]). The structures of the gel phases of KM and KP and mixtures of KP and KS were found to be similar to the structure of the KS gel [31]. In the gel phase the hydrocarbon groups of the amphiphile are apparently in a solid crystalline state, while the polar and aqueous regions are fluid (Winsor [19]). There are thus different degrees of order in different parts of the structure of the gel. The paraffin chains are stiff and parallel, with a high rotational disorder (and probably fairly high translational disorder parallel to the chains) (Chapman [1]). The correlations between the polar groups are loose. When these interactions become strong, for example at low water concentration, the stability of the gel is upset and a crystalline phase precipitates out.

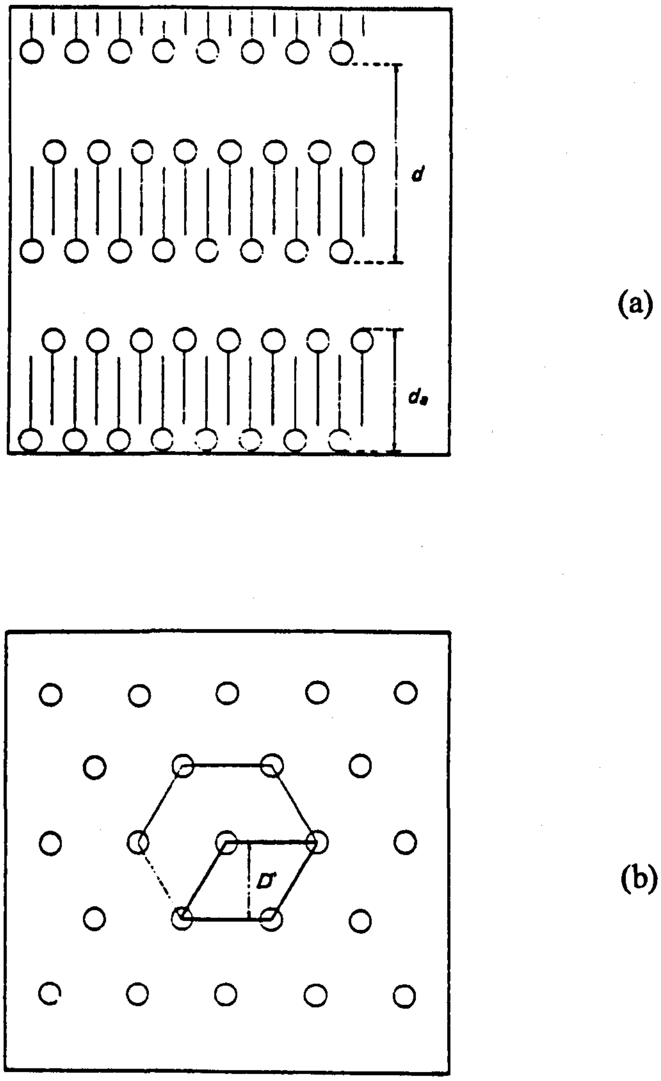

Figure 3.3 The structure of the gel phase of potassium soaps (a) side view and (b) seen from above (from Vincent and Skoulios [30])

Not every soap system can form gel phases (Winsor [19]). Sodium soaps only form coagels and no gels when they crystallise out (Vincent and Skoulios [31]). Whether potassium soaps crystallise out in a gel or coagel depends upon concentration and temperature. For example, (Winsor [19]) a mixture of KS and water cooled from 100°C to room temperature forms a homogeneous and clear gel if it contains less than 70% KS. If it contains more than 70% soap it yields an opaque coagel which is microscopically heterogeneous (Vincent and Skoulios [30]). The following explanation can be given for these phenomena. At low temperatures the tendency for the hydrocarbon chains to crystallise out dominates and the system becomes a coagel [31]. At higher temperatures the hydrocarbon chains melt, the polar groups ionise and the system forms an aqueous mesophase. At intermediate temperatures there are two equally strong tendencies: the polar groups are ionised and the chains are crystallised, which results in a gel structure [31]. In the coagel the tendency of the chains to crystallise makes the soap insoluble in water and phase separation appears (Vincent and Skoulios [32]). For the sodium soaps the tendency to ionise is insufficient to give rise to the separation of the polar groups and to form a gel phase [31]. Sodium oleate however was found to form a clear gel when it crystallises out in the presence of sodium silicate. There has always been an industrial interest in gel phases, as transparent soaps have a high consumer appeal. An X-ray study of the structure of transparent soap was undertaken by McBain *et al.* in 1944 [33]. In this study they proved that the investigated soap (Pears soap) was definitively crystalline and not amorphous as was believed at that time. Their conclusion was that the investigated soap was transparent, because the crystalline particles it was made up of, were too small to provide optical discontinuities when compared with the wavelength of ordinary light.

3.4 Phases between the T_c and the T_i line

The T_i-line in the surfactant phase diagram represents the temperature (as a function of concentration) above which the long range crystalline and liquid crystalline order break down. The region between the T_c- and the T_i-line indicates the compositions and temperatures where the surfactant-water system can exist in a variety of aqueous and thermotropic mesophases. These phases are a consequence of the dual character of the amphiphiles. In aqueous surfactants solutions the apolar hydrocarbon chains associate together in fluid arrangement leaving the polar groups in association with the polar water molecules (*e.g.* Reiss-Husson and Luzzati [4]). The forces involved, the Van der Waals forces (between hydrocarbon chains) and electrostatic forces (between ions and dipoles) result in the formation of aggregates of molecules, the simplest of which is the spherical micelle (see section 3.5.1). The structure of the aggregate depends on temperature, concentration and shearing (*e.g.* Winsor [19]). However, for all the different aqueous phases the pattern of the structure is defined mainly by the polar groups while the lipophilic parts of the molecules form liquid-like associations (Gray and Winsor [22]). The mesophases which can be formed by the surfactants under consideration will now be discussed in order of increasing surfactant concentration.

3.5 The Aqueous Mesophases

In this section some of the generalities of the aqueous mesophases will be explained. The elucidation of these structures is not only of great interest to the detergent industry but also for the study of biological systems, as biological membranes are formed by similar aggregates made up by amphiphiles *e.g.* (Chapman [1], Reiss-Husson [4] and Luzzati and Husson [28]). The aqueous mesophases have been studied by numerous different methods. Rosevear [34] for example was one of the first to look for a method to distinguish between two of the lyotropic liquid crystalline phases (the hexagonal and lamellar phase, see sections 3.5.2 and 3.5.3 respectively) as the detergent industry had an urgent need for this. Rosevear [34] used polarised light microscopy and published photomicrographs and a description of the characteristic optical features of the hexagonal and the lamellar liquid crystalline phase to make identification of an unknown sample possible. Luzzati *et al.* [11,28,35-38], Gallot and Skoulios [39], and Reiss-Husson and Luzzati [4] have extensively studied the aqueous mesophases by X-ray diffraction and with the use of a polarising microscope. Luzzati *et al.* studied the aqueous mesophases of C12 to C18 for sodium and potassium soaps, determined the structures of the lamellar and hexagonal phase [11] and discovered some phases in the intermediate zone between these phases [36]. The structure of some of these phases is supported by electron miscroscopic evidence (Gray and Winsor [22]).

In liquid crystals, (both lyotropic and thermotropic), the distinction has to be made between short and long range order. The short range order is dependent on the state of organisation of the hydrocarbon chains (and of the water molecules), whereas the long range order is dependent on the secondary structure which is composed of the structural aggregates within the system (Gray and Winsor [22]). In general, liquid crystalline phases have long range order, but a highly disordered short range conformation. The hydrocarbon chains of an amphiphilic liquid crystal are usually considered to be in the liquid state. This is supported by a weak and diffuse 4.5Å reflection in the X-ray pattern, which is identical in position and appearance to that for liquid hydrocarbons [19,22]. In addition to this band, a diffuse band corresponding to 3.2Å, which is characteristic of liquid water is also common to all aqueous mesophases (Winsor [19]). The diffraction pattern for an amphiphilic liquid crystal is further characterised by a series of sharp reflections corresponding to interplanar spacings ranging from 10 to above 100Å (Gray and Winsor [22]). For all the liquid crystalline phases the *ratios* of the spacings of the small-angle lines, which are characteristic for each phase, are independent of temperature, but the *spacings* vary continuously with the temperature (Luzzati and Husson [28]). The spacings decrease as the temperature increases (Luzzati *et al.* [11, 28 and 37], which is explained by the liquid nature of the hydrocarbon chains.

In judging the plausibility of a proposed structure two parameters have proven to be useful: firstly the dimensions of the unit aggregates composing the liquid crystalline structure (such as the thickness of the layers in the lamellar phase or the distances between the cylinders in the hexagonal phase) and secondly the available interfacial area per polar head group (Gray and Winsor [22]). The available interfacial area per polar head group represents the molecular crowding at the surfactant-water interface within a particular structure of the amphiphile system. This parameter can be calculated on the basis of X-ray diffraction data and partial specific volumes of soap and water (Gray and Winsor [22]), this is explained in more detail in appendix A. Even in the anhydrous phases the hydrophilic groups are supposed to segregate out from the hydrocarbon regions so that even in that case the area per polar head group can be defined (Chapman [1]).

3.5.1 Dilute isotropic soap phases

At low surfactant concentrations no aggregates are formed by the soap molecules. However, the concentration of surfactant molecules is the highest on the water surface due to the repulsion between the hydrocarbon chains and the water molecules. At concentrations higher than the critical micelle concentration (c.m.c.) and above the Krafft temperature (the temperature above which a surfactant becomes soluble) the simplest form of an aggregate of amphiphiles is formed: the spherical or Hartley [40] micelle. A schematic picture of a spherical micelle is shown in figure 3.4. This micellar phase was called the S_I phase by Winsor [19]. The c.m.c.'s for the surfactants under consideration are all very low (see table 3.2).

surfactant	**temperature (°C)**	**c.m.c. (mol/l)**	**Krafft point (°C)**
NaL	20-70	2.5×10^{-2}	36
NaM	50-70	6.5×10^{-3}	53
NaP	50-70	1.7×10^{-3}	62

Table 3.2 C.m.c.'s and Krafft points for sodium surfactants from Brandrup *et al.* [41]

The XRD pattern of this phase shows the diffuse band around 4.5Å due to the liquid hydrocarbon chains [1,35] and one or two broad peaks in the small angle region [1]. The Hartley micelle is a spherical aggregate of amphiphile molecules with the polar groups on its surface and the hydrocarbon chains forming a fluid core. Although the

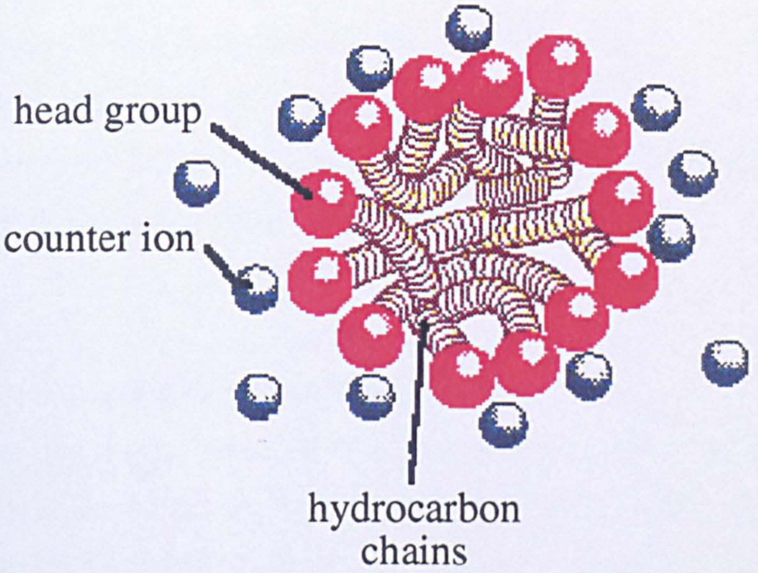
head group
counter ion
hydrocarbon chains

Figure 3.4 Schematic of a spherical micelle (from Tiddy [42])

counter ions are dissociated from the headgroups, at least 60% lie within a few Ångströms of the micelle surface.

Micellar solutions are amorphous in contrast to micellar liquid crystalline solutions and show no birefringence. At higher concentrations the spherical micelles transform to a different aggregate structure, for sodium laurate, myristate, palmitate and stearate this has been studied by Reiss-Husson *et al.* [35]. All types of micelles are of a statistical character, the form changes locally with temperature and concentration fluctuations (Winsor [19]). The word micelle is used by some authors only to denote a spherical micelle, but is used by others as another term for the aggregate units which are found in liquid crystals. In old surfactant literature the term micelle was also used to describe the unit cell of soaps in the solid state.

3.5.2 The hexagonal liquid crystalline phase

At higher surfactant concentrations (typically around 40% soap) and at temperatures above the T_c-line, the hexagonal phase is formed (see figure 3.5). This phase was historically called "middle phase" and was much feared by soap makers due to its high viscosity, see chapter 1. Winsor [19] used M_l to denote this phase, others used the symbol H_l and Ekwall [43] called it E. To avoid confusion, here the term *hexagonal* or *"normal" hexagonal phase* will be used, as this name describes the structure of this phase. This aqueous liquid crystalline phase consists of amphiphile molecules which form cylindrical fibres or rods of indefinite length. These fibrous micelles contain a fluid hydrocarbon interior with the polar groups of the amphiphile molecules on their surface. Within local uniform domains the cylinders are parallel and disposed in a regular two-dimensional hexagonal array with intervening water molecules (see figure 3.5). In a confined space such as between a microscope slide and cover slip the cylinders are oriented parallel to the glass surfaces. The diameter of the cylinders is usually about 10-30% less than the thickness of two "all-trans" surfactant chains (Tiddy [2]) and diminishes with dilution. The distance between the cylinders varies with water content over the range of 8-50Å [2], increasing with increasing water content. The hexagonal structure shows negative birefringence. The structure has been confirmed with electron microscopy (*e.g.* Eins [44], Balmbra *et al.* [45]). Clunie *et al.* [46] suggested a different rod-like structure for this phase, where the rods are chains of spherical micelles, linearly aggregated like a string of beads. The lack of a discontinuity in the density or in the X-ray long-spacings for the transition from the isotropic to the hexagonal phase, led them to conclude there to be little change in structure. However, as a consequence of "the string of beads model", the phase would be nearly isotropic, which is inconsistent with the observed optical sign (Gray and Winsor [22]). Because of this and on the basis of other arguments (Luzzati and Reiss-Husson [47]) the structure of the rods to be circular cylinders as originally suggested by Luzzati *et al.* [37] has been generally accepted.

The X-ray diffraction pattern of the hexagonal phase not only shows a diffuse band at 4.5Å, corresponding to a fluid hydrocarbon micellar interior, but is further characterised by a series of Bragg spacings in the ratio $1:1/\sqrt{3}:1/\sqrt{4}:1/\sqrt{7}:1/\sqrt{12}$, characteristic of parallel fibers in two-dimensional hexagonal array (Gray and Winsor [22]). This ratio is based on the equation for the d-spacings for the hexagonal crystal system, given in chapter 2:

$$\frac{1}{d_{hkl}^2}=\frac{4}{3}\left(\frac{h^2+k^2+hk}{a^2}\right)+\frac{l^2}{c^2} \tag{3.1}$$

Since the hexagonal liquid crystalline phase is only periodic in two-dimensions (*i.e.* there is no *c*-axis) the latter term in the equation can be ignored so that equation 3.1 simplifies to:

$$\frac{1}{d_{hk}^2}=\frac{4}{3}\left(\frac{h^2+k^2+hk}{a^2}\right) \tag{3.2}$$

From this it can be demonstrated that:

$$d_{100}=d_{110}\sqrt{3}=d_{200}\sqrt{4}=d_{210}\sqrt{7}=d_{220}\sqrt{12} \tag{3.3}$$

which explains the ratio given above. From the d-spacings the distance between the axes of the cylinders (which is equal to the a axis of the unit cell) can be calculated. If in addition the concentration and the specific volume of the amphiphile are known, the diameter of the cylinders can be calculated and the average surface on the cylinder which is available to each hydrophilic group can be determined (Luzzati and Husson [28]). The effective area per polar head group increases with increasing dilution, as well as with increasing temperature (Gallot and Skoulios [39]). It is however almost independent of the surfactant chainlength [1,39], see appendix A. The available area per polar head group in the micelles of the hexagonal phase is always markedly greater than the available area in the lamellar phase of the corresponding soap at higher concentration (Gallot and Skoulios [39]).

3.5.3 The lamellar phase

This phase is commonly found in soap-water systems containing between 60 and 80% soap. As is the case for almost all soap phases the nomenclature of the phase depends on the author. Historically this phase was called "soap boilers' neat phase", or simply "neat phase". However the term "neat phase" is also used to describe a thermotropic liquid crystalline phase. Some authors call this the G-phase (*e.g.* Winsor [19], others call it N or L and Ekwall [43] who used an alphabetic way to denote the various soap phases, distinguishes between two different lamellar structures D and B, although this is probably incorrect (Tiddy [2]). To avoid confusion, here the term *lamellar phase* is used as this term directly describes the structure of the phase.

The lamellar phase is formed at higher surfactant concentrations than the hexagonal phase, at temperatures above the T_c-line. The lamellar phase is much less viscous than the hexagonal phase, although the surfactant concentration of the former is higher. This is readily understood on the basis of the structures of the two phases. The structure of the lamellar phase is that of a *smectic* (from the Greek for soapy) liquid crystal, *i.e.* a layered structure with molecules perpendicular to the layers. The lamellar phase consists of alternating surfactant bilayers (with mobile hydrocarbon chains) and water layers (see figure 3.5). The layers extend over large distances, commonly of the order of microns or more (Tiddy [2]). The layers can easily slide

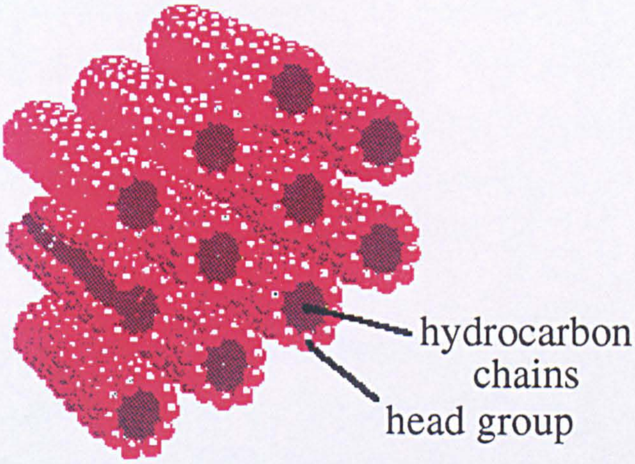
hydrocarbon chains
head group

Figure 3.5 Schematic of the hexagonal liquid crystalline phase, top figure and of the lamellar liquid crystalline phase, bottom figure (from Tiddy [42])

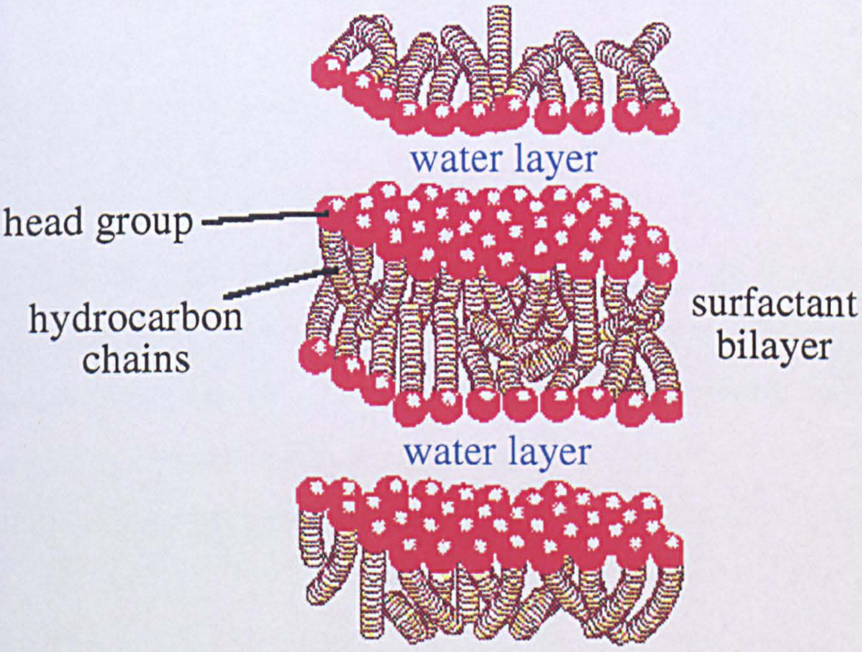
water layer
head group
hydrocarbon chains
surfactant bilayer
water layer

over one another, which explains why the viscosity of the lamellar phase is lower than that of the hexagonal phase. The structure of cell membranes of biological cells is thought to be essentially the same as that of the lamellar phase. Therefore to understand the behaviour of this phase as a function of concentration and temperature is of great biological interest, in order to elucidate the interactions between cells and to clarify the processes that occur on the cell periphery (*e.g.* LeNeveu *et al.* [48]). For theoretical considerations of interactions between biological membranes based on the analogy with lamellar liquid crystals see *e.g.* Goldstein *et al.* [49, 50].

For a given surfactant sample the difference in thickness of the water layers is usually less than about 0.5Å. The water layer thickness itself can vary from about 8 to over 100Å, depending on the water content (addition of water increases the thickness of the water layer) while the surfactant layer thickness is generally about 10-30% less than the length of two all-trans surfactant chains (Tiddy [2]). The thickness of the bimolecular amphiphile leaflets, d_a, diminishes as the water content is increased but at the same time the thickness of the water layers, d_w, increases. Therefore the observed d-spacing, which is the sum of d_a and d_w, varies in a rather complex manner with concentration (Winsor [19]). This was also observed by Parsegian *et al.* [51] who studied the processes taking place when water is removed from the lamellar phase of lecithin, a model system for the study of interactions between biological cells.

Not only the spacings between the layers but also the effective area per polar head group depends on concentration and temperature [11, 17, 28, 37-39]. The effective area per carboxylate group increases with increasing dilution (Winsor [19]) and is just as in the hexagonal phase independent of the surfactant chainlength (Gallot and Skoulios [39]). The thickness of the bimolecular soap leaflets and the effective area per polar head group may be calculated directly from the X-ray long spacing, the composition of the system and the partial specific volumes of its components [11, 22, 28, 36-38], see appendix A. Optical microscopy and X-ray diffraction studies indicate preferred orientation of the lamellae within the sample parallel to the container walls (Winsor [19], Gray and Winsor [22]). With convergent light a uniaxial interference cross can be identified as positive [19,22]. Evidence for the lamellar structure comes from a number of X-ray diffraction studies (*e.g.* Luzzati *et al.* [37]). Apart from the diffuse band at 4.5Å, the interlamellar spacings of the lamellar phase give rise to sharp diffraction bands at low angles in the ratios 1:1/2:1/3:1/4. The intensity falls of steeply for the higher orders and often only the first reflection is visible. The lamellar structure has also been observed using electron microscopy (*e.g.* Eins [44] and Balmbra [45]).

3.5.4 The Reversed Hexagonal Phase

At higher surfactant concentration than the lamellar phase some amphiphiles form the inverse form of the hexagonal phase. This *reversed hexagonal phase* also consists of rods which are packed on a two-dimensional hexagonal lattice, but here the water and the polar groups together form the micellar core and the apolar groups are on the outside of the rods. This phase was called M_2 by Winsor [19], H_2 by others and F by Ekwall [43]. Here it will be referred to as the *reversed hexagonal phase.* This phase is optically negative like the normal hexagonal phase (Gray and Winsor [22]). Again the diameter of the cylinders and the distances between them vary with temperature and concentration. Although some surfactants can form both the normal and the reversed hexagonal phase, in general, for systems where the polar groups are large in relation to the hydrocarbon portion, the formation of the "normal" hexagonal phase is favoured, while if the hydrocarbon part is relatively bulky the reversed hexagonal phase is formed (Gray and Winsor [22]).

Many lipids of biological interest can form the reversed hexagonal phase (*e.g.* Gruner [52]). Gruner pointed out that an important difference between the *reversed* and the *normal* hexagonal phase is that in the reversed hexagonal phase some molecules have to be stretched out further than others, in order to fill the hydrocarbon matrix between the polar regions (see figure 3.6). A consequence of this is that in the normal hexagonal phase the lipid cylinders are rotationally symmetric about the cylinder axis, whereas those in the reversed hexagonal phase have a six-fold symmetry axis.

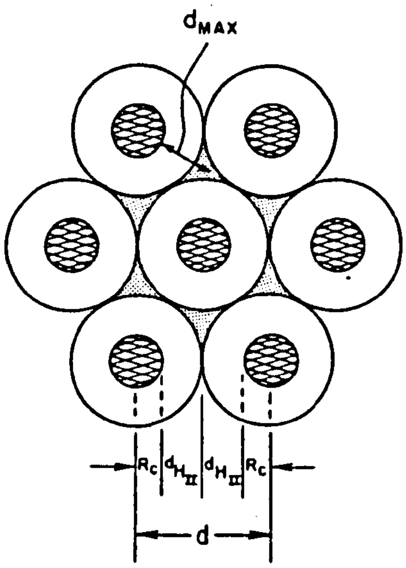

Figure 3.6 The reversed hexagonal phase (from Gruner [52]). The cross-hatched regions represent water cylinders of radius R_c, while the circles and stipled areas represent the lipid hydrocarbon chains. The hydrocarbon chains thus have to extend to different lengths to fill the hydrocarbon regions

The fact that the same liquid crystalline structures are formed by many different molecules (*e.g.* soaps, di-block copolymers and polar biomembrane lipids) with different functional groups led Gruner [52] to suggest that it might be possible to explain the phase transitions between various liquid crystalline structures, such as the transition from the lamellar to the reversed hexagonal phase, with a phenomenological description that does not take into account the different molecular interactions. The model takes the approach that the combination of all the forces that are present in a surfactant layer lead to a specific spontaneous curvature of the layer. If the layer has a different curvature (either too high or too low) this will be energetically unfavourable. In any liquid crystalline structure this energy term, the so called *bending energy*, competes with the *hydrocarbon packing energy* term. This is the unfavourable energy caused by gauche conformations in the hydrocarbon chain, which are energetically unfavourable by about 0.5kcal/mol per gauche conformation.

These gauche conformations effectively lead to a shortening of the molecule relative to the all trans configuration. The model presented by Gruner was developed for systems in which a thermotropic transition occurs from the lamellar to the reversed hexagonal phase on heating and explains this transition in the following way: in the lamellar phase there is no geometrical constraint for the molecules to have different lengths. In the reversed hexagonal phase however, some of the hydrocarbon tails have to be stretched further than others in order to fill the hydrocarbon matrix. Therefore in the reversed hexagonal phase there will be more gauche conformations present than in the lamellar phase. This means that for the lamellar phase the hydrocarbon packing energy is lower than for the reversed hexagonal phase. However, for the lamellar phase the bending energy is higher since else no transition could occur to the reversed hexagonal phase. The two different energy terms depend in a different way on the temperature. Therefore the lamellar to reversed hexagonal transition can occur if a temperature exists at which the sum of the two energy terms of the reversed hexagonal phase is lower than this sum for the lamellar phase.

Gruner's theory predicts that the larger the water core of the cylinders in the reversed hexagonal phase, the more unfavourable the hydrocarbon packing energy becomes, thus leading to a transition to the lamellar phase. This is consistent with reality as the reversed hexagonal phase (when present) is always found in the phase diagram at a lower water content than the lamellar phase. In addition the theory shows that the transition from the lamellar to the reversed hexagonal phase can be facilitated by the addition of hydrophobic substances, such as alkanes. These will go into regions where the hydrocarbon chains are stressed, thus allowing the lipid chains to relax. Mixing surfactants of different chainlengths can achieve the same effect. In general, packing chains in specific shapes results in a conformation distribution which is different from that of the corresponding isotropic liquid hydrocarbons (alkanes), which means that there is an energy penalty, the value of which depends on the structure formed.

3.6 The intermediate phases

The best known soap phases have been discussed in the previous sections: the gels and coagels below the T_c curve, and the following aqueous phases: the isotropic monomer solution at very low surfactant concentrations, the isotropic micellar solution at temperatures above the Krafft temperature and at concentrations above the c.m.c., the hexagonal, the lamellar and the reversed hexagonal liquid crystalline phases. These aqueous phases as well as their structures are the best known aqueous surfactant phases, since they occur over a wide concentration and temperature range and in addition consist of relatively simple structural aggregates (spheres, rods or lamellae). Some theories have been developed in order to explain the transitions between the different phases. Winsor [19] for instance attempted this on the basis of the *R-theory*. In this, R is defined as the ratio of the tendency of the amphiphile layer to become convex toward the organic layer and the tendency of the amphiphile layer to become convex toward the water layer. When both tendencies are balanced R equals one, as is the case for the lamellar liquid crystalline phase. If the concentration or the temperature is changed these tendencies change, thus R changes and the structure of the phase changes. Factors that decrease repulsion between head groups (*e.g.* hydration) increase R, resulting in phase changes in the direction spherical micelle→hexagonal→lamellar phase. Phase changes in the opposite direction result in a reduction in R. This theory however does not lead to any quantitative predictions concerning surfactant phase behaviour. Eins [44] calculated transition concentrations for the lamellar and hexagonal phases of some potassium soaps using the X-ray data from Husson *et al.* [38]. These relatively simple calculations are based on the volume fractions of water and amphiphiles: the calculated values agree remarkably well with the observed transition concentrations. However, in order to perform such calculations the structure and its dimensions first have to be known. The agreement in calculated and observed values however, does show that volume relations play an important role in the configuration and transformation of liquid crystalline structures.

These theories however, do not provide a mechanistic understanding of the transformation process between the lamellar and the hexagonal liquid crystalline phase. More insight into this phase transformation can be obtained from the study of structures of a variety of liquid crystalline phases which have been found to exist intermediate in composition between the lamellar phase and the "normal" hexagonal phase. Here the term *intermediate phases* will be used to refer to these phases. For the sodium soaps the number of intermediate phases and their structures have not yet unequivocally been determined. This is due to the difficulty of preparing these phases as they only form over a very narrow concentration and temperature range. The structures which have been proposed for the intermediate phases of the sodium soaps (and potassium soaps as they are very similar) are explained in the following sections, together with an overview of intermediate phases which have recently been found for other surfactant and polymer systems. These structures are explained here as very similar structures are proposed in chapter 7 for the intermediate phases of sodium soaps.

3.6.1 The intermediate phases of sodium soaps

In the 1940s, when McBain *et al.* [8,9] undertook extensive phase diagram studies for saturated sodium and potassium soaps, it was believed that no phases existed between the regions in the phase diagram for middle and neat soap (now known as the hexagonal and lamellar liquid crystalline phase respectively). At intermediate compositions the system was simply supposed to be composed of a mixture of these two phases. The first to discover the existence of intermediate phases for a number of sodium (see table 3.3) and potassium soaps were Luzzati *et al.* [36 and 37] and Husson *et al.* [38] in the late 1950s and in the 1960s. They found no intermediate phases for NaL, but discovered two intermediate phases for NaM, NaP and NaS, and found even four intermediate phases for KP. For KP this makes six lyotropic liquid crystalline phases in total; in order of increasing soap concentration: *hexagonal, deformed hexagonal, rectangular, complex hexagonal, cubic and lamellar.*

At the time this order was accepted to be generic for all soap systems. For some soaps some of these phases do not form but no inversion of the order was observed.

Surfactant	**hexagonal**	**deformed hexagonal**	**complex hexagonal**	**lamellar**
NaL	----0.59			0.59----
NaM	----0.54	0.54-------0.55	0.55-------0.59	0.59----
NaP	----0.51	0.51-------0.52	0.52-------0.56	0.56----
NaS	----0.50	0.50-------0.51	0.51-------0.54	0.54----

Table 3.3 Phase boundary concentrations (in wt%) for sodium soaps (concentrations have not been determined with great precision, from Husson *et al.* [38])

Luzzati *et al.* [36, 37] and Husson *et al.* [38] did not find rectangular or cubic phases for any of the sodium soaps. Structures for the intermediate phases as they were proposed by Luzzati *et al.* [36, 37] and Husson *et al.* [38] for the sodium soaps are explained below, the cubic and rectangular phases found for the potassium soaps are discussed in the next section.

- The *deformed hexagonal* phase (called phase O) is supposed to be formed by a deformation of the lattice of the normal hexagonal phase whereby the lattice becomes orthorhombic (Luzzati and Husson [28]). This is thought to be accompanied by a deformation of the cylinders, the circular cross-section becoming elliptical (Luzzati *et al.* [28,36]). This phase as well as the *complex hexagonal* phase (see below) were found in systems of certain sodium and potassium soaps but were not observed for NaL, KL and KM (Luzzati [36]).

- The *complex hexagonal* phase. X-ray patterns for the complex hexagonal phase (called H_c by Ekwall [43]) display up to six reflections, which satisfy the two-dimensional hexagonal criteria, its microscopic appearance is furthermore typical of a hexagonal phase Luzzati *et al.* [37]. Its large cell-parameter (almost twice that of the normal hexagonal phase in the same system) points to a complex structure. For the complex hexagonal phase Luzzati *et al.* [36, 37] and Husson *et al.* [38] proposed a structure of cylinders packed on a hexagonal lattice as for the normal hexagonal phase, but here the cylinders are made up of double layers of surfactants with a water core inside the cylinders and water filling the space between the cylinders. Some proposed structural dimensions can be found in *e.g.* [38]. Balmbra, Bucknall and Clunie [45] however, proposed the reversed structure on the basis of electron microscope studies. Both proposed structures of the complex hexagonal phase are now considered as rather unlikely as the curvature on the inside of the cylinders is different from the curvature on the outside of the cylinders Leigh *et al.* [53].

The first to discover the existence of an intermediate phase for NaL were Madelmont and Perron [12] in the 1970s. In subsequent research a second intermediate phase for NaL was found (Madelmont and Perron [16]). However, their DTA (differential thermal analysis) results did not provide any structural information about these phases. Madelmont and Perron therefore assumed [14,15] these phases (which they referred to as I_1 and I_2 for intermediate phase one and two respectively) to be identical to the two phases (deformed hexagonal and complex hexagonal) found earlier by Luzzati *et al.* [36-38] for the other sodium soaps. In further DTA studies Madelmont and Perron also found two intermediate phases for NaM [14, 15], NaP and NaS [18] although for the latter two soaps their observation of the lower concentration intermediate phase is dubious since they did not manage to observe the transition from what they assumed to be the deformed hexagonal phase to the normal hexagonal phase.

Later optical microscopy and NMR studies by Rendall *et al.* [54] confirmed the existence of two intermediate phases for sodium laurate. Although the structures of these phases could not be determined from optical microscopy or NMR results, both intermediate phases showed birefringence and could thus not be cubic. Therefore, like Madelmont and Perron [14, 15], Rendall *et al.* [54] assumed the lower concentration intermediate phase to have a deformed hexagonal structure relying on what Luzzati *et al.* [36-38] had found. For the second intermediate phase (the one of higher surfactant concentration) Rendall *et al.* [54] proposed a lamellar structure with thin bilayers (they assumed a surfactant layer thickness of 15Å and a head group separation of *ca.* 10Å), however they did not exclude the possibility of other structures ("structures based on rods, discs or other shapes"). For the other sodium soaps (NaM, NaP and NaS) Rendall *et al.* [54] found only one intermediate phase, which is inconsistent with the results of Luzzati *et al.* [36-38].

Only one (anisotropic) intermediate phase for NaL (between 57 and 60.5 wt% surfactant) was found by Kilpatrick and Bogard by optical microscopy and NMR studies [55]. They did however discover the existence of a cubic phase formed in a ternary system of NaL, toluene and water and in a ternary system of NaL, n-decane and water. Blackburn and Kilpatrick [56] and Kilpatrick, Blackburn *et al.* [57] later obtained a similar result for NaM using NMR: only one (anisotropic) intermediate phase was found for NaM. A two phase region was found to exist between the transition from the hexagonal to this intermediate phase (Blackburn and Kilpatrick [56]). In addition to this, as had been observed for NaL, Kilpatrick, Blackburn *et al.* [57] demonstrated the existence of a cubic phase formed in ternary systems consisting of NaM, water and one of the following hydrocarbons: n-decane, n-hexadecane or toluene. This cubic phase was not observed in the ternary system of NaM, water and n-decanol.

From the above it is clear that the number and structural nature of intermediate phases for sodium soaps have not unequivocally been determined. In the following section an overview is provided of intermediate phases that have been observed to occur in other systems.

3.6.2 Intermediate phases observed for other surfactant systems

Most of the literature presented in the previous sections is rather old. In more recent years several intermediate phases have been found, for other surfactants than sodium soaps. These will be discussed here, as this will lead to an improved understanding of the intermediate phases of the sodium soaps. For other surfactants than sodium soaps, as well as for some polymer systems, intermediate phases have been found which can all be divided into the following three classes depending on the exact way that the surfactant aggregates are connected: *ribbon*, *mesh* and *bicontinuous* structures. First a concise description of these structures is provided, after which some examples are given.

- The first class of structures is that of the *ribbon structures*, where the rod shaped aggregates of the hexagonal phase are distorted into biaxial ribbons (with probably an elliptical cross-section) which are packed in a regular array. By some authors (*e.g.* Blackburn and Kilpatrick [58]) this is called the R-phase (R for ribbon), although others use this symbol to describe the rhombohedral mesh phase (*e.g.* Kékicheff and Cabane, [59]) (see second class of structures below). A ribbon type structure was first proposed by Luzzati who called it the deformed hexagonal phase. In a ribbon phase there is only two-dimensional long range order and there are no connections between the rods.

- The second class of intermediate phases is that of the *mesh structures*. A mesh structure is a layered structure where the layers are made up of rods that are linked together. An alternative but equivalent way to describe this structure is to say that it is a lamellar structure consisting of alternating water layers and surfactant bilayers, where the bilayers contain water filled holes of certain shapes at regular positions in the layers, thus forming a three-dimensional lattice. This lyotropic liquid crystalline phase thus exhibits three-dimensional long range order. The two main types of mesh phases which have been found are tetragonal and rhombohedral (hexagonal). For each of these types two alternatives are possible: a "normal" mesh phase, where the mesh consists of the surfactant molecules, with water filled holes, or alternatively in the case of a reversed mesh phase, the mesh is made up of the aqueous phase and the holes are filled with the hydrocarbon chains of the surfactants. The first to propose mesh structures were Luzzati *et al.* [60]. They proposed a hexagonal and a tetragonal mesh structure for high temperature thermotropic liquid crystalline phases of strontium myristate and calcium stearate respectively. It is possible that the rectangular phase proposed for the potassium soaps is really a tetragonal mesh phase.

Random mesh phases, *i.e.* disrupted or defected lamellar phases (called L_α^H) have also been found (*e.g.* Kékicheff *et al.* [59, 61]). In the random mesh phases the surfactant bilayers contain water filled holes, which have no inter-planar correlations. These holes cause a broad diffraction ring in the X-ray or neutron scattering pattern at low angle. The defects serve to increase the curvature of the lamellar phase and possibly to reduce the bilayer separation. The appearance of defects and increased interface curvature in the lamellar phase is thought to be a gradual process. Fairhurst, Leaver and Holmes [62] suggested that the defects arise from fluctuations within the lamellar phase which create dimples in the surfactant bilayers. These dimples increase in depth until the bilayers are fully perforated (see figure 3.7). On transformation to an ordered mesh phase the holes become regularly ordered with inter-planar correlations.

The third class of intermediate phases is formed by the so called *bicontinuous structures*. In the mesh phases there are no connections between the layers, so that there is no continuous surfactant phase; the water phase is continuous throughout however, because of the holes in the surfactant layers. When in a mesh phase at certain positions connections between the layers are formed, the structure will contain both a continuous aqueous phase and a continuous surfactant phase and is therefore called *bicontinuous*. It is also possible that the connections between the layers are made in such a way that two equivalent surfactant networks are created, which are interwoven but unconnected; the space between these two networks is filled with a continuous aqueous phase. The reversed situation also occurs, where there are two equivalent interwoven but unconnected aqueous networks, separated by a continuous surfactant phase (in either case the polar headgroups of the surfactants will be in contact with the aqueous phase). Although these structures are really tri-continuous because there are two equivalent unconnected continuous phases (surfactant or aqueous) separated by one continuous phase (aqueous or surfactant), these structures are still called bicontinuous. The best known bicontinuous structures (which in reality are tri-continuous) are the so called *bicontinuous cubic structures* (different types of cubic structures also exist which do not contain continuous

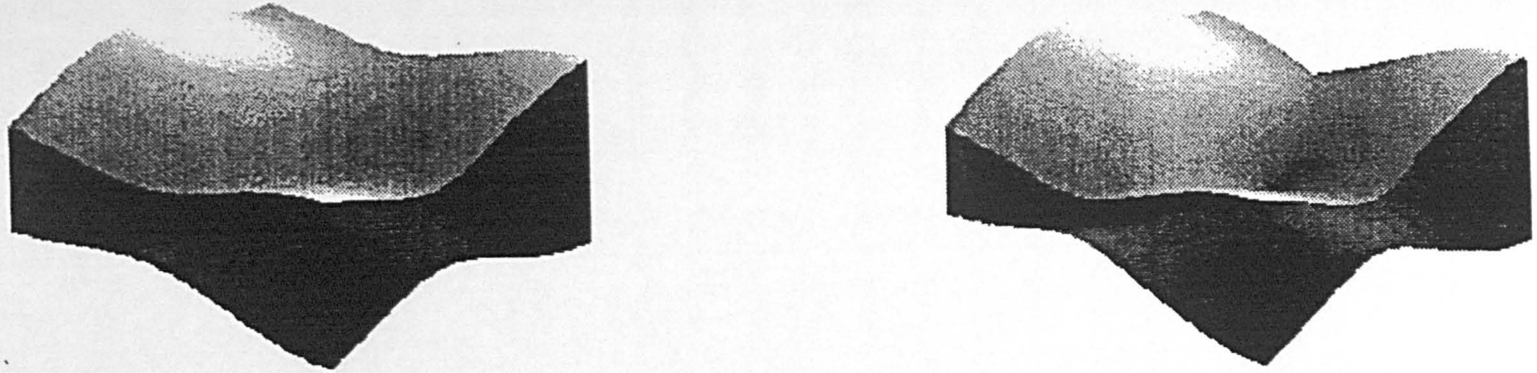

Figure 3.7 Showing the formation of defects in the lamellar phase from dimples which gradually increase in depth until the surfactant bilayers are fully perforated (from Fairhurst *et al.* [62])

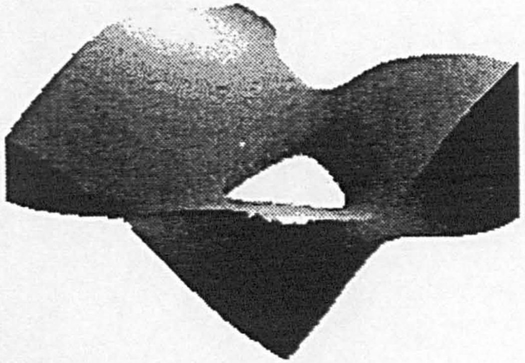

- surfactant or aqueous regions). The first to propose bicontinuous structures for cubic phases were Luzzati *et al.* [63].

Evidence for all three classes of structures has been derived from NMR, optical microscopy and X-ray and neutron scattering data. The first to find structures of all classes was Luzzati. It can be extremely difficult to experimentally distinguish between a mesh and a bicontinuous structure, as these phases are closely related; *e.g.* all that is required to transform a tetragonal mesh phase to a bicontinuous phase is for the surfactant rods in the tetragonal mesh phase to interconnect the planar lattices [58] as is shown later in this section. Such a transformation does not affect the symmetry of the structure and therefore only causes very subtle changes in the XRD patterns. The use of oriented samples for X-ray and neutron diffraction studies has proved to be a valuable aid in determining the structures of the intermediate phases. This technique has also led to a better understanding of transitions between liquid crystalline phases. In principle such a transition can take place either by destruction of the first structure and subsequent formation of the next one, or alternatively might occur in a more organised way in which structural elements from the second phase grow from structural elements of the first phase. Such *epitaxial growth relations* have been shown to exist in certain systems through the use of oriented samples.

In the following section examples are given to illustrate the three types of structures explained above. A large section is devoted to cubic structures which is the result of the variety of different structures which have been proposed for these phases, which are the are the best known intermediate phases. Although the mesh structures were originally proposed in the 1960s by Luzzati for thermotropic liquid crystals, it has only recently been realised that these structures also occur as lyotropic phases intermediate in the phase diagram between the hexagonal and lamellar phase region.

- **Cubic phases**

There has been much speculation on the structures of cubic phases. These phases have also been called "viscous isotropic phases" due to their appearance and are denoted with I in Ekwall's alphabetical system [43] and with V, C or Q by others. Cubic phases are isotropic and therefore do not show birefringence (Tiddy [2]). Luzzati *et al.* [36] give some dimensions of cubic phases. They observed a cubic phase for KL, KM and KP [36,37]. The corresponding sodium soaps however, did not form this phase [36]. Luzzati [28, 47] first postulated a cubic structure consisting of spherical aggregates, packed on a face-centred cubic lattice. They originally suggested [37, 38] the spheres to consist of micelles containing the amphiphiles and called this the cubic I phase [47] (Ekwall [43] called this phase I_{f1} while others called it C_1). Later however, Luzzati *et al.* proposed an alternative model, formed by water spheres embedded in a hydrocarbon matrix; which they called the *reversed cubic* phase, or the cubic II phase [47] (Ekwall calls this I_{f2}, others C_2). Luzzati *et al.* [47] first concluded the cubic II structure to be more probable than the cubic I, on the basis of calculations of the area per polar head group and as a hydrocarbon matrix would explain the high viscosity of the cubic phase. Later however, Luzzati [63] concluded the cubic phases to be bicontinuous: "the structure of the cubic phase is formed of rod-like elements, all identical and crystallographically equivalent, linked three by three into two three-dimensional networks, mutually interwoven and otherwise unconnected. In some cases the rods are filled by the paraffin chains, in others by the polar moieties". Luzzati *et al.* [1] recognised however, that the suggested cubic structures are still questionable. X-ray diffraction patterns for cubic phases show the 4.5A band and two sharp and strong small angle reflections, the spacings ratio of which is $1/\sqrt{3}:1/\sqrt{4}$; occasionally weak spacings with ratios of $1/\sqrt{8}:1/\sqrt{11}$ were also observed, which are characteristic for a face-centred cubic lattice (Luzzati *et al.* [37, 63]). Mariani, Luzzati *et al.* [64] further demonstrated the variety of cubic structures which can be formed by surfactant systems, they proposed structures for six bicontinuous cubic phases for surfactants found in biological systems and did not exclude the existence of even more cubic phases. This further illustrates the biological significance of liquid crystalline phases since these structures were found in conditions close to those prevailing in living organisms (Mariani, Luzzati *et al.*[64]).

Nowadays it is generally believed that there are two different types of cubic structures, bicontinuous and non bicontinuous depending on the position they occupy in the phase diagram. If the cubic phase is found between an isotropic micellar phase (normal or reversed) and a hexagonal phase (normal or reversed) the structure is likely to be non bicontinuous, but made up of aggregates such as spherical micelles, which are possibly deformed and packed on a cubic lattice (primitive, body-centred or face-centred). If the phase is found between the lamellar phase and a hexagonal phase (either normal or reversed) it is probable that the structure is bicontinuous. The phase sequence thus becomes with increasing surfactant concentration: isotropic micellar, non bicontinuous cubic, hexagonal, bicontinuous cubic, lamellar, reversed bicontinuous cubic, reversed hexagonal, reversed non bicontinuous cubic and reversed isotropic micellar. Different types of cubic phases thus constitute intermediate phases between all the other phases. It has been suggested that in principle all lipid systems have the ability to form cubic phases as intermediate phases but that their formation is kinetically hindered, Gruner [52]. Reviews on cubic phases have been given by Fontell [65, 66]. Some structural alternatives for cubic phases are discussed and an overview is provided of more than 100 substances for which cubic phases have been observed [66].

The bicontinuous cubic phases are thought to be built on *infinite periodic minimal surfaces* (IPMS) *e.g.* Larsson [67]. A surface of *constant mean curvature* is a surface for which the average of the two principle curvatures is constant everywhere on the surface ($(C_1 + C_2)/2 = \text{constant}$). A *periodic minimal surface* (PMS) is a special case of a constant mean curvature surface but one for which the constant equals zero. A periodic minimal surface is thus a three-dimensional (non flat) surface, which is free from self-intersections and which has zero mean curvature everywhere, *i.e.* every point on the surface is a saddle point for which the sum of the two principal curvatures is zero. An *infinite* periodic minimal surface is a PMS which exhibits crystallographic periodicity. These surfaces were known in mathematics before they were discovered to occur in liquid crystals. It important to note that the IPMS is not formed by the interface between the hydrocarbon and the aqueous region. In the "normal" bicontinuous cubic phases the IPMS is found in the centre of the surfactant bilayers, where it is sandwiched between both halves of the surfactant bilayers. Three different types of infinite minimal periodic surfaces have been found to occur in cubic phases *e.g.* Larsson [67] (see figure 3.8):

1. the *primitive* (P) IPMS, which corresponds to a body-centred cubic lattice; the term "primitive" does not refer to a primitive lattice but denotes the fact that this was the first and simplest IPMS to be discovered in mathematics.
2. the *diamond* (D) IPMS, which corresponds to a primitive cubic lattice. This IPMS is called diamond as the channel systems on each side of the surface form a diamond lattice. In polymer systems this structure has been called the *ordered bicontinuous double diamond* (OBDD) structure but is also referred to as the tetrapod-network structure because the structure can also be regarded as being made of connected rods *e.g.* Bates and Fredrickson [68].
3. the *gyroid* (G) surface, which like the primitive IPMS corresponds to a body-centred cubic lattice but has different symmetry elements.

Computer simulations of IMPS surfaces by Thomas *et al.* [69] compared well with experimental results found for polymer systems. Theoretical considerations of the curvature of cubic systems justify the position of the cubic phase in the phase diagram between the lamellar and the hexagonal phase (Anderson, Gruner *et al.* [70]). The realisation that the bicontinuous cubic phases are built on infinite periodic minimum surfaces is a refinement of the rod models of cubic structures and demonstrates ways how a single surface without self-intersection can separate two continuous regions. Although it is easier to visualise bicontinuous cubic phases as networks of rods, the IPMS representation is in many cases probably a more realistic one. The continuity of the hydrocarbon and water regions can be confirmed by NMR diffusion measurements (Larsson [67]). Two-dimensional sections through bicontinuous cubic phases have been found to be analogous to the structures of cell

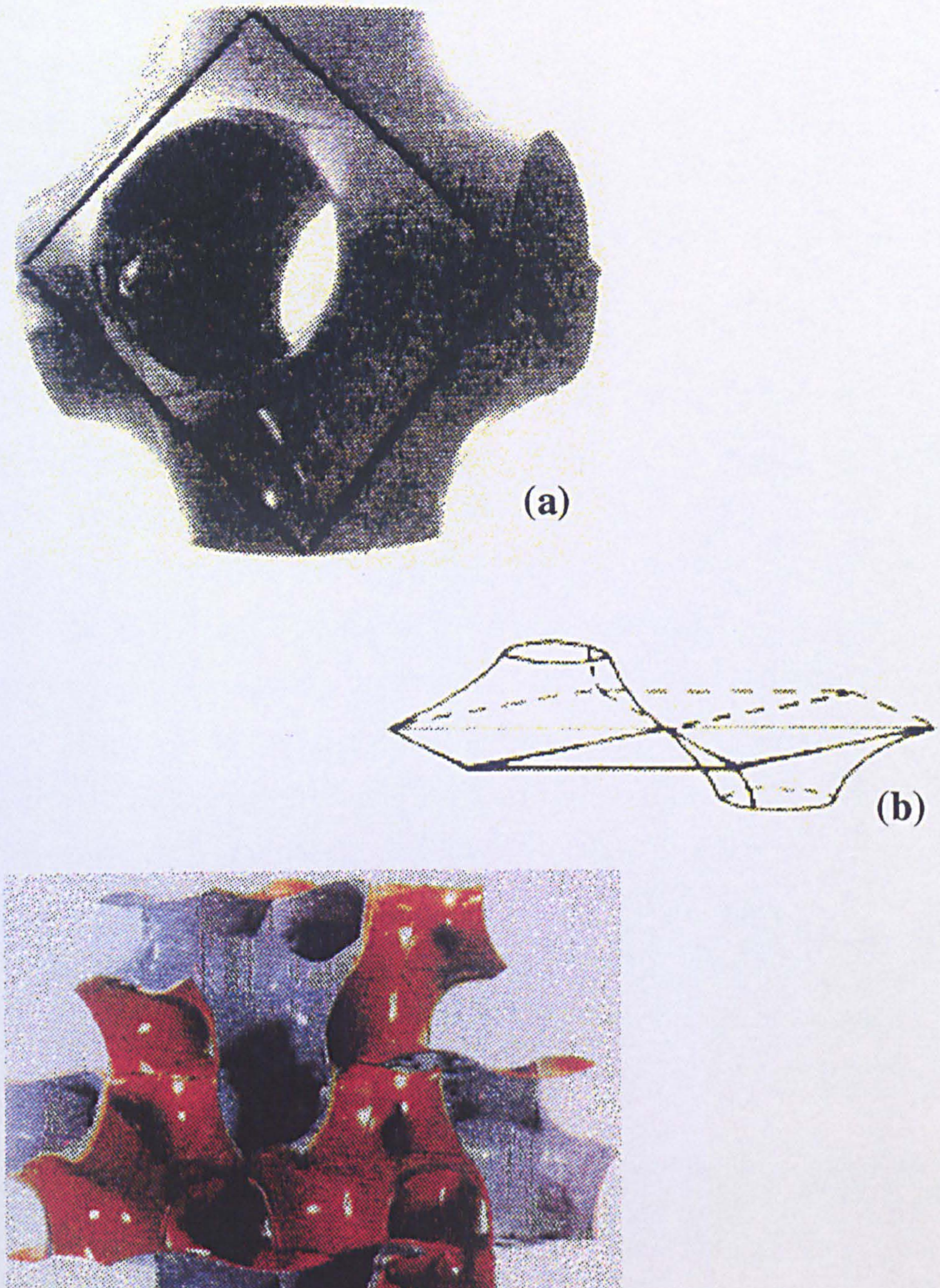

Figure 3.8 The three infinite periodic minimal surfaces which have been found to occur in liquid crystalline systems: a. the primitive IPMS, b. the diamond IPMS and c. the gyroid IPMS (from Larsson [67])

membranes (Larsson [67]). Larsson [67] reported of a variety of biological systems in which transitions between such two-dimensional analogues of bicontinuous cubic phases and lamellar phases play an important role. This and the fact that bicontinuous cubic phases have been found to occur in a variety of systems (soaps, biological lipids and polymers) underlines that bicontinuous cubic phases are not a crystallographic oddity of surfactant systems but are generic structures which occur in many different systems, found in the phase diagram between the hexagonal and the lamellar liquid crystalline phase.

An example of a polymer system which forms bicontinuous cubic phases is the polystyrene-polyisopropene (PS-PI) system, which forms different cubic phases depending on the volume fractions of PS and PI. Thomas *et al.* [71] found a structure consisting of two translationally displaced, mutually interwoven but unconnected three-dimensional networks of polystyrene (PS) rods embedded in a polyisopropene (PI) matrix. This phase occurred between the hexagonal and the lamellar phase. The reversed phase of the same polymer system, where the rods are formed by polyisopropene, embedded in a polystyrene matrix was found by Hasegawa *et al.* [72]. The total phase sequence for this polymer system with increasing fraction of PS was thus thought to be as shown in table 3.4 (*e.g.* Bates [73]). Later however, Förster *et al.* [74] found a cubic phase different from the OBDD one with PI rods in a PS matrix. In addition Förster *et al.* [74] found a perforated (layered mesh) intermediate phase, probably consisting of PI rods linked by threes, forming hexagonally shaped holes.

For another di-block copolymer system, poly(ethylenepropylene)-poly(ethylethylene) (PEP-PEE), Almdal *et al.* [75] found three ordered phases using oriented samples: an undulated (rippled) lamellar phase, a lamellar phase with holes in the PEE layers and an ordered phase which was thought to be a bicontinuous phase. The formation of this phase might be initiated by the formation of holes in the PEP layers and connections between the layers. No detailed structure was proposed for this phase however.

phase sequence on increasing fraction of PS	**consisting of**
body-centred cubic	PS spheres in PI matrix
hexagonal	PS cylinders in PI matrix
OBDD	PS rods in PI matrix
lamellar	alternating lamellae of PS and PI
OBDD	PI rods in PS matrix
hexagonal	PI cylinders in PS matrix
body-centred cubic	PI spheres in PS matrix

Table 3.4 showing the phase sequence of the polymer PS-PI system from Bates [73]

- **Intermediate phases of anionic surfactants**

In the previous section some examples have been given of systems that form cubic phases. This section concentrates on non-cubic intermediate phases. An anionic surfactant of which the phase behaviour has been studied extensively is sodium dodecyl sulphate (SDS). This surfactant is of special interest here because it has the same chainlength and counter ion as NaL, only the head group is different. Leigh *et al.* [53] found one intermediate phase for SDS for which they proposed a deformed hexagonal structure on the basis of X-ray diffraction data. However it is odd that their optical microscopy studies of this phase indicated the rods to be perpendicular to the glass microscope slides, whereas the rods of the normal hexagonal phase are known to be oriented parallel to glass surfaces. The existence of another intermediate phase for the SDS-water system was found by Kékicheff and Cabane [76], who discovered a defected lamellar phase. An indication for this phase was the appearance of a diffuse diffraction ring in neutron diffraction patterns of oriented SDS samples. The correlations between these pores or channels in the surfactant bilayers were supposed to exist only between two or three layers. The correlations between the defects was observed to increase near the phase boundary with the deformed hexagonal phase, the defects were thought to become staggered in position between adjacent bilayers. The defects can be therefore be regarded as the first step of the surfactant layers breaking up into rods.

This mesh or bicontinuous phase, with correlations between the holes in the layers was further investigated using synchrotron radiation, which led to the discovery of four lyotropic intermediate phases (Kékicheff and Cabane [77]. These are in order of increasing concentration: hexagonal, a ribbon phase ordered on a two-dimensional monoclinic lattice (called the M_α phase), a rhombohedral phase (mesh or bicontinuous, called R_α), a bicontinuous cubic phase (called Q_α), a tetragonal mesh phase (called T_α) and the lamellar phase. Later neutron scattering [59] studies on oriented SDS samples confirmed this phase sequence and demonstrated epitaxial relations between some of the phases.

Less intermediate phases but a similar phase sequence was found for cesium myristate (CsM) by Blackburn and Kilpatrick [78]: isotropic micellar, hexagonal, ribbon phase, bicontinuous cubic phase, lamellar phase. From their NMR and microscopy data the exact structure of the cubic and ribbon phase could not be determined. No two phase region was observed between the hexagonal phase and the ribbon phase. This indicates that the hexagonal phase changes continuously until the rod phase is formed. The other phase transitions (ribbon to lamellar, ribbon to cubic, hexagonal to cubic) in CsM were all found to take place through a two phase region [56].

A comparison of the intermediate phases observed for different surfactant systems led Kékicheff and Tiddy [61] to assume that the formation of a bicontinuous cubic phase depends on the balance between the type of polar head group (which determines mainly the interfacial curvature) and restrictions on alkyl chain conformational freedom (which increases with increasing chainlength). To investigate this they studied the intermediate phase region of the lithium perfluoroctanoate/water system ($CF_3(CF_2)_6COOLi$). In this system the chains have a much lower flexibility than hydrocarbon chains and therefore a non-cubic intermediate phase was expected instead of a bicontinuous cubic phase. Using synchrotron radiation this was confirmed experimentally, with a tetragonal mesh phase being found, consisting of rods probably with an elliptical cross section, linked by fours to form surfactant layers with square holes. The distance between the layers was found to be almost identical to that in the lamellar phase. The water filled holes were found to be ordered on a body-centred tetragonal lattice. The holes of one layer thus coincide with junctions from adjacent layers. Since the junctions of the rods are probably thicker than the rest of the rods, Kékicheff and Tiddy [61] assumed that the high viscosity of this phase could be explained by the fact that it was body-centred. This means that flow of this phase causes junctions to move and coincide. The X-ray pattern for this phase showed texture, indicating the presence of large crystallites. The name T_1 was proposed for this phase. The symbol T_2 would denote the reversed phase, where the rods consist of water molecules and the continuous phase is formed by the surfactant molecules. The X-ray patterns of the lithium perfluoroctanoate/water system also indicated the persistence of defects or holes in the lamellar phase, which was consistent with NMR diffusion measurements (Kékicheff and Tiddy [61]). On increasing the temperature the diffuse peak in the X-ray patterns for the holes became broader and less intense indicating that at higher temperatures the correlations between the holes are lost.

- **Intermediate phases of non-ionic surfactants**

Other systems which have been widely studied in order to investigate the formation of intermediate phases are the non-ionic poly(oxyethylene) surfactants of the type $CH_3(CH_2)_{n-1}(OCH_2CH_2)_mOH$ or short C_nEO_m. The apolar part is a normal alkyl chain and the head group is formed by the poly(oxyethylene) glycol group, $-(OCH_2CH_2)_mOH$. These surfactants have the advantage that the size of both the alkyl chain and of the poly(oxyethylene) head group can be varied almost continuously so that these surfactants can be used as model systems to investigate the influence of these parameters on the phase diagram. The disadvantage of these substances is that they cannot be used for assessing the effect of counter ion size on surfactant phase behaviour, as they are non-ionic surfactants and thus do not have a counter ion.

Mitchell and Tiddy *et al.* [79] proposed a model phase diagram for poly(oxyethylene) surfactants, on the basis of interfacial curvature, the order of possible phases is (with increasing surfactant concentration): L_1 (isotropic micellar solution), I_1 (small micelles packed on a body or face-centred cubic lattice), H_1 (normal hexagonal phase), V_1 (cubic normal bicontinuous), L_α (lamellar phase), V_2 (reversed bicontinuous cubic phase), H_2 (reversed hexagonal phase). This sequence was derived on the basis of considerations of interfacial curvature of the different structural elements, the available area per polar head group, and experimental evidence of a large number of poly(oxyethylene) surfactants. In this sequence the interfacial curvature goes from positive in the isotropic micellar phase through zero curvature in the lamellar phase, to a negative curvature in the reversed phases.

Rançon and Charlovin [80] demonstrated with neutron diffraction experiments, the existence of epitaxial growth relations between lattice planes of the lamellar, cubic and hexagonal phase, for the non-ionic surfactant hexaethylene glycol mono-n-dodecyl ether-water system ($C_{12}EO_6$). Such epitaxial growth relations contribute to a better understanding of the overall transformation process between the lamellar to the hexagonal liquid crystalline phase. In subsequent research of oriented samples of the same non-ionic surfactant, Rançon and Charlovin [81] observed the occurrence of structural fluctuations both in the lamellar and in the hexagonal phase close to the transition to the cubic phase. These fluctuations in the lamellar phase lead to the fragmentation of the surfactant layers into cylinders parallel to the layers. These cylinders form a metastable hexagonal phase, from which the cubic phase is grown. The fluctuations in the normal (stable) hexagonal structure cause deformations of cylinders which are correlated from cylinder to cylinder. These deformations are likely to be the onset of ruptures and connections of cylinders in the formation of the cubic phase.

For a non-ionic surfactant with the same head group but a longer chainlength, hexaethylene glycol n-hexadecyl ether ($C_{16}EO_6$) Funari *et al.* [82] found an intermediate phase which appeared to be isotropic (cubic) on heating but which was anisotropic (possibly a mesh phase) on cooling. The system was also found to form a gel phase (symbol L_β) and in addition a *nematic* phase was discovered intermediate in composition between the isotropic micellar phase and the hexagonal phase. In a nematic (from the Greek for thread) phase there is alignment of the structural units in one direction, without any regular ordering. There is thus no long range order, only orientational order. In this case the nematic phase was thought to consist of micellar cylinders, arranged in one direction (this type of nematic is called N_C to differentiate it from a nematic phase formed by disc shaped micelles N_D). A defected lamellar phase (symbol $L_\alpha{}^H$) was also observed for this non-ionic surfactant, in composition between the other intermediate phase (cubic or mesh) and the lamellar phase. The defected lamellar phase exhibited a broad peak at small angle in the XRD pattern. The defects in the surfactant bilayers were thought to consist of uncorrelated water filled holes of elongated rectangular shape.

The intermediate phase region of this non-ionic surfactant ($C_{16}EO_6$) was further studied by Fairhurst, Leaver and Holmes [62]. Again on cooling from the lamellar phase a non cubic intermediate phase was observed that was not found to occur on heating from the hexagonal phase. On cooling from the lamellar phase the following phase sequence was found to take place: lamellar, defected lamellar, mesh phase, bicontinuous cubic (with the gyroid infinite periodic minimal surface), hexagonal and a two phase region of the hexagonal phase and a gel phase on further cooling. On heating from the hexagonal or two phase region the mesh phase was not observed, instead the cubic phase persisted into the region in the phase diagram, where the mesh phase had been found on cooling. Both a cubic and a mesh phase sample were prepared and were kept at constant temperature for three months to investigate the stability of both phases. After this period no changes were found to have occurred however. A rhombohedral layered mesh structure was proposed for the intermediate phase in which the surfactant rods have six fold connections. This structure was previously found for another non-ionic surfactant ($C_{30}EO_9$, see below).

The lyotropic phase behaviour of the non-ionic surfactant: nonaethylene glycol mono(11-oxa-14,18,22,26-tetramethylheptacosyl) ether, ($C_{30}EO_9$), was studied by Burgoyne, Holmes and Tiddy [83]. This system showed a non cubic intermediate phase, which unlike most intermediate phases was found to exist over a wide concentration range. For this intermediate phase the following four structures were considered: 1. a body-centred tetragonal layered mesh structure, 2. a body-centred bicontinuous tetragonal structure, 3. a rhombohedral layered mesh structure consisting of surfactant rods linked by threes to form hexagonally shaped water filled holes in the surfactant layers and 4. a rhombohedral layered mesh structure where the surfactant rods have six fold connections (see figure 3.9). Both rhombohedral variants could also be bicontinuous. Although optical microscopy observations indicated a layered structure, it could not be concluded decisively which the correct structure was. No defective lamellar phase was found in this system. A nematic rod phase was observed (by microscopy) to exist in between the isotropic micellar solution and the hexagonal phase. In subsequent studies of the same surfactant ($C_{30}EO_9$) Fairhurst, Holmes and Leaver [84] used a shear stress cell to produce oriented samples of the intermediate phase. The thus produced texture in the diffraction rings definitely ruled out the tetragonal mesh and bicontinuous phases. The structure was concluded to be the rhombohedral mesh phase with six fold connections between the rods. The induced orientation effects in the diffraction rings demonstrated the existence of epitaxial relations between the hexagonal and the mesh phase: the layers of the mesh phase were shown to grow parallel to the cylinders of the hexagonal phase (Fairhurst, Holmes and Leaver [84]).

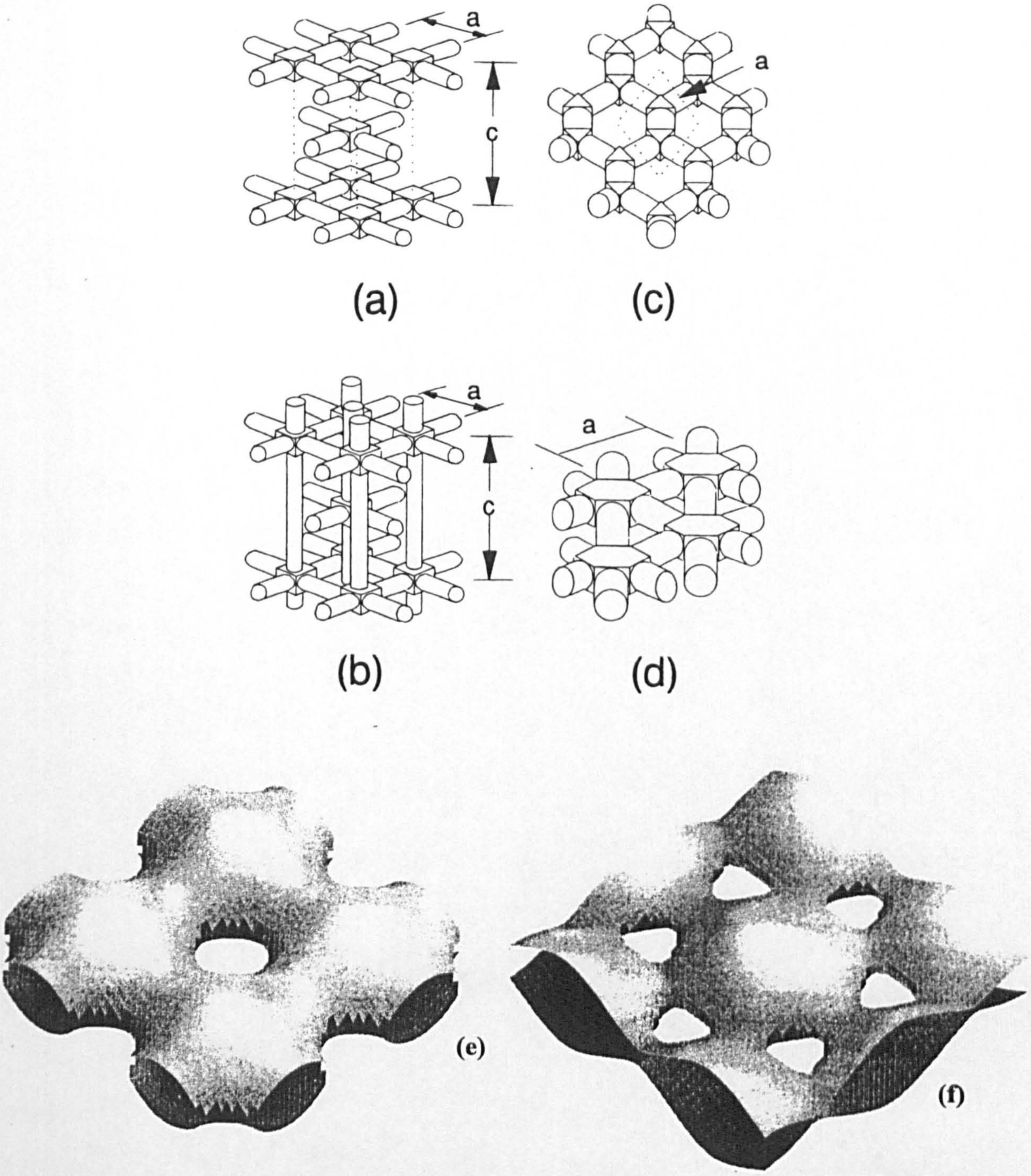

Figure 3.9 Possible structures proposed for intermediate phases of $C_{30}EO_9$ (from Burgoyne, Holmes and Tiddy [83]). The figure shows: (a) a centred tetragonal mesh structure, (b) a bicontinuous centred tetragonal structure, (c) one layer of a type of hexagonal mesh from which both a rhombohedral mesh and bicontinuous structures can be constructed and (d) one layer for a bicontinuous hexagonal structure. In figure (e) and (f) more realistic representations are shown of one layer of a centred tetragonal and a rhombohedral mesh structure respectively.

3.7 Trends in surfactant intermediate aqueous phase behaviour

In this section the influence of chainlength, head group, and counter ion on the type of intermediate phase formed is discussed, as has become apparent from a comparison of the phase behaviour of a large number of surfactants. A number of researchers do not consider the cubic phase as an intermediate phase and have occupied themselves with the question why some systems form cubic phases while others form intermediate phases (*i.e.* non-cubic intermediate phases). The phase behaviour of SDS has clearly demonstrated that this is not the right question to ask since SDS exhibits both cubic and non-cubic intermediate phases. The occurrence of a cubic phase for a certain surfactant therefore clearly does not imply that the surfactant does not also have the ability to form other types of intermediate phases.

The curvature of the aqueous/hydrocarbon interface depends on two parameters (*e.g.* Blackburn and Kilpatrick [58]):

1. The hydrocarbon volume, which depends on two factors: 1. the volume taken up by the hydrocarbon chain, which depends on chainlength, flexibility and structure. The chainlength can vary between the maximum all-trans length and a shorter value which depends on the flexibility of the chain. In a fluorinated carbon chain less gauche conformers will be present than in a hydrogenated carbon chain; the flexibility of the chain is also affected by the degree of saturation. 2. the presence of organic additives, such as fatty acids or long chain alcohols.
2. The area per polar head group. This is determined by inter- and intra-aggregate electrostatic forces, which depend on the head groups, degree of hydration, size of the counter ion and counter ion position relative to the head groups.

The effect of temperature on interfacial curvature is not well understood (Blackburn and Kilpatrick [58]. On the one hand an increase in temperature leads to a reduced hydration of the head groups and counter ions thus enabling a closer approach of these two charged entities, so that electrostatic repulsion between the head groups is reduced and which should result in a less curved interface. On the other hand the increase in temperature leads to an increase in entropy of the hydrocarbon chains and thus leads to the creation of more gauche conformers which reduces the effective chainlength, thus causing an increased surface curvature.

An increase in head group size leads to an increase in interfacial curvature, whereas an increase in chainlength acts to decrease the interfacial curvature. In general, independent of surfactant type, the interfacial curvature and the available area per polar head group decrease in the sequence: isotropic micellar solution, hexagonal phase, intermediate phases, lamellar phase, reversed intermediate phases, reversed hexagonal phase, reversed isotropic micellar solution ([Tiddy [20]). Cubic phases have certain interfacial curvatures which result from a balance of head group and chainlength size. This balance is achieved by short chainlength surfactants or by longer chainlength surfactants with larger head groups. Sodium soaps with a chainlength up to C_{10} form cubic phases, while from C_{12} upwards other types of intermediate phases are found. This is explained by Burgoyne *et al.* [83] in the following way: in bicontinuous cubic phases the surfactant bilayers are positioned on infinite periodic minimal surfaces in order to reduce interfacial curvature energy. The head group region however is *not* a periodic minimal surface. The infinite periodic minimal surface lies at the centre of the bilayer and roughly marks the location of the terminal methyl groups. An increase in surfactant chainlength moves the head group region further away from the IPMS, thereby increasing its surface curvature energy. As the chainlength (or the rigidity of the chain) is increased there comes a point where it is energetically more favourable for the system to form a structure which is not based on a minimal surface and a non cubic intermediate phase is formed. If the chainlength remains constant but the size of the head group is increased, as is the case with SDS in comparison to NaL, the surfactant can again can accomplish the interfacial curvature required for a cubic phase.

A comparison of the phase behaviour of sodium myristate which forms a non cubic intermediate phase and cesium myristate, which forms a cubic intermediate phase illustrates the influence the size of the counter ion on surfactant phase behaviour (Blackburn and Kilpatrick [58]). Sodium ions are smaller than cesium ions and can therefore approach the head groups more closely than cesium ions can and thus reduce the ionic repulsion between the carboxylate groups more than cesium ions can. The reduced repulsion of the head groups effectively leads to a reduction of the required area per polar head group and therefore leads to smaller surface curvature. This implies that the interfacial curvature of the non-cubic intermediate phase of NaM is less than the cubic phase of CsM. That not all non cubic intermediate phases have less interfacial curvature than cubic phases is demonstrated by SDS, where a non cubic intermediate phase is found in the phase diagram on either side of the cubic phase. One of these phases will thus have an interfacial curvature larger than that of the cubic phase, while the interfacial curvature of the other intermediate phase is smaller than that of the cubic phase.

The effect of the required area per head group and hydrocarbon volume on surfactant phase behaviour was further demonstrated by Blackburn and Kilpatrick [58], who investigated the effect of the following additives on the lyotropic phase behaviour of cesium myristate: salts (CsOH and CsCl), fatty acid (myristic acid) and a long chain alcohol (1-tetradecanol). Although ternary systems are outside the scope of this review, the results of this study demonstrate the influence of the area per head group and volume of the hydrocarbon chain on the phase behaviour of binary surfactant/water systems and in addition illustrate surfactant phase behaviour during soap boiling. Instead of the cubic intermediate phase formed without additives, Blackburn and Kilpatrick found that the addition of CsOH or CsCl enabled the formation of a non cubic intermediate phase (thought to consist of a planar network of rods, either tetragonal or rhombohedral). The electrolytes reduce the repulsive electrostatic interactions between the head groups, so that less curved structures are favoured by the system. Ternary systems of CsM, water and either fatty acid (cesium myristate) or 1-tetradecanol did not exhibit the non-cubic intermediate phase. The CsM-water-myristic acid system still formed the cubic phase. The addition of either myristic acid or the long chain alcohol led to a significantly larger area in the phase diagram for the lamellar phase. The effect of both substances is to increase the hydrocarbon volume and thus to decrease the preferred interfacial curvature. The observed influence of fatty acid and electrolyte concentration on the lyotropic structure formed, illustrates the phase behaviour of soaps during their manufacture: at the initial stages of soap boiling a large excess of fatty acids is present, inhibiting the formation of the unwanted viscous hexagonal phase. As the concentration of fatty acids decreases through the conversion to soaps, the risk of the formation of the hexagonal phase arises but this is avoided by the addition of salt or brine.

A mathematical model for calculating the free energy (based on an electrostatic and an interfacial term) of the lamellar and hexagonal phase, was proposed by Blackburn and Kilpatrick [85], with the aim of predicting which phase would be favoured by a surfactant-water system under certain conditions. The predictions of the model were compared with experimental results for sodium and cesium laurate. The model predicted the right trend but the predicted values compared poorly with the experimental results. Further work needs to show the feasibility of the model to predict the correct phase boundaries for the hexagonal, lamellar and possibly even for the intermediate phases.

3.8 Thermotropic mesophases

When low moisture content (or anhydrous) soap is heated, it gradually changes from the solid into the liquid state. Numerous phase transitions are known to occur in the wide temperature gap between the collapse of the three-dimensional crystalline structure and complete melting (Chapman [1]). The substance is therefore said to be in a mesomorphic state (intermediate form), the mesophases being thermotropic liquid crystalline phases. This phenomenon is also called "double melting". The formation of the thermotropic phases is the result of a balance between the strong electrostatic attraction between counter ions and head groups, and the weak attractive forces between alkyl chains. The former cause a tendency to form regular crystals, the latter forces are the driving force towards the liquid state (*e.g.* Tiddy [2]). The thermotropic phases are formed at temperatures between the T_c and the T_i curves which correspond to a temperature range from about 120°C up to around 350°C (*e.g.*

Pacor and Spier [86]). The structures formed under these conditions are explained in this section. These phases have not found any applications in the surfactant industry, as they only exist at very high temperatures. They are briefly discussed here however to provide a complete picture of surfactant phase behaviour and to demonstrate the variety of liquid crystalline structures formed by amphiphiles. Apart from the thermotropic liquid crystalline structures, anhydrous soap also exhibits a number of polymorphic crystalline structures up to about 120°C. Especially in early literature on soap phases the distinction between crystalline and liquid crystalline phases was not always clearly made.

3.8.1 Thermotropic liquid crystalline soap phases

Vold *et al.* [87, 88] used microscopy and dilatometry to demonstrate the existence of thermotropic liquid crystalline phases. First they found two phases for NaP, called the waxy and subneat soap phase and later [88] recognised six mesophases for this soap. These are, in order of increasing temperature: the curd fiber phase (which is a crystalline and not a liquid crystalline phase), subwaxy, waxy, subneat, neat and isotropic liquid (also called "nigre"). The transition temperatures are: curd to subwaxy 117°C, subwaxy to waxy 135°C, waxy to subneat 208°C, subneat to neat 253°C and neat to isotropic liquid 292°C. All transitions are reversible. Small quantities of water were found to cause profound changes in the transition temperatures [87]. With the addition of a small percentage of water, the anhydrous phases are brought a short distance within the hydrous region in the phase diagram, in the form of "tongues" inclining sharply downward [10]. In a subsequent study [89] Vold published the transition temperatures for NaL, NaM, NaP and NaS, also for the then known superwaxy phase, which lies between the waxy and the subneat phase. This makes the total phase sequence on increasing the temperature: the curd fiber phase (a crystalline phase), subwaxy, waxy, superwaxy, subneat, neat and isotropic liquid. Vold [89] assumed the lower temperature transitions to be associated with the arrangements of the hydrocarbon chains and the higher temperature transitions to be associated with the rearrangement of the polar groups of the molecules. De

Bretteville and McBain [90] studied the thermotropic phases of NaS by X-ray diffraction but did not determine any structures. They supposed the subwaxy and waxy phase to be crystalline and the soap to become liquid crystalline when the superwaxy phase is formed. This was contradicted by Nordsieck *et al.* [91] who found that the subwaxy and waxy phases are liquid crystalline as well.

Later, Skoulios and Luzzati [92, 93] used X-ray diffraction to investigate the thermotropic liquid crystalline phases of anhydrous sodium soaps. They found the following X-ray characteristics for all these phases: sharp peaks above 10Å and diffuse peaks between 3 and 5Å. The same diffuse band around 4.5Å was found as for the aqueous liquid crystalline phases, indicating the liquid nature of the hydrocarbon chains. Another indication for this was that the lamellar layers of the neat phase contract with increasing temperature. The following structures were proposed:

- For the subwaxy, waxy, superwaxy and subneat phase a ribbon-like structure was proposed: the carboxyl groups are localised in double layers forming ribbons of indefinite length. The space between the ribbons is filled by the liquid hydrocarbon chains (see figure 3.10a). The polar groups are thought to be organised in a crystalline manner, at least in a first approximation. The ribbons are parallel to one another and are ordered in an orthorhombic array which becomes almost hexagonal in going from subwaxy to subneat by increasing the temperature (Skoulios and Luzzati [92, 93]). The ribbons for potassium soaps are ordered in a two-dimensional oblique structure, the exact structure depends on the temperature (Gallot and Skoulios [94]). A characteristic peak appears in the X-ray spectrum for the ribbon-like structure around 3Å (Skoulios and Luzzati [92, 93]). In the subneat to neat transition the organisation of the carboxyl groups collapses [92, 93]. Pacor and Spier [86] later used DTA and DSC to show a large heat effect associated with the subneat to neat transition, which agrees with a major molecular arrangement from two- to one-dimensional order.

- The neat phase was found to have a smectic lamellar structure (Skoulios and Luzzati [92, 93]). Apart from the diffuse 4.5Å band the neat phase shows a number of spacings above 10Å with a ratio of 1:1/2:1/3:1/4:1/5. The intensity of these peaks decreases monotonically. This indicates a lamellar structure where the polar groups are localised in double layers of indefinite length, separated by liquid hydrocarbon chains, similar to the structure of the aqueous lamellar phase. A DTA study of Madelmont and Perron [16] of the phase diagram of NaL showed that the structure of the aqueous lamellar phase is directly derived from the structure of the anhydrous neat phase. These phases are thus essentially the same and therefore the corresponding areas in the phase diagram should be connected.

- For NaL a new phase was found (Skoulios and Luzzati [92, 93]) between 200 and 215°C (between superwaxy and subneat), which showed five sharp peaks above 10Å, apart from the diffuse band at 4.5Å. The existence of this phase was later confirmed by Pacor and Spier [86] using DTA and DSC. Skoulios and Luzzati [92, 93] proposed a structure in which discs are formed by double layers of polar groups. The spaces between the discs are filled by the liquid hydrocarbon chains. The discs are organised in an orthorhombic lattice [92, 93] (see figure 3.10b). The exact structure of the discs depends on the temperature (Gallot and Skoulios [94]).

- The isotropic liquid phase was found not to be amorphous but to resemble the structure of the neat phase (Skoulios and Luzzati [92, 93]). It is possible that in the isotropic liquid phase small regions exist where groups of molecules form a similar structure to that of the neat phase. In their DTA/DSC study Pacor and Spier [86] found a small heat effect for the neat to isotropic transition, which is consistent with a model of the isotropic phase as a liquid which is organised similarly to the neat phase.

An NMR study by Lawson and Flautt [95] confirmed the phase transitions previously reported and in addition showed the existence of another phase for NaM, between the waxy and superwaxy phase. Subsequent X-ray studies were carried out for liquid

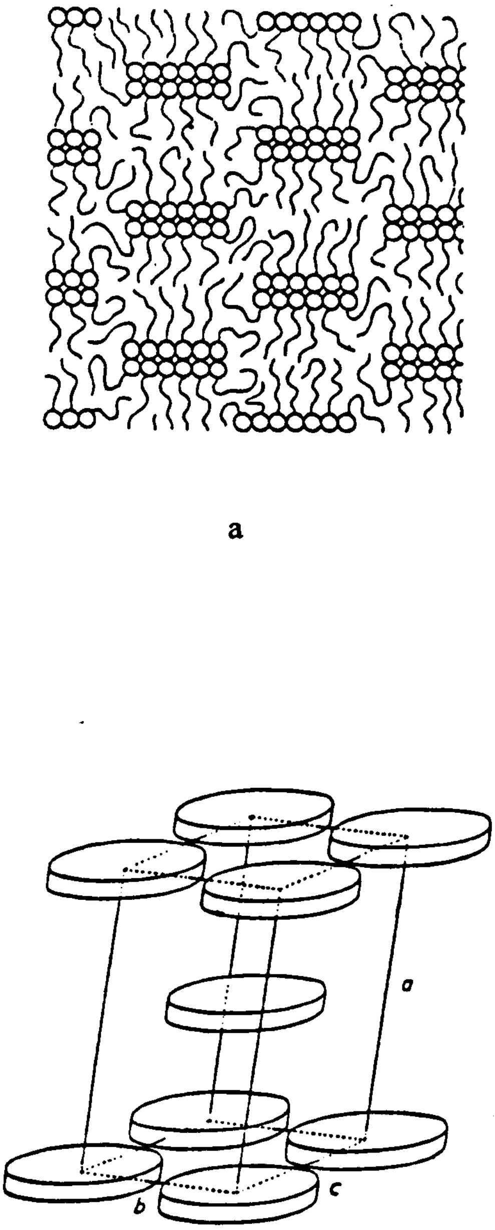

a

b

Figure 3.10 Schematic representation of (a) the ribbon-like structure of the subwaxy, waxy, superwaxy and subneat phase and (b) a disc structure from Chapman [1]

crystalline phases of anhydrous soaps of other cations: *e.g.* Gallot and Skoulios [94, 96] for potassium soaps, and [60 and 97-100] for divalent soaps. KP and KS were found to form a ribbon-like structure [94], where the ribbons were organised in an oblique pattern [94, 96]. A disc-like structure was found to exist for KM, the other potassium soaps did not form this phase [94]. All potassium soaps formed another type of lamellar phase at temperatures above the neat phase (above 270°C). Gallot and Skoulios [94] called this phase, in which both polar groups and hydrocarbon chains are in the liquid state, the *labile lamellar phase*.

For thermotropic phases of divalent soaps (calcium and strontium) Luzzati *et al.* [1, 60] found three-dimensional networks of rods forming tetragonal and hexagonal mesh phases as well as cubic phases [60, 100], whereas the monovalent sodium and potassium soaps only form lamellar structures in which the polar groups are localised in lamellar regions, such as ribbons, discs and infinite planar sheets. Luzzati *et al.* [1, 60] therefore concluded that the structure of the thermotropic phase formed mainly depends on the polar groups [1].

3.9 Crystalline soap phases

In the following section the crystalline polymorphs of sodium soaps are discussed. Although the existence of many polymorphs has been reported in literature, no full structure of a sodium soap has yet been determined. Thiessen and Spychalski [101, 102] were amongst the first to study soaps with X-ray diffraction, some unit cells parameters were published (see table 3.7). Later Thiessen and Stauff [27, 103] discovered the existence of two polymorphs of sodium palmitate and stearate, of which they managed to grow single-crystals. The two forms were labelled α and β. The α form was unstable and was thought to have an orthorhombic structure, the stable β form was thought to have a monoclinic structure. Crystallisation from alcohol results in the α form. The transition between the two polymorphic forms was found to occur around the melting point of the corresponding fatty acid. This point is called the *genotypic point* [26] (for NaP about 42°C and for NaS about 50°C). Vold *et* *al.* [88] also found an indication of a crystalline polymorphic transition at the genotypic point as Thiessen and Stauff [26,27,103] had reported, but assumed this transition to be associated with a minor structural change. The transition is irreversible. Thiessen and Stauff explained the polymorphic transition in terms of interactions between the polar groups of the soap molecules. They assumed there to be two ways in which two soap molecules can form a "double molecule"; either *trans* in which case the α polymorph is formed or *cis* which results in the β form (see figure 3.11). Evidence for this would be that soap crystallised from an apolar solvent results in the β form while soap crystallised from alcohol forms the α form. The alcohol molecules have a dipole which interferes with the associations between the soap dipoles so that the stable β structure cannot be formed. Later, Buerger *et al.* [104] showed that the α and β form are different hydrates. Not only could the α form be converted to the β form by heating or by grinding, the reversed transition from the β to the α form was also found to be possible and to occur when some water was added to the β form whilst heating the sample. The hydrate nature of sodium palmitate was investigated by McBain *et al.* [29] who found that much of the water in soap curd is not actual water of hydration but is held in there by the capillary forces of the soap fibers. Buerger *et al.* [104] showed the α form to be monoclinic instead of orthorhombic and later (Buerger [105, 106]) determined the unit cell parameters for the α form of NaP and NaS (see table 3.8). The unit cells were thought to contain 16($NaP.1/2H_2O$) and 16($NaS.1/2H_2O$) molecules respectively.

A third crystalline polymorphic form of sodium stearate was found by De Bretteville and McBain [107]. This form was called γ to conform with the notation of Thiesssen and Stauff. However, this form was called the ω form by Proctor & Gamble laboratories (Ferguson *et al.* [108]). De Bretteville and McBain [107] produced this γ form by drying sodium stearate, obtained from the reaction between stearic acid and sodium alcoholate, at 105°C. In addition, it was found (Ferguson *et al.* [108, 109]) that rapid chilling from the lamellar liquid crystalline phase induces the formation of the γ phase while slow cooling induces the β form. Thus not only the crystal size and orientation depend on the processing of the material, but also the phases present in

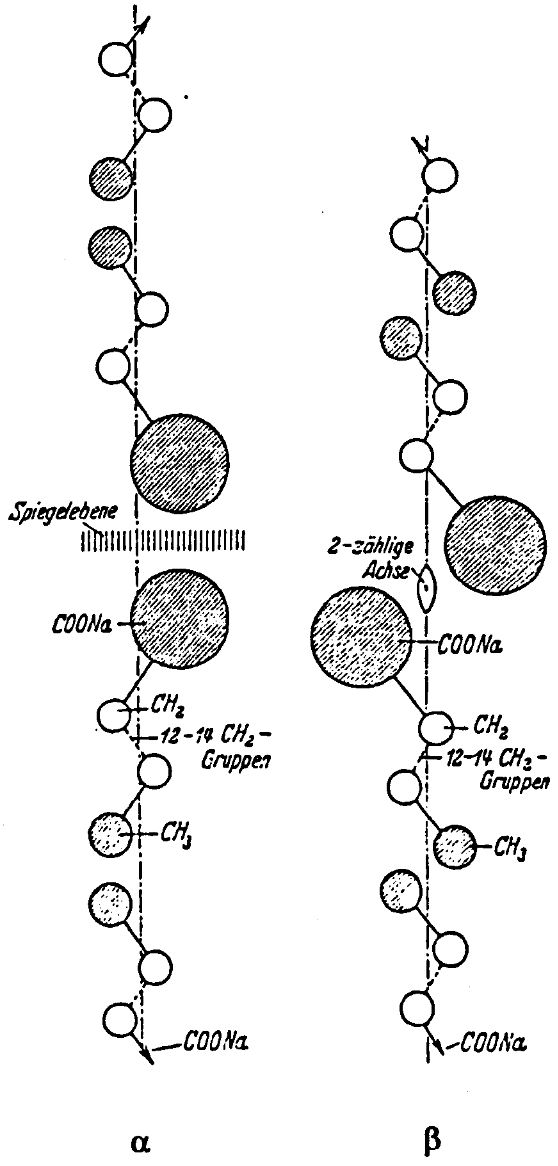
Spiegelebene
COONa
CH₂
12-14 CH₂-Gruppen
CH₃
COONa
α
2-zählige Achse
COONa
CH₂
12-14 CH₂-Gruppen
CH₃
COONa
β

Figure 3.11 The α and β form of sodium soaps according to Thiessen and Stauff [27, 103]

the final product (Ferguson et al. [108, 109] and Vold *et al.* [110]). These phases affect factors like the hardness, solubility and transparency of the final product [10]. An example of processing conditions which can lead to a polymorphic phase transition is the extrusion of soap through an opening. This was found to convert either the γ to the β phase or the β to the γ phase, depending on the exact conditions used (Ferguson [109]). The degree of stirring of the sample during crystallisation can also affect the structure formed (Ferguson *et al.* [108, 109]). Vold *et al.* [110] studied a number of commercially available soap bars and found that the hardness of a soap bar not only depends on the crystalline structure but also on the degree of orientation and size of the crystallites. These parameters depend strongly on the processing history of the soap bar. In addition the hardness of the soap bar was found to be different in the centre from the outside. This effect was thought to be due to the fact that during cooling the cooling rate in the centre is different from that in the outside.

The following long spacings were found to be characteristic for the different forms of sodium stearate: α form 51.8Å, β form 46.6Å, γ form 44.6Å (De Bretteville and McBain [107]). Buerger *et al.* [104] showed that the β form of NaS could be converted to the γ form by heating and concluded that the α form is most hydrated, the β form has an intermediate hydration state and the γ form is least hydrated. Analysis indicated the following hydration states: α=NaS.1/2H_20, β=NaS.1/8H_20 and the γ form was thought to be anhydrous. The hydrate nature of soap has been investigated by several authors; McBain *et al.* [29] for example had already found the existence of a large number of definite hydrates of soaps. McBain *et al.* [8] found that NaM to NaS all form hemihydrates, whereas NaL does not. NaP also forms other hydrates up to NaP.10H_2O [4]. Later Ferguson [109] listed the existence of 16 different definite hydrate forms (ranging from NaP.1/8H_2O to NaP.30H_2O) previously reported and argued that the different polymorphic forms are not related to different hydrates.

The fourth polymorphic form of sodium soaps was described by Ferguson *et al.* [108] and was called δ. This form can be obtained by rapid cooling from dilute solution or by extrusion at relatively high moisture content (Ferguson *et al.* [108, 109]). Characteristic d-spacings for the different phases were found to be independent of the chainlength of the soaps present in the sample (whether single soaps or mixtures), thus enabling the identification of the various polymorphic forms present in commercial soaps (Ferguson *et al.* [108, 109], see table 3.5).

polymorph	**characteristic spacings (Å)**
α	2.45 and 3.65
β	2.75
γ	2.95
δ	2.85 and 3.55

Table 3.5 Characteristic d-spacings for the different forms of soap (from Ferguson *et al.* [108, 109])

Buerger *et al.* [24] later discussed the existence of *seven* distinct soap phases. It was claimed that both the β and the γ form (which they called ω) were in reality mixtures of at least two phases: for the γ form these phases were labelled κ and η; the β phase was thought to be made up of ε and ζ. In addition they found a phase which they called μ. The phase separation of the β phase into the ε and ζ phase and the separation of the γ phase into the κ and η phase was found to occur after severely working the sample. Which polymorphic structure can be formed depends on the chainlength of the soap, see table 3.6.

Buerger *et al.* [24] suggested that these seven forms have fundamentally different crystal structures, each of which can exist as a number of different hydrates. For example α is more hydrated that α' etc. This would indicate the existence of a very large number of (pseudo) polymorphic forms. In addition to these forms, later another form was found for NaP, called the σ form by Gardiner, Buerger *et al.* [111], who studied NaM, NaP and NaS by dehydration and X-ray techniques. Their studies were consistent with previous studies in showing the α form of NaS to be a hemihydrate (a hydrate containing half a molecule of water per soap molecule) which changes to the β form on losing 3/8 H_2O per mole of soap. Several other changes in hydration state were observed and the following was concluded for the various phases of NaP: ζ=$NaP.3/8H_2O$, β=ζ'=$NaP.1/8H_2O$, ε=$NaP.1/2H_2O$, ε'=$NaP.1/8H_2O$, δ=$NaP.1/2H_2O$, δ'=$NaP.1/6H_2O$, and σ=NaP (anhydrous) (Gardiner, Buerger *et al.* [111]). The effect of mechanical working on the phase formed in NaP was studied by Buerger *et al.* [25]. Although the machine used for the mechanical working did not resemble any of the equipment used during industrial soap making, it was shown that different soap phases could be produced depending on the processing conditions.

form	**NaL**	**NaM**	**NaP**	**NaS**
α				x
β consisting of				
ε			x	x
ζ	x	x	x	x
γ consisting of				
κ	x	x		
η				
δ			x	x
μ		x		

Table 3.6 Showing the different polymorphs each soap can form according to Buerger *et al.* [24]

unspecified forms	**NaL**	**NaM**	**NaS**
[101]	orthorhombic a=7.6 b=? c=30.1	orthorhombic a=7.2 b=5.0 c=33.9	orthorhombic a=7.6 b=4.9 c=42.9
[102]		orthorhombic a=3.8 b=5.0 c=34.8	orthorhombic a=4.0 b=5.0 c=44.8

Table 3.7 Cell parameters of unspecified forms of sodium soaps

form	**NaM**	**NaP**	**NaS**
α [27, 103]		orthorhombic a=8.06 b=9.24 c=47.70	orthorhombic a=8.04, b=9.24, c=51.77
[104, 105]		monoclinic 16(NaP.1/2H_2O) per unit cell a=9.13 b=8.01 c=91.85 β=?	monoclinic 16(NaS.1/2H_2O) per unit cell a=9.16 b=8.00 c=103.96 β=93.72°
[106]		monoclinic 16(NaP.1/2H_2O) per unit cell a=9.13 b=8.01 c=91.85 β=94°	monoclinic 16(NaS.1/2H_2O) per unit cell a=9.16 b=8.00 c=103.96, β=93.2°
[112]	monoclinic NaM.1/2H_2O a=9.32 b=8.00 c=82.63 β=93.75°	monoclinic NaP.1/2H_2O a=9.23 b=8.01 c=92.94 β=94°	monoclinic a=9.21 b=8.03 c=113.45 β=93.5°
β [27, 103]		monoclinic a=7.83 b=5.40 csinβ=42.10	monoclinic a=7.80 b=5.33 csinβ=46.10
[104]			NaS.1/8H_2O
γ(=ω) [104]			NaS anhydrous

Table 3.8 Proposed cell parameters for various sodium soaps polymorphs

Minor and Lingafelter [112] found that crystallisation of NaS from alcoholic solution could result in two different polymorphs, one being the α form, the other remained unidentified. In the same paper Minor and Lingafelter published cell parameters for the monoclinic α form of NaM, NaP and NaS, see table 3.8. The value of the c axis of the unit cell given by Minor and Lingafelter is about 10Å larger than that reported by Buerger *et al.* [104, 105]. The variety of cell parameters which have been published for sodium soaps is illustrated by table 3.7 and 3.8.

Later, in the 1970s DTA studies of Madelmont and Perron [16] showed the existence of three polymorphic structures for the hemihydrate of NaL [11] as well as for NaM [14]. They labelled these polymorphs C_1, C_2 and C_3. The transitions between these forms were found to be reversible. For NaL the C_1 form was found to exist up to 68°C, the C_2 from between 68°C and 104°C and the C_3 form between 104°C and 133°C (Madelmont and Perron [16]). It is not known to which Greek letter labels these soap phases correspond.

Recently, Gupta [113] undertook a DSC study of commercial soap bars, with the purpose of quantifying by DSC measurements the relative amounts of the polymorphic forms present in a soap bar. In this way some of the properties of soaps can be predicted on the basis of simple DSC measurements, since the relative amounts of the various polymorphic forms are responsible for the key functional properties of the soap bar, such as the amount of lather, the dissolution rate, the development of cracks in the bar during its use and the swelling of wet soap. With the developed method Gupta was able to identify the relative amounts of the β, δ and γ (=ω) form present in commercial soaps and proposed equations with which the lathering value and the solubility index of a soap bar can be predicted when the relative amounts of the various polymorphic forms are known. This is based on the various properties of the different polymorphic forms presented in table 3.9

From the previous section it is clear that the number of polymorphs of sodium soaps has not been established beyond doubt and no crystal structure has yet been determined. Therefore in the following a concise overview of polymorphism in potassium soaps is given, since one structure has been determined for KP and as the structures of sodium and potassium soaps are likely to be similar. For potassium soaps four forms were found by Vand *et al.* [114] designated A, B, C and D, where the A, B and C form were thought to be anhydrous and the D form hydrated. The angle of tilt was thought to decrease in the order A, B, C, D. The monoclinic A form was obtained for soaps with a chainlength ranging from C_4 to C_{10} crystallised from alcohol, the (probably triclinic) B phase was formed by soaps from C_{12} to C_{18} crystallised from alcohol and the C polymorph was formed by all soaps after heating. The D form was observed at lower temperatures (not specified). The unit cell parameters and space group of a single crystal of the A form of potassium caprate (KC_{10}) were determined: a=8.09, b=5.63, c=28.81, β=108°, $P2_1/a$ and four molecules per unit cell. It is not known if there are any direct structural relations between the A, B, C and D form of the potassium soaps and the α, β, γ and δ form of the sodium soaps.

soap properties	β	γ	δ
firmness (arbitrary units)	8.0 (most firm)	7.2	3.0 (least firm)
% rub off (in water)	2.4	0.5	1.7
soaking (in water)	swells and disintegrates	no swelling or disintegration	cracks with little swelling
solubility	rapidly soluble	poorly soluble	medium solubility
lathering	easy lathering	poor lathering	medium lathering

Table 3.9 Physical properties of the β, γ and δ forms of soap (from Gupta [113])

Polymorphism in potassium soaps was further studied by Lomer [115], who determined cell parameters of the A, B and C forms of potassium soaps, ranging from

C_4 to C_{18}. Lomer found that on cooling from the C phase all soaps reverted back to their original phase with one exception. This is KL which crystallises from alcohol in the B phase, transforms on heating to the C phase but transforms to the A phase on cooling. This phase however is unstable and reverts over a period of months to the original B phase. The above described polymorphism of potassium soaps is summarised in tables 3.10 and 3.11.

Polymorphism in potassium soaps	
C_4-C_{10}	$\text{crystallisation from alcohol} \longrightarrow \text{A form} \underset{\text{cooling}}{\overset{\text{heating}}{\rightleftarrows}} \text{C form}$
C_{12}	$$\begin{tikzcd} \text{crystallisation from alcohol} \arrow[r] & \text{B form} \arrow[rr, "\text{heating}"] & & \text{C form} \arrow[dl, "\text{cooling}"] \\ & & \text{A form} \arrow[ul, "\text{time}"] & \end{tikzcd}$$
C_{14}-C_{18}	$\text{crystallisation from alcohol} \longrightarrow \text{B form} \underset{\text{cooling}}{\overset{\text{heating}}{\rightleftarrows}} \text{C form}$

Table 3.10 Polymorphism in potassium soaps from Lomer [115]

KC_{12}	B → C (heating)	54°C
KC_{12}	C → A (cooling)	54°C
KC_{14}	B → C (heating)	61°C
KC_{16}	B → C (heating)	68°C
KC_{18}	B → C (heating)	78°C

Table 3.11 Transition temperatures for potassium soaps (from Lomer [115])

Several years later Dumbleton and Lomer [116] solved the structure of the B form of KP (see figure 3.12). For this purpose they managed to grow single crystals of KP which looked like extremely thin plates. The B form was found to be triclinic with unit cell parameters: a=4.15, b=5.60, c=37.82; α=93.0°, β=91.4°, γ= 92.4°. The space group is $P\bar{1}$ with two molecules per unit cell, crystallographic density=1.109g/cm^3. The potassium and oxygen atoms form double layers, which are separated from each other by the hydrocarbon chains, the structure is thus very similar to that of a lamellar liquid crystal (see figure 3.13).

From the above it is clear that the exact number of sodium soap polymorphs and their structures are not yet known. At least four different forms exist (which may be mixtures of phases) of which three are found in commercial soap bars (the β, γ and δ form). These different forms can be obtained by different processing conditions: the rate of stirring and cooling during crystallisation, heating, milling and extrusion all affect the relative amounts of the various polymorphs present in the final product. Some of these phase transformations that occur during processing might take place through a liquid crystalline phase. Important properties of commercial soaps such as the amount of lather, the dissolution rate, the development of cracks in the bar during its use etc., highly depend on the mixture of crystal structures present in the product. The lack of fundamental knowledge of the soap phases (such as crystal structures) is likely to be due to the fact that results are difficult to reproduce since a sample's crystal structure depends strongly on its processing history and chemical composition.

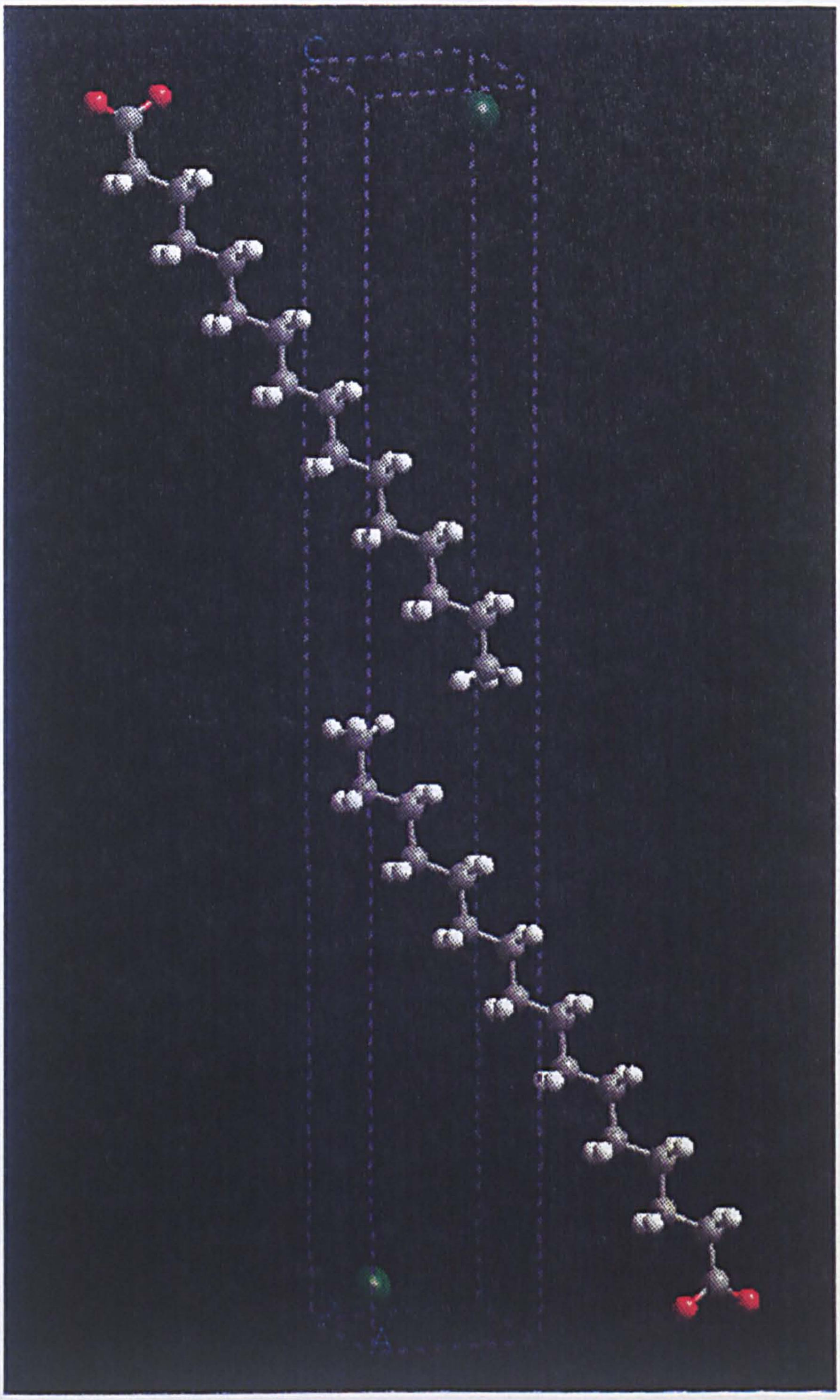

Figure 3.12 Crystal structure of potassium palmitate. Unit cell parameters: a=4.15, b=5.60, c=37.82, α=93.01, β=91.40, γ=92.40, space group P–1 (from Dumbleton and Lomer [116])

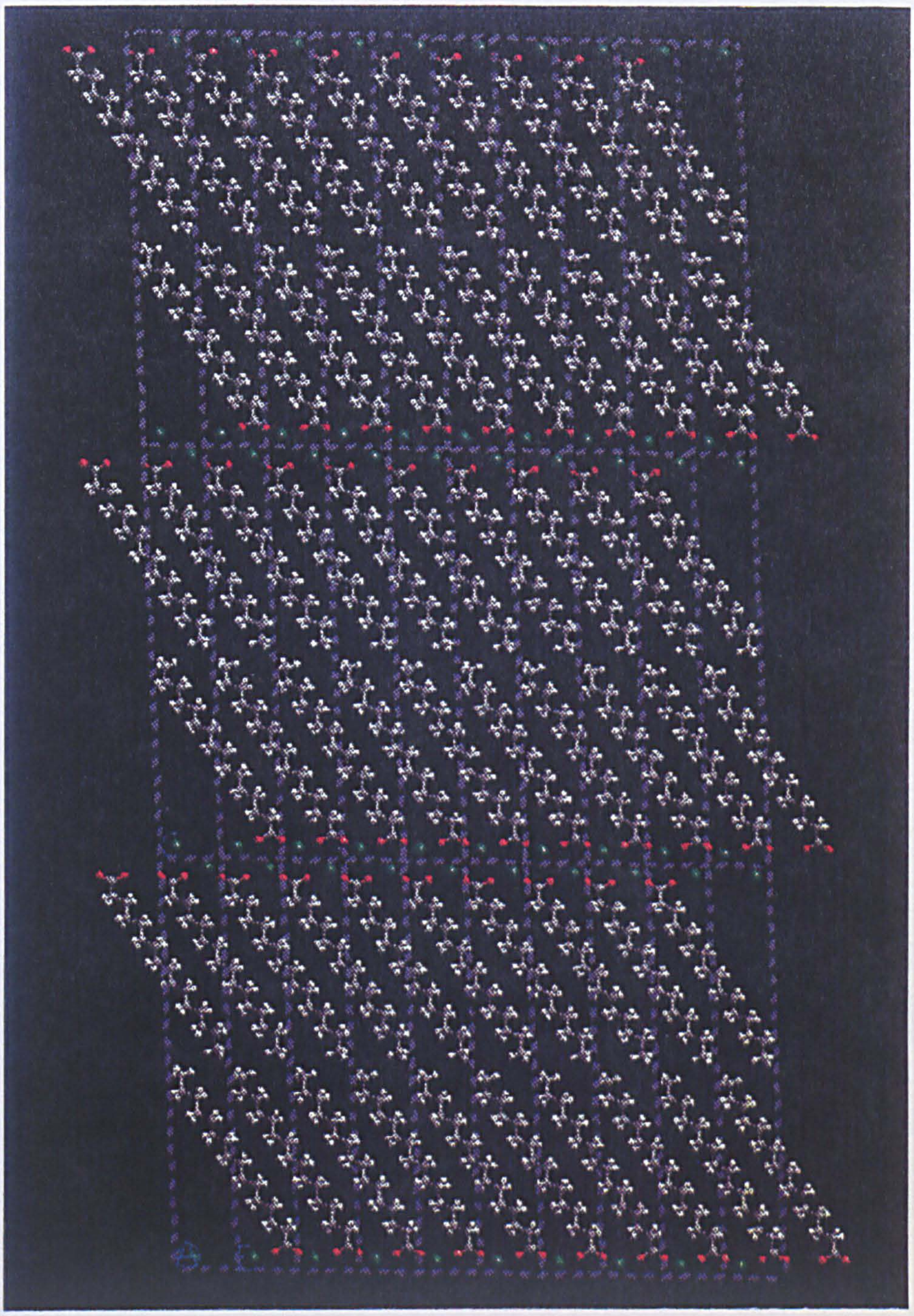

Figure 3.13 A series of unit cells of potassium palmitate illustrating the resemblance with a lamellar liquid crystalline phase (based on structure from Dumbleton and Lomer [116])

3.10 Summary of surfactant phase behaviour

From this chapter it is clear that soaps have the ability to form a large variety of crystalline and liquid crystalline structures. Apart from chainlength, head group and counter ion, the structure formed depends on temperature, concentration and processing history. Despite the great commercial importance of these systems, there still remains much uncertainty about the existence and exact nature of a number of solid and liquid crystalline soap phases and the transitions between them.

The manifold of phases formed by surfactants can be graphically depicted in binary phase diagrams. At temperatures and compositions below the T_c curve sodium soaps exist as a coagel, between the T_c and the T_i curve, the short range order breaks down and a liquid crystalline (lyotropic or thermotropic) is formed. In lyotropic liquid crystals, although the headgroups are confined to the hydrophobic-water interface and the water to the water channels, the molecules are in every other way in a fluid form and randomly diffuse over many unit cells each second (Gruner [52]).

Most of the literature on sodium soaps is rather old, while in recent years different types of lyotropic phases have been discovered for other surfactant systems. These systems have been discussed here in order to demonstrate the effect of counter ion, head group, chainlength and additives on surfactant aqueous phase behaviour. An increase in head group size leads to an increase in interfacial curvature. A smaller counter ion can achieve a closer approach of the headgroups, thus reducing their electrostatic repulsions and therefore leads to a decrease in interfacial curvature. A longer (or less flexible) apolar chain has the same effect. Therefore for systems with a bulky hydrophilic group with respect to the hydrocarbon moiety, the hexagonal phase range will be more extended. When *vice versa* the hydrocarbon chains are bulkier, the lamellar phase range will be more extended. These effects are generic for a large number of systems ranging from polymers to biological lipids.

The three most powerful methods for studying liquid crystals have proved to be:

1. X-ray (or neutron) diffraction for exact determination of aggregate size and available area per polar head group. The interpretation of the results has been greatly aided by the use of oriented samples, which in addition have revealed epitaxial relations between certain liquid crystalline phases.
2. NMR provides information on order, rotation and diffusion of molecules and can in some cases be used to distinguish bicontinuous from non bicontinuous structures.
3. Polarised light microscopy, with which phases can be identified by comparing their characteristic textures and through a qualitative assessment of the viscosity of the liquid crystalline phase, in general:

$$\text{viscosity}_{\text{cubic}} > \text{viscosity}_{\text{hexagonal}} > \text{viscosity}_{\text{lamellar}}$$

The variety of lyotropic mesophases is summarised in table 3.12 which illustrates the varying types of order which can be found in a phase sequence (amorphous, one-, two-, or three-dimensional long range order). The symbols most frequently encountered in literature are also given in table 3.12. A subscript "1" usually refers to normal phases (water continuous with a positive interfacial curvature), whereas the subscript "2" usually denotes a reversed phase (hydrocarbon continuous with negative interfacial curvature). The lamellar structure with zero interfacial curvature constitutes a natural connection between normal and reversed phases. The interfacial curvature as well as the available area per polar head group decrease in going through a phase sequence from the normal phases through the lamellar phase to the reversed phases. In addition the available area per polar head group increases with increasing temperature but is almost independent of the length of the hydrocarbon chain (Gallot and Skoulios [39], or see appendix A). No example is known of a surfactant which forms all phases listed in table 3.12.

The number of intermediate lyotropic liquid crystalline phases and their molecular structures for aqueous single sodium soap systems have not unambiguously been established; the structure of the complex hexagonal phase is probably incorrect. In addition no data at all is available up to date on the existence of intermediate phases for binary sodium soap mixtures with water. For these reasons an investigation was undertaken which focused on the crystallisation of single and mixed sodium soap systems from liquid crystalline phases. The results are presented in chapter 7.

Phase	**symbols used**	**type of order**
aqueous surfactant monomer solution	W	amorphous
nematic rod phase	N_C	orientational order, no long range order
isotropic micellar	L_1	amorphous
cubic phase consisting of small micelles (spheres, rods or discs) packed on a cubic lattice, can be primitive, fcc or bcc	I_1, I''_1, S_{1c}	3-D
hexagonal or middle phase	H_1, H_α	2-D
intermediate phases		
• deformed hexagonal, consisting of deformed rods or ribbons with probably elliptical cross-section 1. if packing is undetermined 2. if packing is 2-D monoclinic	H_{1d} or, R M_α or $M_{\alpha\text{-}2d}$	2-D
• rhombohedral (planar networks of rods, the rods have either three or six fold connections)	Rh, R_α	
• complex hexagonal	H_c	2-D
• bicontinuous cubic possibly with infinite periodic minimal surfaces	V_1, VI, Q_1, I'_1	3-D
• rectangular	R_1	
• tetragonal	T_1, T_α	
• defected lamelllar (lamellar phase with defects at irregular positions)	L_α^H	
lamellar or neat phase	L_α	1-D
reversed intermediate phases		
• reversed tetragonal mesh phase	T_2	
• reversed bicontinuous cubic possibly with infinite periodic minimal surfaces	V_2, Q_2, I'_2	3-D
reversed hexagonal	H_2	2-D
cubic phase consisting of small reversed micelles (spheres, rods or discs) packed on a cubic lattice	I_2, I''_2	3-D
reversed spherical micelles	L_2	amorphous
crystalline solid, various polymorphs	S, C, X	3-D
gel phase	L_β	3-D

Table 3.12 Demonstrating the variety of symbols used to denoted the same phases

3.11 References used in this chapter

1. Chapman D (ed), *Biological Membranes: Physical Fact and Function*, chapter 3 page 71 (by Luzzati), Academic Press, London and New York (1968)
2. Tiddy GJT, *Physical Reports* **57**, pages 1-46 (1980)
3. Davidsohn J, Better EJ and Davidsohn A, *Soap Manufacture* volume 1 (1953) Interscience publishing company, New York
4. Reiss-Husson F and Luzzati V, *Advances in Biological and Medical Physics* **11**, 87 (1967)
5. Hartshorne NH, *The microscopy of liquid crystals*
6. Glatter O, *Journal de Physique IV* 3, 27 (1993)
7. Glatter O, Scherf G, Schillén K and Brown W, Characterisation of a Poly(ethylene oxide)-Poly(propylene oxide) Triblock Copolymer (EO_{27}-PO_{39}-EO_{27}) in Aqueous Solution, submitted to *Macromolecules* (1994)
8. McBain JW and Lee WW, *Oil and Soap* **20**, 17 (1943)
9. McBain JW and Sierichs WC, *The Journal of the American Oil Chemists' Society*, p 221 (June 1948)
10. D Swern (ed), *Bailey's Industrial Oil and Fat Products*, **vol 1, 4th ed**, J Wiley and Sons (1979)
11. Luzzati V, Mustacchi H and Skoulios AE, *Nature* **180**, 600 (1957)
12. Madelmont C and Perron R, *Bulletin de la Société de Chimique de France*, **12 pt 1**, 3259-3263 (1973)
13. Madelmont C and Perron R, *Bulletin de la Société de Chimique de France*, **12 pt 1**, 3263-3268 (1973)
14. Madelmont C and Perron R, *Bulletin de la Société Chimique de France*, **9-10 pt 1**, 1795-1798 (1974)
15. Madelmont C and Perron R, *Bulletin de la Société Chimique de France*, **9-10 pt 1**, page 1799-1805 (1974)
16. Madelmont C and Perron R, *Bulletin de la Société Chimique de la France* **3-4 pt 1**, 425-429 (1974)
17. Madelmont C and Perron R, *Bulletin de la Société de Chimique de France* **3-4 pt 1**, 430-434 (1974)

18.Madelmont C and Perron R, *Colloid & Polymer Sci* **254**, 581-595 (1976)

19.Winsor, PA, *Chemical Reviews* vol 68 no.1, 1-38 (1968)

20.Tiddy GJT, *Modern Trends of Colloid Science in Chemistry and Biology*, edited by Eicke, Birkhäuser Verlag Basel (1985)

21.Bleasdale TA and Tiddy GJT, *The structure, dynamics and equilibrium properties of colloidal systems*, edited by Bloor DM and Wyn-Jones E, Kluwer Academic Publishers (1990)

22.Gray GW and Winsor PA (eds), *Liquid Crystals & Plastic Crystals*, volume 2, J Wiley and Sons(1974)

23.Gunstone FD, Harwood JL and Padley FB, *The Lipid Handbook*, (sec. ed., 1994) chapter 8, Chapmann and Hall London and New York (1986)

24.Buerger MJ, Smith LB, Ryer FV and Spike JE Jr, *Proceedings of the National Academy of Sciences* **31**, 226 (1945)

25.Buerger MJ, Smith LB and Ryer FV, *The Journal of the American Oil Chemists' Society* **24**, 193 (1947)

26.Thiessen PA, *Angewandte Chemie* **51**, 318 (1938)

27.Thiessen PA and Stauff J, *Zeitschrift für physikalische Chemie* A **176**, 397 (1936)

28.Luzzati V and Husson F, *Journal of Cell Biology* **12**, 207 (1962)

29.McBain JW, Vold MJ and Johnston SA, **63**, 1000 (April 1941)

30.Vincent JM and Skoulios A, *Acta Crystallographica* **20**, 432 (1966)

31.Vincent JM and Skoulios A, *Acta Crystallographica* **20**, 441 (1966)

32.Vincent JM and Skoulios A, *Acta Crystallographica* **20**, 447 (1966)

33.McBain JW and Ross S, *Oil and Soap*, p 97 (1944)

34.Rosevear, FB, *Journal of the American Oil Chemists' Society* **31**, 628 (1954)

35.Reiss-Husson F and Luzzati V, *Journal of Physical Chemistry* **68**, 3504 (1964)

36.Luzzati V, Mustacchi H and Skoulios AE, *Discussions of the Faraday Society* **25**, 43 (1958)

37.Luzzati V, Mustacchi H and Skoulios AE, Husson F, *Acta Crystallographica* **13**, 660, (1960)

38.Husson F, Mustacchi H and Luzzati V, *Acta Crystallographica* **13**, 668 (1960)

39.Gallot B and Skoulios AE, *Kolloid-Zeitschrift und Zeitschrift für Polymere* **208**, 37 (1966)

40.Hartley GS, *Progress in the Chemistry of Fats and other Lipids* **3**, 19 (1955)

41.Brandrup J and Immergut EH (eds), Polymer Handbook, second ed., John Wiley & Sons (1975)

42.Tiddy GJT, Daresbury Laboratory Annual Report 1995-1996

43.Ekwall P, Mandell L and Fontell K, *Molecular Crystals and Liquid Crystals*, **8**, 157 (1969)

44.Eins S, *Molecular Cystals and Liquid Crystals*, **11**, 119 (1970)

45.Balmbra RR, Bucknall DAB, Clunie JS, *Molecular Cystals and Liquid Crystals*, **11**, 173 (1970)

46.Clunie JS, Corkhill JM and Goodman JF, *Proceedings of the Royal Society of London* A, **285**, 520 (1965)

47.Luzzati V and Reiss-Husson F, Nature **210**, 1351 (1966)

48.LeNeveu DM, Rand RP, Parsegian VA and Gingell D, *Biophysical Journal* **18**, 209, (1977)

49.Goldstein RE and Leibler S, *Physical Review Letters* **61**, 2213 (1988)

50.Goldstein RE and Leibler S, *Physical Review A*, **40 (2)**,1025 (1989)

51.Parsegian VA, Fuller N and Rand P, *Proc Natl Acad Sci* **76 (6)**, 2750 (1979)

52.Gruner SM, *J Phys Chem* **93**, 7562 (1989)

53.Leigh ID, McDonald MP, Wood RM, Tiddy GJT and Trevethan MA, *J Chem Soc, Faraday Trans 1*, **77**, 2867 (1981)

54.Rendall K, Tiddy GJT and Trevethan MA, *J Chem Soc Faraday Trans 1*, **79**, 637-649 (1983)

55.Kilpatrick PK and Bogard MA, *Langmuir* **4**, 790 (1988)

56.Blackburn JC and Kilpatrick PK, *Langmuir* **8 (6)**, 1679 (1992)

57.Kilpatrick PK, Blackburn JC and Walter TA, *Langmuir* **8 (9)**, 2192 (1992)

58.Blackburn JC and Kilpatrick PK, *Journal of Colloid and Interface Science*, **157**, 88 (1993)

59.Kékicheff P and Cabane B, *Acta Cryst* **B44**, 395 (1988)

60.Luzzati V, Tardieu A and Gulik-Krzywicki T, *Nature* **217**, 1028 (1968)

61.Kékicheff P and Tiddy GJT, *Journal of Physical Chemistry* **93**, 2520 (1989)

62.Fairhurst CE, Leaver MS and Holmes MC, *The structure and morphology of the intermediate phase region in the non-ionic surfactant $C_{16}EO_6$/water system* (to be published)

63.Luzzati V, Tardieu A, Gullik-Krzywicki T, Rivas E and Reiss-Husson F, *Nature* **220**, 485 (1968)

64.Mariani P, Luzzati V and Delacroix H, *J Mol Biol* **204**, 165 (1988)

65.Fontell K, *Mol Cryst Liq Cryst* **63**, 59 (1981)

66.Fontell K, *Colloid Polym Sci* **268**, 264 (1990)

67.Larsson K, *J Phys Chem* **93**, 7304 (1989)

68.Bates FS and Fredrickson GH, *Anu Rev Phys Chem* **41**, 525 (1990)

69.Thomas EL, Anderson DM, Henkee CS and Hoffman D, *Nature* **334**, 598 (1988)

70.Anderson DM, Gruner SM and Leibler S, *Proc Natl Acad Sci* **85**, 5364 (1988)

71.Thomas EL, Alward DB, Kinning DJ, Martin DC, Handlin DL (Jr), Fetters LJ, *Macromolecules* **19**, 2197 (1986)

72.Hasegawa H, Tanaka H, Yamasaki K and Hashimoto T, *Macromolecules* **20**, 1651 (1987)

73.Bates FS, *Science* **251**, 898 (1991).

74.Förster S, Khandpur AK, Zhao J, Bates FS, Hamley IW, Ryan AJ and Bras W, *Macromolecules*, **27**, 6922 (1994)

75.Almdal K, Koppi KA, Bates FS and Mortensen K, *Macromolecules* **25**, 1743 (1992)

76.Kékicheff P and Cabane B, *J Physique Lett* **45**, 813 (1984)

77.Kékicheff P and Cabane B, *J Physique* **48**, 1571 (1987)

78.Blackburn JC and Kilpatrick PK, *Journal of Colloid and Interface Science* 149 (2) 450 (1992)

79.Mitchell DJ, Tiddy JT, Waring L, Bostock T and McDonald MP, *J Chem Soc Faraday Trans 1*, **79**, 975 (1983)

80.Rançon Y and Charlovin J, *J Phys Chem* **92**, 2646 (1988)

81.Rançon Y and Charlovin J, *J Phys Chem* **92**, 6339 (1988)

82.Funari SS, Holmes MC and Tiddy GJT, *The Journal of Physical Chemistry* **98**, 3015 (1994)

83.Burgoyne J, Holmes MC and Tiddy JT, *The Journal of Physical Chemistry* **99**, 6054 (1995)

84.Fairhurst CE, Holmes MC and Leaver MS, *Langmuir* **12**, 6336 (1996)

85.Blackburn JC and Kilpatrick KP, *Ind Eng Chem Res* **35**, 2823 (1996)

86.Pacor P and Spier HL, *The Journal of the American Oil Chemists' Society* **45**, 338 (1968)

87.Vold RD, Rosevear FB and Ferguson RH, *Oil and Soap*, p48-51 (March 1939)

88.Vold RD and Vold MJ, *Journal of the American Chemical Society* **61**, 808 (1939)

89.Vold RD, *Journal of the American Chemical Society* **63**, 2915 (1941)

90.De Bretteville A Jr and McBain JW, *Journal of Chemical Physics* **11**, 426 (1943)

91.Nordsieck H, Rosevear FB and Ferguson RH, *The Journal of Chemical Physics* **16**, 175 (1948)

92.Skoulios AE and Luzzati V, *Nature* **183**, 1310 (1959)

93.Skoulios AE and Luzzati V, *Acta Crystallographica* **14**, 278 (1961)

94.Gallot B and Skoulios AE, *Kolloid-Zeitschrift und Zeitschrift für Polymere* **210**, 143 (1966)

95.Lawson KD and Flautt TJ, *The Journal of Physical Chemistry* **69 (12)**, 4256 (1965)

96.Gallot B and Skoulios AE, *Acta Crystallographica* **15**, 826 (1962)

97.Spegt PA and Skoulios AE, *Acta Crystallographica* **16**, 301 (1963)

98.Spegt PA and Skoulios AE, *Acta Crystallographica* **17**, 198 (1964)

99.Spegt PA and Skoulios AE, *Acta Crystallographica* **21**, 892 (1966)

100.Luzzati V and Spegt PA, *Nature* **215**, 701 (1967)

101.Thiessen PA and Spychalski R, *Zeitschrift für physikalische Chemie A* **156**, 435 (1931)

102.Spychalski R, *Rocz Chem* **11**, 427 (1931)

103.Thiessen PA and Stauff J, *Zeitschrift für physikalische Chemie A* **177**, 398 (1936)

104.Buerger MJ, Smith LB, De Bretteville Jr A and Ryer FV, *Proceedings of the National Academy of Sciences USA* **28**, 526 (1942)

105.Buerger MJ, *Proceedings of the National Academy of Sciences USA* **28**, 529 (1942)

106.Buerger MJ, *The American Mineralogist* **30**, 551 (1945)

107.De Bretteville A Jr and McBain JW, *Science* **96**, 470 (1942)

108.Ferguson RH, Rosevear FB and Stillman RC, *Industrial and Engineering Chemistry* **35**, 1005 (1943)

109.Ferguson RH, *Oil and Soap* **21**, 6 (1944)

110.Vold RD and Lyon LL, *Industrial and Engineering Chemistry* **37**, 497 (1945)

111.Gardiner KW, Buerger MJ and Smith LB, *Journal of Physical Chemistry* **49**, 417 (1945)

112.Minor JE and Lingafelter EC, *J Am Chem Soc* **71**,1145 (1949)

113.Gupta S, *J Am Oil Chem Soc* **68 (6)**, 450 (1991)

114.Vand V, Lomer TR and Lang A, *Nature* 159, 507 (1947)

115.Lomer TR, *Acta Crystallographica* **5**, 11 (1952)

116.Dumbleton JH and Lomer TR, *Acta Crystallographica* **19**, 301 (1965)

Chapter 4

Experimental procedures and equipment

Chapter 4 Experimental procedures and equipment

4.1 Introduction

In this chapter the various experimental procedures and equipment are described that were used for the work presented here. First in section 4.2 the preparation of the soaps is explained. In section 4.3 a description is given of the equipment used for purification and characterisation of fatty acids. In section 4.4 the equipment is described that was used to study the nucleation process of soaps and in section 4.5 the equipment is discussed that was used for *in-situ* X-ray diffraction studies using synchrotron radiation. A brief description of the experimental facilities used at the synchrotron sources is included. A considerable amount of the equipment had to be designed and developed especially for this project. Amongst these are: the zone refiner, parts of the slow cool rig (*e.g.* the submersible stirrer and the water-tight lids for the sample vials), the crash cool rig and the X-ray cells used for *in-situ* crystallisation studies.

4.2 Soap preparation

The soaps were prepared by neutralisation of the fatty acids (obtained from *Sigma* with a stated purity of at least 99%), rather than commercially acquire the soaps, in order to ascertain that the soaps would be properly neutralised. In chapter 3 it was shown that even small amounts of fatty acids or electrolytes can significantly alter the phase behaviour of surfactants. Neutralisation was carried out using the so called *alcoholic solution route*. This involves dissolution of the fatty acid in the same weight of warm ethanol and subsequent neutralisation with sodium hydroxide as a 30% solution. This produces the right ethanol/water ratio for both the fatty acid and the soap to remain dissolved during the conversion. The following reaction takes place:

$$\underset{\text{(Fatty acid)}}{CH_3(CH_2)_nCOOH} + NaOH \rightarrow \underset{\text{(soap)}}{CH_3(CH_2)_nCOONa} + H_2O$$

The reaction mixture is continuously stirred and warmed to approximately 80°C. The caustic is added slowly and meanwhile samples are taken from the reaction mixture to check neutralisation using the so called 'magic mixture' (which is described below) as an indicator. Some drops of this are added to some drops of the reaction mixture. When the magic mixture turns pink the fatty acid has been fully neutralised. Most of the solvent is then distilled off from the reaction mixture, after which the soap is further dried in a vacuum oven, until no further weight loss (due to evaporation of the solvent) occurs. After this, soap samples of various water contents can be prepared by mixing the dried, ground soap with a known amount of distilled water which can then be used for subsequent studies.

The 'magic mixture' can be prepared in the following way: 85% vol. ethanol is mixed with 15% vol. water and a few drops of phenolphthalein. This solution will be slightly acidic because of the ethanol. The mixture is then made slightly alkaline by dropwise adding 0.1M NaOH until a faint colour has been obtained. The excess caustic is subsequently neutralised with CO_2 by breathing into the solution until it becomes almost colourless. This way it is ensured that the pH value of the indicator will be very close to the transition point.

4.3 Procedures and equipment used for purification and characterisation of fatty acids

In this section the procedures and equipment used for the purification and characterisation of fatty acids is described. It is well known that small quantities of impurities, such as close homologues, can have dramatic effects on the nucleation and crystallisation process of long-chain hydrocarbons. Soaps are very difficult to purify by zone refining due to their high melting point (around 300°C). At lower temperatures the solid would be in equilibrium with a thermotropic liquid crystalline phase rather than an isotropic melt. The high viscosity of the liquid crystalline phase would make diffusion of impurities in the liquid zones very slow, thus rendering the purification process very inefficient. Therefore in order to obtain pure soaps, fatty acids were purified using a re-designed multi-pass zone refiner, which is described in section 4.3.1. The purified material was subsequently characterised with the following techniques: gas chromatography to identify the impurities, differential scanning calorimetry to investigate the effect of the impurities on the melting point and X-ray diffraction to assess to influence of impurities on the crystal structure. The equipment for these techniques is described in sections 4.3,2, 4.3.3 and 4.3.4 respectively. Most of the experimental work involved in the purification and analysis of the fatty acids was carried out by van Lamsweerde [1]. The feasibility of zone refining fatty acids has previously been shown by Schaeppi [2] and Narang [3].

4.3.1 Multi-pass zone refiner used for purification of fatty acids

Figure 4.1 shows a picture of the zone refiner with cooling and heating apparatus, used for purification of fatty acids (see chapter 5). The basis of this apparatus is a zone refiner that has previously been described in literature (McArdle [4]). This apparatus was improved significantly however, since during operation this zone refiner was found to have inadequate temperature control over the heating and cooling zones. The basic principle has remained the same however. The fatty acid to purify was melted into a long, round-bottomed glass tube (length 900mm, internal diameter and external diameter 14mm and 17mm respectively). This tube was then placed inside the zone refiner, where its vertical translation through the heating and cooling zones was accomplished by means of a cam with a 45mm step (equal to the distance between two zones), see figure 4.1. The cam was driven by a motor, running at 1rpm through a 1:100 gearbox, which resulted in an upward movement of the glass tube of 27mm/hr. In this way the molten zones travelled slowly down the tube until the next heater was reached. At that point the cam would cause the tube to drop, hereby aligning the molten zone with the preceding heater. In this way each molten zone moved down until it reached the bottom of the tube. This is schematically shown in figure 4.2. In addition, the tube was rotated around its axis at 1rpm in order to accomplish uniform heat transfer around the tube and to provide agitation of the molten zones. There were 12 heating zones (width=6mm) and 11 cooling zones

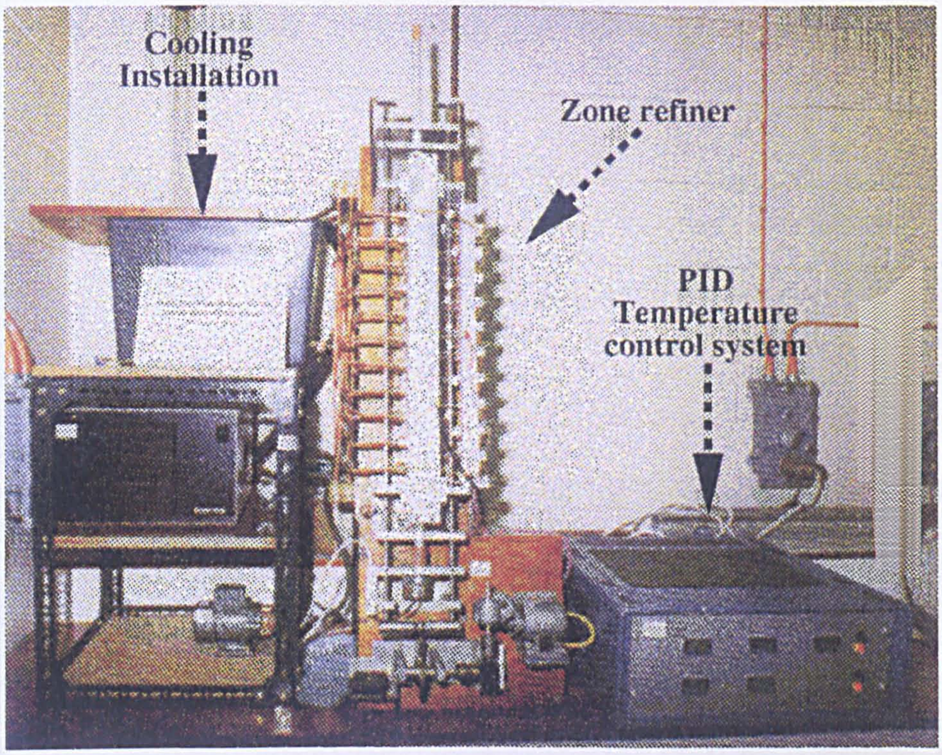
Cooling Installation
Zone refiner
PID Temperature control system

Figure 4.1 Multi–pass zone refiner, the picture above shows the whole installation, the one on the right shows the cam mechanism for translating the sample tube

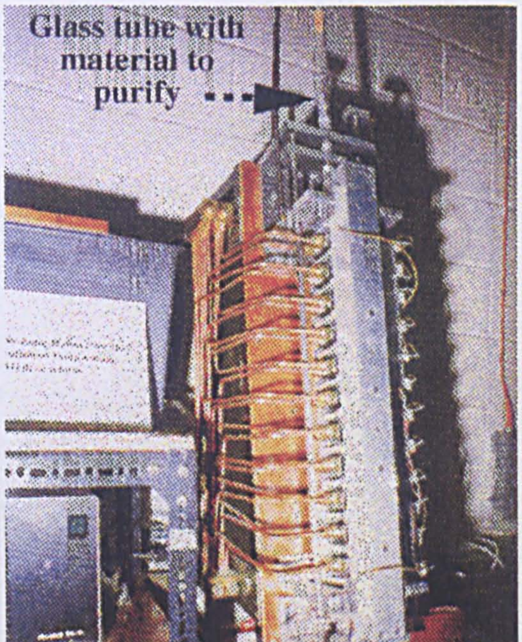
Glass tube with material to purify
Cam

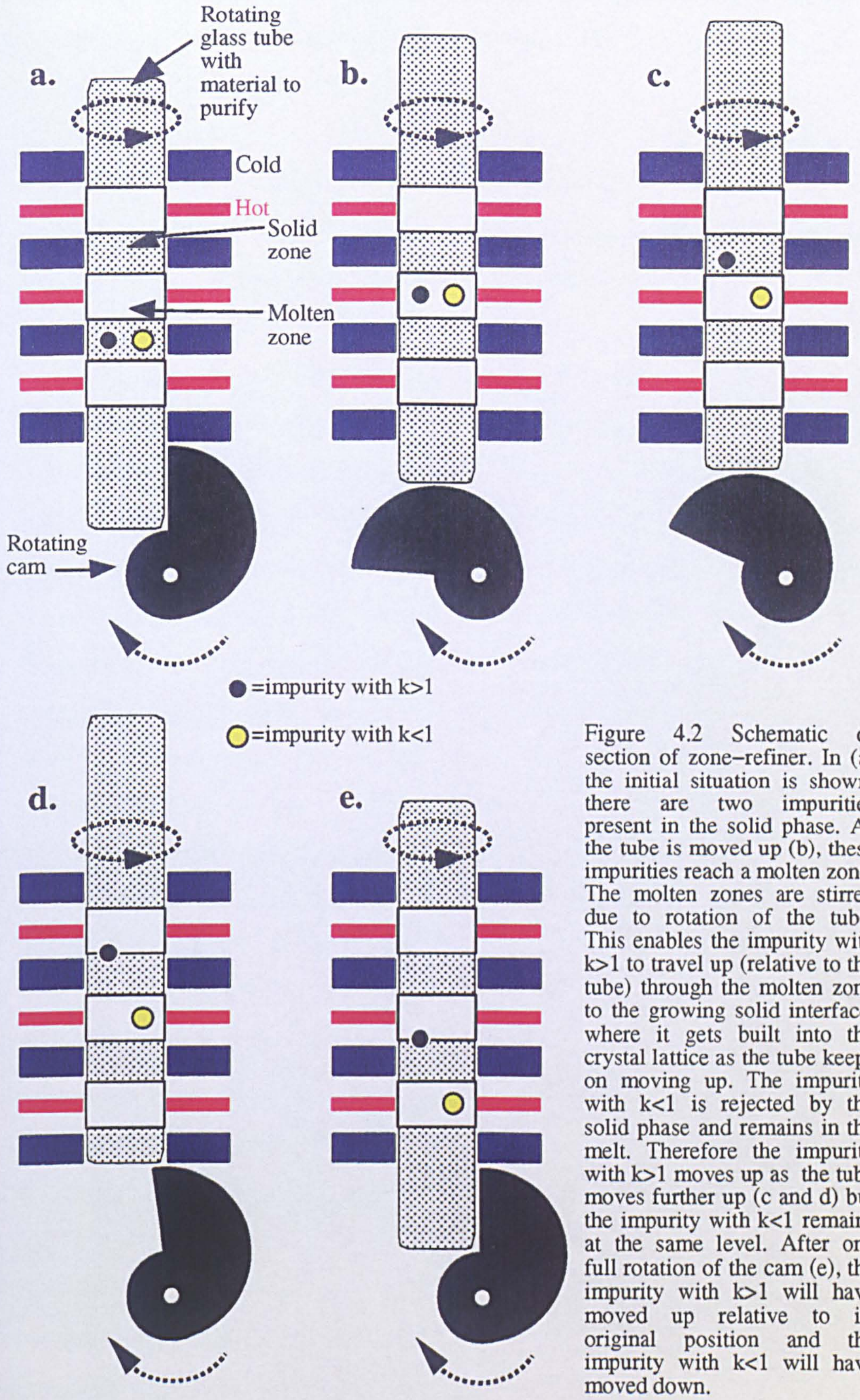
a.
Rotating glass tube with material to purify
Cold
Hot
Solid zone
Molten zone
Rotating cam
b.
c.
● =impurity with k>1
○=impurity with k<1
d.
e.

Figure 4.2 Schematic of section of zone–refiner. In (a) the initial situation is shown; there are two impurities present in the solid phase. As the tube is moved up (b), these impurities reach a molten zone. The molten zones are stirred due to rotation of the tube. This enables the impurity with k>1 to travel up (relative to the tube) through the molten zone to the growing solid interface, where it gets built into the crystal lattice as the tube keeps on moving up. The impurity with k<1 is rejected by the solid phase and remains in the melt. Therefore the impurity with k>1 moves up as the tube moves further up (c and d) but the impurity with k<1 remains at the same level. After one full rotation of the cam (e), the impurity with k>1 will have moved up relative to its original position and the impurity with k<1 will have moved down.

(width=19mm) with a distance between a heating and adjacent cooling zone of 10mm. In this way multi-pass zone refining was accomplished, which reduces the time required to purify the material in comparison with single-stage zone refiners, which only have one heating zone.

The following modifications were made to the original zone refiner:

- In order to be able to control and manipulate the temperature of the cooling and heating fins in a precise manner the following changes were made:

  1. The original zone refiner had only one heating element at the back of the heating block. As a results of this, a large temperature difference was found to exist between the middle zone and the outer ones. In addition, this heater was controlled by a conventional thermostat, which caused large temperature fluctuations. In order to achieve better temperature control over the heating fins, cartridge heaters were inserted directly into the fins and were controlled from *Cal Control 3200* PID (proportional, integral, derivative) temperature controllers with auto-tuning and feed-back from type N thermocouples. Five PID controllers were used; each controlling two or three heating zones. In this way the maximum temperature fluctuation of a heating zone from the set-point was found to be 0.2°C. The thermocouples were secured inside the heating fins with titanium putty to enable operation at high temperatures. The heaters were switched on and off by the PID controllers through the use of solid state relays, rather than relying on mechanical ones, as solid state relays are much more suitable for continuous operation.

  2. The cooling side was improved in the following way: the original zone refiner relied on a flow of tap water at the back of the cooling block for cooling. This was found to provide insufficient cooling as the heat had to be conducted all the way through the aluminium block. Therefore water channels were made in the actual cooling fins, to ensure more efficient cooling. The cooling fins were all connected in a parallel manner with a small tank so that water could be circulated, instead of

using tap water. The water in the tank was cooled using a *Haake EK12* cooling element controlled by an adjustable thermostat with 0.1°C accuracy Re-circulation of the cooling water has two advantages over the use of tap water. Firstly the temperature can be much better controlled and can be held constant and secondly inhibitor can be added to the water, in order to prevent corrosion of the aluminium cooling fins. The water was circulated by a magnetically coupled induction motor driven centrifugal pump at a rate of 7*l*/min. This type of pump was chosen as it can be operated continuously for long periods of time, since it does not have brushes like other electro-motors.

- A thermal cut-out system was installed, with feed back from a thermocouple that was placed inside the cooling block of the zone refiner. In this way, if anything would go wrong (*e.g.* leakage or evaporation of the cooling water, or failure of the pump or the cooling unit), the whole system would be switched off automatically thus ensuring that the sample would cool down to room temperature and solidify. In this way melting of the solid zones due to failing cooling conditions was prevented, which would cause unwanted re-mixing of pure and impure material.

- The motor that rotated the cam for vertical translation of the glass tube was replaced by an induction driven motor, so that the apparatus could be run continuously without having to change the brushes.

- A mechanical counter was added to automatically count the number of passes

All these modifications served to ensure continuous operation of the zone refiner without faults that could lead to unwanted re-mixing of the sample, which would mean that purification would have to be started all over again.

At the end of the zone refining process, the zone refiner would be switched off to let the molten zones solidify. The glass tube was then cut into 12 equal sections by etching it with a glass cutter in the relevant places and touching the etchings with a hot glass rod. The tube then snapped cleanly at the etchings, producing sections of approximately equal size.

4.3.2 GC analysis

Gas chromatography (GC) analysis was used in order to identify and quantify the impurities present in the unpurified and purified fatty acids. As these materials are not volatile enough for direct GC analysis they first had to be converted into their methyl-esters by the following procedure:

1. The fatty acid was converted to its corresponding methyl-ester by refluxing one gram of it with 2 ml of boron tri-fluoride methanol complex for 10 min:

$$\underset{\text{(fatty acid)}}{CH_3(CH_2)_nCOOH} + CH_3OH \xrightarrow{BF_3} \underset{\text{(methyl-ester)}}{CH_3(CH_2)_nCOOCH_3} + H_2O$$

2. The methyl-ester was then extracted from this mixture with heptane. For this, 5ml of heptane was added to the reaction mixture which was then again refluxed for 10 min.
3. The solution was subsequently transferred into a conical flask, to which a saturated NaCl solution was added. This caused phase separation so that two layers were formed.
4. The top layer (which was the organic layer containing the ester) was then taken of with a pipette and was shaken with anhydrous sodium sulphate, in order to remove entrained water.
5. This was left to settle so that the solid material would sink to the bottom. The heptane solution could then be taken out with a pipette, which after dilution was ready for GC analysis. The samples had to be stored in a refrigerator in order to prevent degradation.

The gas chromatograph (GC) used to determine the nature and concentration of the impurities present in fatty acids was a *Hewlett Packard 5890 series II* Gas Chromatograph with data handling software. Splitless injection was used with a 50m long polar column. The column head pressure was 170kPa with helium as the carrier gas. The 1μ*l* samples were injected into the column which, initially at 100°C, was ramped after 3 minutes to 200°C at 10°C/min. The impurities were determined by analysing known samples of fatty acid of different chainlengths (C_8-C_{18}) and comparing their retention times with those of the impurity peaks. The software enabled integration of the area underneath the peaks by manually drawing the individual baselines. Initially a different GC was used, which seemed to be capable of detecting lower levels of impurities, this GC became unavailable however.

4.3.3 Differential scanning calorimetry

Differential scanning calorimetry (DSC) analysis was carried out on samples of purified and unpurified fatty acids, in order to investigate the influence of impurities on the melting and crystallisation temperature and the enthalpy of melting and crystallisation. For this, a *Mettler DSC 820*, with *Mettler-Toledo TA8000* software was used. A typical sample weight was 0.0073g. The samples were heated and cooled between 30 and 60°C at a rate of 2°C/min. An inert atmosphere was provided around the sample pan by a continuous flow of nitrogen gas.

4.3.4 X-ray diffraction

A *Siemens D-5000* X-ray diffractometer linked to *Siemens Diffrac AT version 3* software was used to study the influence of impurities on the crystal structure of the material. This diffractometer used a copper X-ray tube run at 40kV/30mA and was equipped with an *BRAUN PSD-50M* 10cm position sensitive detector. The sample temperature could be accurately controlled with a *Cryocool* cryostat/heater temperature control system. The samples were ground up using a mortar and pestle and filled into 1mm quartz glass capillaries.

4.4 Procedures and equipment used for nucleation studies of soaps

Two different automated nucleation rigs were used for studying the nucleation process of single and mixed surfactant systems from isotropic micellar solutions: one rig was used for slow cool experiments with the aim of measuring the metastable zone width and saturation temperature of the sample. After these parameters had been determined crash cool experiments were performed with the second nucleation rig (the so called *crash cool rig*), in order to measure the induction times of the samples as a function of supersaturation.

Prior to the nucleation experiments the samples were warmed up to a temperature where all solid soap had dissolved and were subsequently filtered to remove residual heterogeneous particulate contaminants, using a porosity 2 sintered glass filter, since it has been found that such impurities play an important part in the formation of the critical size molecular clusters formed during nucleation (Nyvlt [5]). All glassware involved in the filtration process was pre-heated in an oven at 120°C. In this way crystallisation during filtration was prevented. Approximately 15ml of each sample was used for nucleation studies.

These nucleation rigs are described in sections 4.4.2 and 4.4.3 respectively. In both cases optical turbidity was used as the criterion to establish at which temperature the sample had nucleated and dissolved. For the slow cool rig a commercially available turbidity meter was used, but for the crash cool rig a turbidity meter was developed, which is described in section 4.4.1. The basic principle of both turbidity meters is the same.

4.4.1 Turbidity meter

The specially for the crash cool apparatus developed turbidity meter mainly consisted of a turbidity probe which was connected with optical fibers to the actual turbidity meter. The turbidity probe was made of a stainless steel cylinder with a disc of polished stainless steel attached to it, which served as a mirror. The probe was put into a stirred solution so that the solution continuously flowed through the gap between the cylinder and the mirror. The probe worked as follows: light entered the probe through an optical fiber, shone through the solution in the gap, hit the mirror and was reflected back into the probe, into a second optical fiber. Nucleation and dissolution could thus be detected by detecting changes in the amount of light that was transmitted through the solution. When solid particles were being formed in the solution these would block off the light, causing the amount of light transmitted through the solution to decrease. When the solid material dissolved, the turbidity of the solution would decrease again. The precipitation and dissolution temperatures of the sample could thus be determined by simultaneously measuring the temperature of the solution.

It was found to be a problem with the above described technique that the turbidity probe could pick up unwanted incident light, which would cause fluctuations in the turbidity measurements. This problem was overcome in the following way: the light source used for the turbidity meter was an ultra bright red LED (light emitting diode). A crystal based oscillator made this LED switch on and off with a frequency of 6kHz. The light was guided through the optical fiber, ending in the turbidity probe. The light coming back from the turbidity probe through the second fiber was detected with a photo-diode with integral amplifier. The signal from this photo-diode was filtered so that only light could come through that oscillated with a frequency of 6kHz. In this way only the signal from the LED was detected and unwanted incident light was filtered out. The measured turbidity using this technique was not 'absolute', 100% did not indicate a totally clear solution, nor did 0% indicate a totally opaque sample. However, the signal did provide an effective measure of the onset of the crystallisation process.

4.4.2 Slow cool apparatus

In figure 4.3 a schematic picture is shown of the automated rig used for slow cool experiments for studying the nucleation process of soaps. Apart from some

Figure 4.3 Diagram of rig used for slow cool experiments (part of figure from Taggart [9])

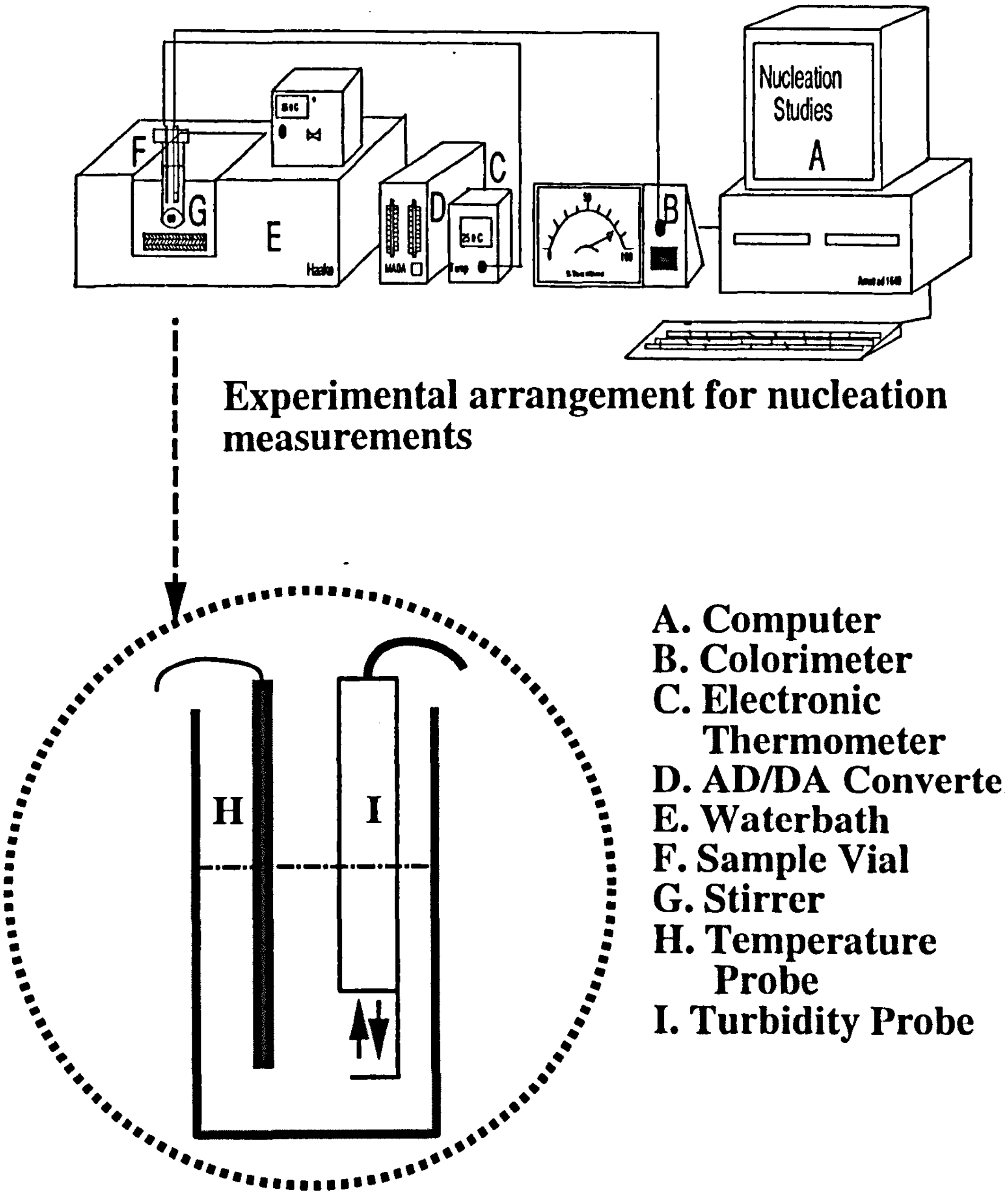

Experimental arrangement for nucleation measurements

A. Computer
B. Colorimeter
C. Electronic Thermometer
D. AD/DA Converte
E. Waterbath
F. Sample Vial
G. Stirrer
H. Temperature Probe
I. Turbidity Probe

Expanded view of sample vial, showing turbidity and temperature probe

improvements (better stirrer and water tight lid), this apparatus has been described before in literature (*e.g.* Roberts *et al.* [6] and Gerson *et al.* [7]) and preliminary results from this study have also been published by van Gelder *et al.* [8]. The aim of the experiments was to determine the metastable zone width and saturation temperature of the samples by extrapolating the data back to the equilibrium situation (zero cooling/heating rate). From this the enthalpy and entropy of dissolution could be obtained, as was explained in chapter 2.

The rig worked as follows: the sample was placed in a glass vial, inside a *Haake F3-CH* thermostatically controlled water bath, where it was agitated by means of a teflon magnetic stirrer flea. The stirring motion of this flea was induced by a submersible stirrer (described below), which was placed inside the water bath, below the glass vial. A stainless steel fibre optic light probe and a platinum resistance thermometer (*PT100*) were immersed in the solution through a liquid-tight lid (which is briefly described below). At the onset of crystallisation the turbidity of the solution increased and could thus be detected by monitoring the percentage of light transmitted through the solution. The light probe is connected to a *Brinkmann PC800* colorimeter, a commercially available turbidity meter, which transferred the signal to a computer through an analogue to digital converter. The signal from the temperature probe was also fed through the analogue to digital converter to the computer. Data points were registered every 30 seconds. The temperature of the bath and consequently of the sample was controlled from the computer. In this way the sample could be subjected to cooling/heating cycles at a desired rate of temperature change.

The submersible stirrer was especially designed for the nucleation experiments. A small DC-motor was built into a small sealed aluminium box, which could be placed inside the water bath, underneath the sample vial. The lead for the motor was fed through a metal cylinder to a variable power supply from which the rate of stirring could be controlled. This rate was held constant for all experiments.

The water-tight lid for the sample vial was made out of two PVC discs, which had openings for the temperature and turbidity probe. Rubber “O”-rings between the two PVC discs were compressed by means of three screws and ensured a tight seal of the probes inside the discs. Another rubber “O”-ring provided a seal between the PVC discs and the glass sample vial.

The nucleation apparatus measured the transmittance of light through the solution to detect the formation and dissolution of crystal nuclei. In all experiments the turbidity of a clear solution was defined as the average turbidity of the sample over a period of 30 minutes at the beginning of each cooling/heating cycle. During this period of time the sample was held at a sufficiently high temperature, where no crystals were detectable. The solution was then cooled through computer control at a pre-set rate until crystallisation started to occur. This was defined to have occurred when the percentage of light transmitted through the solution had dropped by 10% or more of the averaged starting value. The (arbitrary) value of 10% was chosen so that electronic noise (up to 4%) could not be mistaken for nucleation. The sample was then held for two minutes at the temperature were crystals started to form, in order to let the solution equilibrate before the heating phase commenced. Dissolution was defined as occurring when the transmittance came within 10% of the starting value on heating of the sample. In some cases the transmittance of light through the solution had dropped by 10% before the onset of nucleation. In these cases the precipitation temperature was obtained from the turbidity versus temperature plots as the point where a sharp decrease in the transmittance in light through the solution occurred on cooling

Cooling/heating cycles were recorded at the following rates: 0.75, 0.50, 0.25 and 0.10°C/min. Each cycle was carried out at least three times to ensure data reproducibility. If the results from one of the runs looked significantly different from the other runs then these results were discarded and new data was taken until consistency was obtained. As the metastable zone width is defined as the difference between the dissolution temperature and the precipitation temperature at zero cooling rate, it could be obtained by extrapolating the data back to the equilibrium situation (zero cooling/heating rate). The metastable zone width therefore corresponds to the y-intercept of a plot of the difference between the dissolution and the precipitation temperature. The "standard least squares regression" method was used to calculate all lines of best fit. The difference between the dissolution and the precipitation temperature decreased when the rate of temperature change was decreased as the solution was given more time to equilibrate. The saturation temperature is defined as the dissolution temperature at equilibrium (zero heating rate) and could thus be obtained as the y-intercept of a plot of the dissolution temperature as a function of heating rate. The values for the order of nucleation, m , were calculated as the slope of a plot of the logarithm of the rate of temperature change versus the logarithm of ΔT_{max} (see chapter 2).

4.4.3 Crash cool apparatus

After the metastable zone width had been determined with the slow cool experiments, the induction time of the sample could be measured by cooling it very rapidly through its saturation temperature to a pre-set temperature within the metastable zone width. The induction time was measured as the time it took from the moment that the temperature had dropped below the saturation temperature until the moment that the sample started to crystallise. By cooling the sample to a number of different temperatures within the metastable zone, a different degree of supersaturation was induced, so that a series of induction times versus the degree of supersaturation was obtained. From this the interfacial tension and the size of the critical nucleus could be calculated, as was explained in chapter 2. The sample needed to be cooled a fast as possible, so that the induction time corresponding to one specified supersaturation could be measured. Most of the experimental work involved in the crash cool experiments was carried out by Palmer [10]

The apparatus used for crash cool experiments was especially developed for the work presented here; in figure 4.4 a schematic diagram and picture are shown. The

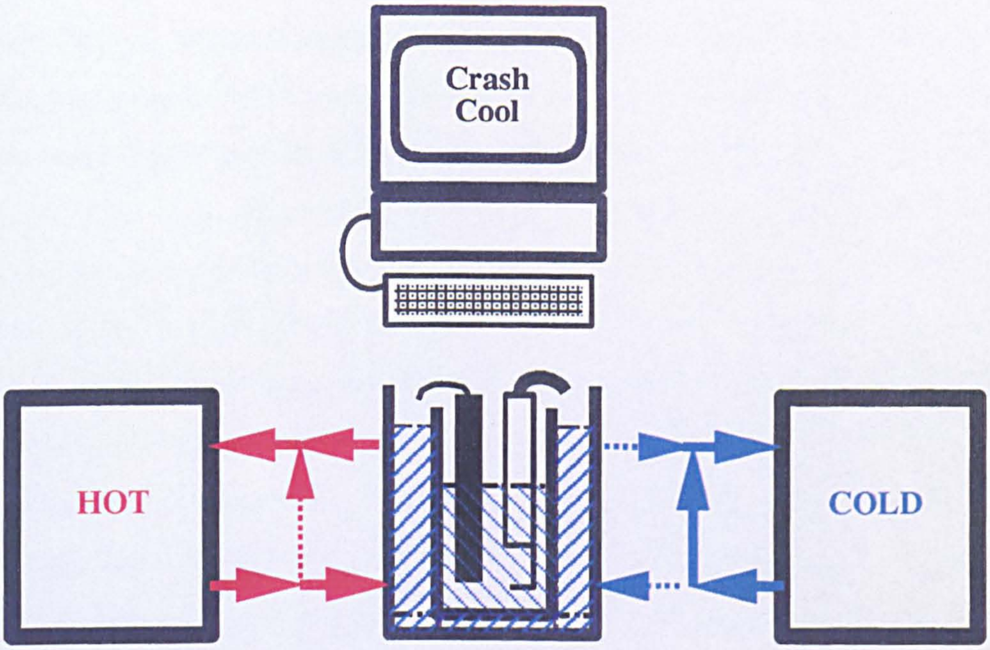
Crash
Cool
HOT
COLD

Figure 4.4 Crash cool rig, schematic (top) and picture (below)

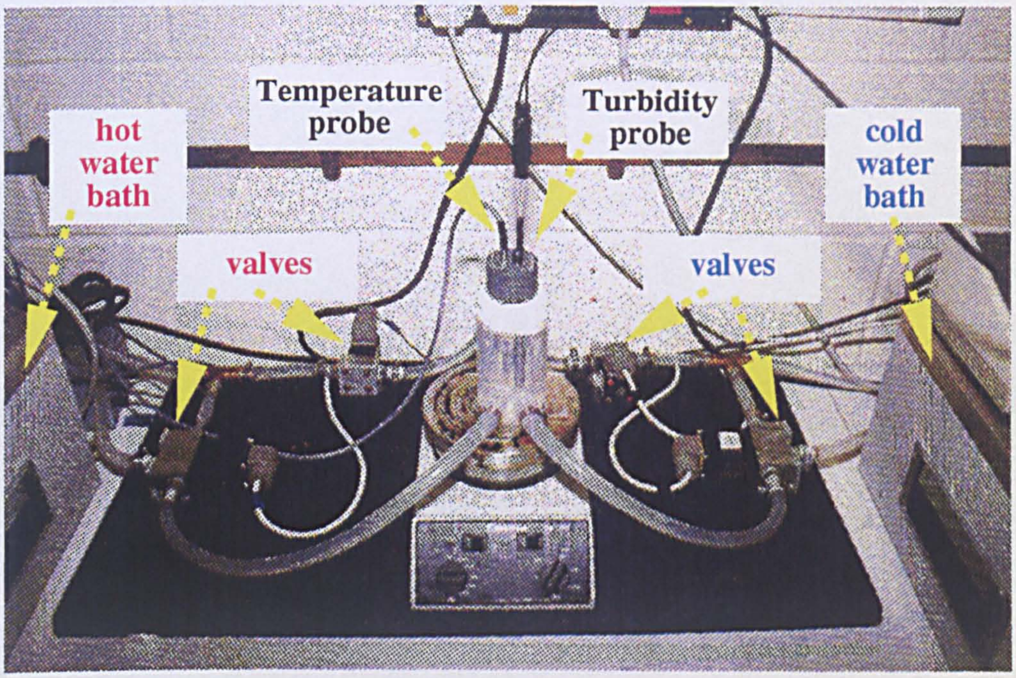
Temperature probe
Turbidity probe
hot water bath
cold water bath
valves
valves

apparatus was very similar to the slow cool rig. The essential difference was that for the crash cool rig two water baths were used, in order to accomplish very rapid cooling. The sample was placed in a glass vial, identical to the ones used for slow cool experiments, with a turbidity and temperature probe inserted through a liquid tight lid. The sample vial was not placed in a water-bath but in a specially designed perspex water jacket. Initially water was circulated through this water jacket around the sample vial, at a temperature high enough to ensure that all solid material was dissolved, for 30 minutes. After this period a set of valves was switched over by computer so that cold water (of a pre-set temperature within the metastable zone) was circulated around the sample, thus inducing supersaturation. As with the slow-cool measurements nucleation was detected by a drop in the amount of light that was transmitted through the solution. The computer registered the induction time as the time it took for the sample to crystallise after the temperature had dropped below the saturation temperature. After crystallisation had occurred the computer switched the valves over so that hot water was circulated around the sample again, in order to dissolve all formed particulate material. The sample was then again kept at this temperature for 30 minutes prior to the next crash cool run. The apparatus was fully automated, the sample could be crash cooled a set number of times to a series of temperatures within the metastable zone width. All induction times corresponding with these temperatures were registered by computer.

At the start of crash cooling, at the moment that the valves were being switched over from the hot to the cold bath, the hot water present in the water jacket would mix with the cold water, thus increasing the temperature of the cold water bath by about five degrees. This water then had to be cooled down again, thus causing a delay before the set-point could be reached. To counteract this effect, the temperature of the cold water bath was set by computer to a temperature five degrees below the actual set point. In this way when the valves switched over, the hot water left in the water jacket would increase the temperature to a value closer to the set-point. In addition, from that moment on, the computer would raise the temperature of the cold water bath to the actual set-point. In this way the sample could be cooled faster than if the cold water bath was initially held at the set-point temperature.

It was found that a limiting factor in achieving rapid cooling of the sample was the poor thermal conductivity of the glass sample vial. Ideally this vial would have to be replaced by a material with good thermal conductivity like a metal, *e.g.* brass. This could cause a problem however if metal-oxides would form on the inside of this sample vial and drop into the solution and interfere with the nucleation process. In addition the sample vial would not be transparent anymore.

4.5 Equipment used for *in-situ* XRD studies of the crystallisation process of soaps

The crystallisation process from the liquid crystalline phases of single and mixed soap systems has been investigated *in-situ*, using synchrotron radiation (see chapter 7). In this section the equipment used for those studies is explained. In section 4.5.1 a description of the X-ray cells is given, followed by a brief description in section 4.5.2 of the experimental facilities at the synchrotron sources used.

4.5.1 X-ray cells for *in-situ* crystallisation experiments

Two *in-situ* X-ray cells have been especially designed for the work presented here, see figure 4.5. Both cells relied on a water jacket for temperature control of the sample. The water was circulated through the cells using a *Haake F3-CH* thermostatically controlled water bath. The temperature of the bath and thus of the cell could be remotely controlled using a *Haake PG-20* temperature programmer.

Both cells were made from brass. In one cell the sample was held inside an "O"-ring between two thin (0.025 mm) mica windows. The other cell (see figure 4.5) mainly consisted of a brass block, in which capillaries filled with the sample could be mounted in a cavity between two brass discs. A small circular aperture (1mm in

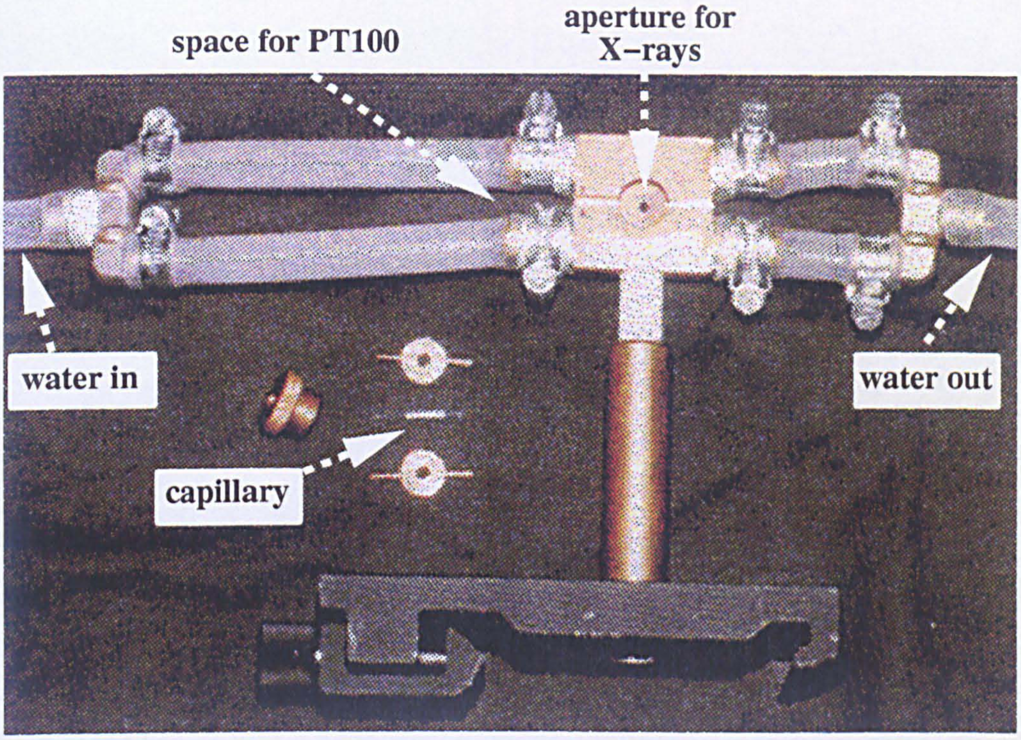
space for PT100
aperture for X-rays
water in
water out
capillary

Figure 4.5 The figure above shows the X–ray cell in which capillaries filled with the sample can be mounted, the figure below shows the X–ray cell where the sample is held between mica windows

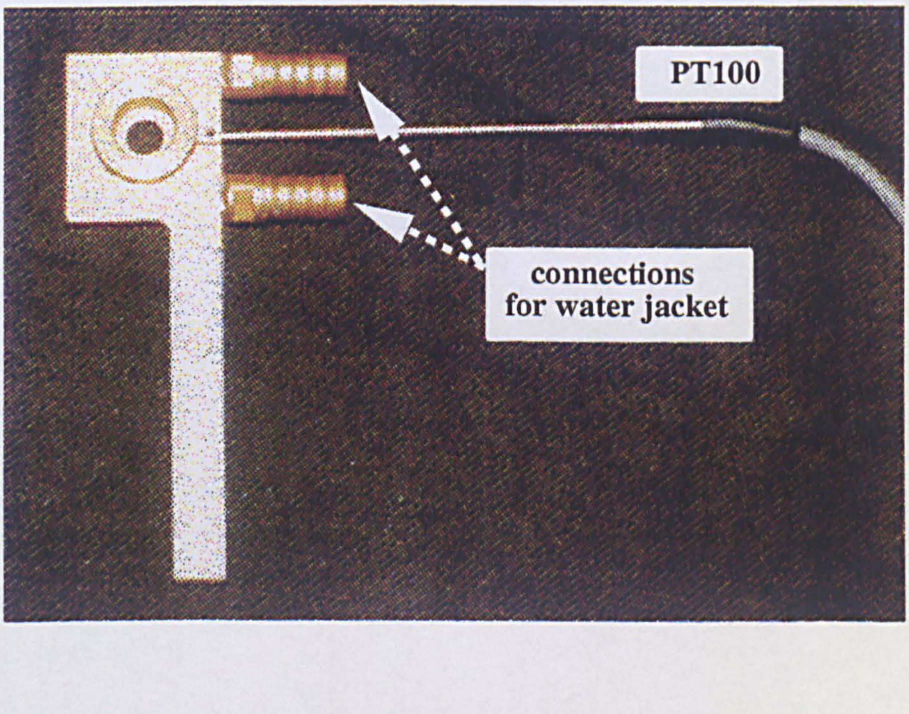
PT100
connections for water jacket

diameter) in the brass block allowed for the X-rays to pass through the sample. A *PT100* platinum resistance temperature probe was placed inside the brass block close to the capillary in order to measure the sample temperature during the experiments. By keeping the size of the aperture in the brass block to a minimum, a uniform temperature throughout the sample is ensured. The capillaries (1.0mm inner diameter) were filled by cutting off the sealed end and subsequently dipping them into the liquid crystals at elevated temperatures. The sample then crystallised inside the capillary which in some case resulted in preferred orientation of the soap fibers (see chapter 7). When filled, the capillary was flame-sealed at both ends to prevent evaporation of water during the experiments.

The surfactant concentration was continuously varied in the experiments by the following technique: either the solid phase in the coagels was slowly dissolved during heating of the sample, thus slowly increasing the concentration or it was slowly crystallised during cooling of the sample, thus effectively continuously depleting the solution. In this way the sample passes through all surfactant phases in the phase diagram, between a solution of surfactant monomers and the phase that is formed at the concentration where all surfactant present in the sample is dissolved. Since X-ray patterns were taken continuously, all these phases could in principle be observed and possibly identified from their X-ray spectra. Difficulties of preparing samples at the exact right concentration, which is the main problem in studying the intermediate lyotropic phases since they only exist over a very limited concentration range, are thus overcome.

In most experiments the samples were subjected to a constant heating/cooling rate of 0.75°C/min during which X-ray data was collected with a counting time of 80 seconds per data frame, so that every °C an X-ray pattern was recorded. In addition crash cool experiments were carried out, by connecting the above described X-ray cell with the arrangement of valves, described for the crash cool rig (section 4.4.3). In this way crystallisation from the liquid crystalline phases, during crash cooling, could be observed *in-situ* with the high intensity X-rays provided by the synchrotron source.

4.5.2 Facilities used at synchrotron sources

In order to study the phase transformations taking place during crystallisation from liquid crystalline phases synchrotron radiation was used. The main advantage of synchrotron radiation over conventional laboratory X-ray sources, is its high intensity which enables processes to be studied on a real-time basis. Two synchrotron sources were used, the *Synchrotron Radiation Source* (SRS) at Daresbury Laboratory (UK) (part of the *Central Laboratory of the Research Councils*) and the *National Synchrotron Light Source* (NSLS) at Brookhaven National Laboratory (USA). In this section a concise description is provided of both these research facilities.

At both synchrotron sources the radiation is produced in the following way: a linear accelerator injects electrons into a booster synchrotron where they are accelerated to a higher energy prior to their extraction into the high energy storage ring. Injection of electrons into the storage ring continues for several minutes until a stored current of up to 300mA has been achieved. The electrons in the storage ring are then 'ramped' in energy by increasing the field strengths in the magnets until the electrons have the operating energy. In the storage ring synchrotron radiation is then produced at the dipole magnets which define the curved trajectories of the electrons. The radiation is led through the beam lines to the experimental stations. Some data about the used synchrotron sources are given in table 4.1. More information can be found at [11, 12].

The station used at the SRS was station 16.1 (*e.g.* Bliss *et al.* [13]). This is a fixed wavelength (1.4Å) high intensity X-ray diffraction station, mainly used for time-resolved studies in the small angle regime. The sample to detector distance can be varied from about 1-9m. For the data presented in chapter 7 this distance was approximately 1m, corresponding to a d-spacings range of 25-100Å. Area detectors and image plate detectors are standard features of this station. Data can be analysed using the *xotoko* software.

parameters	**SRS**	**NSLS**
energy after linear accelerator (MeV)	12	120
energy after booster ring (MeV)	600	750
storage ring		
• energy (GeV)	2	2.6
• maximum operating current (mA)	300	300
• circumference (m)	96	170.1

Table 4.1 Some specifications of the SRS and the NSLS

At the NSLS station X12B was used for SAXS experiments. This station has a variable wavelength (0.92-1.61Å) and is generally used for protein crystallography and for time-resolved X-ray diffraction studies. The sample to detector distance can be varied from 3cm to 2.8m. An area detector is available as well as image plate facilities. For the data presented in chapter 7, an area detector was used with a sample to detector distance of about 1m which resulted in a range covered by the detector of approximately 25-100Å. The raw data was circularly integrated using the program *fi_gui* and analysed with the programs *frnew*, *int_view*, *xmgr* and *geomview*. In figure 4.6 a picture is shown of one of the X-ray cells mounted on the optical rail at station X12B.

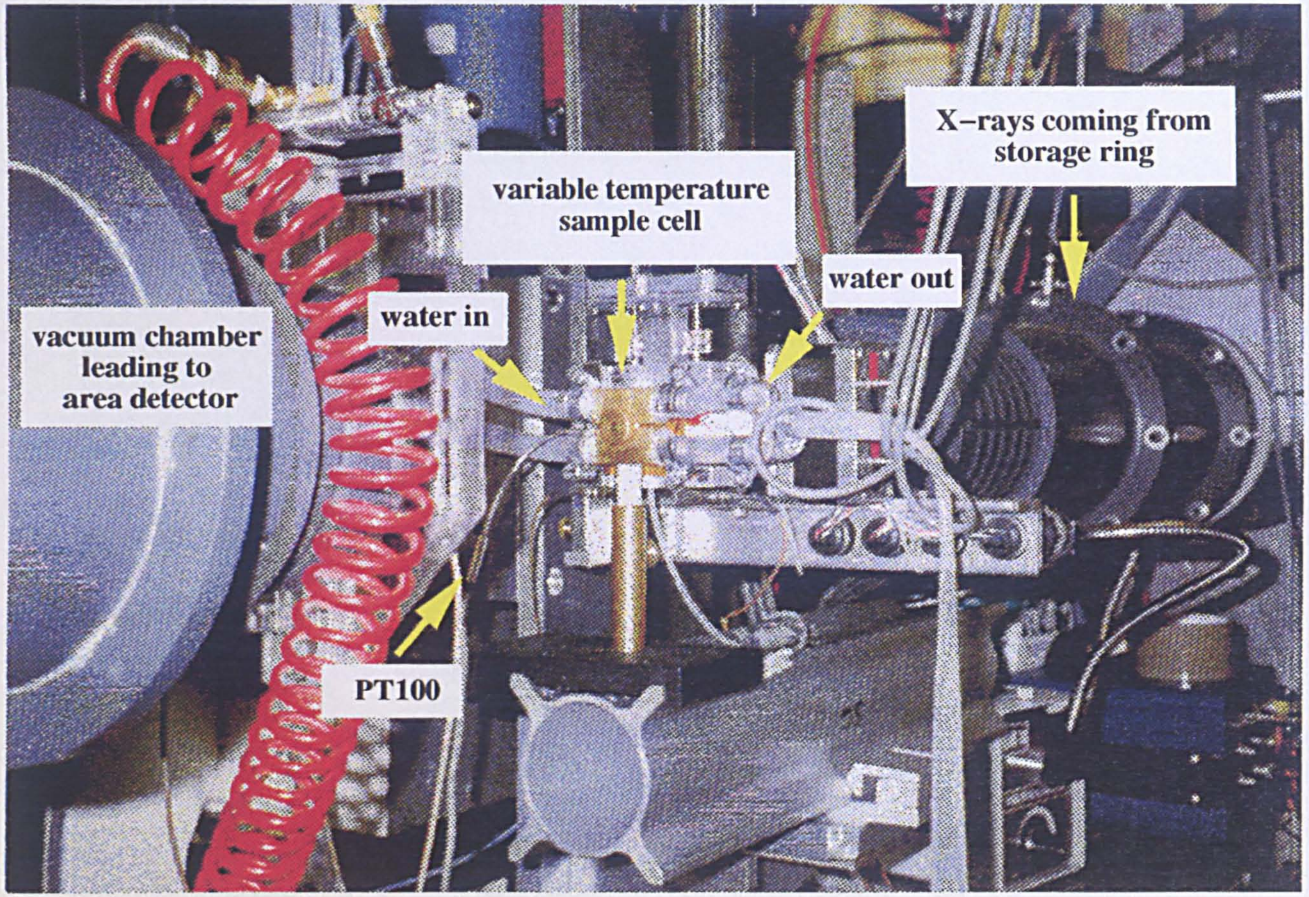
X–rays coming from storage ring
variable temperature sample cell
water out
water in
vacuum chamber leading to area detector
PT100

Figure 4.6 One of the X–ray cells at station X12B of the National Synchrotron Light Source at Brookhaven National Laboratory

4.6 References used in this chapter

1. van Lamsweerde P, *An investigation into the Zone refining of Fatty Acids*, undergraduate thesis Heriot-Watt University, Edinburgh (1997)
2. Schaeppi WH, *Chimia* **16**, 291 (1962)
3. Narang, R.S, *Lattice defects in crystals of long chain compounds*, PhD thesis, University of Strathclyde, Glasgow, (1980)
4. McArdle BJ and Sherwood JN, *Chemistry and Industry* **8**, 268-274 (1985)
5. Nyvlt J, *J Crystal Growth* **3-4**, 377 (1968)
6. Roberts KJ, Sherwood JN and Stewart A, *J Crystal Growth* **102**, 419 (1990)
7. Gerson AR, Roberts KJ and Sherwood JN, *Powder Technology* **65**, 243 (1991)
8. van Gelder RNMR, Roberts KJ, Chambers J and Instone T, *J Crystal Growth* **166**, 189 (1996)
9. Taggart AM, *Nucleation, growth and habit modification of n-alkanes and homologous mixtures in the absence and presence of flow improving additives*, PhD thesis, University of Strathclyde, Glasgow (1995)
10. Palmer G, *Investigation of homogeneous nucleation of natural surfactants using the induction time measurement of crystallisation within the MSZW*, undergraduate thesis Heriot-Watt University, Edinburgh (1997)
11. http//www.dl.ac.uk/SRS/index.html
12. http://www.nsls.bnl.gov
13. Bliss N, Bordas J, Fell BD, Harris NW, Helsby WI, Mant GR, Smith W and Towns-Andrews E, *Rev Sci Instrum* **66 (2)**, 1311 (1995)

Chapter 5

Purification of fatty acids, the first step in obtaining purified soaps

Chapter 5 Purification of fatty acids, the first step in obtaining purified soaps

5.1 Introduction

In this chapter an investigation is presented into the effect of low levels of impurities, such as close homologues on the crystallisation behaviour of lauric acid and myristic acid. These fatty acids were purified with the multi-pass zone refiner described in chapter 4. The feasibility of purifying lauric and myristic acid has previously been shown by Schaeppi [1]. Schaeppi however did not attempt to calculate the distribution coefficients of the impurities. Soaps are difficult to purify by zone refining due to their high melting temperatures (~300°C), therefore soap of a high purity can more readily be obtained by purifying the starting materials in soap production, the fatty acids, and subsequently converting these to soaps. The next step would then be to assess the effect on the impurities on the nucleation and crystallisation process of soaps.

The data on the fatty acids are presented in three major parts. First in section 5.2 general observations on purified fatty acids are given. The purity of the samples has been analysed by gas chromatography, the results for this are given in section 5.3. To investigate the influence of impurities on the melting point, enthalpy of melting and the occurrence of phase changes, differential scanning calorimetry (DSC) was used, these results are presented in section 5.4. X-ray diffraction measurements were carried out on unpurified and purified samples, in order to assess the effect of impurities on the crystal structure of fatty acids, the results for this are given in section 5.5. The results are discussed in section 5.6 followed by conclusions in section 5.7. At the end of the chapter recommendations are given for future work in section 5.8.

5.2 General observations

Samples of lauric and myristic acid were melted into a glass tube and were zone refined for 371 (26 days) and 783 (54 days) passes respectively. The length of the molten zones was found to be approximately 14mm with a solid zone length of approximately 31mm (see figure 5.1). At the end of the zone refining process, the material in the glass tube was cooled down to room temperature in order to let the molten zones solidify. Clear differences in colour were observed in the fatty acids along the glass tube in which they were purified. The original fatty acids, before purification, were white. After zone refining lauric acid for 371 passes the top of the tube was brilliantly white, whereas the bottom 5 sections were pale yellow. The myristic acid after 783 passes was colourless and transparent at the top changing to a creamy colour around the middle of the tube.

A difference in hardness of the material along the ingot was also observed. The sample at the top of the lauric acid tube was very hard and brittle and produced a statically charged powder on grinding with a mortar and pestle. The sample from the bottom of the tube was much softer and greasy, producing plates on grinding. The same was found for myristic acid although the top sample was slightly softer than the top sample of lauric acid and did not produce a statically charged powder on grinding.

The observed differences in colour and hardness along the ingot indicate that the material in the top of the ingot had become purer and the bottom section had become less pure than the starting material. This would mean that most of the impurities have a segregation coefficient smaller than unity, since most of the impurities seem to have travelled down the ingot with the molten zones.

5.3 Gas chromatography (GC) results

Gas chromatography (GC) analysis was used to identify the impurities present and to quantify their distribution along the sample ingot. All fatty acid samples first had to be converted to their methyl-esters since fatty acids are not volatile enough for GC

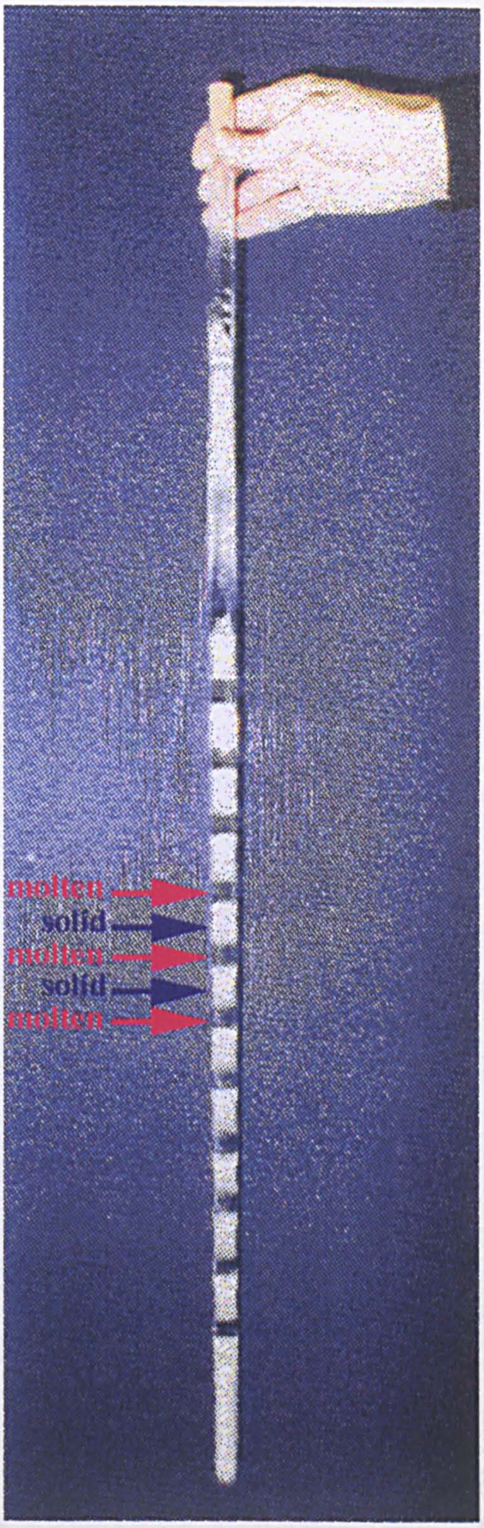
molten
solid
molten
solid
molten

Figure 5.1 Showing the molten and solid zones in a sample tube filled with lauric acid

analysis. The experimental procedure for this is described in chapter 4. The impurities in all samples were identified by comparing their retention time to the retention times of known fatty acid samples. The GC results for the lauric acid samples are given in section 5.3.1, followed by the results for the myristic acid samples in section 5.3.2.

For brevity the fatty acids will be called here after the number of carbon atoms in the hydrocarbon chain: C_n stands for $CH_3(CH)_{n-2}COOH$. The fatty acids that were used as reference samples are listed in table 5.1, together with their measured retention times.

fatty acid	**retention time (min)**
C_8	4.60
C_{10}	7.14
C_{11}	8.47
C_{12}	9.81
C_{13}	11.02
C_{14}	12.20
C_{16}	14.57
C_{18}	17.82

Table 5.1 Fatty acids used as reference materials and their retention times

5.3.1 GC results for lauric acid

GC analysis of unpurified lauric acid revealed the presence of a number of impurities, see figure 5.2. The purity of the starting material was determined to be 99.471%. This material was then zone refined for 371 passes, after which the concentrations of all the impurities found in all the sections of the ingot of lauric acid were determined, these are given in table 5.2. During initial analysis with a different GC (see chapter 4), small concentrations of C_{18} were also detected. However, the GC used for all the analysis shown here could not detect the presence of C_{18}.

	impurity							
	C_8	**C_9**	**C_{10}**	**C_{11}**	**C_{12}**	**C_{13}**	**$C_{13i?}$**	**C_{14}**
retention time (min)	4.6	5.9	7.2	8.5	9.8	11	11.2	12.2
initial concentration (%)	0.016	0.0014	0.0693	0.063	99.471	0.0324	0.0234	0.3234
section 1 (top)	0.0052	0.0198	0.003	0.0011	99.957	0.0018	0.001	0.0115
section 2	0.0012	0.0005	0.0014	0.0548	99.824	0.0087	0.0256	0.0836
section 3	0	0	0	0.0144	99.912	0.015	0.0135	0.0447
section 4	0	0	0	0.1974	99.608	0.014	0.1044	0.0763
section 5	0.0048	0.0028	0.0018	0.065	99.777	0.0202	0.0266	0.1013
section 6	0.0019	0.0037	0.0041	0.0064	99.731	0.035	0	0.2181
section 7	0.003	0.0028	0.0117	0.0453	99.595	0.0425	0.0159	0.2837
section 8	0	0	0.0303	0.1667	99.251	0.0473	0.1	0.3881
section 9	0.0049	0.0034	0.0837	0.0438	99.199	0.0593	0.0038	0.6022
section 10	0.0248	0.0031	0.1617	0.2047	98.655	0.0751	0.097	0.7746
section 11 (bottom)	0.084	0.0019	0.3745	0.0709	98.149	0.0985	0	1.2217

Table 5.2 Concentrations of impurities found in the different sections of the ingot of C_{12}

The values from table 5.2 are plotted in figure 5.3 as a function of the length along the ingot, measured from the top. Most of the impurities show a distinct distribution along the ingot. The $C_{13i\ ?}$ represents a peak adjacent to the C_{13} peak and was believed to be a substance with the same chainlength as C_{13}, maybe an unsaturated fatty acid, or a C_{13} isomer. The overall purity of lauric acid can be seen from figure 5.3 to decrease towards the bottom of the ingot.

The segregation coefficients of the impurities in lauric acid were calculated by plotting the logarithm of the concentration versus the distance along the ingot (see figure 5.4) and using the equations for the ultimate distribution given in chapter 2. According to these equations a plot of $\ln c(x)$ versus x should result in a straight line with slope B, since:

$$\ln c(x) = \ln A + Bx \qquad (5.1)$$

where $c(x)$ is the concentration of an impurity as a function of x, which is the distance along the ingot measured from the top and A and B are constants (see chapter 2). The segregation coefficient, k, for an impurity can then be calculated from:

$$k = \frac{Bl}{e^{Bl} - 1} \qquad (5.2)$$

where l is the length of the molten zone (14mm). The initial concentration of an impurity can be calculated from the ultimate distribution with:

$$A = \frac{c_0 BL}{e^{BL} - 1} \qquad (5.3)$$

where L is the length of the ingot (472mm). A verification of assuming the ultimate distribution can be made by comparing the calculated value for c_0 with the measured initial concentration. The calculated values for the segregation coefficients (with correlation coefficients, r^2) and initial concentrations of the impurities are given in table 5.3. The measured values of c_0 are also listed in this table and in most cases show a poor comparison with the calculated values. The segregation coefficients do have reasonable values however, all values are very close to unity. The tabulated correlation coefficients are a measure for how well the data in figure 5.4 fit a straight line; the better the fit, the closer r^2 is to unity. This shows that the best fits were obtained for C_{10}, C_{13} and C_{14}.

	impurity					
	C_8	C_9	C_{10}	C_{11}	C_{13}	C_{14}
B from plot	0.0091	-0.001	0.0201	0.0058	0.0058	0.009
k (r^2)	0.94 (0.73)	1.01 (0.02)	0.87 (1.00)	0.96 (0.30)	0.96 (0.97)	0.94 (0.99)
ln*A* from plot	-7.802	-5.5701	-10.363	-4.6743	-5.0074	-3.9978
A	0.0004	0.0038	0.00003	0.0093	0.0067	0.0184
c_0 calculated	0.0069	0.0030	0.0443	0.0494	0.0354	0.2991
c_0 measured	0.0693	0.0014	0.0160	0.063	0.0324	0.3234

Table 5.3 Segregation coefficients and calculated and measured values of c_0 for impurities in lauric acid

Figure 5.2 GC spectrum for unpurified lauric acid reveals the presence of several impurities

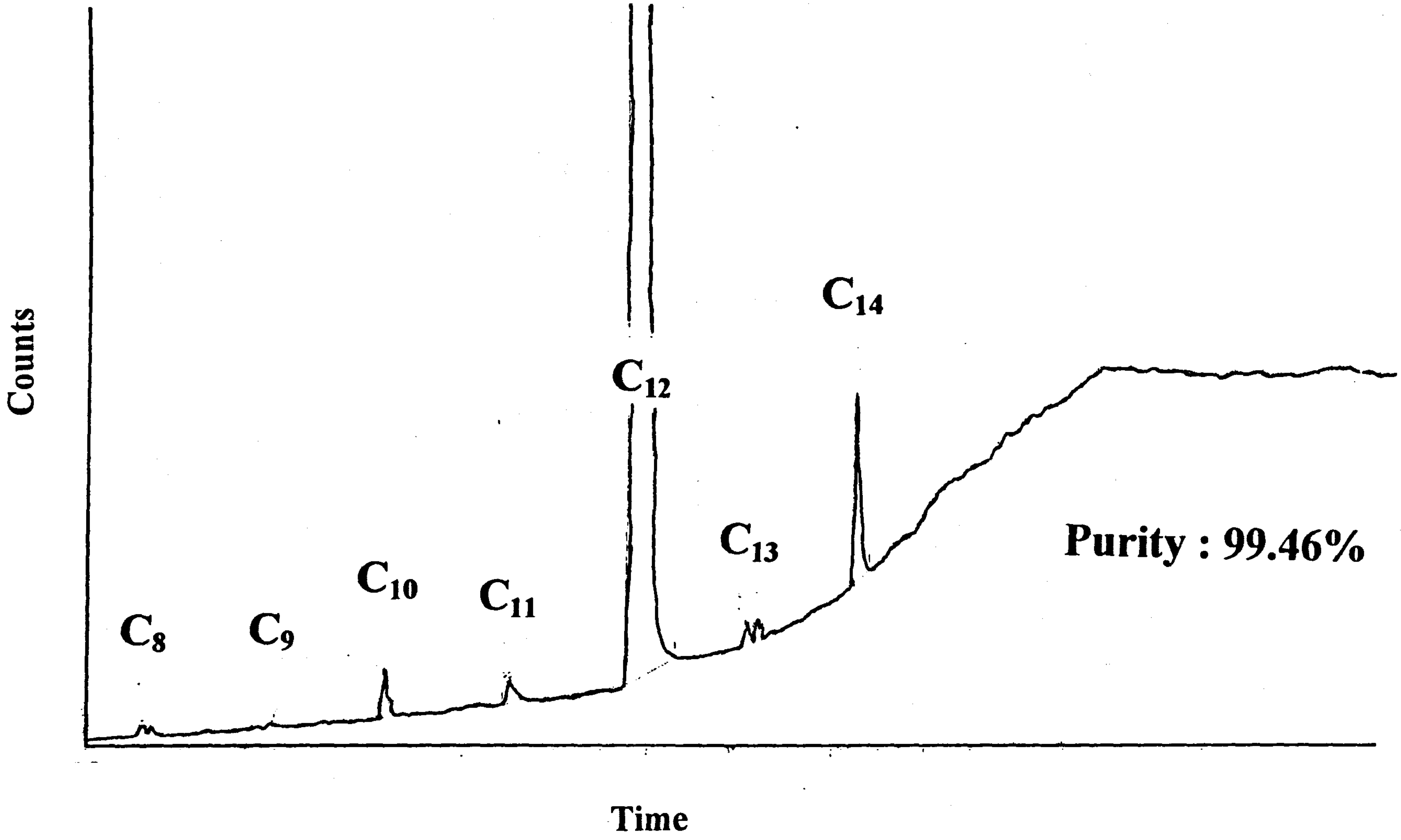

Figure 5.3 Concentration profiles of impurities found in lauric acid

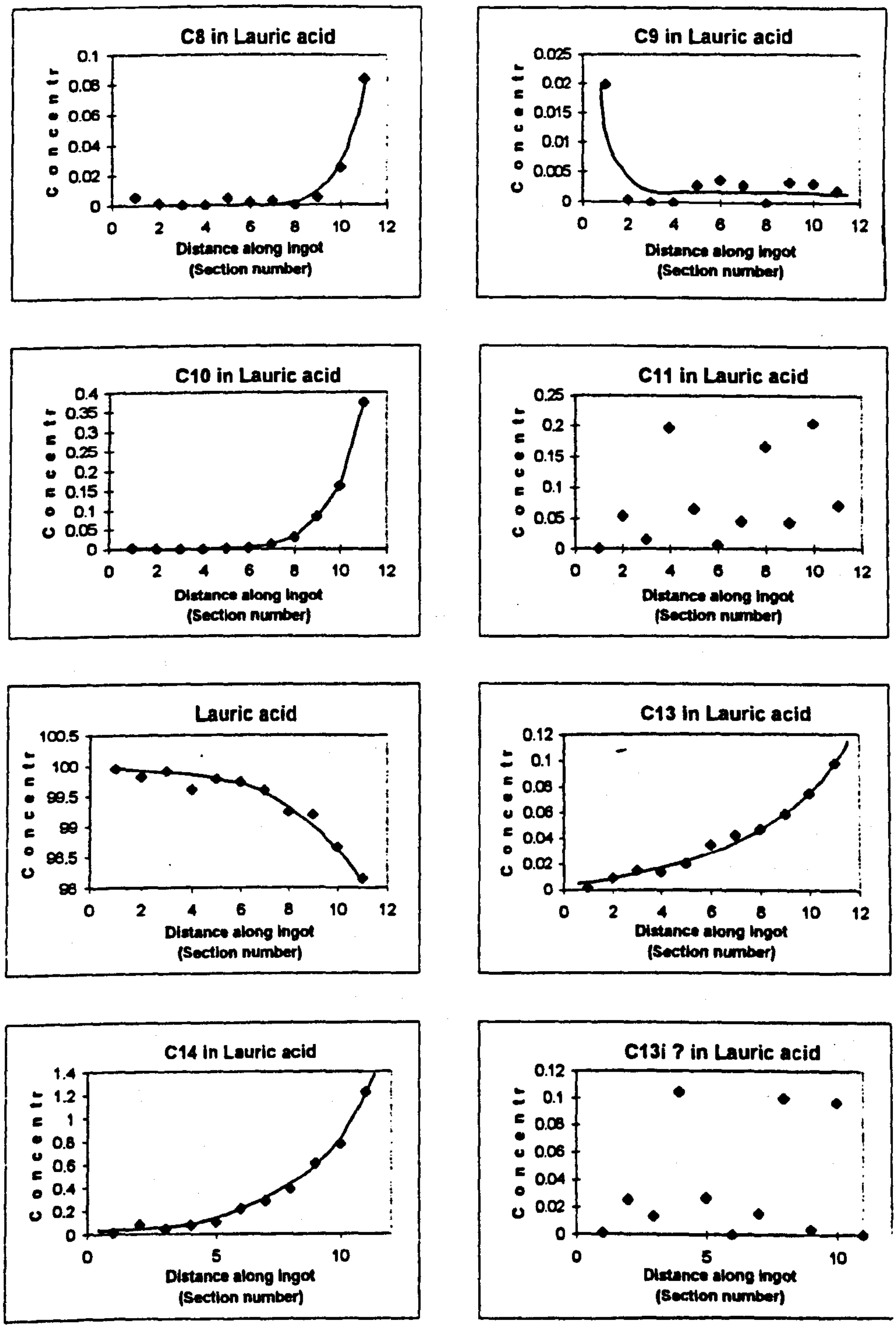

Figure 5.4 Graphs for the calculation of the segregation coefficients of the impurities in lauric acid

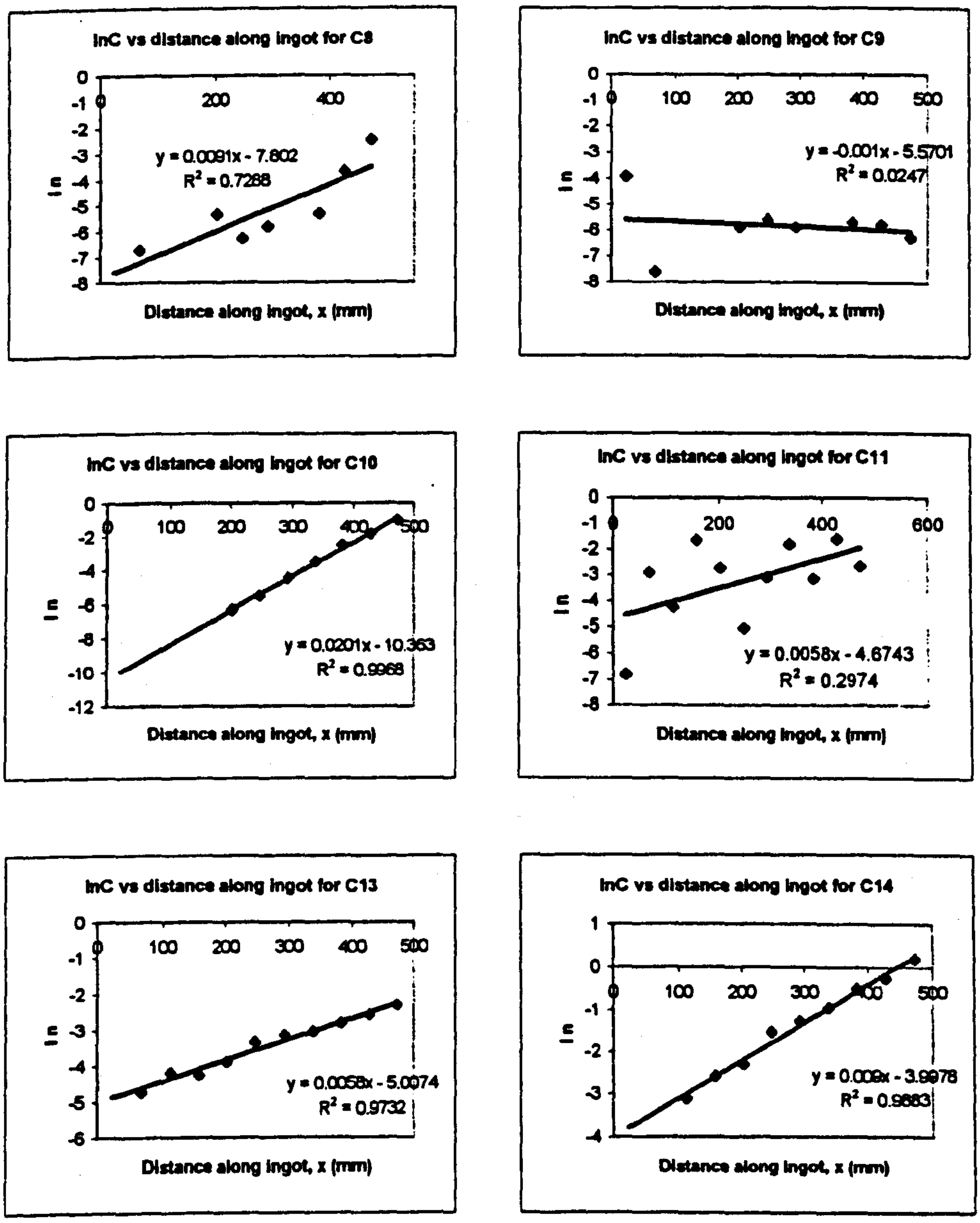

5.3.2 GC results for myristic acid

GC analysis of unpurified myristic acid showed that there were several impurities present, but only in very low concentrations, see figure 5.5. This material was then zone refined for 783 passes, after which the concentrations of all the impurities found in all the sections of the ingot of myristic acid were determined; these are given in table 5.4. The peaks represented by a "?" are for impurities which have not been positively identified. The values from table 5.4 are plotted in figure 5.6 as a function of the length along the ingot, measured from the top. From table 5.4, the overall purity of myristic acid seems to be the highest at the top of the ingot, although no clear distribution can be seen in figure 5.6. The concentration profiles for C_{10}, C_{12} and C_{13} show distinct trends. The concentrations of these impurities all increase towards the bottom of the ingot. The concentration profiles for the other impurities do not show a clear re-distribution.

The segregation coefficients have been calculated for C_{10}, C_{12} and C_{13} (the impurities which showed clear concentration profiles). This was done in the same way as for the impurities present in lauric acid, using the ultimate distribution (see figure 5.7). The results are given in table 5.5. All segregation coefficients are again close to unity as was found for the impurities in lauric acid. Apart from C_{13} the segregation coefficients of the other impurities have a low correlation coefficient, indicating that the obtained values for k are not very reliable. In addition there is a large discrepancy between the measured values of the initial concentrations and the ones calculated with the ultimate distribution.

	impurity								
	C_8	**C_9**	**C_{10}**	**C_{11}**	**?**	**C_{12}**	**C_{13}**	**$C_{13i?}$**	**C_{14}**
retention time (min)	4.6	5.9	7.2	8.5	9.05	9.8	11	11.2	12.2
initial concentration (%)	0.0075	0.0027	0.0047	0.0034	0	0.0162	0.0451	0.0627	99.806
section 1 (top)	0.0017	0.0036	0.0013	0.0072	0.0045	0.0503	0	0.0041	99.901
section 2	0.0084	0.0055	0.0058	0	0	0.0405	0	0	99.591
section 3	0.0062	0.001	0.0022	0.0028	0.0019	0.0242	0	0	99.957
section 4	0.0043	0.0043	0.004	0.0228	0.0074	0.0342	0	0.014	99.909
section 5	0.0098	0.0283	0	0	0	0.0381	0.0074	0	99.917
section 6	0.0085	0.0143	0.0204	0.0535	0	0.0283	0.0113	0	99.813
section 7	0.0081	0.0074	0.0029	0	0	0.0292	0.0145	0	99.927
section 8	0	0.0034	0.0034	0.0208	0.0042	0.0717	0.0257	0.0104	99.852
section 9	0.0065	0	0.003	0	0	0.0452	0.0375	0	99.89
section 10	0.0058	0.0067	0.0052	0.0014	0	0.0429	0.0369	0	99.884
section 11	0.0072	0.0055	0.0064	0.0041	0	0.077	0.0393	0	99.857
section 12 (bottom)	0.0086	0.0085	0.0095	0.0322	0	0.1389	0.0443	0.0138	99.744

Table 5.4a Concentrations of impurities found in all sections of the ingot of C_{14}

	impurity			
	$C_{15?}$	C_{16}	$C_{17?}$	C_{18}
retention time (min)	13.36	14.57	16	17.82
initial concentration (%)	0.0256	0.0137	0	0.0121
section 1 (top)	0.0158	0	0	0.0111
section 2	0.0975	0.1762	0.0161	0.0595
section 3	0.0052	0	0	0
section 4	0	0	0	0
section 5	0	0	0	0
section 6	0.0078	0	0.0053	0
section 7	0.0112	0	0	0
section 8	0.0086	0	0	0
section 9	0.0176	0	0	0
section 10	0.0168	0	0	0
section 11	0.0191	0	0	0
section 12 (bottom)	0	0	0	0

Table 5.4b Concentrations of impurities found in all sections of the ingot of C_{14}

	impurity		
	C_{10}	**C_{12}**	**C_{13}**
B from plot	0.0021	0.0019	0.0058
k (r^2)	0.99 (0.43)	0.99 (0.38)	0.96 (0.90)
ln*A* from plot	-10.363	-3.5569	-2.5569
A	0.00003	0.02853	0.07754
c_0 calculated	0.0001	0.0474	0.4498
c_0 measured	0.0047	0.0162	0.0451

Table 5.5 Segregation coefficients and calculated and measured values of c_0 for impurities in myristic acid

Figure 5.5 GC spectrum for unpurified myristic acid.

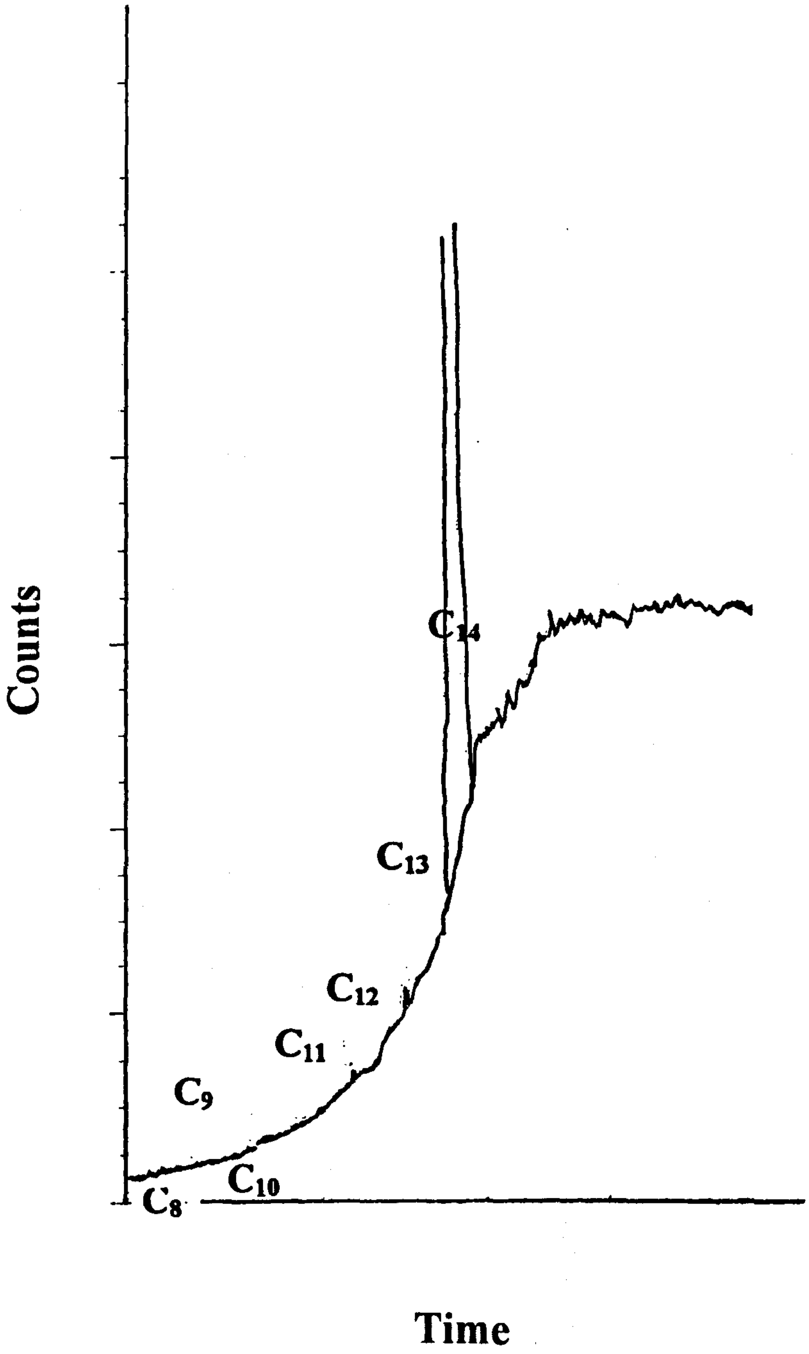

Figure 5.6 Concentration profiles of impurities found in myristic acid.

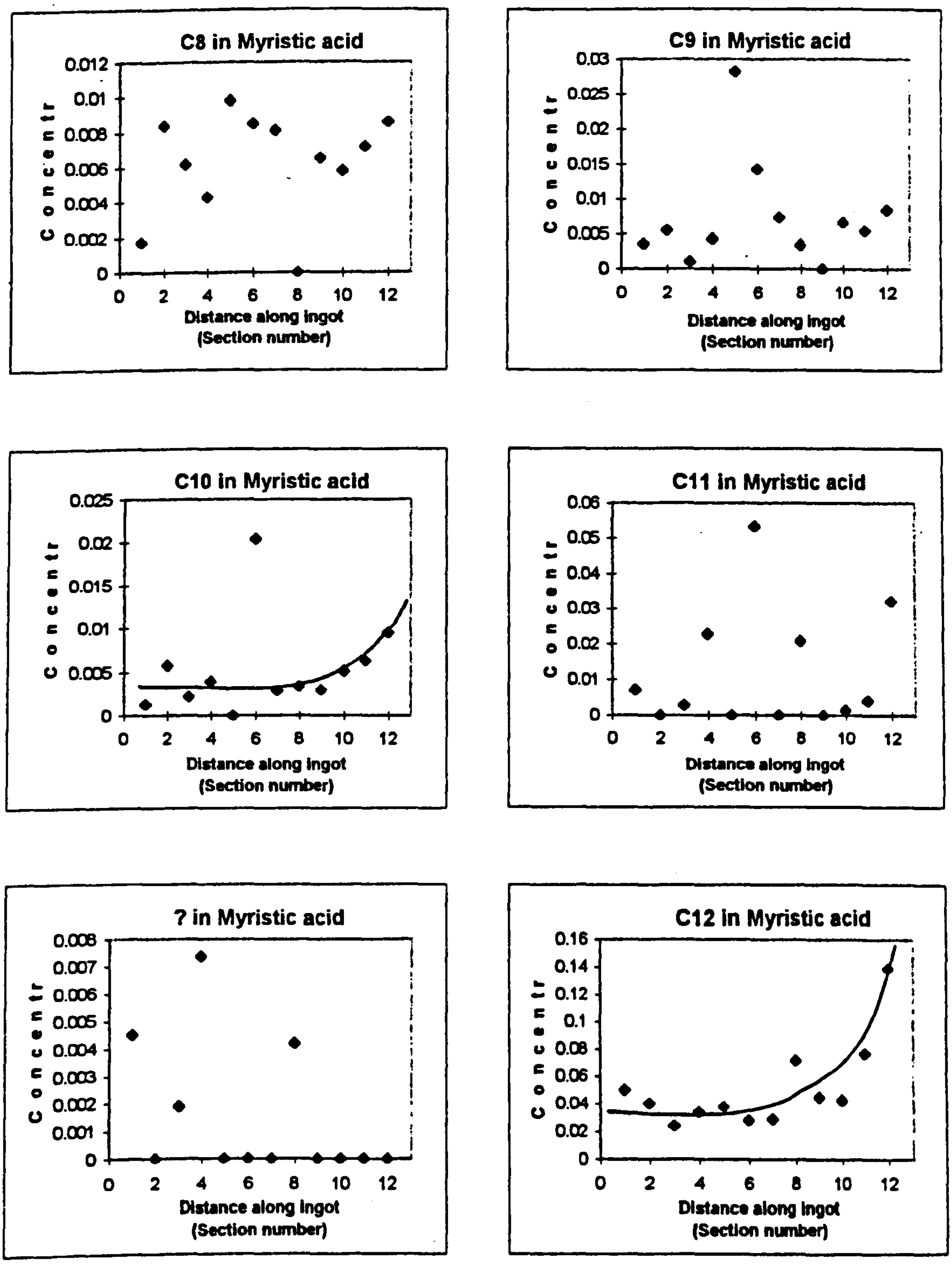

Figure 5.6 Concentration profiles of impurities found in myristic acid (continued)

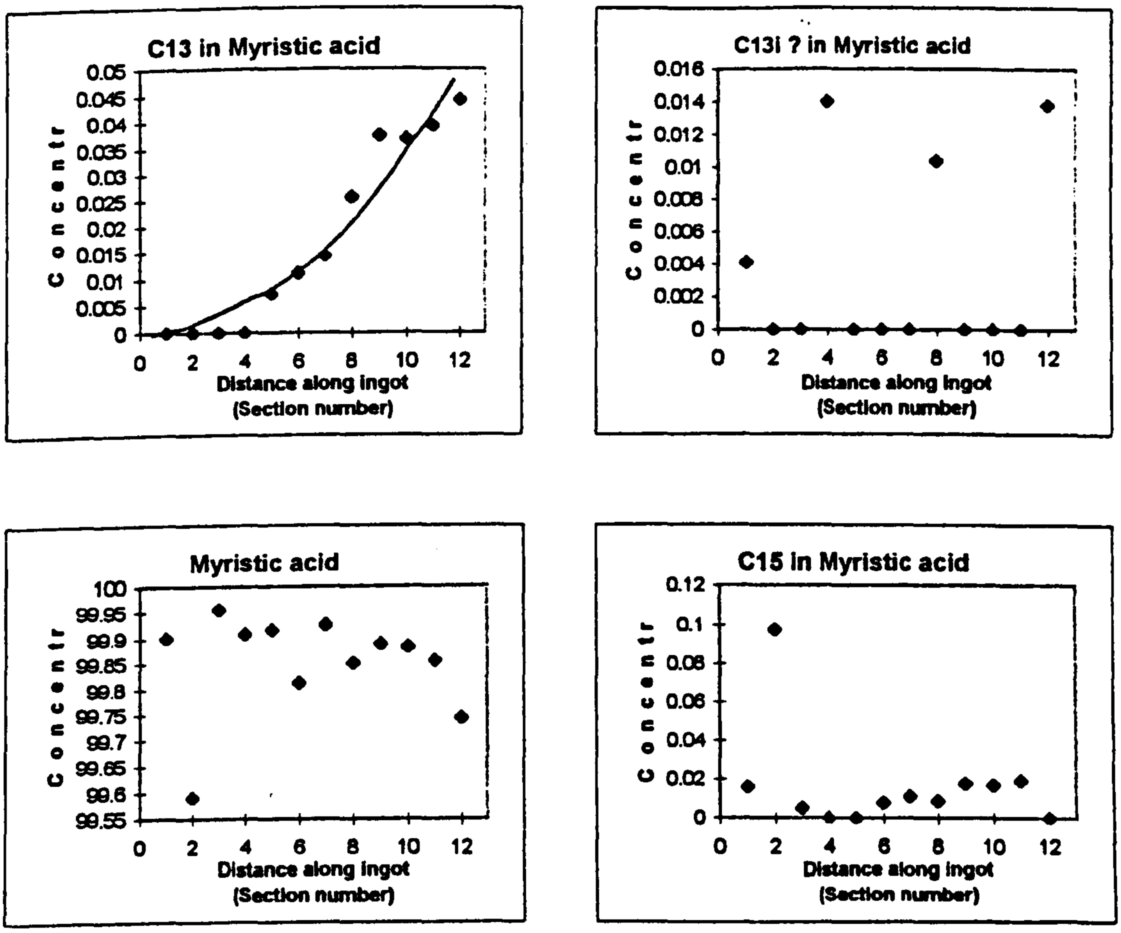

Figure 5.7 Graphs for the calculation of the segregation coefficients of the impurities in myristic acid

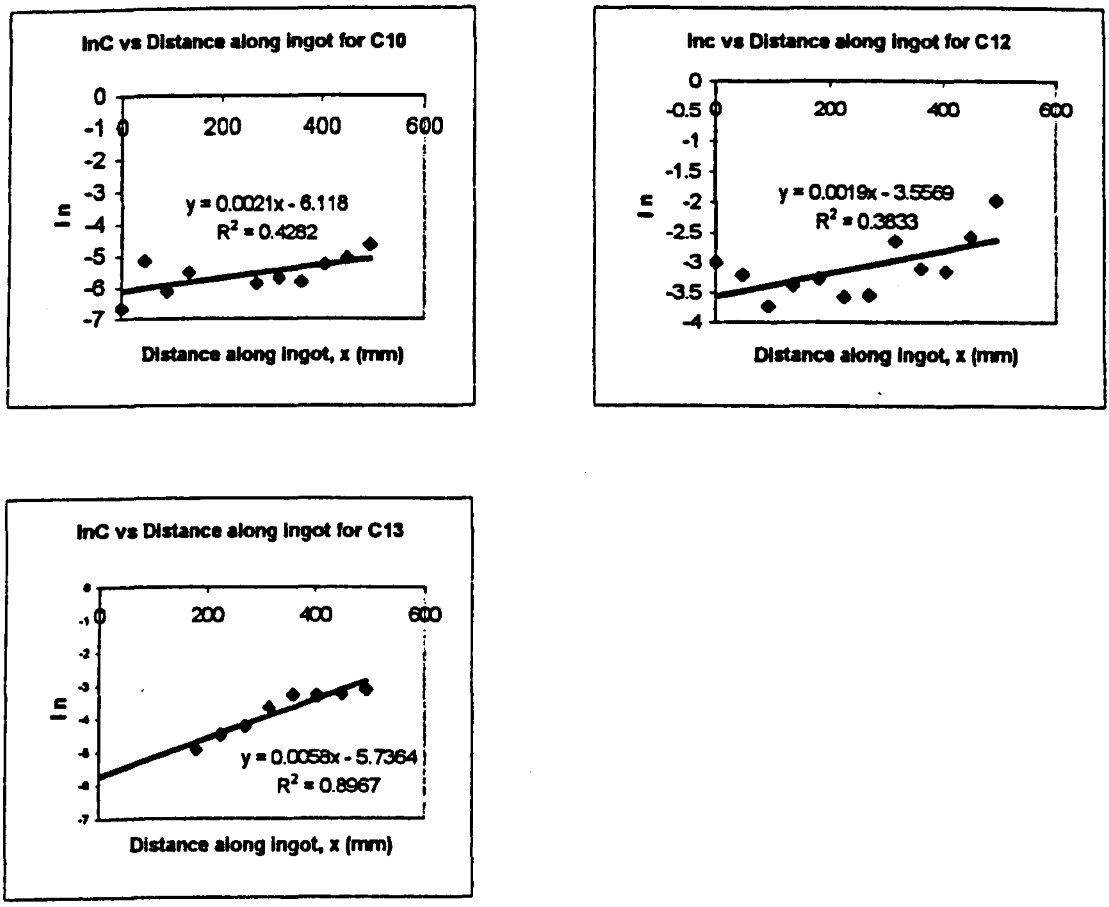

5.4 Differential Scanning Calorimetry (DSC) results

After GC analysis had shown that the top section of the ingot contained the purest material, samples of this section as well as unpurified samples were studied using differential scanning calorimetry (DSC), in order to assess the influence of impurities on the melting point, enthalpy of melting and crystallisation, and on the occurrence of phase transitions. For brevity the term "pure" will be used to refer to the purified samples from the top section of the ingot and the term "impure" will be used to refer to the fatty acid as obtained from *Sigma*. First in section 5.4.1 the DSC results are given for lauric acid, followed by the results for myristic acid in section 5.4.2. All samples were heated and cooled between 30 and 60°C at a rate of 2°C/min with the DSC described in chapter 4.

5.4.1 DSC results for lauric acid

The DSC results obtained for pure and impure lauric acid are summarised in table 5.6. For the impure sample no phase transitions were observed other than melting. However, for the pure sample a small peak was observed in the DSC curve before melting of the sample, indicating a phase transition at 39.94°C. This phase transition appeared to be irreversible, it only occurred when the sample was heated the first time and was not observed on cooling.

	sample (lauric acid)	
	impure	**pure**
melting point (°C)	45.07	45.60
crystallisation temperature (°C)	43.21	41.88
metastable zone width (°C)	1.86	3.72
enthalpy of melting (kJ/mol)	-35.18	-34.68
enthalpy of crystallisation (kJ/mol)	37.43	36.99
temperature at which phase change occurred during heating (°C)	none	39.94
enthalpy of phase change (kJ/mol)	none	-4.38

Table 5.6 DSC results for impure and pure lauric acid

5.4.2 DSC results for myristic acid

The DSC results found for pure and impure myristic acid are given in table 5.7. The enthalpy of melting seems to be incorrect for the impure sample, which is probably due to inaccurate weighing of the sample. The DSC curves for the myristic acid samples are shown in figure 5.8. For the impure sample no other phase transition was observed other than melting. A small peak at 50.03°C in the DSC curve of pure myristic acid shows that a phase transition did take place in this sample. As was found for pure lauric acid this phase transition appeared to be irreversible, it only occurred when the sample was heated the first time and did not take place on cooling.

	sample (myristic acid)	
	impure	**pure**
melting point (°C)	55.41	55.71
crystallisation temperature (°C)	51.97	51.70
metastable zone width (°C)	3.44	4.01
enthalpy of melting (kJ/mol)	-29.53	-44.53
enthalpy of crystallisation (kJ/mol)	46.16	48.31
temperature at which phase change occurred during heating (°C)	none	50.03
enthalpy of phase change (kJ/mol)	none	-3.63

Table 5.7 DSC results for impure and pure myristic acid

5.5 X-ray diffraction (XRD) results

Powder X-ray diffraction (XRD) measurements were carried out on "pure" (the top section of the ingot) and "impure" (obtained from *Sigma*) samples of lauric and myristic acid, in order to assess the influence of impurities on the crystal structure of these fatty acids. The XRD results for lauric and myristic acid are given in sections 5.5.1 and 5.5.2 respectively.

Figure 5.8 DSC curves for myristic acid: (a) unpurified and (b) purified

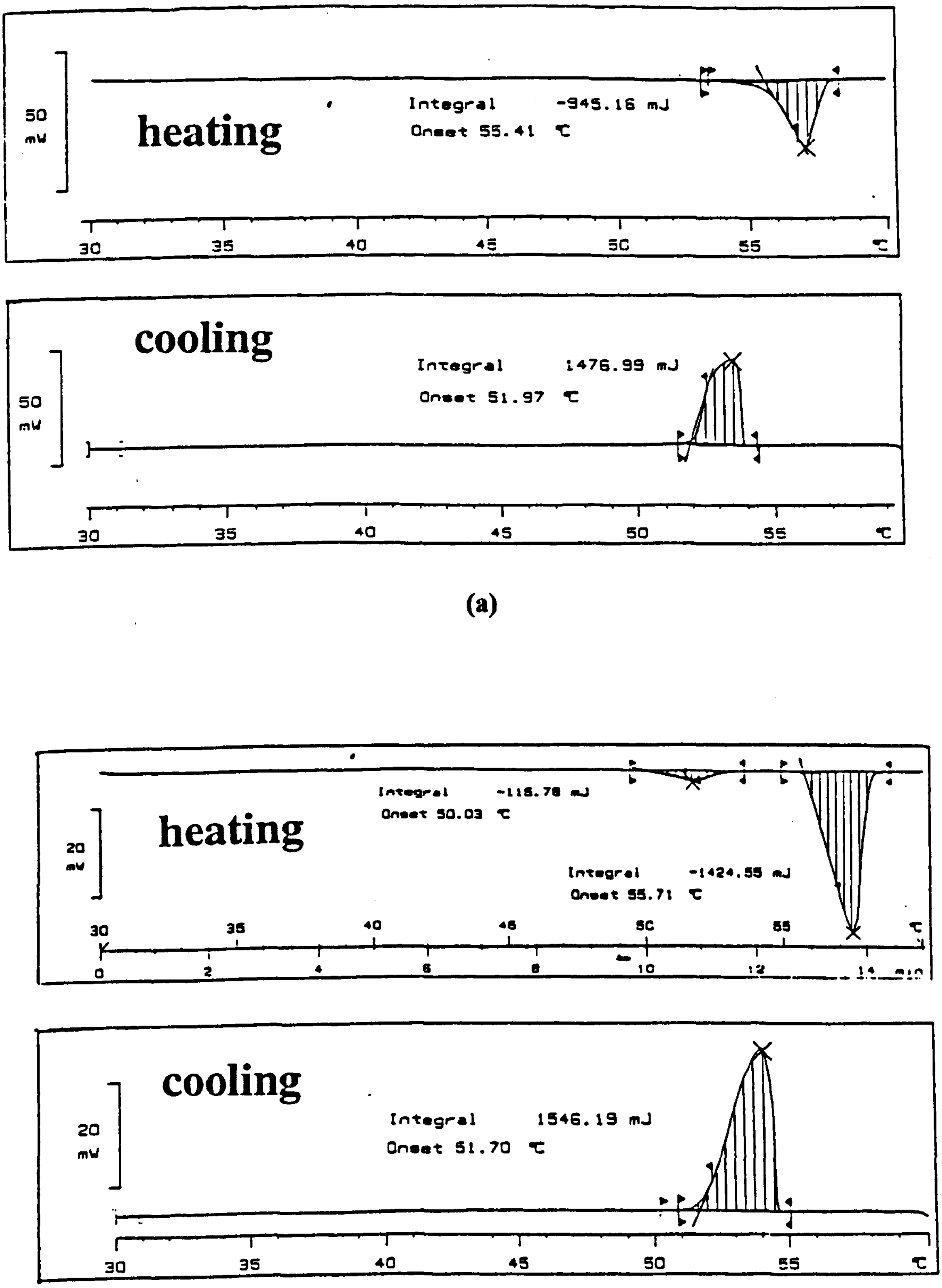

(a)

(b)

5.5.1 XRD results for lauric acid

X-ray spectra were taken of samples of pure and impure lauric acid. These spectra are compared in figure 5.9 and show that the structures of the two samples must be distinctly different. The spectrum of the pure sample was found to match well with the spectrum of the A-super form of lauric acid, which was simulated with data from Goto and Asada [2] using Cerius2 molecular modelling. The impure sample's spectrum was found to match well with the spectrum of the C form of lauric acid, simulated with data from Vand *et al.* [3].

In order to investigate the phase transition found with the DSC measurements, the pure sample of lauric acid was heated up from room temperature to 42°C, just above the temperature at which the phase transition was observed. At this temperature another XRD pattern was taken, which revealed that the structure of the sample had changed. The X-ray pattern of the pure sample taken at 42°C was identical to the pattern of the impure sample. The sample was then melted by increasing the temperature to 60°C and subsequently re-crystallised by cooling it down to 42°C. The XRD spectrum then taken at this temperature was still the same as for the impure sample. After subsequent cooling of the sample to 22°C, the XRD pattern showed a spectrum that was in between the spectra of the pure and the impure sample. Regular scans over a period of 2 weeks showed that the XRD pattern was slowly changing from the one found for the impure sample to the one originally found for the pure sample. This is shown in figure 5.10, where the key peaks are shown from figure 5.9. The peaks labelled 1 & 3 are decreasing in intensity whilst peaks 2 & 4 are increasing. This shows that the phase transition *is* reversible, the structure *does* revert back to the original, after heating and subsequent cooling, but the kinetics of the transformation process are slow.

5.5.2 XRD results for myristic acid

The XRD patterns for pure and impure myristic acid, taken at room temperature are compared in figure 5.11. This shows that the pure and impure samples of myristic acid also have different structures. However, the spectrum of the pure sample resembles that of the impure sample with several significant peaks added. These extra peaks were similar to the peaks in the pure lauric acid (two on either side of the main peak for the impure sample) and hence it seemed that the pure myristic acid sample was a two phase mixture, consisting of some material with the structure of pure myristic acid and some material with the structure of impure myristic acid.

No structures are known for myristic acid, however the XRD pattern of the pure sample was found to match well with the pattern of the γ (=A-super) form of myristic acid from the *Siemens D-5000* data base (no. 8-0806) and the impure sample's spectrum was found to match well with the spectrum of α (=C) myristic acid from the *Siemens D-5000* database (no. 8-0786).

A comparison of the spectra for the lauric acid samples and the myristic acid samples shows that the X-ray patterns for both the pure fatty acids show many similarities and so do the X-ray patterns for both the impure fatty acids.

5.6 Discussion

The results will be discussed in three parts: first in section 5.6.1 the trends and accuracy of the GC results, followed by a discussion on the DSC results in section 5.6.2. Although the last section, 5.6.3, mainly focuses on the XRD results, the consistency is demonstrated of these results with those obtained by the other techniques used.

5.6.1 Trends in the GC results

A number of impurities were found in both the unpurified lauric and myristic acid. From the evenly spaced retention times of the impurities it was assumed that these were fatty acids of different chainlengths. This was confirmed by GC analysis of samples of C_8, C_{10}, C_{11}, C_{13}, C_{14}, C_{16} and C_{18}. The retention times of all these

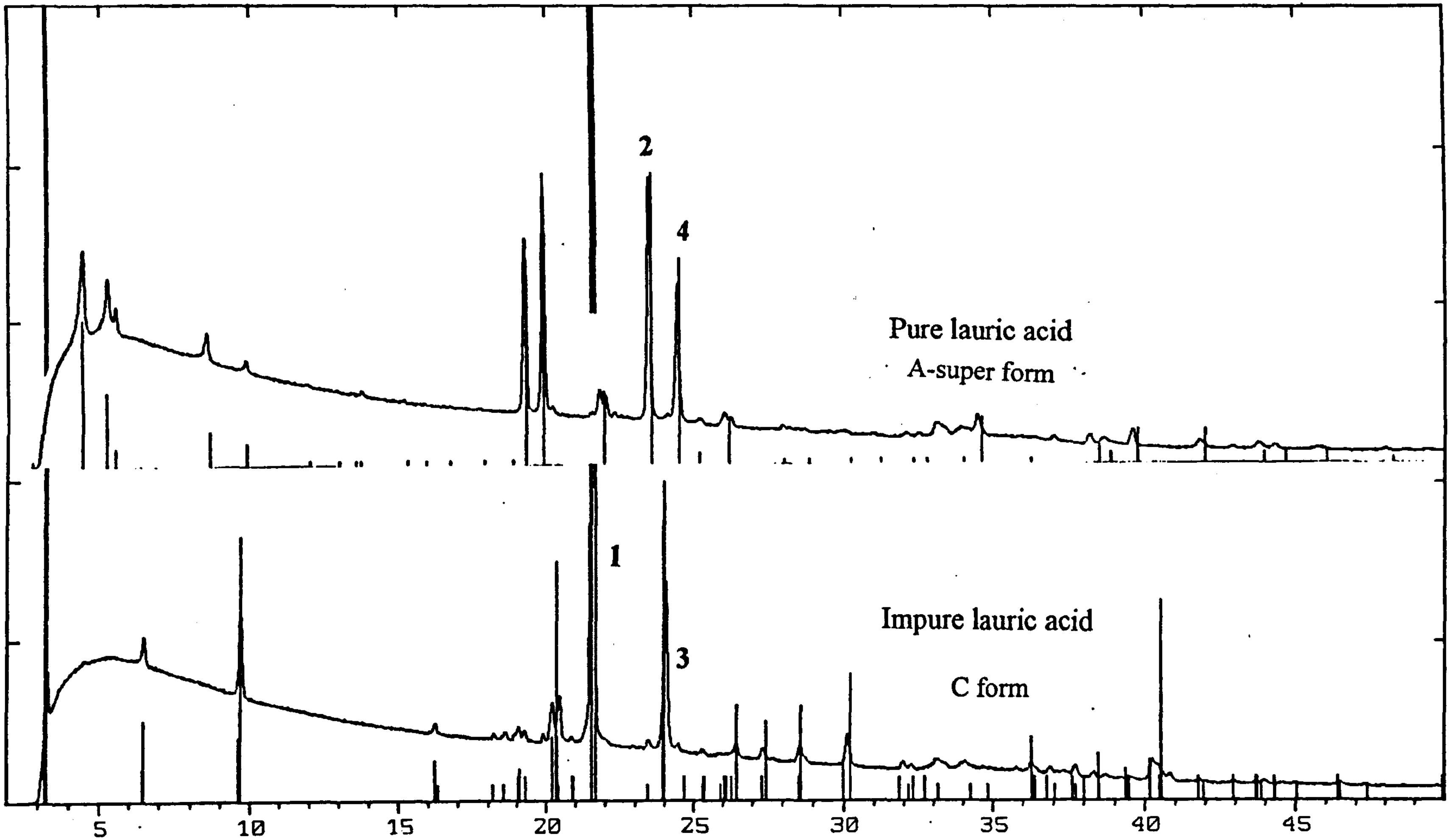

Figure 5.9 XRD patterns for pure and impure lauric acid show distinct differences

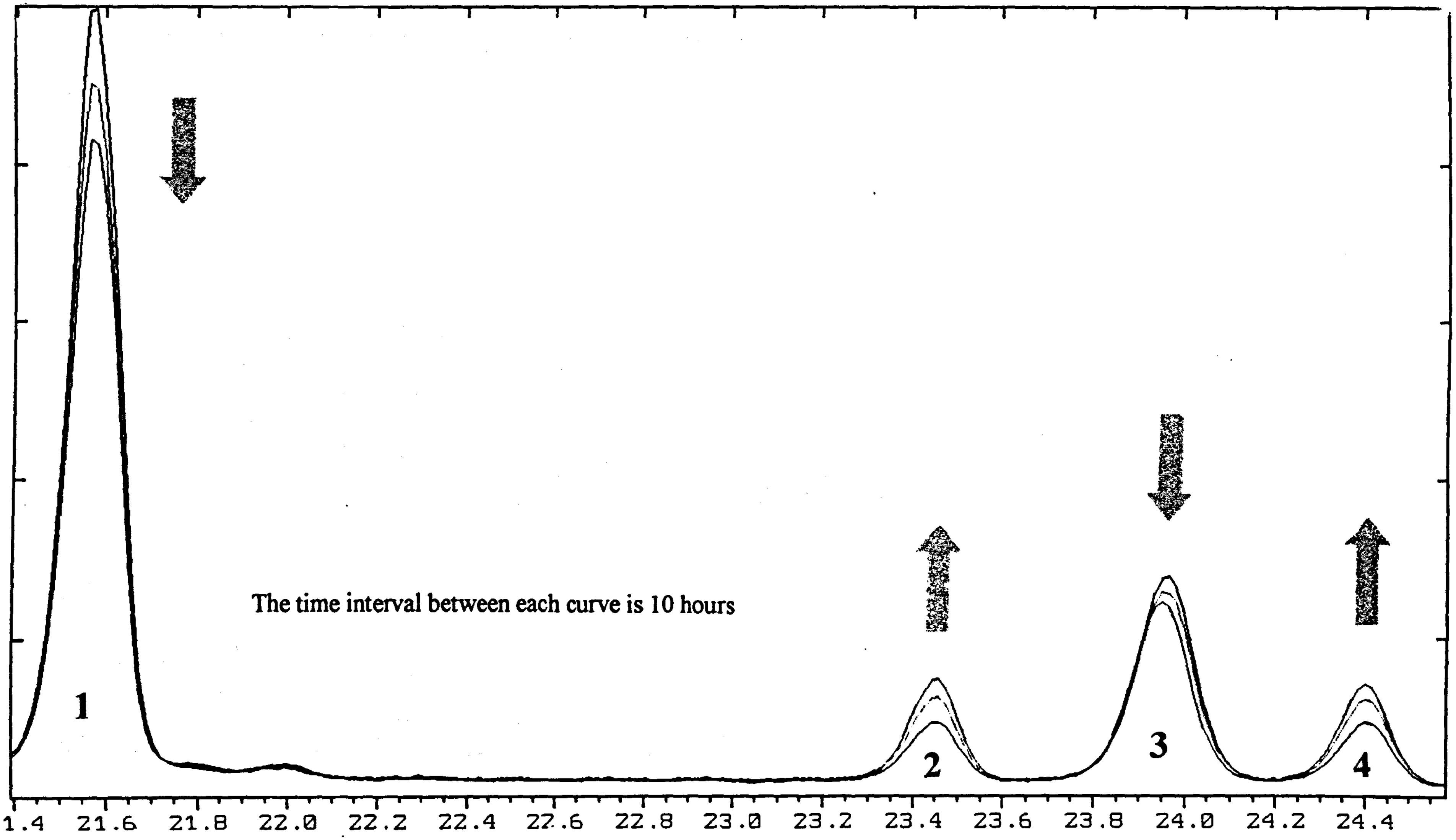

Figure 5.10 XRD patterns of lauric acid after heating and subsequent cooling showed that the material was slowly reverting back to its original structure; peaks 2 & 4 increased while peaks 1 & 3 decreased in intensity

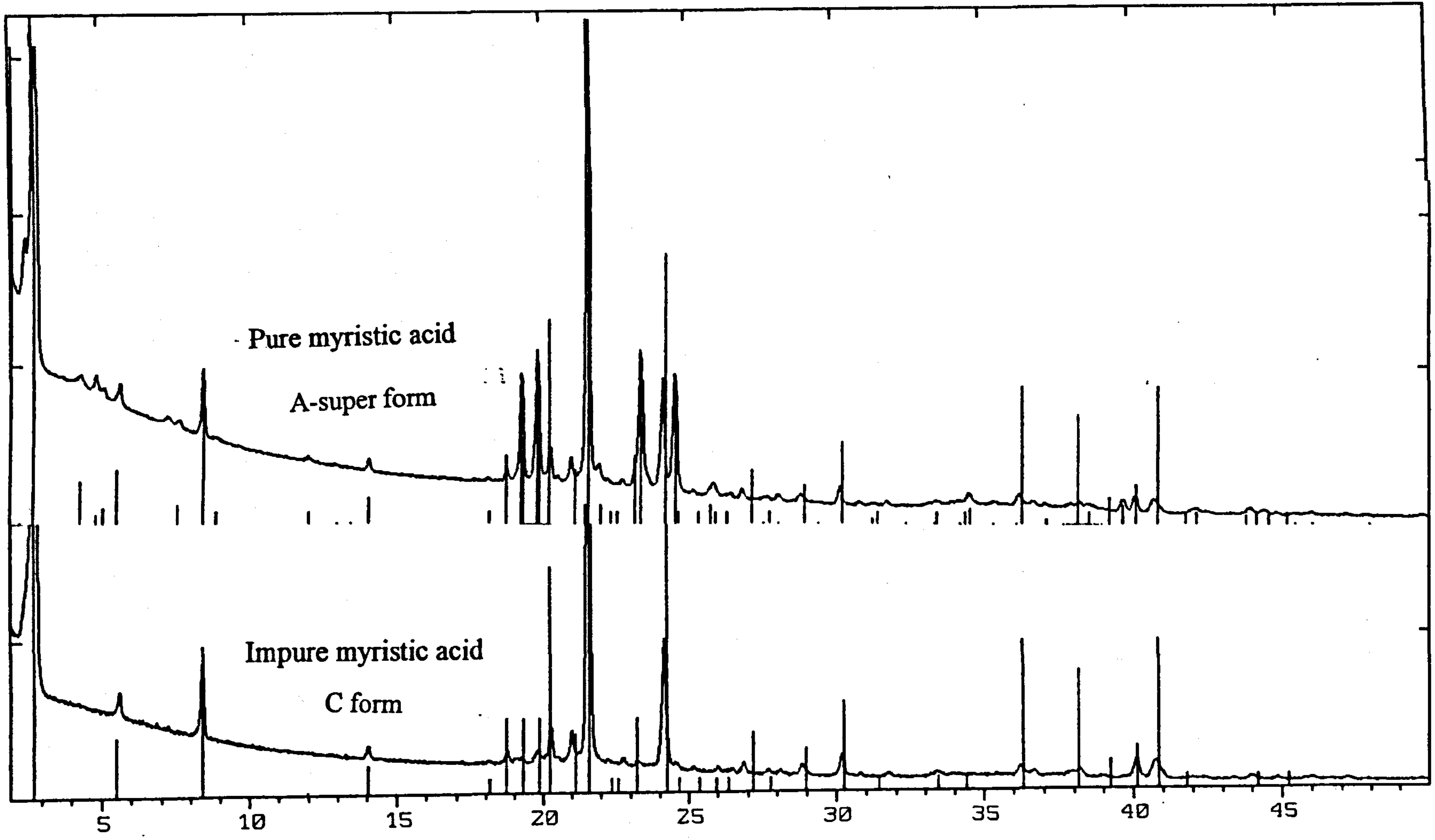

Figure 5.11 XRD patterns for pure and impure myristic acid show distinct differences

samples matched the times of the impurity peaks. Samples of C_9, C_{15} and C_{17} were not analysed but the peaks obtained at 5.9, 13.4 and 16.0 minutes were assumed to be due to these substances respectively. This assumption could be made because the peaks were equally spaced in between the surrounding identified peaks.

5.6.1.1 Lauric acid

The GC analysis (figure 5.2) of the unpurified lauric acid (C_{12}) revealed the presence a number of impurities. The concentrations of these impurities were between 0.0014 and 0.3234% which meant there was enough material present to be able to detect a concentration gradient along the ingot after refining, the smallest peaks detectable and accurately quantifiable over the noise using the GC and data handling software being ~0.001%. The overall purity of the unpurified sample was found to be relatively high: 99.471%.

The concentration profiles along the ingot, after purification, of most of the impurities (C_8, C_9, C_{10}, C_{12}, C_{13} and C_{14}) show a clear re-distribution along the ingot. Apart from C_9 the concentrations of most of the impurities (C_8, C_{10}, C_{11}, C_{13} and C_{14}) increased towards the bottom of the tube, indicating that the segregation coefficients for these impurities must be less than 1, as they had been brought down to the bottom of the tube in the molten zones. The concentration profiles for C_{11} and the unidentified peak at 11.2 min ($C_{13i?}$, which was thought to be an isomer of the C_{13} ester) showed no obvious trend. The concentrations in sections 4, 8 and 10 of the ingot do not seem to fit in with the rest of the data for C_{11} and $C_{13i?}$ (see concentration profiles, figure 5.3). These samples were esterified and analysed on the same day and hence a common error during their preparation or analysis could account for their similar vagrancy. The concentration profile for the overall purity of lauric acid, shown in figure 5.3, also indicates that some error had occurred in analysing sections 4, 8 and 10, as these points seem to be slightly out with the overall trend.

The segregation coefficients for the impurities were calculated from the concentration profiles, using the equations for the ultimate distribution. The best correlation coefficients for these calculations were obtained for C_8, C_{10}, C_{13} and C_{14}. The segregation coefficients found for these impurities were all very close to but slightly smaller than one. The C_9 was the only impurity that showed a segregation coefficient larger than unity, although only slightly larger: 1.01. The correlation coefficient for this value was very poor however. This could be due to the very low initial concentration of C_9 which means that after re-distribution the concentration in some sections will be even lower and is therefore very difficult to detect accurately. The correlation coefficient for the segregation coefficient of C_{11} was very low as well, as was also indicated by the poor quality data of the concentration profile.

The initial concentrations calculated from the ultimate distribution did not compare very well with the measured values for these concentrations. The values found for the segregation coefficients seem to be very reasonable however. A possible explanation for this is that not all impurities could be detected due to the fact that the GC conditions could not be optimised for the analysis of methyl-esters of fatty acids. This could cause two opposing effects:

1. All concentrations have been calculated by dividing the area under an impurity peak by the total area under all peaks. If there are more impurities present than are detected, than the total area would be larger than measured, therefore the real concentrations of the detected peaks would be *lower* than measured.
2. The fact that the GC conditions were not optimised could cause the detected peaks to be smaller than they should be. This would mean that the detected impurities are present in *higher* concentrations than the measured values.

These two opposing effects might result in the observed discrepancies between the calculated and measured values for c_0. Additional reasons might be:

1. the assumption was made that the sensitivity of the detector would be identical for all fatty acid homologues. This is not necessarily the case and could be investigated by studying samples of known concentrations and calibrating the areas underneath the peaks

2. the length of a molten zone l, was not constant for all the zones, which would influence the calculated value of c_0
3. there was no cooling zone above the top heating zone; as the tube was filled above this level, impurities from this part of the tube could have mixed with the main part of the tube.

5.6.1.2 Myristic acid

GC analysis of unpurified myristic acid showed only very low concentrations of impurities to be present (the overall purity was found to be 99.81%), in addition there was a significant amount of noise after the C_{14} peak, which meant that fatty acids with a longer chainlength than C_{14} could not be accurately detected. The four shortest chainlength impurities (C_8, C_9, C_{10} and C_{11}) had concentrations below 0.0075%. Because of this most of these impurities did not show a clear trend in their concentration profile after zone refining.

Good concentration profiles along the ingot of myristic acid after zone refining were obtained for C_{10}, C_{12} and C_{13}. The graphs indicate that the segregation coefficients for these impurities must be smaller than unity as the concentrations increase towards the bottom of the tube. The segregation coefficients were calculated using the equations for the ultimate distribution. Similar to the segregation coefficients for the impurities found in lauric acid, they were all very close to, but slightly smaller than unity. The initial concentrations calculated with the ultimate distribution again do not match very well with the measured values. This is probably due to the same reasons that were given above for lauric acid. In addition the position of the C_{14} peak was at the point where the background signal starts to increase and therefore any peaks coming after it were distorted or even hidden by the noise.

Although the measured concentrations of the impurities may not be highly accurate, it has been shown that the purity of both fatty acids after zone refining was the highest at the top of the ingot, and that most impurities have a segregation coefficient smaller than unity, which is consistent with this. It was to be anticipated that the values for the segregation coefficients are very close to unity as all the impurities were fatty acid homologues. These form solid solutions with the mother phase, thus making purification difficult to achieve.

5.6.2 DSC discussion

DSC analysis of both fatty acids revealed that the purified samples had a higher melting point and a lower crystallisation temperature than the unpurified samples. Both these effects result in a larger metastable zone width for the purified samples than for the unpurified samples. This shows that even very low levels of impurities can affect the nucleation and crystallisation behaviour of fatty acids. A higher melting point would be expected for purer samples, as impurities distort the crystal lattice so that less energy is needed to disrupt the lattice. However, no significant difference was found between the enthalpy of melting of the purified and unpurified samples. The difference in crystallisation temperature between the unpurified and purified samples clearly shows the effect of impurities on the nucleation process of lauric and myristic acid. When the concentration of impurities is lower a higher degree of undercooling is needed for the material to crystallise, as there are less impurities present around which a stable nucleus can be formed.

DSC analysis further showed the occurrence of a phase transformation in the purified samples of both fatty acids. This phase transition took place for both purified samples on heating but not on cooling. Initially this phase transition was therefore thought to be irreversible, but X-ray diffraction experiments (see next section) showed that the purified material did revert back to its original structure, but only slowly. The fact that the impure samples showed no phase change on heating indicated that they were in a different phase from the purified fatty acids. This was confirmed by the XRD measurements.

The enthalpy of the phase transition is larger for the lauric acid than for the myristic acid. This is consistent with the XRD results, which showed the pure myristic acid to be a mixture consisting of two phases, whereas the pure lauric acid seemed to exist as a single phase. Therefore a larger proportion of the material in the lauric acid sample was undergoing a phase change than in the myristic acid sample, which would explain a larger enthalpy for the phase transition.

5.6.3 General discussion

The XRD results are best discussed in relation to the observations of all the techniques used, therefore, instead of discussing the XRD results in isolation, in this section an overall discussion is given. The XRD measurements showed the X-ray spectra for the purified samples to be distinctly different from the ones for the unpurified samples. In addition, the X-ray diffraction experiments confirmed the occurrence of the phase transformation in the purified fatty acids that had been observed by DSC analysis. The XRD spectrum of purified lauric acid changed from the pattern for the pure material to the one for the impure material when the sample was heated to a temperature just above the transition temperature that had been observed with the DSC. When the sample was cooled past the transition temperature the spectrum changed back over a period of two weeks.

Fatty acids are well known to exhibit polymorphism (*e.g.* Garti and Sato [4], and Gunstone *et al.* [5]). Different polymorphs of fatty acids were originally labelled A, B and C on the basis of decreasing long spacings (increasing angle of tilt) in the order A, B, C. Later however, other structures have been found. The polymorphism of lauric and myristic acid is summarised as follows: the most common form for both lauric and myristic acid is the C (=α) structure which is formed by crystallisation from the melt (*e.g.* Thibaud and Dupré La Tour [6]). In addition to this a number of other structures are known to form depending on the crystallisation conditions. The B form has only been observed by Thibaud and Dupré La Tour [7], who introduced the α, β, γ notation where α=C, β=B and γ=A-super [6].

Both fatty acids can form the A-super (originally named A or γ) form, which can be obtained by crystallisation from certain solvents (*e.g.* Stenhagen and von Sydow [8] and von Sydow [9]). This form has not been observed for any other fatty acid (von Sydow [10] and Kobayashi *et al.* [11]). The structure of this form of lauric acid was partly solved by von Sydow [12] and was further refined by Goto and Asada [2], who had obtained the A-super form by a slow solution mediated transition from the C form in isooctane at room temperature. A spontaneous but very slow transformation (2 years) in the solid state has been shown to take place in the case of lauric acid from the C to the A-super form by Lomer [13]. In the case of myristic acid this transition has not been observed to occur spontaneously at all (not even after a period of 2 years), but can however be initiated by grinding the substance (Lomer [13]). The transition then takes place over a period of several days. On heating, a solid state transformation occurs in both fatty acids from the A-super to the C-form at a couple of degrees below their melting point (Lomer [13]).

In addition to the A-super, B and C forms, for lauric acid the A_1 form has been found by crystallisation from diethyl ether (Lomer and Spanswick [14] and Lomer [15]) and for myristic acid the A_2 and A_3 forms have been found (Kobayashi *et al.* [11]). This A_2 form was obtained by crystallisation from isooctane and was found to transform to the A_3 form at low temperatures (around 140K). Lauric acid only formed the A-super form, for which no transformation was observed on cooling to 30K ([Kobayashi *et al.* [11]).

The different forms can be distinguished by their XRD patterns. The crystal structures of the A-super, the A_1 and the C form of lauric acid have all been determined. No structure has been published for myristic acid. Cell parameters and transition temperatures from literature, for the polymorphs obtained here, are given in table 5.8 and 5.9 respectively.

The polymorphic forms of lauric and myristic acid found here have been identified by a comparison of the observed XRD patterns with patterns either simulated from known structures (in the case of lauric acid) or from the *Siemens D-5000* database (in the case of myristic acid). The purified lauric acid has been identified to exist at room temperature in the A-super form (also called γ), which transformed to the C (also called α) form on heating to a couple of degrees below the melting point. The purified myristic acid appeared to consist of a mixture of the A-super and the C form. The unpurified samples were shown to be in the C form (also called α). Apart from identification from the XRD pattern the C form was further confirmed by a comparison between the melting points of both fatty acids observed here and those reported in literature (see table 5.9). The melting point of the samples determined here compares well with previously published melting points of the fatty acids in the C form (see table 5.9). The melting points found here were slightly higher than those in literature, indicating that the samples were purer. Although the structure of the A-super and the C form of myristic acid are not known, the close similarities between the XRD spectra of lauric and myristic acid indicate that these structures must be very similar to the structure of the A-super respectively the C form of lauric acid.

polymorph	**cell parameters**	**no. of mol. per unit cell**	**space group**	**theor. density (g/cm^3)**
lauric acid • A-super (=γ) [2]	a=5.415 b=25.964 c=35.183 α=69.82° β=113.14° γ=121.15°	12	$A\bar{1}$	1.04
• C (=α) [3]	a=9.524 b=4.965 c=35.39 monoclinic, β=129.22°	4	$P2_1/a$	1.034
myristic acid • A-super (=γ) [13]	a=22.2 b=5.14 c=37.2 monoclinic, β=100.83°	12	not known	1.09
• C (=α) [16]	a=9.509 b=4.968 c=40.71 monoclinic, β=129.12°	4	not known	1.02

Table 5.8 Literature data for the A-super and the C form of lauric and myristic acid, the crystallographic data for myristic acid may not be accurate as the full crystallographic structures have not been solved

	lauric acid C form			myristic acid C form		
	literature	impure	pure	literature	impure	pure
crystallisation temperature (°C)	43.75 [17]	43.21	41.88	53.65 [17]	51.97	51.70
melting point (°C)	44.8 [3]	45.07	45.60	54.4 [17]	55.41	55.71
transition temp. (°C) A-super→C	35°C [10]	-	39.94	43°C [6] 44°C [8, 2]	-	50.03

Table 5.9 Comparison of literature data and data found here for crystallisation, melting, and transition temperatures of lauric and myristic acid

The temperatures found here for the transition from the A-super to the C form for both fatty acids are significantly higher than the ones previously reported. This might be due to the higher purity, as the crystal lattice of the A-super structure of the samples is more stable than the one previously found so that the transition only occurs at a higher temperature. Another explanation might be that the transition was detected here at a heating rate of 2°C/min. It may be possible that the transition was initiated at a lower temperature but due to the slow kinetics of the transformation process was only detected some time later at a higher temperature.

The spectrum for purified myristic acid revealed the sample to be a mixture of the A-super and the C form. Two possible causes for this are: 1. the material is not pure enough yet. 2. The kinetics of the transformation from the C to the A-super form might be slower for myristic acid than for lauric acid. As the transition occurs in the solid state the process is likely to be more difficult with increasing chainlength.

In figure 5.12 the transformation process is illustrated between the C and the A-super form of lauric acid. In all known fatty acid structures the molecules form hydrogen bridges between the carboxyl groups. In the C form distinct alternating layers exist of carboxyl groups and methyl end groups. In the A-super form this is not the case, the molecules alternate in direction in groups of three, so that no distinct layers in the crystal exist with only carboxyl or only methyl end groups. This means that during the transformation form the C form to the A-super form (and vice versa) major structural changes have to take place, as can be seen from a comparison of the structures of these forms of lauric acid in figure 5.12. This figure shows that in the transformation from the C to the A-super form groups of molecules have to be translated approximately the length of one molecule, along the direction of the hydrocarbon chain. In addition, in the A-super form there are two different molecular conformations present whereas in the C form all molecules have the same conformation The angle of tilt in the A-super form is also different from that in the C form. The phase transition occurs without a significant change in density, as can be seen from table 5.8. If one molecule starts to shift this will force other molecules to move as well. This rationalises the observation that even very low levels of impurities can inhibit the phase transition; if the movement of molecules is blocked at one point then no molecule can move.

The transition process from the C to the A-super form has only previously been found to occur for lauric acid over a period of two years and for myristic acid only after grinding and waiting for several days. Here *in-situ* XRD observations of purified lauric acid crystallised from the melt and subsequently cooled to room temperature, have shown that for pure enough material the transformation takes place over a period of two weeks rather than two years. In addition the transition has been shown to be enantiotropic since it was observed to be reversible with at a specific transition temperature. Ostwald's step rule for a crystallisation process states that the initially obtained structure after crystallisation is not always the *most* stable form but the *least* stable form, that is closest in terms of free energy change to the original state (see chapter 2). Successive polymorphic transformations can lead to more stable structures, until the most stable form at those conditions has been reached. This would indicate that the difference in free energy between the C form and the melt is smaller than for the A-super form and the melt. This is plausible since the ordering of

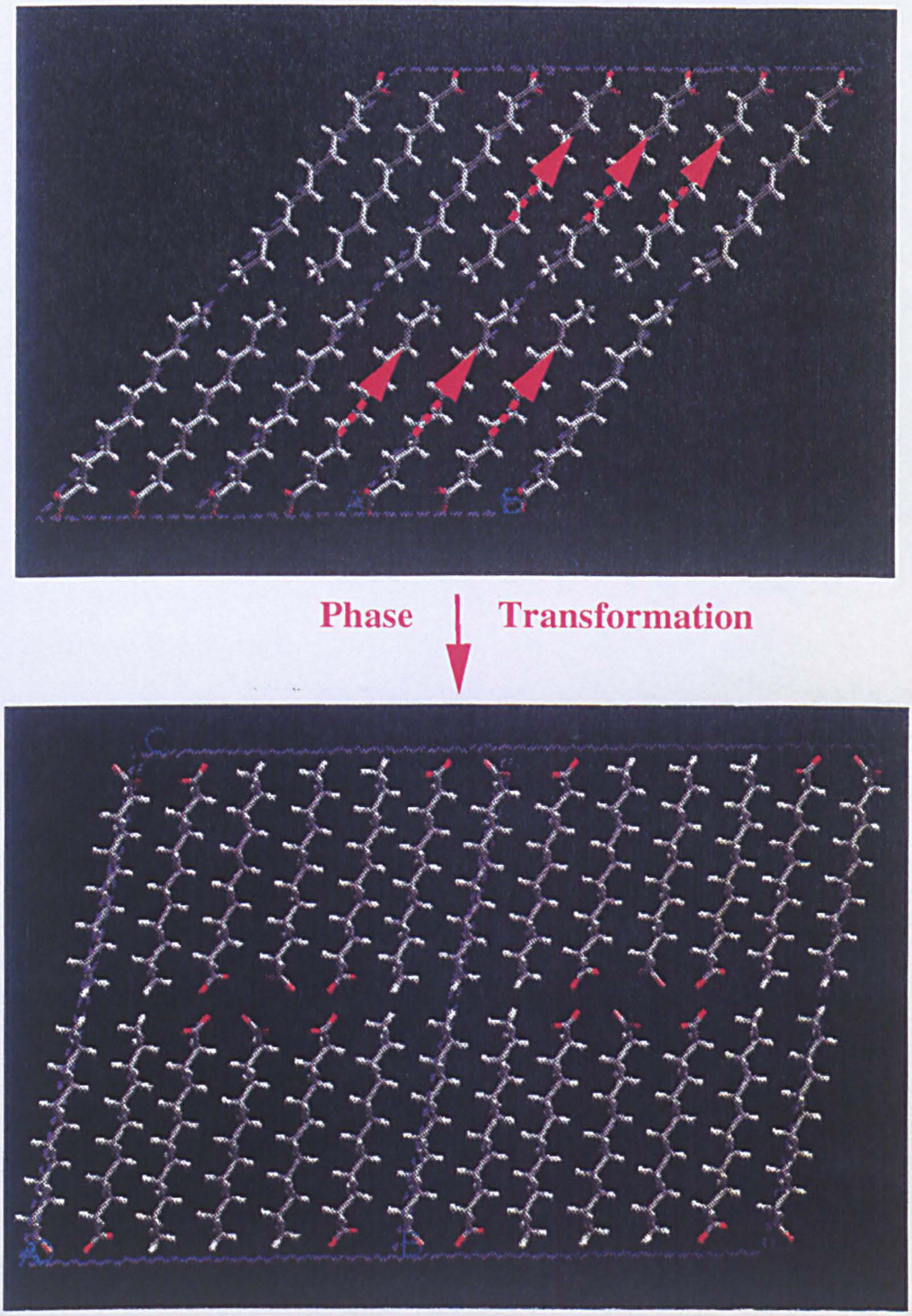

Figure 5.12 Illustrating the transformation in the solid state for lauric acid from the C (α) form to the A–super (γ) form. The top figure shows three units cells of the C form and illustrates the major movement of molecules necessary for the transformation to the A–super form, of which two unit cells are shown in the bottom figure. The crystal structures are based on data from Vand *et al.* [3] for the C form and from Goto and Asada [2] for the A–super form

the fatty acid molecules in the molten state is more likely to resemble the structure of the C form than that of the A-super form, as the structure of the C form is similar to that of a lamellar liquid crystal with alternating polar and apolar layers (here formed by the carboxyl and the methyl end groups respectively).

If the fatty acids above a certain purity would crystallise in the A-super structure from the melt, then in the sample tube during zone refining different solid forms would be present at the same time, depending on the position in the tube. At the top of the ingot the A-super structure would form, since the purity has been shown to be the highest in the top section, and in the bottom part the C form would exist. Therefore in the top section there would be an equilibrium between the liquid phase and the A-super form, while below a certain height an equilibrium would exist between the liquid phase and the C form. The distribution coefficients for these two equilibria would probably be different, since the solid state structures are different. For this reason the simultaneous existence of the equilibria of the molten phase with both the A-super and the C form would affect the values of the observed distribution coefficients and of the initial concentration calculated from the ultimate distribution. Although the *in-situ* X-ray diffraction experiments have shown that even for the purest material obtained here, the C form is still the one initially formed from the melt, the transition to the A-super form starts immediately when the sample is cooled below the transition temperature (which definitely occurs during zone refining, as the temperature of the cooling water was held at 11°C). A major molecular rearrangement has been shown to take place during the transformation processes which take place during the C to A-super transition and again when this particular section of the sample is heated, during the A-super to C transition. The assumption made in zone refining theory that solid state diffusion is negligible is thus not correct in this case and a redistribution of the impurities in the solid phase might occur. It is not known to what extent this affects the calculated values of the initial concentrations and the distribution coefficients.

The results have shown that impurities can have a dramatic effect on the structure of both fatty acids. The spontaneous transition from the C to the A-super form, which is the most stable form at room temperature, is inhibited by the presence of even very low levels of impurities, which were at the detection limit of the GC method used. This illustrates two points previously made by Pfann [18]:

1. the true properties of a substance are not known until it has been obtained in ultra pure form
2. since some properties of a material are affected even by levels of impurities which are hard to detect by analytical methods, in some cases it is easier to assess the purity of the material by monitoring a specific property of the material (*e.g.* melting point or in this case the crystal structure)

5.7 Conclusions

- GC analysis of the fatty acids revealed the following:
    1. Significant amounts of impurities were present in unpurified lauric acid, the concentrations of these impurities were lower in unpurified myristic acid.
    2. Zone refining effected a re-distribution of the impurities; for both fatty acids the purity after zone refining increased towards the top of the ingot. From GC analysis this was not apparent for myristic acid, but visual observation, DSC and XRD analysis showed the material to be in a different state from before. This illustrates that at very low levels of impurities it might be easier to assess the purity of a material from monitoring its properties than from analytical methods.
    3. Using the equations for the ultimate distribution, the segregation coefficients were calculated for a number of impurities in both the fatty acids. All segregation coefficients were found to be close to unity, indicating that the other homologues fatty acids are very difficult to separate from the main one using zone refining. The initial concentrations of the impurities calculated from the ultimate distribution differed

significantly from the measured values. This is probably due to the fact that the GC conditions could not be optimised for the analysis of methyl-esters of fatty acids. In addition solid state diffusion takes place during the transformation from the C to the A-super form and vice versa. This might affect the calculated values of the segregation coefficients and of the initial concentration.

- DSC analysis showed:
    4. Melting point and crystallisation temperature are both affected by low levels of impurities. Purer material was found to have a higher melting point, a lower crystallisation temperature and thus a larger metastable zone width than less pure material.
    5. A phase change to occur in the purified fatty acids on heating that did not take place in the unpurified samples.

- XRD experiments revealed:
    1. The purified lauric acid to be in the A-super (=γ) form at room temperature and both unpurified fatty acids to be in the C (=α) form.
    2. The purified myristic acid to consist of a mixture of the A-super and the C form.
    3. The phase transition observed in purified material during DSC studies to be the transition from the A-super to the C-form.
    4. The ability of purified fatty acids to change *spontaneously* and *reversibly* in the solid state from the C to the A-super structure and vice versa over a period of two weeks. This transition has previously only been reported in literature to occur over a period of two years (for lauric acid) or only after grinding and waiting for several days (for myristic acid).

The XRD spectra of both purified fatty acids were very similar and so were both spectra for the unpurified samples. Although the structure of the A-super and the C form of myristic acid are not known these are thus likely to be very similar to the respective structures of lauric acid.

- Overall conclusions

  Even low levels of impurities were shown to have a dramatic effect on the crystallisation process of fatty acids. Although these levels of impurities can be difficult to detect by analytical means, they can still affect the crystallisation and melting temperatures and inhibit the material from forming its most stable structure. The latter is readily understood when comparing the two different structures and realising the major molecular re-arrangement which occurs during the phase transformation. The physical properties of fatty acids were also observed to be affected by small amounts of impurities, the refined samples were optically clearer and much harder to grind than the unpurified material.

5.8 Suggestions for future work

- A dramatic effect has been shown of low levels of impurities on the crystallisation process and physical properties of fatty acids. The next logical step would be to convert the purified fatty acids to soaps, in order to assess the effect of impurities on the nucleation and crystallisation process and other physical properties of soaps.

- It would be interesting to study the dependence of the obtainable purity on the number of passes in order to investigate what the minimum number of passes is required for the ultimate distribution.

- Other chainlengths of fatty acids can be purified to investigate if the effects of impurities found here are generic for a series of fatty acids.

- It could be investigated which impurities inhibit the fatty acids from forming the A-super structure. This could be attempted by mixing different chainlength fatty acids with the purified material. These “impurity” fatty acids must themselves be of a high purity, otherwise a mixture of chainlengths is mixed in, instead of a single component.

- The GC conditions need to be optimised in order to be able to detect low levels of impurities more accurately. Peaks could have been hidden or damped in the excessive noise due inappropriate set-up of the GC.

- The degree of agitation of the molten zones during zone refining could be improved by making the motor which rotates the tube alternate in direction and by using an acceleration motor profile. In this way the liquid phase mixing and hence mass transport would be improved, which perhaps makes the zone refining process overall more efficient.

5.9 References used in this chapter

1. Schaeppi WH, *Chimia* **16**, 291 (1962)
2. Goto M and Asada E, *Bulletin of the Chemical Society of Japan* **51 (1)**, 70 (1978)
3. Vand V, Morley WM and Lomer TR, *Acta Cryst* **4**, 324 (1951)
4. Garti N and Sato K (eds), *Crystallization and polymorphism of fats and fatty acids*, Marcel Dekker Inc, New York and Basel (1988)
5. Gunstone FD, Harwood JL and Padley FB, *The Lipid Handbook*, (sec. ed., 1994), Chapmann and Hall London and New York (1986)
6. Thibaud J and Dupré La Tour F, *C R Acad Sci Paris*, **191**, 200 (1930)
7. Thibaud J and Dupré La Tour F, *C R Acad Sci Paris*, **190**, 945 (1930)
8. Stenhagen E and von Sydow E, *Arkiv för Kemi* **6 (29)**, 309 (1953)
9. von Sydow E, *Acta Chemica Scandinavica* **9**, 1685 (1955)
10. von Sydow E, *Arkiv för Kemi* **9 (19)**, 231 (1956)
11. Kobayashi T, Kobayashi M and Tadokoro H, *Mol Cryst Liq Cryst* **104**, 193 (1984)
12. von Sydow E, *Acta Chemica Scandinavica* **10**, 1 (1956)
13. Lomer TR, *Nature* **176**, 653 (1955)
14. Lomer TR and Spanswick RM, *Acta Cryst* **14**, 312 (1961)
15. Lomer TR, *Acta Cryst* **16**, 984 (1963)
16. Abrahamsson S and von Sydow E, *Acta Cryst* **7**, 591 (1954)

17.Francis F and Piper SH, *J Amer Chem Soc* **61**, 577 (1939)

18.Pfann WG, *Zone Melting*, Robert E Krieger Publishing Company Inc, Huntington, New York, second ed. (1978)

Chapter 6

Nucleation studies of single and mixed straight chain surfactants from dilute aqueous solutions

Chapter 6 Nucleation studies of single and mixed straight chain surfactants from dilute aqueous solutions

6.1 Introduction

In this chapter the results are given of an investigation into the nucleation process of natural surfactants from isotropic micellar solutions. Dilute surfactant systems of single and mixed sodium laurate (NaL), sodium myristate (NaM) and sodium palmitate (NaP) samples have been studied, in order to investigate the effect of chainlength and the mixing of surfactants on their nucleation behaviour. The experimental procedures for sample preparation and filtration as well as the equipment used for the nucleation studies are described in chapter 4. Slow cool experiments were carried out with the aim of measuring the metastable zone widths and the saturation temperatures of the samples. The results for this are given in section 6.2. In the second part of this chapter (section 6.3) the results are discussed that were obtained with the crash cool rig which was especially developed for the work presented here (see chapter 4). The objective of the crash cool experiments was to measure the induction time as a function of supersaturation. From these measurements, with the use of homogeneous nucleation theory, the size of the critical nucleus and the solid-liquid interfacial tension have been estimated. The conclusions drawn from the slow and crash cool measurements are given in section 6.4. The chapter finishes with recommendations for future work in section 6.5.

6.2 Slow cool experiments

Slow cooling/heating cycles were used, to obtain the metastable zone width (MSZW), the order of nucleation as defined in chapter 2 and the saturation temperature in order to determine the enthalpy and entropy of dissolution. With the apparatus used no liquid crystalline systems could be studied, due to their high viscosity. Therefore only nucleation behaviour from isotropic micellar solutions has been investigated. The upper limit of the solution concentration was thus determined by the transition concentration between the isotropic micellar solution and the hexagonal liquid crystalline phase; this concentration decreases with increasing chainlength. The results for the single surfactant samples are given in section 6.2.1, for the surfactant mixtures in section 6.2.2.

6.2.1 Results and discussion: single surfactants

The single surfactant systems studied are listed in table 6.1. Some typical results of cooling/heating cycles for single surfactant samples are shown in the figures 6.1-6.3. From these figures it is clear that the onset of nucleation during cooling can be detected by a dramatic increase in turbidity. As the solid dissolves on heating the transmittance of light through the sample increases until it has reached the value for a clear solution. The small decrease in turbidity after the onset of crystallisation and the small increase in turbidity just before dissolution were artefacts of the system. As the soap crystallised out, a white coagel was formed, which reflected the light back into the turbidity probe. The afore mentioned small changes were thus due to reflectance of light by the sample rather than transmission of light through the solution. The small decrease in turbidity was thus caused by the hardening of the coagel which filled up the open space in the turbidity probe. On heating, the coagel became soft so that less light was reflected back into the turbidity probe. The effect is illustrated in figure 6.4 where part of the cooling curve of a sodium laurate solution is compared to the corresponding part of the cooling curve for docosane ($C_{22}H_{46}$) in dodecane ($C_{12}H_{26}$). The alkane did not form a coagel when it crystallised but formed a suspension. The alkane sample therefore did not show the small decrease in turbidity after the onset of crystallisation.

Single surfactants
5, 10, ,15, 20, 25% NaL
5, 10, ,15, 20% NaM
5, 10, ,15% NaP

Table 6.1 Single surfactant samples studied; percentages are by weight

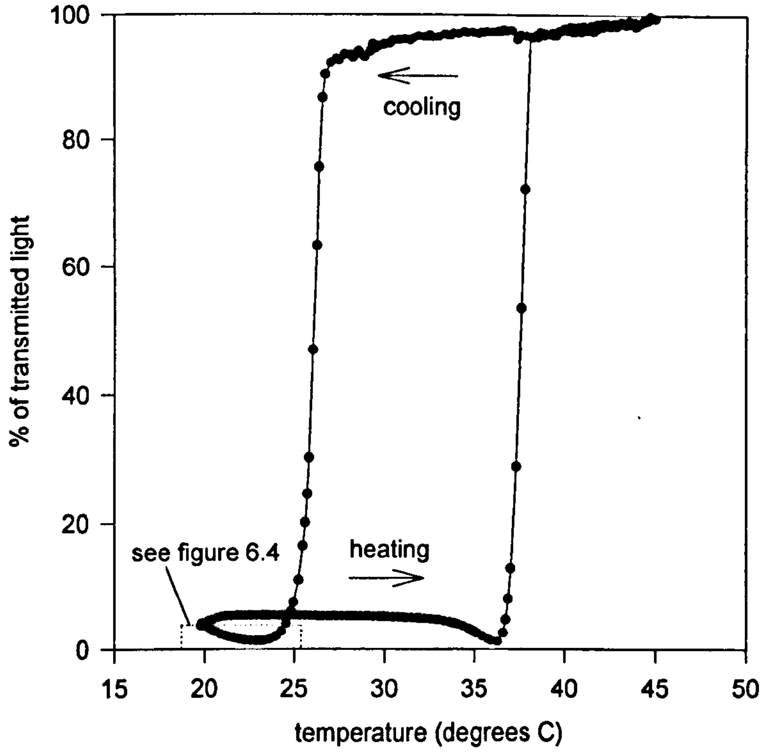

Figure 6.1 Turbidity versus temperature curve for a 10% NaL sample; cooling/heating rate=0.75°C/min

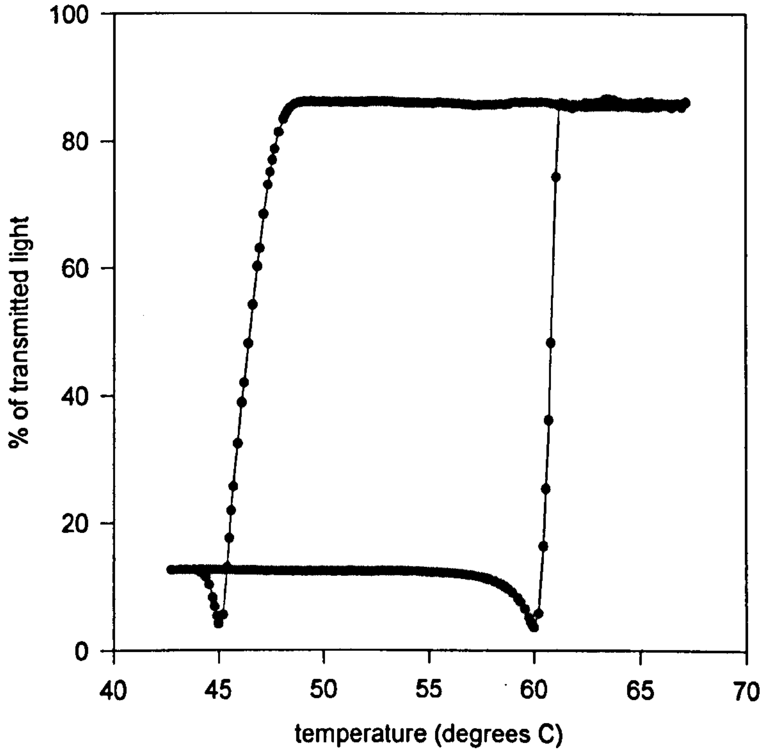

Figure 6.2 Turbidity versus temperature curve for a 15% NaM sample; cooling/heating rate=0.50°C/min

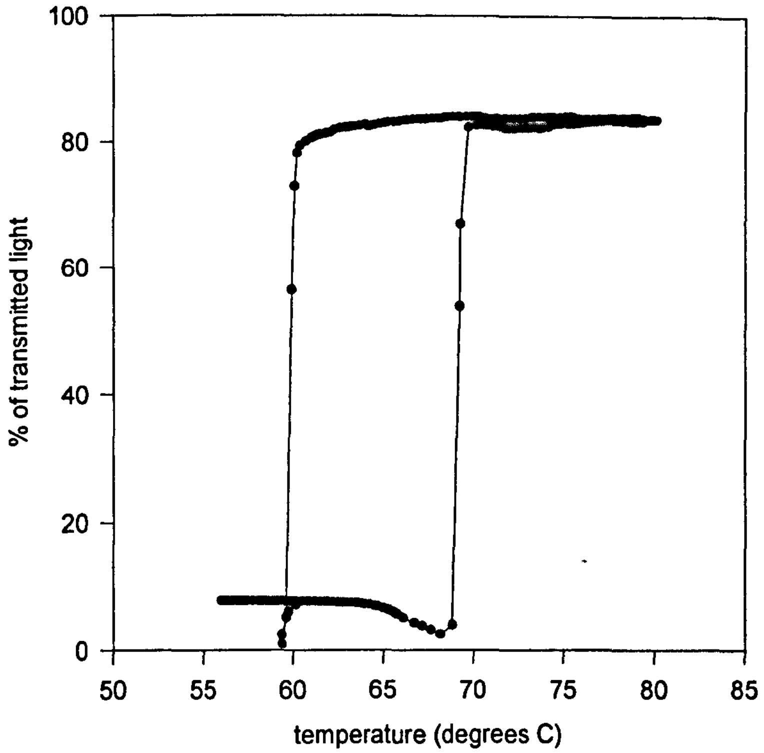

Figure 6.3 Turbidity versus temperature curve for a 10% NaP sample; cooling/heating rate=0.75°C/min

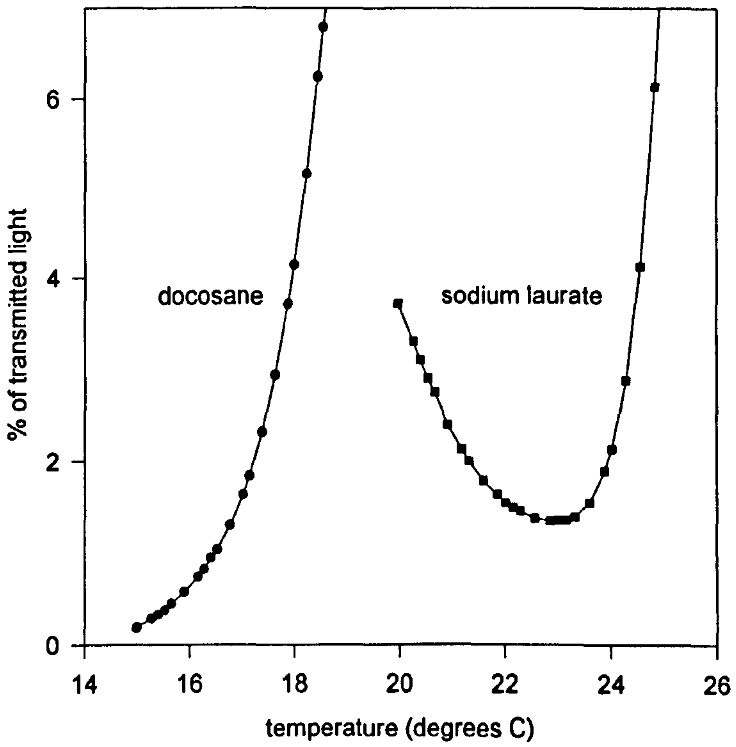

Figure 6.4 Comparison of part of the cooling curve for a 10% sodium laurate sample and a 10 mole% docosane in dodecane sample, cooling rate=0.75°C/min

By extrapolation of the precipitation and dissolution temperatures to zero cooling rate (as was explained in chapter 4) the metastable zone widths, the apparent order of nucleation, *m* and the saturation temperatures have been determined at different concentrations of NaL, NaM and NaP. These values are given in table 6.2. From this table it is clear that the saturation temperature increased with increasing chainlength, the saturation temperatures for NaP were the highest, then the ones for NaM and the saturation temperatures for NaL were the lowest. For all three surfactants the saturation temperature increased with increasing solution concentration, although the correlation coefficients for the saturation temperatures for the sodium myristate solutions are quite low. The observation that the saturation temperature increased with chainlength can be explained by the fact that as the chainlength gets longer the surfactant becomes more hydrophobic, thus becoming less soluble. The metastable zone width and the apparent order of nucleation seemed to decrease with increasing chainlength and concentration, although there are deviations to these trends.

wt% soap	**MSZW (°C)**			**m**			**T_{sat} (°C)**		
	NaL	NaM	NaP	NaL	NaM	NaP	NaL	NaM	NaP
5	6.81 (0.86)	4.56 (0.78)	3.42 (0.99)	3.72 (0.89)	3.44 (0.87)	2.56 (0.98)	32.12 (0.97)	49.25 (0.13)	65.45 (0.95)
10	7.25 (0.92)	4.12 (0.91)	4.19 (0.96)	4.37 (0.90)	2.96 (0.95)	2.55 (0.98)	36.49 (0.87)	53.44 (0.77)	68.01 (0.95)
15	5.10 (0.92)	3.01 (0.98)	3.82 (0.99)	2.91 (0.97)	1.48 (0.98)	3.32 (0.98)	39.45 (0.91)	59.82 (0.69)	69.49 (0.86)
20	4.33 (0.90)	2.75 (0.95)	-	2.43 (0.97)	2.31 (0.98)	-	43.02 (1.00)	56.76 (0.04)	-
25	3.05 (0.95)	-	-	2.06 (0.97)	-	-	45.25 (0.97)	-	-

Table 6.2 Nucleation parameters for single surfactant systems; correlation coefficients are given between brackets

From the saturation temperatures the values for the enthalpy and entropy of dissolution have been calculated using the Van 't Hoff equation (see chapter 2). The values are given in table 6.3. Both the entropy and the enthalpy of dissolution increased with increasing chainlength. This reflects that more energy is needed to dissolve the longer chainlength surfactant and that there is a larger difference in disorder between the dissolved state of the surfactant and the solid state as the chainlength gets larger. The good fit between the data and the Van 't Hoff equation indicates ideal solution behaviour. This would mean that the interactions between the surfactant molecules and between surfactant and water molecules would be the same. This is clearly not the case since their interactions with water cause the surfactant molecules to form micelles.

Surfactant	ΔS_d **(J/mol K)**	ΔH_d **(kJ/mol)**	**correlation coefficient**
NaL	317.3	110.5	0.99
NaM	463.0	163.8	0.80
NaP	792.9	284.5	0.99

Table 6.3. Entropies and enthalpies of dissolution calculated with the van 't Hoff equation (see chapter 2)

6.2.2 Results and discussion: surfactant mixtures

The surfactant mixtures which have been studied are listed in table 6.4. These samples were subjected to the same cooling/heating cycles as the single surfactants had been. In many cases the observed nucleation behaviour was significantly different however, this will be further discussed below.

NaL:NaM=1:3, 1:1, 3:1	20% surfactant, 80% water
NaL:NaM=1:1	10% surfactant, 90% water
NaL:NaP=1:3, 1:1, 3:1	10% surfactant, 90% water
NaM:NaP=1:3, 1:1, 3:1	10% surfactant, 90% water

Table 6.4 Surfactant mixtures studied; ratios are molar ratios, percentages are by weight

6.2.2.1 The NaL/NaM mixtures

The turbidity versus temperature curves for the NaL/NaM mixtures showed the same general shape as had been observed for the single surfactant samples. An example is shown in figure 6.5. For the NaL/NaM mixtures as a 20% surfactant solution the metastable zone widths and saturation temperatures are given in table 6.5 together with the values for single surfactants as 20% soap solutions for comparison. From this table it seems that a 1:1 surfactant mixture resulted in an intermediate MSZW, whereas when one of the components of the mixture dominated, the metastable zone became larger indicating that crystallisation was inhibited. The apparent order of reaction for nucleation was higher for all the NaL/NaM mixtures than for the two individual components. The saturation temperature increased with an increasing fraction of NaM in the mixture.

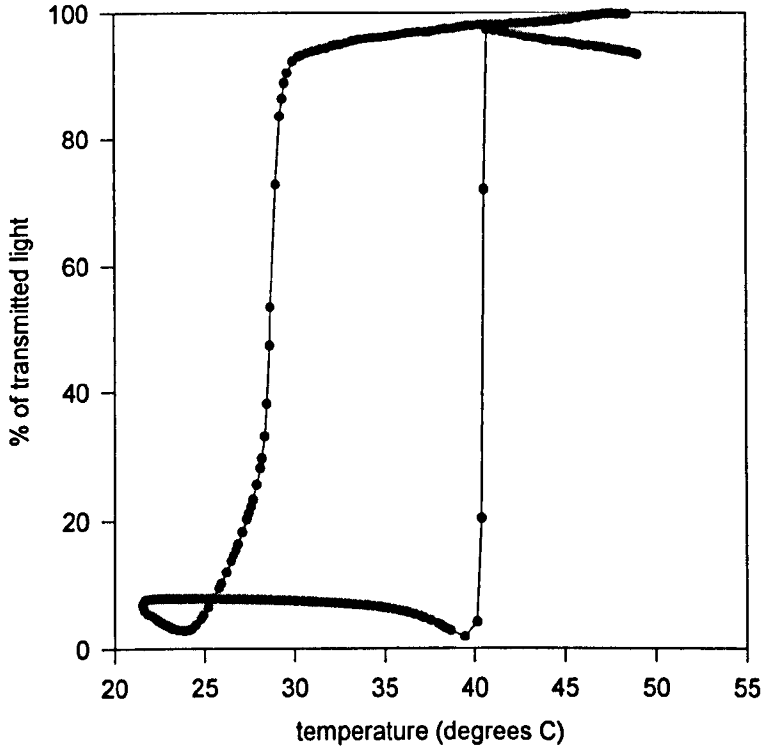

Figure 6.5 Turbidity versus temperature curve for a NaL:NaM=3:1 mixture containing 20% soap; cooling/heating rate=0.75°C/min

6.2.2.2 The NaL/NaP mixtures

All the NaL/NaP mixtures showed turbidity versus temperature curves which were significantly different from the ones obtained for the single surfactant samples. Some examples are shown in figures 6.6-6.9. The turbidity of the solutions of these mixtures seemed to increase and decrease in a two step process. This indicates the existence of two metastable zones, which have been marked in figure 6.6 as number one and two. It has been attempted to estimate the sizes of these two zones as well as both the "saturation temperatures". The reproducibility of some of the data is quite poor however. In addition, care had to be taken to cool and heat the sample sufficiently to ensure that both metastable zones were recorded. This is illustrated by comparing figure 6.6 and figure 6.7. Both figures correspond to the same sample and cooling/heating rate. The reason that figure 6.7 does not clearly show the second metastable zone is that the sample had not been cooled as far as was the case for the experiment shown in figure 6.6. Values for the metastable zone widths and saturation temperatures are given in the table 6.6. The poor reproducibility of some the data is reflected by the low values for the correlation coefficients. However, both "saturation temperatures" showed the same trend, both increased with an increasing amount of NaP present in the mixture. Metastable zone number two showed the same trend. No trend appeared obvious for the first metastable zone.

6.2.2.3 The NaM/NaP mixtures

Of the NaM/NaP mixtures two (the NaM:NaP=1:1 and NaM:NaP=1:3) showed a similar shape of the turbidity versus temperature curve as the single surfactants, see figures 6.10 and 6.11. Figure 6.11 however illustrates that in some cases, after heating and cooling, the transmittance of light through the sample did not reach the initial value anymore. This phenomenon had also been observed during an experiment with a single surfactant sample containing 10% NaP, as is shown in figure 6.12.

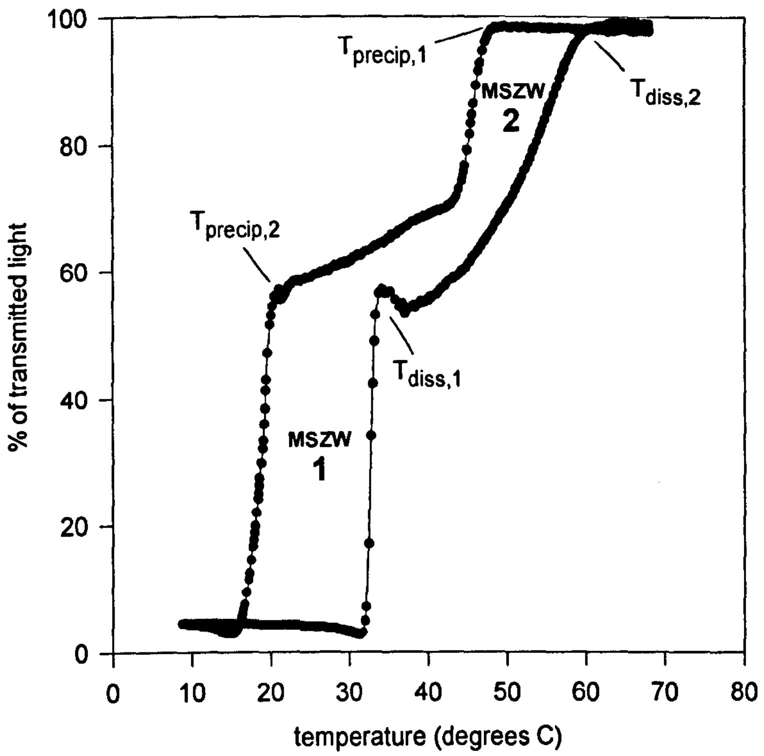

Figure 6.6 Turbidity versus temperature curve for a NaL:NaP=3:1 mixture containing 10% soap; cooling/heating rate=0.75°C/min. The figure illustrates the two step increase and decrease in turbidity

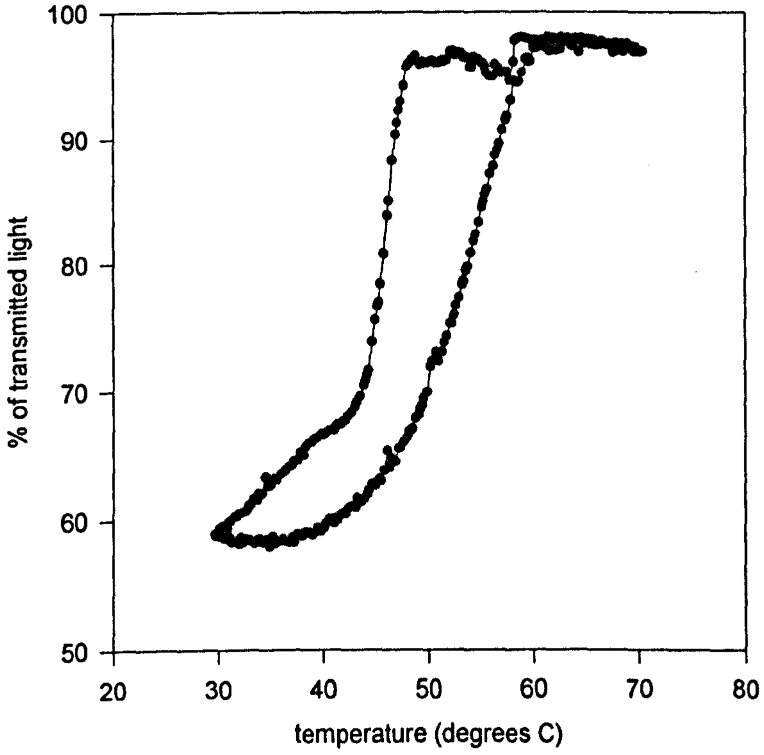

Figure 6.7 Turbidity curve for the same sample as in figure 6.6 with identical cooling and heating rate. Comparison of these two figures illustrates that care had to be taken to cool the sample far enough to see the two step increase in turbidity

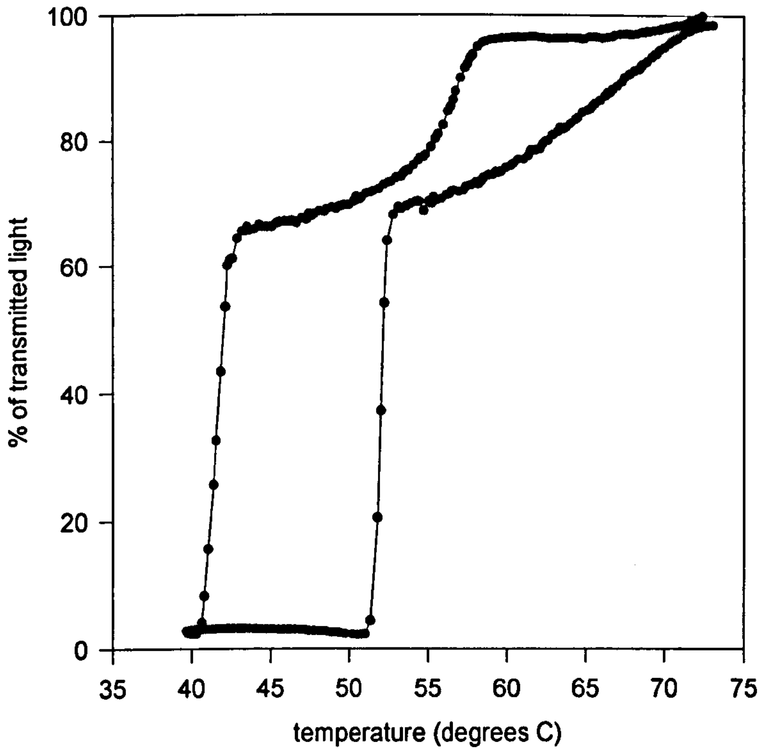

Figure 6.8 Turbidity versus temperature curve for a NaL:NaP=1:1 mixture containing 10% soap; cooling/heating rate=0.75°C/min

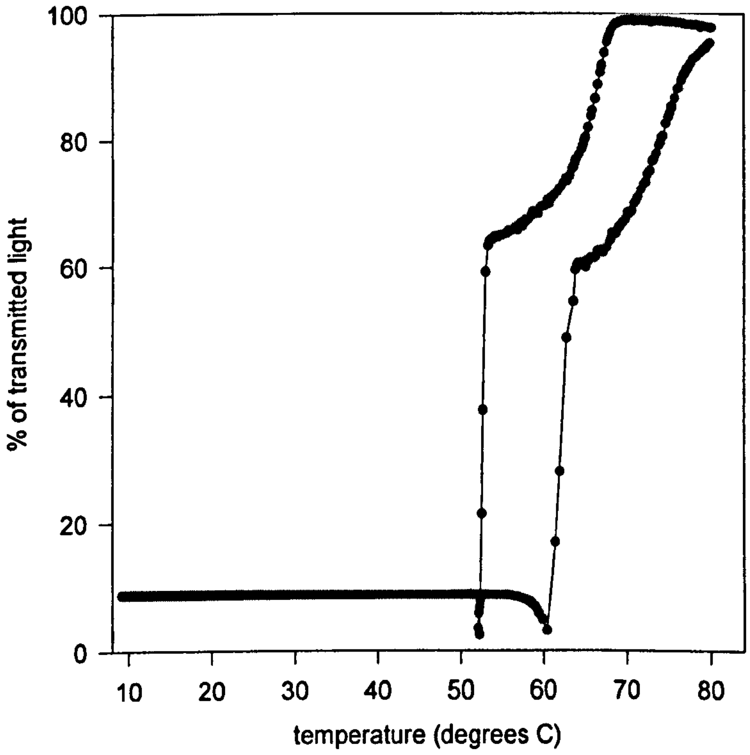

Figure 6.9 Turbidity versus temperature curve for a NaL:NaP=1:3 mixture containing 10% soap; cooling/heating rate=0.75°C/min. The sample was cooled far below the precipitation temperature to investigate if any further changes in turbidity would occur

The NaM:NaP=3:1 mixture, showed a two step precipitation and dissolution behaviour (see figure 6.13), similar to that observed for the NaL/NaP mixtures. Although for the NaM:NaP=3:1 sample the two step process was observed in all experiments, the correlation coefficients for the saturation temperatures were quite low. The MSZWs of all the NaM/NaP mixtures appeared to be larger than those for the individual surfactants. The saturation temperature increased with an increase of the fraction NaP in the mixture. An exception to this formed the NaM:NaP=3:1 sample which exhibited two "dissolution temperatures".

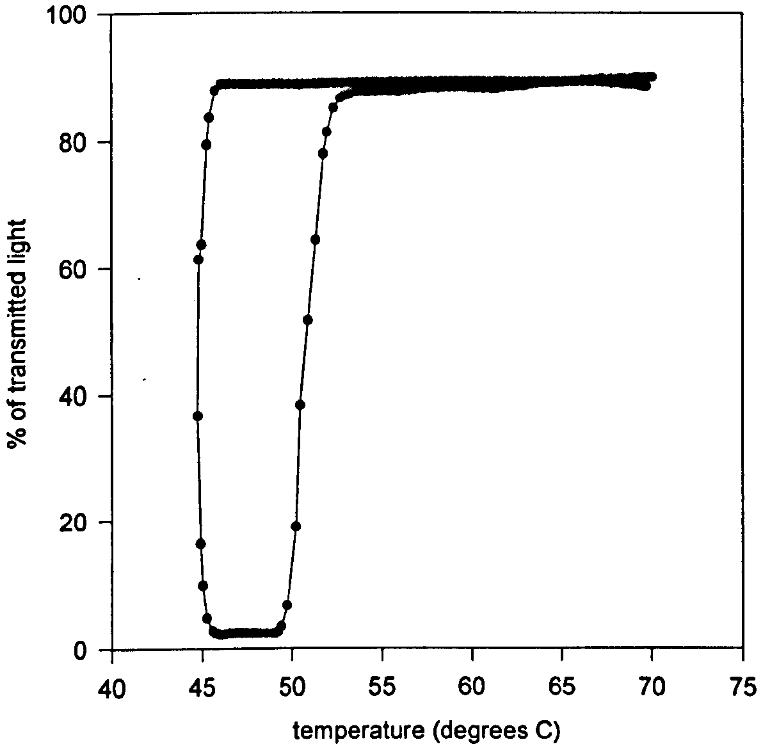

Figure 6.10 Turbidity versus temperature curve for a NaM:NaP=1:1 mixture containing 10% soap; cooling/heating rate=0.75°C/min. No further changes in turbidity occurred on heating the sample above the first metastable zone

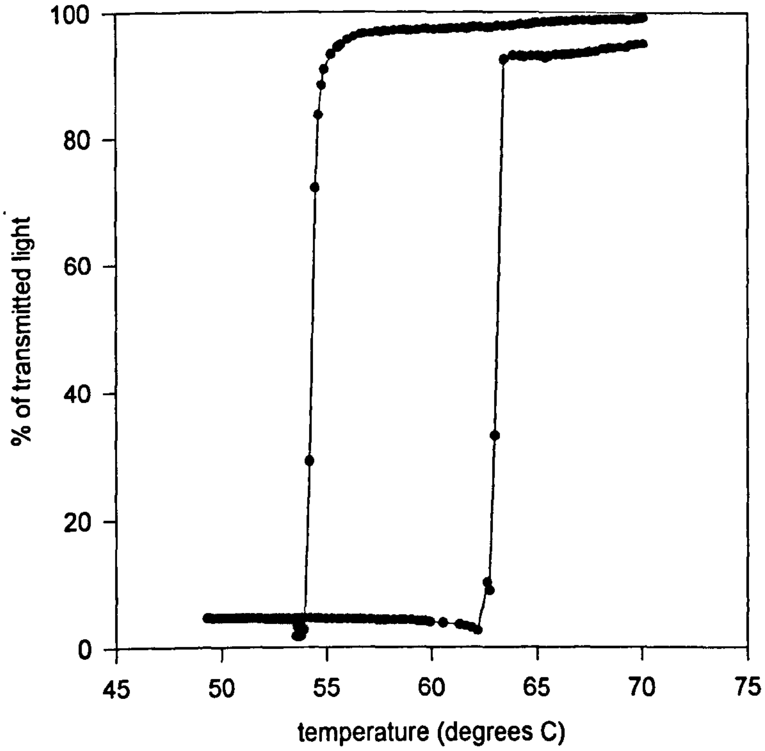

Figure 6.11 Turbidity versus temperature curve for a NaM:NaP=1:3 mixture containing 10% soap; cooling/heating rate=0.75°C/min. The figure illustrates that after heating and cooling the transmittance of light through the sample did not always reach the initial value anymore

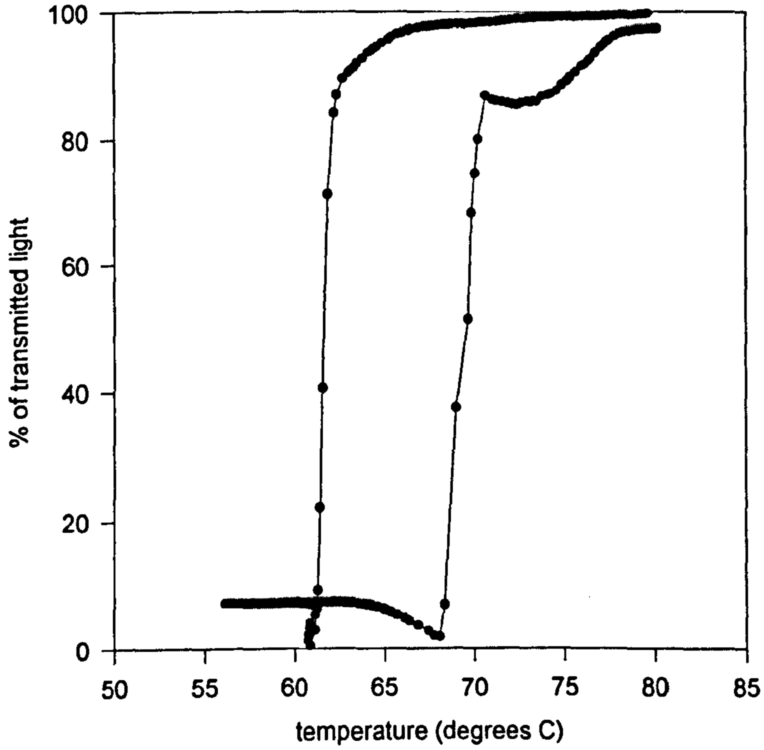

Figure 6.12 Turbidity versus temperature curve for a 10% NaP sample, cooling/heating rate=0.75°C/min. The figure illustrates that in some experiments with NaP the transmittance of light through the sample did not always reach the initial value anymore after cooling and subsequent heating

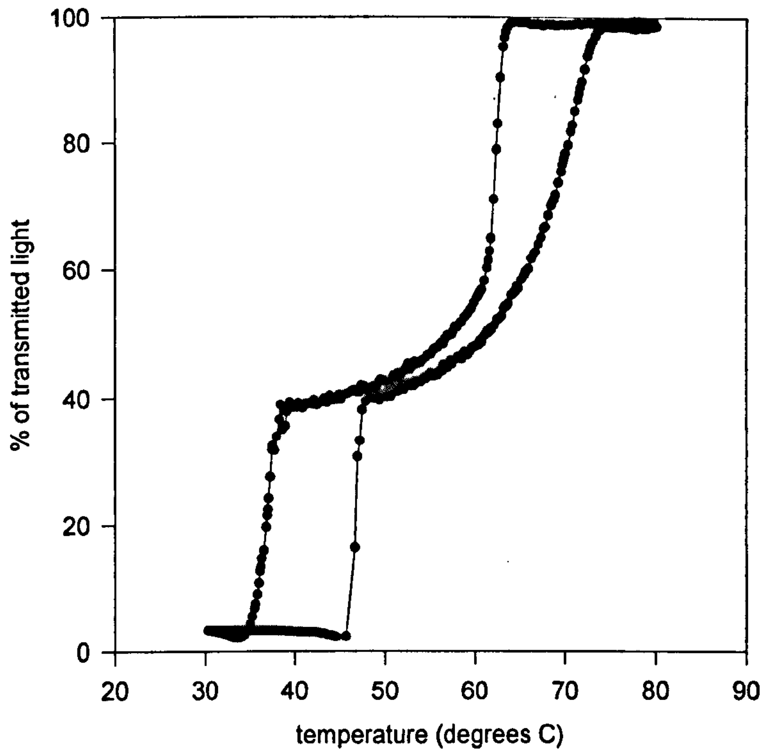

Figure 6.13 Turbidity versus temperature curve for a NaM:NaP=3:1 mixture containing 10% soap; cooling/heating rate=0.75°C/min. The figure shows the two step precipitation and dissolution behaviour that had also been observed for the NaL/NaP mixtures

NaL:NaM=	**MSZW** (°C)	**m**	**T_{sat}** (°C)
1:0	4.33 (0.90)	2.43 (0.97)	43.02 (1.00)
3:1	5.73 (0.88)	3.35 (0.94)	39.39 (0.54)
1:1	3.99 (0.93)	3.33 (0.97)	43.64 (0.78)
1:3	7.45 (0.93)	3.84 (0.95)	54.20 (0.97)
0:1	2.75 (0.95)	2.31 (0.98)	56.76 (0.04)

Table 6.5. Nucleation parameters for NaL/NaM mixtures compared with single surfactant systems as 20% by weight soap solutions. Correlation coefficients are given between brackets

NaL:NaP=	MSZW 1 (°C)	MSZW 2 (°C)	T_{sat} 1 (°C)	T_{sat} 2 (°C)
1:0	7.25 (0.92)		36.49 (0.87)	
3:1	10.48 (0.38)	7.40 (0.76)	39.17 (0.75)	59.42 (0.00)
1:1	6.15 (0.94)	7.84 (0.66)	52.55 (0.21)	70.49 (0.10)
1:3	5.50 (0.97)	11.00 (0.10)	64.00 (1.00)	80.00 (0.50)
0:1	4.19 (0.96)		68.01 (0.95)	

Table 6.6. Nucleation parameters for NaL/NaP mixtures compared with single surfactant systems as 10% by weight soap solutions. Correlation coefficients are given between brackets

NaM:NaP=	MSZW 1 (°C)	MSZW 2 (°C)	m	T_{sat} 1 (°C)	T_{sat} 2 (°C)
1:0	4.12 (0.91)		2.96 (0.95)	53.44 (0.77)	
3:1	6.45 (0.61)	5.16 (0.94)		48.79 (0.34)	73.01 (0.67)
1:1	6.96 (0.02)		2.18 (0.26)	55.61 (0.60)	
1:3	4.52 (0.86)		3.28 (0.92)	62.14 (0.90)	
0:1	4.19 (0.96)		2.55 (0.98)	68.01 (0.95)	

Table 6.7. Nucleation parameters for NaL/NaP mixtures compared with single surfactant systems as 10% by weight soap solutions. Correlation coefficients are given between brackets

6.2.2.4 Discussion

The slow cool results for the surfactant mixtures can be summarised as follows: the results seem to indicate a two-step precipitation and dissolution process for all the NaL/NaP mixtures as well as for the NaM:NaP=3:1 mixture. This two step process might be caused by phase separation of the two components of the sample during nucleation, which then dissolve at different temperatures on subsequent heating. This seems to contradict the results of *in-situ* crystallisation X-ray diffraction (XRD) experiments where no segregation was observed (see chapter 7). However, the XRD experiments were carried out on stagnant samples. It is possible that the observed two step process is dependent on the degree of sample agitation during nucleation and subsequent crystal growth. The degree of stirring during nucleation is well known to affect for example the polymorphic form of stearic acid and triglycerides (see *e.g.* Garti and Sato [1]). Variations in the stirring rate could then explain the poor reproducibility of some of the data.

It is not known why the NaL/NaM samples and the other NaM/NaP mixtures (NaM:NaP=1:1 and NaM:NaP=1:3) did not show the two step process. These samples showed the same general shape of the turbidity versus temperature curve as had been observed for the single surfactant systems. From figure 6.12 it could be argued that NaP is causing the two step process as this figure seems to indicate a discontinuity in the dissolution process. However this would not be consistent with the fact that the NaM:NaP=1:1 and NaM:NaP=1:3 mixtures did not show the two step process although they both contain a higher fraction of NaP than the NaM:NaP=3:1 sample. The NaL/NaM samples and the NaM/NaP samples have a difference in chainlength of 2 CH_2 groups, whereas this difference for the NaL/NaP mixtures is 4 CH_2 groups. It is likely that the smaller the difference in chainlength between the two components the easier a solid solution is formed. It is thus possible that the mixtures that did not exhibit phase separation during cooling formed solid solutions, whereas for the other samples the difference in chainlength was too large for this. This would not explain why the NaM:NaP=3:1 sample *did* show phase separation but it is possible that NaM and NaP do not form solid solutions in all ratios.

The determined metastable zone widths of the mixtures were larger than the metastable zone widths of the individual components of the mixture (with one exception). This indicates that the micelles in an isotropic micellar solution of a mixture of chainlengths is more stable than micelles consisting of only one chainlength. Intuitively this can be understood in the following way: when a spherical micelle is made up of surfactant molecules of uniform chainlength, this can lead to molecular crowding in the core of the micelle. This crowding will be less when two different chainlengths are present, since in that case not all the molecules are reaching into the centre of the micelle. This could possibly explain the observed larger metastable zone widths for the surfactant mixtures. In addition, it may be that mixed systems are more difficult to nucleate as the system is forming a solid solution. The saturation temperatures of the surfactant mixtures seemed to increase when a larger amount of longer chainlength was present in the mixture, similar to the trend observed for the saturation temperatures of the single surfactants. There were some exceptions to this however.

6.3 Crash cool experiments

In section 6.3.1 the results are discussed of the crash cool experiments that have been carried out on the samples listed in table 6.8, with the aim of determining a series of induction times as a function of supersaturation, from which the interfacial energy and the size of the critical nucleus have been estimated. These samples exhibited a single metastable zone width in the slow cool experiments. The data needed for the calculations are given in table 6.8 and 6.9. The enthalpies of dissolution and the saturation temperatures have been determined using slow cool experiments (see previous paragraph). The molecular volume, v_m, was calculated from the density, ρ ($v_m = \frac{MW}{\rho N_A}$, where MW is the molecular weight and N_A is Avogadro's constant). The height, h, of a critical nucleus has been taken as the d_{001} spacing, obtained from X-ray diffraction measurements (see chapter 7).

The supersaturation, σ, at the temperatures that the samples were cooled down to has been calculated using the van 't Hoff equation (see chapter 2):

$$\ln \sigma = \frac{\Delta H_d}{R}\left(\frac{1}{T_p} - \frac{1}{T_{sat}}\right) \tag{6.1}$$

where ΔH_d is the enthalpy of dissolution, R is the gas constant, T_p is the temperature at which precipitation was observed and T_{sat} is the saturation temperature. The critical nucleus was assumed to have a cylindrical shape (the height of the cylinder being equal to the d_{001} spacing) so that the following equation (see chapter 2) could be used to calculate the interfacial tension γ between the solution and the nucleus:

$$\ln\left(\frac{1}{\tau}\right) = \ln A' - \frac{2\pi\gamma^2 v_m h}{k^2 T^2 \ln\sigma} \tag{6.2}$$

The radius of the critical nucleus was subsequently calculated from (see chapter 2):

$$r^* = \frac{2\gamma v_m}{kT\ln\sigma} \tag{6.3}$$

The volume of the critical nucleus has been calculated from the critical radius by assuming a cylindrical nucleus, the number of molecules in a critical nucleus was subsequently determined by dividing the volume of the nucleus by the molecular volume.

sample	ΔH_d (kJ/mol)	**MSZW** (°C)	T_{sat} (°C)
10% NaL	110.5	7.25	36.49
10% NaM	163.8	4.12	53.44
10% NaL:NaM=1:1	87.11	7.21	37.14

Table 6.8 Enthalpies of dissolution, MSZWs and saturation temperatures of the studied samples

soap	ρ (10^6 g/m^3)	v_m (Å^3)	h (Å)
NaL	1.15	322	31.6
NaM	1.13	369	36.5
NaL:NaM=1:1	1.14	346	34.5

Table 6.9 Data needed for calculations. Densities of soaps from Southam and Puddington [2].

6.3.1 Crash cool results and discussion

An example of a turbidity versus time curve resulting from a crash cool experiment is shown in figure 6.14. The induction times obtained from these curves are tabulated in tables 6.10-12. Graphs were made of $\ln(1/\tau)$ versus $\frac{1}{T^2 \ln\sigma}$, these are shown in figures 6.15-6.17. The equations for the lines of best fit through the data points are given in table 6.13, together with the values for the interfacial energy, γ, that have been determined from the slopes of these equations. The radius of the critical nucleus, r^* as a function of supersaturation is listed in tables 6.10-12, together with the volume of the critical nucleus, V^* and the number of molecules it contains, N.

A good correlation was found between the experimental data and the theoretical relationship between the induction time and supersaturation of the samples. The results clearly showed an increase in induction time of the samples when cooled to a temperature closer to the upper limit of the metastable zone. In addition, the results showed an increase in the size of the critical nucleus with decreasing supersaturation. Although (especially at high supersaturation) the calculated number of molecules per critical nucleus, N, seems rather small, the number of molecules per nucleus does follow the trend predicted by theory: the critical nucleus is larger at lower supersaturation. A source of error in the calculated number of particles in the critical nucleus is the fact that the measured induction time is the sum of the real induction time and the time it takes before the critical nucleus has reached a detectable size. This time can only be neglected when it is small in comparison to the real induction time, *i.e.* it is assumed that growth of a nucleus after it has achieved critical size is very rapid in comparison to the time it takes to form the critical nucleus.

The deviation of linearity of the data in figures 6.15-6.17 could indicate that the nucleation mechanism changes below a certain supersaturation. This could mean a change from homogeneous nucleation at high supersaturation to heterogeneous nucleation at lower supersaturation. If this is the case then two lines should be fitted through the data instead of one.

Nucleation was not always observed to occur. Sometimes the appearance of the solution seemed to alternate between clear and slightly cloudy. For these cases the induction times have been calculated using the equations in table 6.5 and are given in

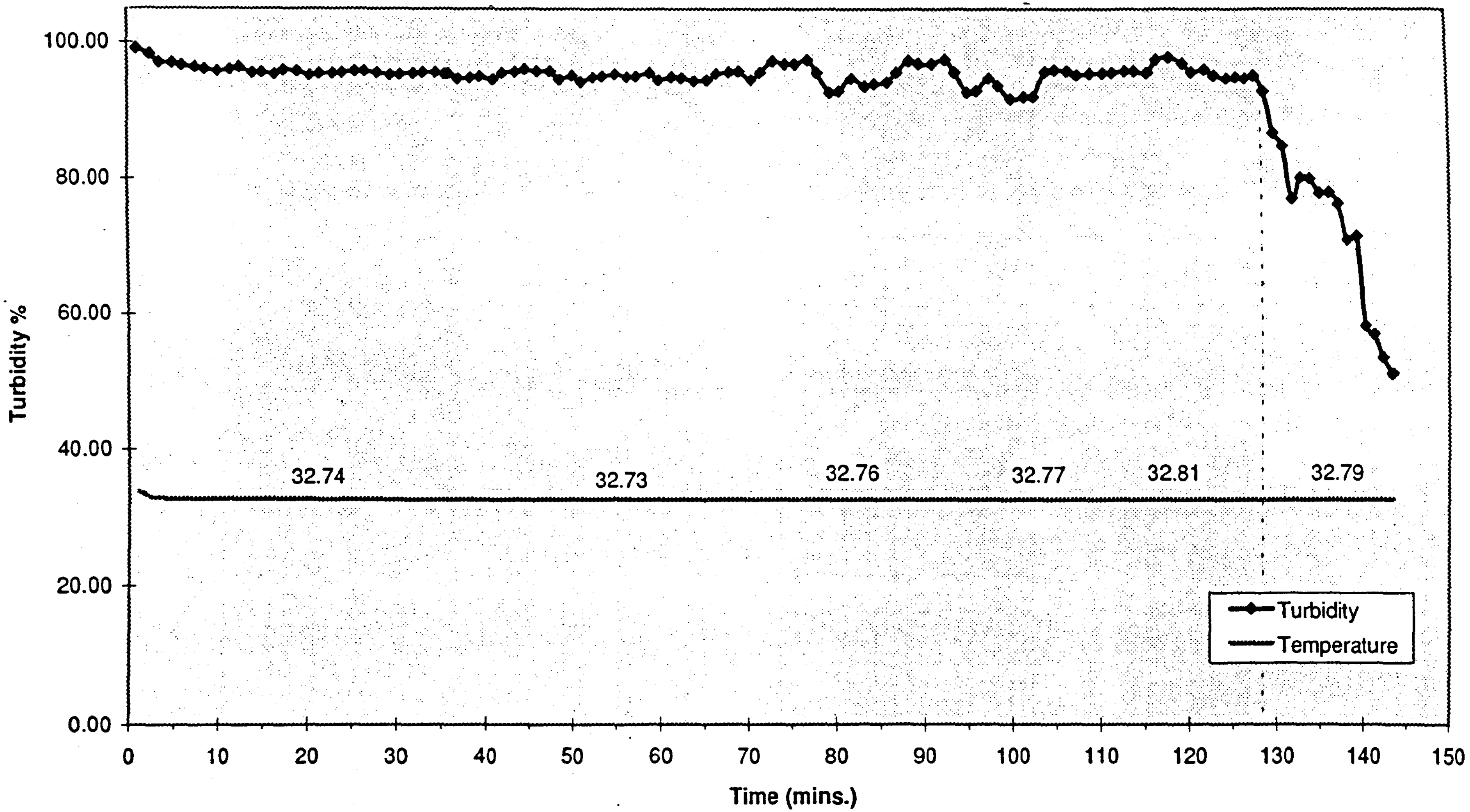

Figure 6.14 Typical example of the result of a crash cool experiment for a NaL:NaM=1:1 mixture containing 10% soap

tables 6.2-4 between brackets. These calculated values show that the induction times were too long to have been observed in practice, as in some cases it would have taken several months before nucleation would have occurred. The alternating appearance of the sample could indicate that clusters were formed which were smaller than the critical size, so that they were not stable and re-dissolved, as predicted by theory (see chapter 2). The size of the critical nucleus has also been calculated for these situations where no nucleation was observed, the values for this are given in tables 6.2-4 between brackets.

T (°C)	$\ln\sigma$	σ	τ (min)			r^* Å	V^* 10^3 Å^3	N
			run 1	run 2	run 3			
28.60	1.12	3.06	3.55	3.55	3.55	4.69	2.18	3.2
29.30	1.02	2.77	5.10	5.00	6.10	5.15	2.63	3.8
29.60	0.98	2.66	11.50	11.50	8.50	5.37	2.86	4.2
30.32	0.87	2.39	19.00	25.30	19.30	6.00	3.57	5.2
30.70	0.82	2.27	23.00	26.75	23.00	6.39	4.05	5.9
31.20	0.75	2.12	46.00	50.00	43.50	7.00	4.86	7.1
32.17	0.61	1.84	63.00	70.00	86.00	8.57	7.28	10.6
33.10	0.48	1.62	(38.7 days)	(38.7 days)	(38.7 days)	(10.9)	(11.8)	(17.3)

Table 6.10 Induction time data and sizes of critical nuclei for 10% NaL solution. Values between brackets have not been observed but have been calculated with the use of the equation given in table 6.13

In figure 6.18 a graph is shown of the number of particles in the critical nucleus versus the supersaturation of the samples studied. This graph demonstrates that at the same supersaturation the critical nuclei in the NaL sample require most molecules, the critical nuclei in the NaM sample require the smallest number of molecules and the critical nuclei in the mixture require an intermediate number of molecules. This cannot be explained by the fact that the NaM molecules are more hydrophobic than the NaL molecules due to the longer chainlength, because the comparison is made at constant supersaturation. The driving force for crystallisation is thus the same for NaL and NaM. A possible explanation for the observed trend might be that the attractive forces between the NaL molecules are smaller than between the NaM molecules because the former are smaller molecules. Therefore during the formation of the nucleus the NaM molecules are held together more strongly than the NaL molecules, so that the nucleus can be stabilised with less molecules. The observation that the critical nuclei in the mixture require an intermediate number of molecules is consistent with this.

T (°C)	$\ln\sigma$	σ	τ (min)			r^* Å	V^* 10^3 Å^3	N
			run 1	run 2	run 3			
49.44	0.75	2.12	24.00	23.00	19.50	3.59	1.48	1.4
49.94	0.65	1.92	30.50	30.50	25.50	4.11	1.93	1.8
50.44	0.56	1.75	50.00	52.50	51.00	4.79	2.63	2.5
50.94	0.47	1.60	134.00	137.00	124.00	5.75	3.79	3.5
51.44	0.37	1.45	187.00	187.50	190.50	7.19	5.92	5.5
51.94	0.28	1.32	286.00	260.00	192.00	9.58	10.5	9.8
52.44	0.19	1.21	(42.9 hrs)	(42.9 hrs)	(42.9 hrs)	(14.4)	(23.7)	(22.2)
52.94	0.09	1.09	(676 days)	(676 days)	(676 days)	(28.8)	(94.7)	(88.6)

Table 6.11 Induction time data and sizes of critical nuclei for 10% NaM solution. Values between brackets have not been observed but have been calculated with the use of the equation given in table 6.13

T (°C)	$\ln\sigma$	σ	τ (min)			r^* Å	V^* 10^3 Å^3	N
			run 1	run 2	run 3			
29.80	0.85	2.34	20.50	20.50	19.50	4.19	1.90	2.2
30.80	0.74	2.10	29.10	23.20	24.10	4.82	2.51	2.9
31.80	0.62	1.86	73.00	68.00	58.10	5.67	3.48	4.1
32.80	0.51	1.67	133.00	124.50	128.00	6.89	5.15	6.0
33.80	0.40	1.49	233.00	236.00	191.00	8.79	8.36	9.8
34.80	0.29	1.34	(1651)	(1651)	(1651)	(12.1)	(15.9)	(18.6)
35.80	0.18	1.20	(63.9 days)	(63.9 days)	(63.9 days)	(19.5)	(41.2)	(48.2)

Table 6.12 Induction time data and sizes of critical nuclei for 10% NaL:NaM=1:1 mixture. Values between brackets have not been observed but have been calculated with the use of the equation given in table 6.13

sample	correlation between induction time and supersaturation	γ (x10^{-3} J/m^2) (r^2)
10% NaL	$\ln\left(\frac{1}{\tau}\right) = -2.182 - \frac{39.04\times10^4}{T^2\ln\sigma}$	3.410 (0.89)
10% NaM	$\ln\left(\frac{1}{\tau}\right) = -1.902 - \frac{11.70\times10^4}{T^2\ln\sigma}$	1.623 (0.84)
10% NaL:NaM=1:1	$\ln\left(\frac{1}{\tau}\right) = -0.781 - \frac{18.21\times10^4}{T^2\ln\sigma}$	2.150 (0.93)

Table 6.13 Correlations found between induction time and supersaturation, and values for the interfacial energy

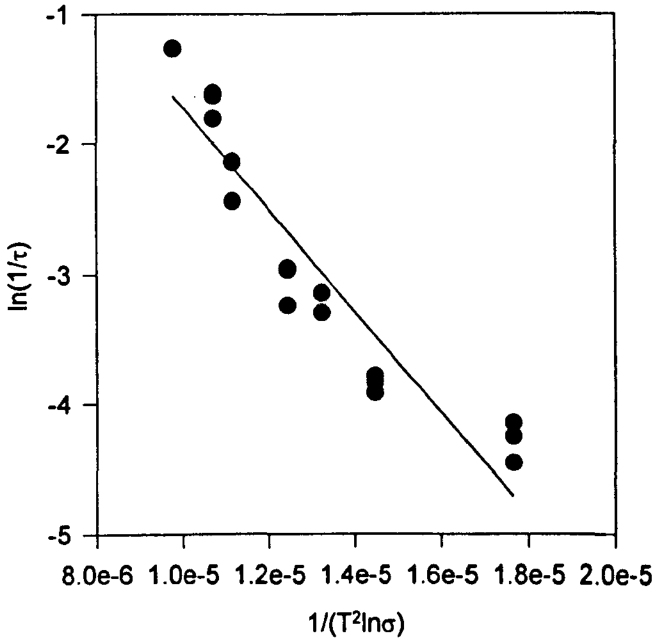

Figure 6.15 Showing the correlation between the induction time and the supersaturation for a 10% NaL sample

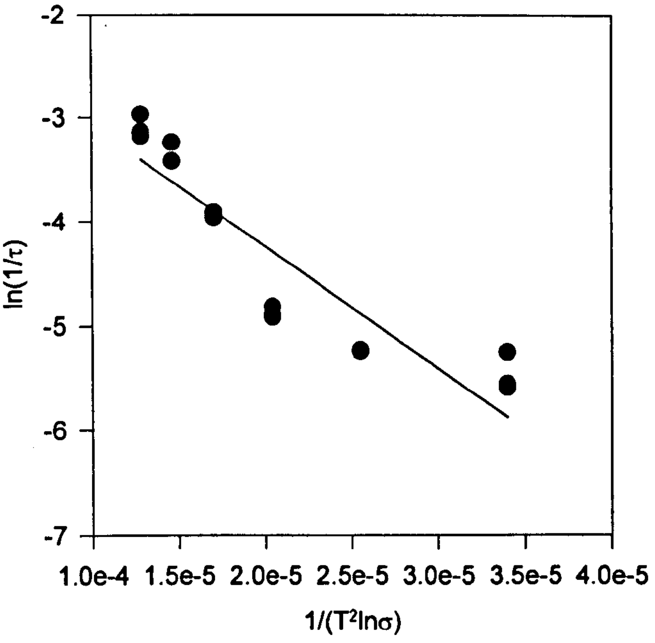

Figure 6.16 Showing the correlation between the induction time and the supersaturation for a 10% NaM sample

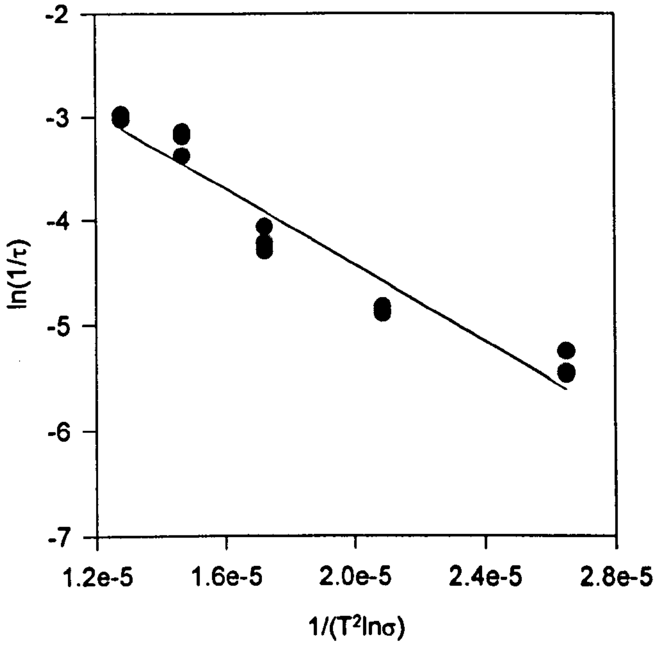

Figure 6.17 Showing the correlation between the induction time and the supersaturation for a NaL:NaM=1:1 10% soap sample

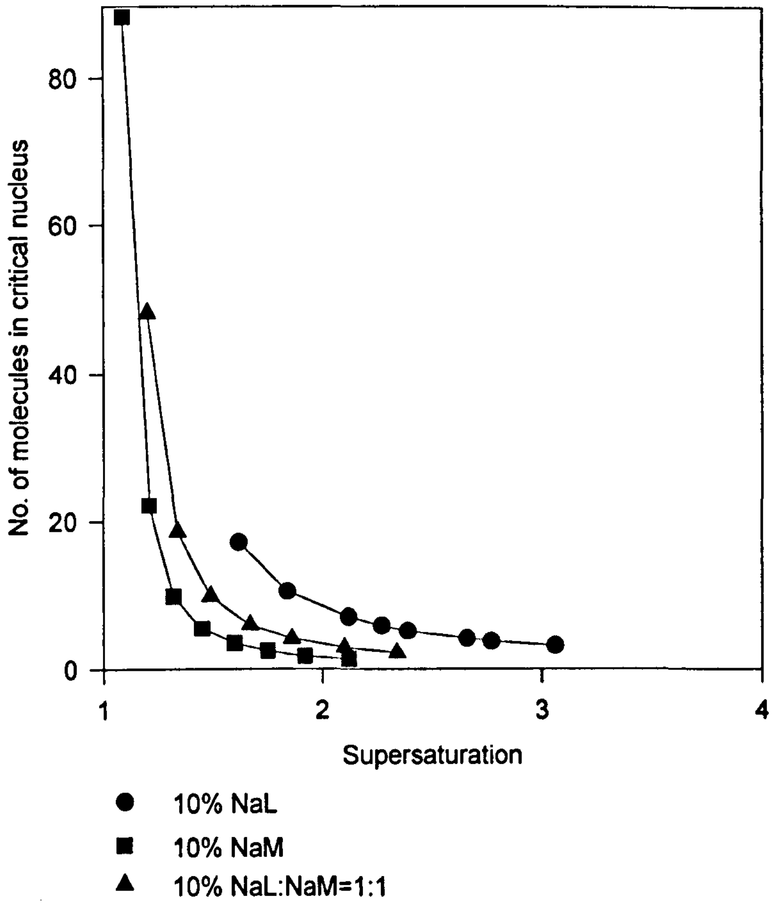

Figure 6.18 Comparison of the number of molecules in the critical nucleus for the different samples. At the same supersaturation, for NaL most molecules are required to form a stable nucleus, for NaM the least and for the 1:1 mixture an intermediate number of molecules is needed

6.4 Conclusions of slow and crash cool experiments

6.4.1 Slow cool experiments

The following trends were noted from the nucleation studies:

Single surfactants:

- For the single surfactants studied, the saturation temperature clearly increased with increasing chainlength and concentration.

- The metastable zone width and the apparent order of nucleation appeared to decrease with increasing concentration and chainlength although there were deviations to this.

- Both the enthalpy and entropy of dissolution increased with increasing chainlength.

Surfactant mixtures

- The results indicated a two step nucleation and dissolution process for all the NaL/NaP mixtures as well as for the NaM:NaP=3:1 mixture. This two step process might be caused by phase separation of the two surfactants in the mixture during nucleation. It is possible that this process is affected by the degree of agitation.

- The NaM:NaP=1:1, the NaM:NaP=1:3 as well as all the NaL/NaM mixtures showed the same general shape of turbidity versus temperature curves as had been observed for the single surfactant samples.

- The metastable zone width of the mixtures appeared to be larger for the mixtures than for the single surfactant samples. This indicates that micelles consisting of a mixture of chainlengths are more stable than micelles made up of molecules of uniform chainlength. This might be explained by molecular crowding effects near the core of the micelle. Alternatively it might just indicate that mixed systems simply do not nucleate as easily as single systems.

- The saturation temperature of the surfactant mixtures increased when a larger amount of longer chainlength component was present in the mixture, mirroring similar behaviour to the single surfactants. There were exceptions to this trend however.

In cases there were examples of poor reproducibility for some of the data, which could have been caused by:

- The effect of impurities, such as other homologues surfactants and dust particles present in the solution, on the nucleation process. How pronounced the effects of even minor levels of impurities can be, has been demonstrated in the previous chapter.

- As the surfactants start to crystallise not a suspension but a coagel is formed. The magnetic stirrer can become trapped in this coagel, so that the sample is no longer agitated. As the sample is re-heated the stirrer has to break free from the soap mass before the sample is stirred again. The dissolution temperature is thus affected by the moment that the stirrer can break free from the coagel.

- The degree of agitation might influence the observed two step nucleation and dissolution process.

6.4.2 Crash cool experiments

The crash cool results need to be interpreted very carefully since only two different chainlengths and one mixture has been studied. However, the results do indicate the following trends:

- A good correspondence was found between the experimental data and the theoretical relation between the induction time and the supersaturation; the lower the supersaturation the longer the induction time and the more molecules are required to form a stable nucleus.

- The shorter the chainlength the more molecules are needed per critical nucleus. This might be explained in terms of attractive forces between the molecules which are stronger as the chainlength gets longer, thus stabilising the critical nucleus.

6.5 Recommendations for future work

- The nucleation behaviour of pure soaps (obtained from neutralisation of the purified fatty acids described in chapter 5) could be studied in order to investigate the influence of minor levels of impurities such as close homologues on the nucleation process of surfactants. Impurities might be a cause of the observed two step phase separation behaviour.

- The nucleation behaviour of soaps with a different head group, counter ion and chainlength can be investigated in order to study the effect of these parameters on the nucleation process and to investigate the generics of the nucleation behaviour found here.

- The effect of stirring on the two step phase separation process could be examined, by varying the degree of agitation during the nucleation experiments and through the use of *in-situ* X-ray studies of stirred samples. An example of such a study can be found in [3].

6.6 References used in this chapter

1. Garti N and Sato K (eds) *Crystallization and polymorphism of fats and fatty acids*, Marcel Dekker Inc, New York and Basel (1988)
2. Southam and Puddington, *Can J Res Sect B*, **25**, 123 (1947)
3. MacCalman ML, Roberts KJ, Kerr C and Hendriksen B, *J Applied Crystallography* **28**, 620 (1995)

Chapter 7

An in-situ XRD investigation into the crystallisation process of soaps from liquid crystalline phases

Chapter 7 An *in-situ* XRD investigation into the crystallisation process of soaps from liquid crystalline phases

7.1 Introduction

In-situ small angle X-ray scattering (SAXS) studies have been carried out into the processes that take place during crystallisation and dissolution of single and mixed surfactant systems. The data were collected at station X12B at the NSLS and at station 16.1 at the SRS in Daresbury, with specially designed X-ray cells (see chapter 4). The 41 samples investigated are summarised in tables 7.1 and 7.2.

single surfactants		
20% NaL NaM NaP	40% NaL NaM NaP	70% NaL NaM NaP
surfactant mixtures		
20% NaL:NaM=3:1,1:1,1:3 NaL:NaP=3:1,1:1,1:3 NaM:NaP=3:1,1:1,1:3	40% NaL:NaM=3:1,1:1,1:3 NaL:NaP=3:1,1:1,1:3 NaM:NaP=3:1,1:1,1:3	70% NaL:NaM=3:1,1:1,1:3 NaL:NaP=3:1,1:1,1:3 NaM:NaP=3:1,1:1,1:3

Table 7.1 Aqueous samples studied from three concentration regimes (percentages by weight, ratios are molar ratios)

NaL	**% ethanol in solvent**	**% water in solvent**
30%	10	90
30%	60	40
30%	70	30
20%	80	20
10%	100	0

Table 7.2 Sodium laurate samples crystallised from ethanol/water mixtures (percentages by weight, 100% ethanol here refers to standard laboratory ethanol, typically containing 3% water)

The crystallisation behaviour of aqueous single surfactants and three groups of aqueous surfactant mixtures were studied. Two of these groups of mixtures (the NaL-NaM and NaM-NaP mixtures) have a difference in chainlength of two CH_2 groups. For the third group of mixtures, the NaL-NaP mixtures, the difference in chainlength is four CH_2 groups. By studying three different compositions of each group of mixtures (3:1, 1:1 and 1:3) the influence of mixing surfactants of different chainlengths on the crystallisation process has been investigated. Samples of all these compositions were crystallised from three different concentration regimes: the isotropic micellar phase region (samples containing 20wt% surfactant), the hexagonal phase (samples containing 40wt% surfactant) and the lamellar phase region (samples containing 70% surfactant), in order to study the influence of concentration on solid and liquid crystalline phase behaviour. The dilute aqueous samples (containing 20wt% surfactant) were identical to the samples used for nucleation studies. A different experimental parameter is that during the X-ray diffraction studies the samples were stagnant, whereas during the nucleation experiments they were stirred. In addition to the aqueous samples, five NaL samples were crystallised from ethanol-water mixtures (see table 7.2) in order to assess the influence of solvent on the crystal structure of NaL.

All aqueous samples were heated and cooled at least twice in order to ensure data reproducibility. In total this amounted to over 12,000 SAXS data frames equivalent to over 12Giga bytes in raw data. As this is clearly far too much to be shown here in detail, only some representative examples leading to the identification of generic processes are formally presented here. The temperatures at which phase transformations occur cannot be read of the figures shown in this chapter. For this reason these have been collected in appendix B, together with the peak positions of the phases involved in these transformations.

The obtained SAXS results are presented in seven major parts. First in section 7.3 the results are given for all the samples (20%, 40% and 70%, single and mixed and the samples crystallised from ethanol mixtures) at room temperature, where they exist as coagels. This is followed by the results at elevated temperatures for the 20% and 40% surfactant samples in section 7.4. In section 7.5 the phase transitions are discussed that were found to occur in the 70% single and mixed surfactant systems. Epitaxial growth relations between the different phases are shown in section 7.6 based on orientation effects in the diffraction rings. In section 7.7 results from crash cool experiments are presented, followed by additional phases found for some samples in section 7.8. The results section finishes with observations on the micellar phase behaviour of samples containing ethanol in section 7.9. In section 7.10 a detailed discussion is provided. Conclusions are given in section 7.11 and recommendations for future work in section 7.12. First in section 7.2 it is explained how the volume fraction surfactant can be calculated from the weight fraction. This volume fraction is required for calculating the structural parameters for the different aqueous phases.

7.2 Calculation of the surfactant volume fraction

For calculating the parameters that describe the structures of the different aqueous phases, the volume fraction surfactant, ϕ_S, needs to be known. This volume fraction can be calculated from the surfactant concentration in the following way: the assumption is made that two regions of different density can be distinguished (Luzzati *et al.* [1]):

1. the hydrocarbon region occupied by the alkyl chains
2. the aqueous region occupied by the polar head groups, the counter ions and the water molecules

The boundary between these two regions is chosen halfway between the carbon atom and the oxygen atoms of each carboxyl group (Luzzati *et al.* [1]). It is then assumed that the density of the hydrocarbon region, ρ_h, is identical to the density of the alkane with the same chainlength as the surfactant, since in the mesophases the hydrocarbon chains are considered to be in a liquid state. Temperature effects are not taken into account. The density of the aqueous region, ρ_a, has to take into account the oxygen atoms of the carboxyl groups and the cations. This density can be calculated from the total density of the surfactant-water system, ρ_T, (which can be measured) and the density of the hydrocarbon phase but is not required for calculating the surfactant volume fraction.

The total weight of an arbitrary volume V of solution is $V\rho_T$; the weight of the hydrocarbon region in this volume is then $V\rho_T c_h$, where c_h is the weight fraction of surfactant in the solution. The partial volume of the hydrocarbon region, v_h, is then given by:

$$v_h = Vc_h \frac{\rho_T}{\rho_h} \tag{7.1}$$

(since density=mass/volume ⇒ volume=mass/density). The surfactant volume fraction in the solution is equal to the volume taken up by the hydrocarbon region divided by the total volume of the solution:

$$\phi_s = \frac{v_h}{V} = \frac{Vc_h \frac{\rho_T}{\rho_h}}{V} = c_h \frac{\rho_T}{\rho_h} \tag{7.2}$$

The total density, ρ_T, of all surfactant-water systems under consideration here, is taken as $1.00\text{x}10^6$g/m^3. The densities of the alkanes with the same chainlengths as the soaps are given in table 7.3. With these values the surfactant volume fraction ϕ_s, can be calculated with equation 7.2, when c_h is known. For the mixed systems weighted averages were used for the densities of the hydrocarbon regions.

The concentration of surfactant in solution, c_h, varied continuously during the experiments as the surfactant either slowly dissolved or crystallised. This concentration was therefore not known at any point in time. Therefore, in order to be able to calculate structural parameters for the various phases formed by the single surfactant systems, the d-spacing has been used at the point where a phase transition occurred, since the concentrations at these points are approximately known from literature for the single surfactant systems. As there are no data available for the transition concentrations for mixed surfactant systems, weighted averages have been taken of the ones for the single surfactant systems.

alkane	ρ
dodecane ($C_{12}H_{26}$)	0.75
tetradecane ($C_{14}H_{30}$)	0.76
hexadecane ($C_{16}H_{34}$)	0.77

Table 7.3 Densities of alkanes (x10^6g/m^3) from Timmermans [2]

7.3 Single and mixed coagel systems

At room temperature all aqueous soap samples (containing 20wt%, 40wt% and 70wt% surfactant) were coagels. A coagel is a heterogeneous mixture of solid soap and water, where the water is held in between the solid soap regions by capillary forces (see chapter 3). A coagel is best visualised as a soft soap bar. Although a coagel can contain a large amount of water, this is not visible to the eye unless it is pressed out of the material (*e.g.* with a spatula). For all single and mixed surfactants crystallised from water, the solid phase in these coagels gave rise to a single diffraction ring in the SAXS range (approximately 25-100Å) covered by the 2-D SAXS detector. The peak width did not appear to vary with sample composition The concentration regime from which the sample was crystallised (isotropic micellar solution, the hexagonal phase or the lamellar phase) had no influence on the position of this d-spacing. To investigate the effect of cooling rate on the resulting solid structure some samples were subjected to a number of cooling rates (0.75, 0.50, 0.25 and 0.10°C/min). In addition to this, some samples were crash cooled, see section 7.7. However, the observed d-spacing was not found to be affected by the cooling rate used during crystallisation.

The influence of the mother liquor on the resulting solid state structure was investigated by crystallising NaL from different ethanol-water compositions (see table 7.2. The sample crystallised from ethanol without any added water and the sample crystallised from a solvent containing 80% ethanol and 20% water, were found to exhibit diffraction characteristics that were different from all the other samples (aqueous and ethanol-water mixtures). These are the two samples with the highest ethanol content. For the sample crystallised from ethanol without any added water, at room temperature, three peaks instead of one were observed before heating. Two of these were rather weak diffuse peaks that clearly shifted to smaller d-spacing before fading away on heating (see figures 7.1 and 7.2). After subsequent cooling these peaks both re-occurred at smaller d-spacing than before heating. The d-spacing of the strongest peak was slightly smaller than the d-spacing of the other samples. The sample that had been crystallised from a 80% ethanol, 20% water solvent mixture showed before heating only one peak at approximately the same position as the NaL samples crystallised from water. After dissolution by heating and subsequent re-crystallisation by cooling, three peaks were observed, similar to the peaks for the sample crystallised from ethanol without added water.

The values for the observed d-spacings for all samples at room temperature are given in table 7.4 for the samples crystallised from ethanol and in table 7.5 for the aqueous samples.

NaL	**% ethanol in solvent**	**% water in solvent**	**observed d-spacings**
20%	80	20	before heating 31.42 (s)
			after cooling 62.21 (w) 30.80 (s) 23.80 (vw)
10%	100	0	before heating 61.60 (w) 30.35 (s) 24.45 (vw)
			after cooling 56.10 (w) 30.21 (s) 23.71 (vw)

Table 7.4 d-spacings for sodium laurate samples crystallised from ethanol-water mixtures, which showed different diffraction characteristics from all other samples (s=strong, w=weak, vw=very weak)

surfactant	d-spacing (in Å)	
	observed	calculated
NaL	31.64	31.64
NaM	36.46	36.46
NaP	41.80	41.80
NaL:NaM=3:1	33.43	32.85
1:1	34.47	34.05
1:3	35.90	35.26
NaL:NaP=3:1	35.87	34.18
1:1	38.25	36.72
1:3	41.52	39.26
NaM:NaP=3:1	37.68	37.80
1:1	39.65	39.13
1:3	41.34	40.47

Table 7.5 d-spacings of samples crystallised from water

The calculated values in table 7.5 are weighted averages of the values found for the single surfactants (crystallised from water) and are given here for comparison. Table 7.5 shows that the observed values for the mixtures show the same trend as the calculated values, *i.e.* the d-spacing becomes larger when a larger quantity of a larger chainlength is present in the mixture. However, the observed values for the mixtures are larger than the calculated ones. This is illustrated in figure 7.3, where the observed d-spacings from table 7.5 are plotted versus the weighted average number of carbon atoms in the hydrocarbon chain. This figure shows three different linear relations between observed d-spacings and average chainlength, for:

1. the single surfactants
2. the mixtures with a difference in chainlength of two CH_2 groups (the NaL-NaM and NaM-NaP mixtures)
3. mixtures with a difference in chainlength of four CH_2 groups (the NaL-NaP mixtures)

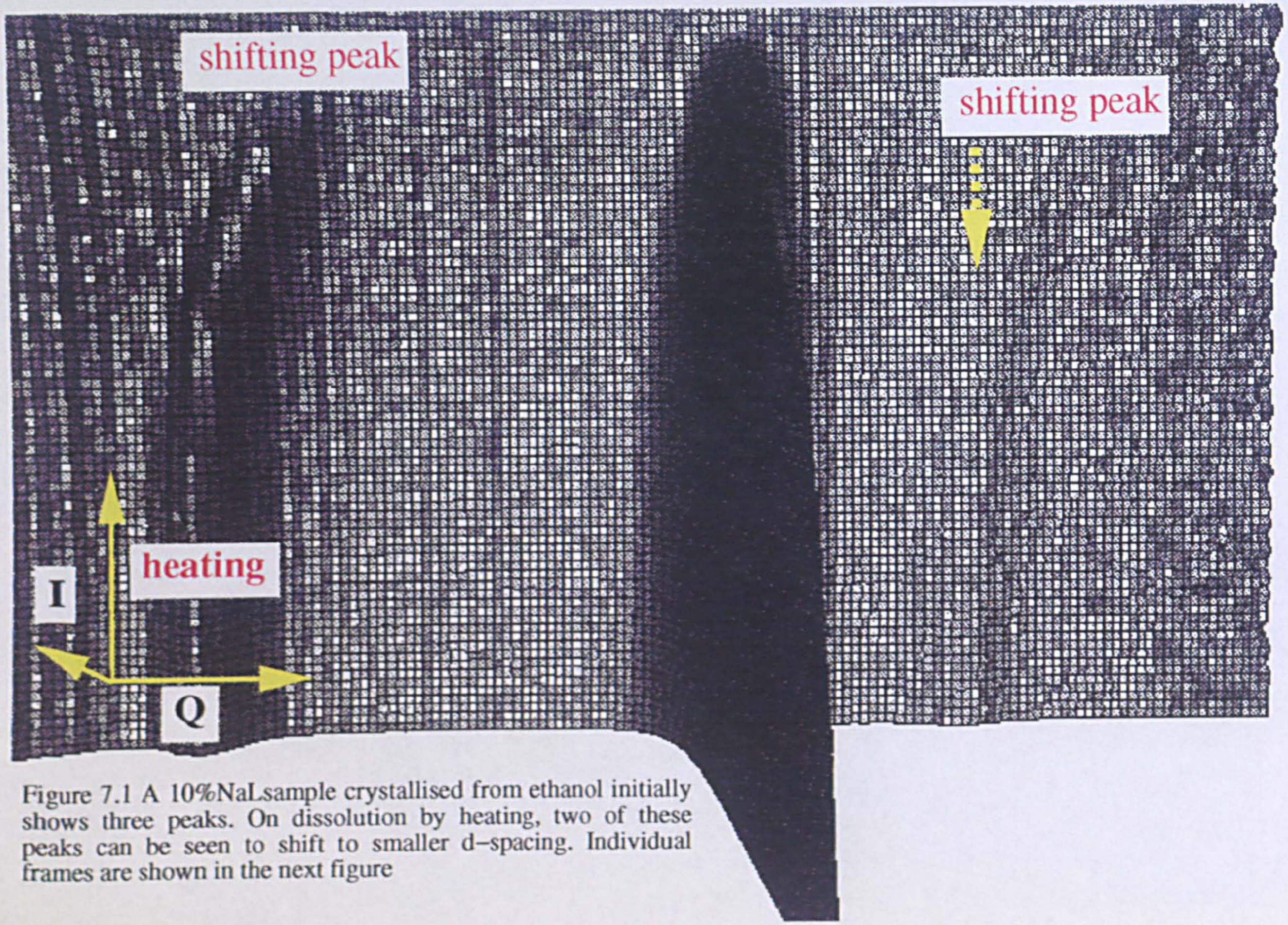

Figure 7.1 A 10%NaLsample crystallised from ethanol initially shows three peaks. On dissolution by heating, two of these peaks can be seen to shift to smaller d–spacing. Individual frames are shown in the next figure

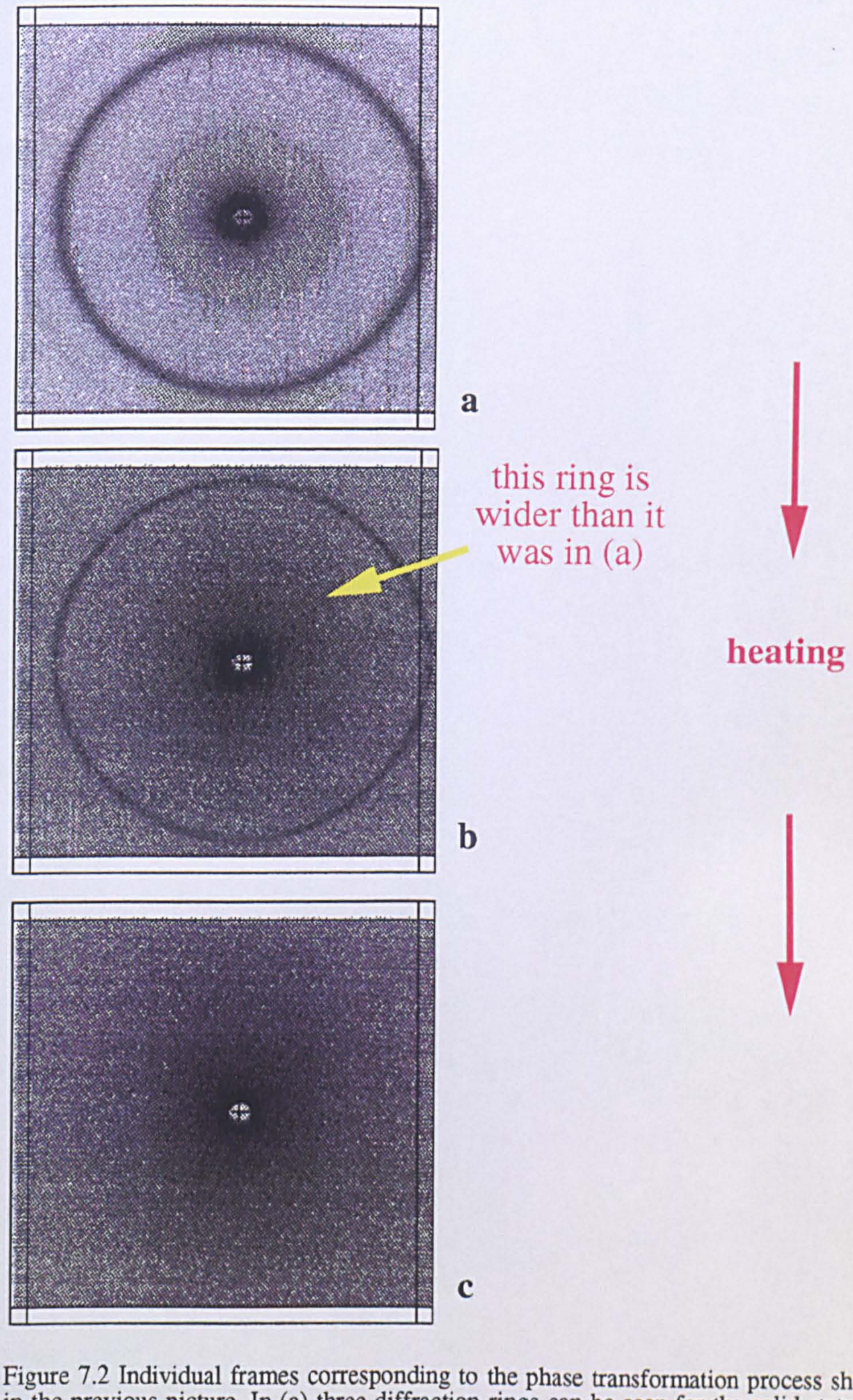
a
this ring is wider than it was in (a)
b
heating
c

Figure 7.2 Individual frames corresponding to the phase transformation process shown in the previous picture. In (a) three diffraction rings can be seen for the solid state. As the sample is heated, two of these rings shift (b) until all soap has dissolved (c). Figure (b) and (c) have been printed with extra contrast to enhance possible weak rings

Figure 7.3 reveals that in the chainlength range of interest here (from 12 to 16 carbon atoms), mixtures of NaL-NaP (difference in chainlength of four CH_2 groups) result in larger d-spacings than mixtures of NaL-NaM and NaM-NaP (difference in chainlength of two CH_2 groups). Because of this, the difference between the observed and the calculated spacings is the largest for the NaL-NaP mixtures.

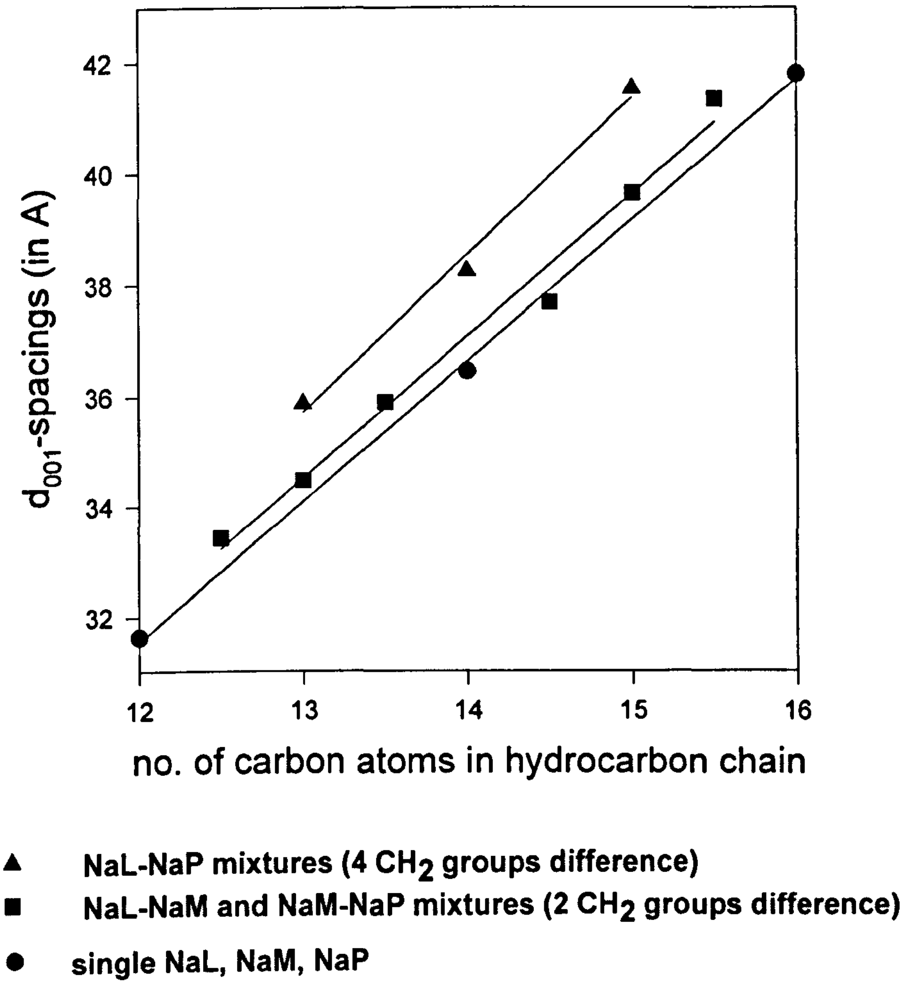

Figure 7.3 d-spacings for single and mixed coagels, as a function of the average number of carbon atoms in the hydrocarbon chain

The slopes of the lines of best fit through the data points are given in table 7.6. From the slope of the line for the single surfactant samples, an estimation was made of the tilt angle, *i.e.* the angle between the hydrocarbon chain of the surfactant molecules and the base plane of the unit cell. A structure similar to that of KP was assumed, where there are two molecules in the unit cell with parallel hydrocarbon chains, oriented tail to tail. When a similar structure is assumed for the sodium soaps, then an addition of *one* CH_2 group per molecule would mean that the distance in the direction of the hydrocarbon chains would increase by an amount equal to the distance between alternate carbon atoms (since the length of both molecules in the unit cell would increase), which is 2.557Å (Dumbleton and Lomer [3]). The slope of the line for the observed d-spacings for the single sodium surfactants indicates that the d_{001} spacing increases by 2.54Å on addition of one CH_2 group to the chainlength of one molecule. The tilt angle, τ, can then be calculated from $\sin(\tau)=2.54/2.557$. From this the tilt angle is approximately 83°. The same calculation for the NaL-NaM and NaM-NaP mixtures results in a tilt angle of approximately 90°. The d_{001} value for the NaM:NaP=3:1 mixture is slightly below the line of best fit. This might be due to experimental uncertainty or it could indicate that for this mixture the crystal structure is different. It is noteworthy here that the nucleation behaviour of this composition was also different from that of the other NaM-NaP and the NaL-NaM samples (see chapter 6).

surfactant	**slope of line (in Å/CH_2 group) (r^2)**
single surfactants NaL, NaM, NaP	2.54 (0.999)
mixtures NaL-NaM, NaM-NaP	2.56 (0.985)
mixtures NaL-NaP	2.83 (0.992)

Table 7.6 Slopes of the lines in figure 7.3 with correlation coefficients, r^2, between brackets

For the NaL-NaP mixtures the increase in d-spacing per CH_2 group is larger than the increase in the length of the molecules given by the distance between alternate carbon atoms. This indicates that the molecular packing of these mixtures (with a chainlength difference of four CH_2 groups) is less dense from that of the single surfactants. Care must be taken in interpreting these results however, since only three data points are available.

In some cases the peak for the solid phase was found to shift on heating to a slightly larger d-spacing. This is illustrated in figure 7.4. The reverse was also seen, on cooling the peak corresponding to the solid phase would after appearing shift to a slightly smaller d-spacing. These effects were very small however and since they were observed for mixed and single surfactant samples they were probably caused by thermal expansion and contraction of the crystal lattice.

7.4 Dissolution and crystallisation of 20 and 40wt% surfactant systems

Single and mixed surfactant systems were studied as 20 and 40wt% surfactant samples (see table 7.1), in order to assess the effect of mixing different chainlengths on the formation of the isotropic micellar phase and the hexagonal liquid crystalline phase, and on the crystallisation process from these phases. In this way the X-ray data for this part of the heating/cooling cycle could be identified when investigating more concentrated samples. In the following sections the different phases observed for the 20 and 40wt% surfactant samples are discussed, in the order that they occurred during the dissolution process.

7.4.1 The dissolution process of the 20 and 40wt% samples

Some typical examples of the transformation process between a coagel and the normal hexagonal liquid crystalline phase for a 40% single surfactant sample during heating of the sample are shown in figures 7.4-7.6. As the coagel was heated up, the solid started to dissolve; when the soap concentration exceeded the c.m.c. (critical

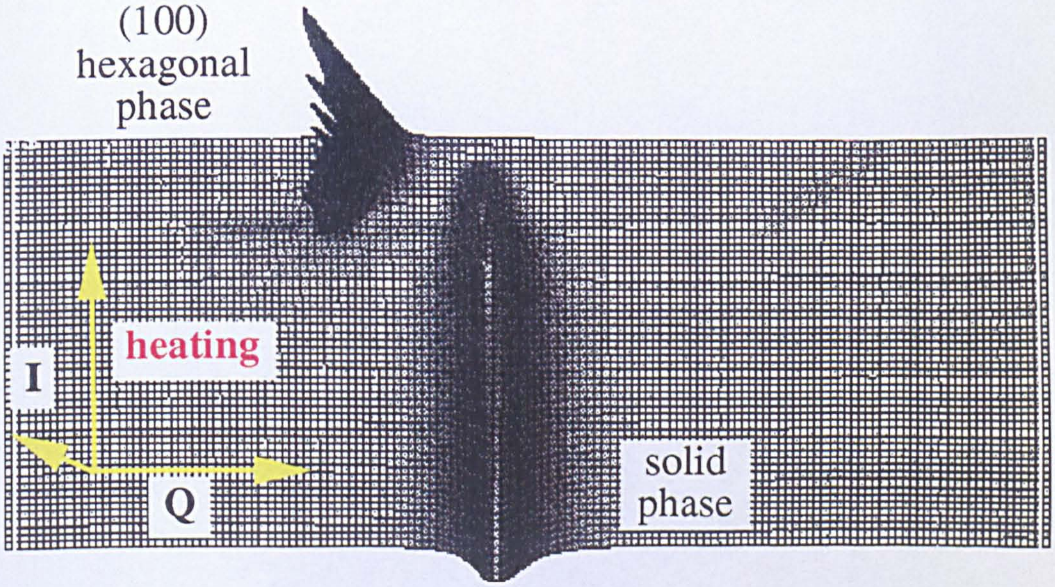

Figure 7.4 Changes in the integrated SAXS patterns, corresponding to the transformation process between the solid phase and the hexagonal liquid crystalline phase on heating. The top figure shows this for a NaL:NaP=1:3 40% soap sample. The peak for the hexagonal phase shifts to smaller d–spacing as more soap dissolves. The peak for the solid phase shifts to slightly larger d–spacing before disappearing.

Figure 7.5 Illustrating the same process as in the figure above, but for a NaM:NaP=1:1 40% soap sample.

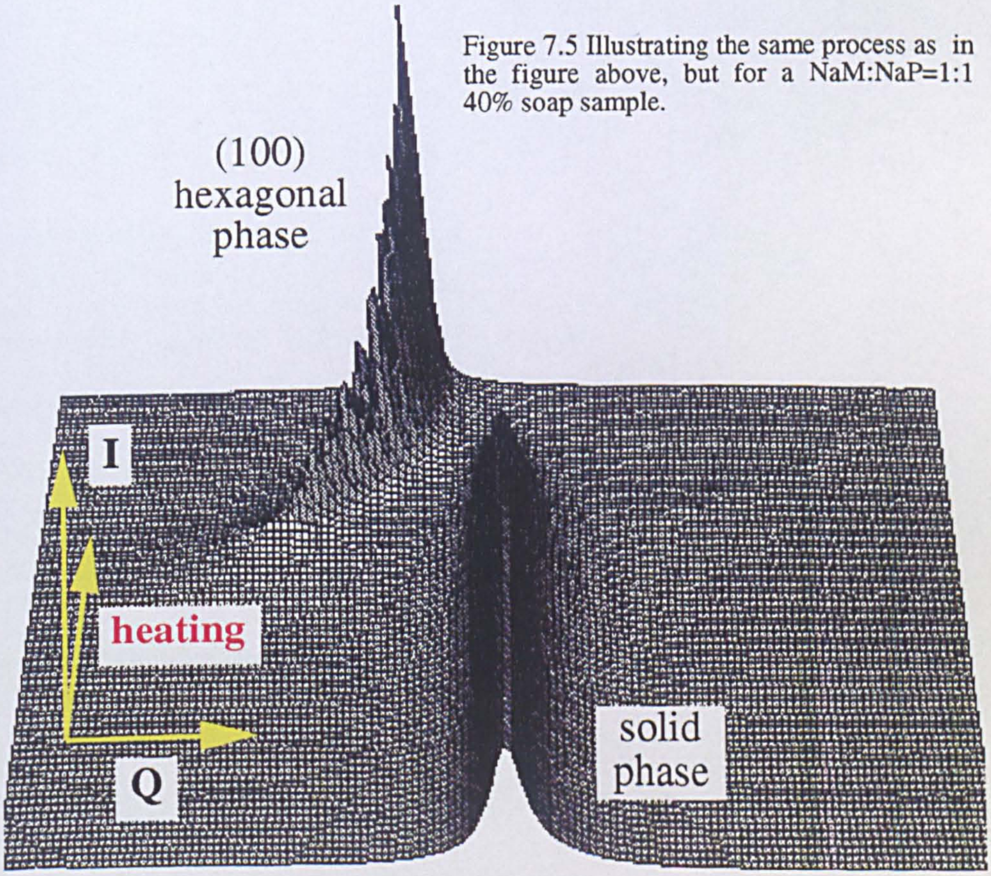

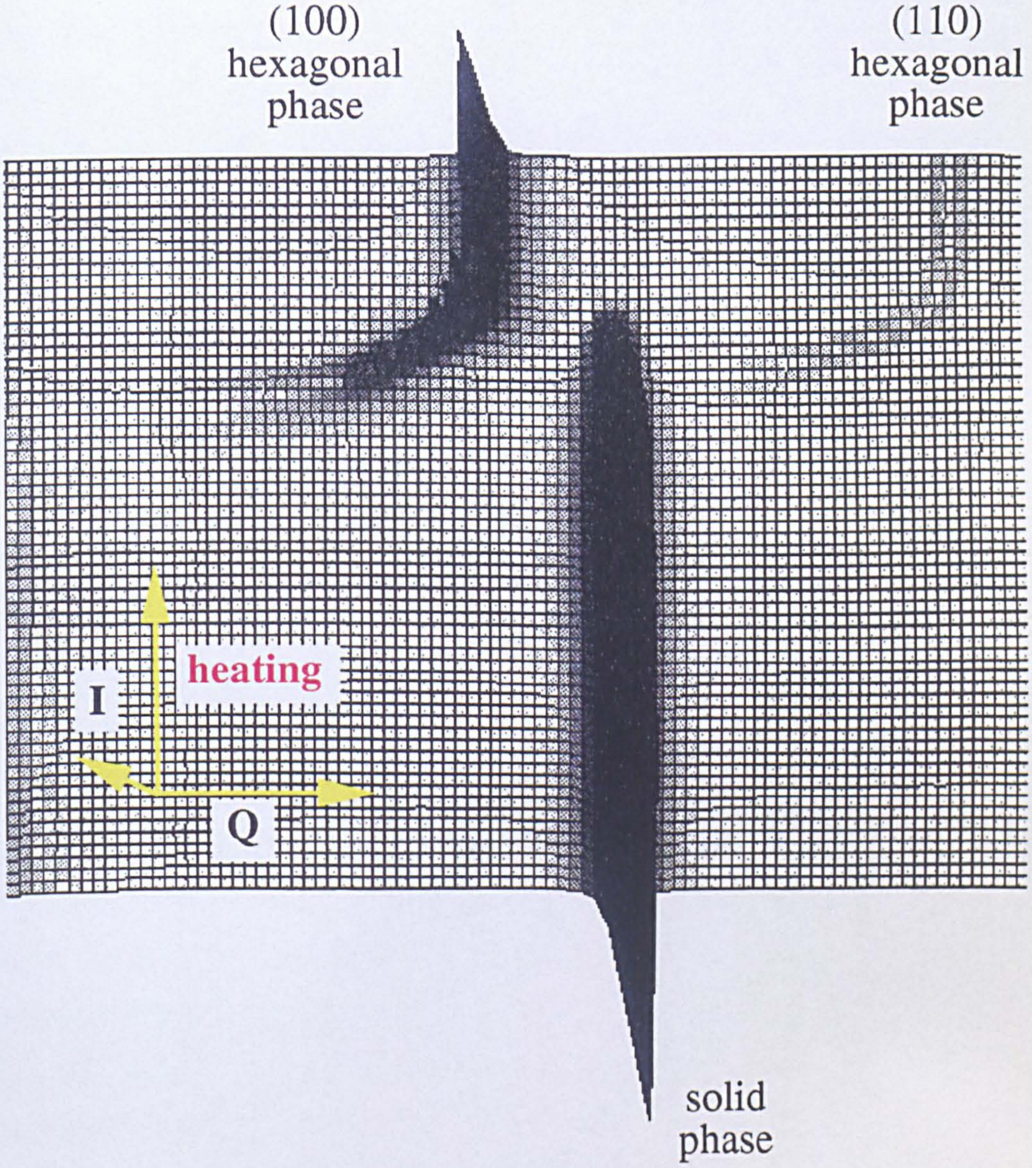

Figure 7.6 Variable temperature SAXS data showing the transformation process taking place during dissolution of a 40% NaP sample. The (110) peak of the hexagonal phase is just visible

micelle concentration), spherical micelles were formed, which resulted in the appearance of a diffuse diffraction ring in the SAXS spectrum, the d-spacing of which corresponds to the average distance between the micelles, see figure 7.7. For this isotropic micellar phase all 20 and 40wt% soap samples exhibited only one diffraction ring. When the sample was heated up further, more soap dissolved, resulting in a smaller d-spacing for the diffuse diffraction ring. For the 40wt% samples at a certain point (when the transition concentration was reached) a transformation occurred from the isotropic micellar solution to the hexagonal liquid crystalline phase, see figure 7.7. This phase gave rise to one or two sharp diffraction rings in the SAXS range covered by the detector, which were easily indexed as the (100) and the (110) peaks, see figure 7.6. As more soap dissolved the peak corresponding to the solid phase became weaker and the peaks for the hexagonal phase grew in intensity. In addition it can clearly be seen from figures 7.4-7.6 that the peaks for the hexagonal phase shifted to a smaller d-spacing as the coagel peak died out. The oscillations in the intensity of the (100) peak for the hexagonal phase are an artefact of the graphics software, caused by the shifting peak.

In some samples preferred orientation was present of the solid soap inside the capillaries. This caused texture in the diffraction rings in the form of two arcs with a higher intensity than the rest of the ring. It was found that if this orientation was present for the solid phase, then it was passed on to the hexagonal phase. This is shown in figure 7.8. This effect was found to be reversible on repeated heating and cooling of the samples: on cooling the orientation was passed on from the hexagonal phase to the solid phase and on heating the orientation was passed on from the solid to the hexagonal phase (see figure 7.8).

Figures 7.7 and 7.9 show SAXS patterns for the transition between the isotropic micellar solution and the hexagonal liquid crystalline phase and vice versa. The broad peak is caused by the isotropic micellar phase, the sharp peak is the (100) peak of the hexagonal phase. Reiss-Husson and Luzzati [4], found that for sodium soaps the (100) peak for the hexagonal phase coincided with the centre of the peak for the

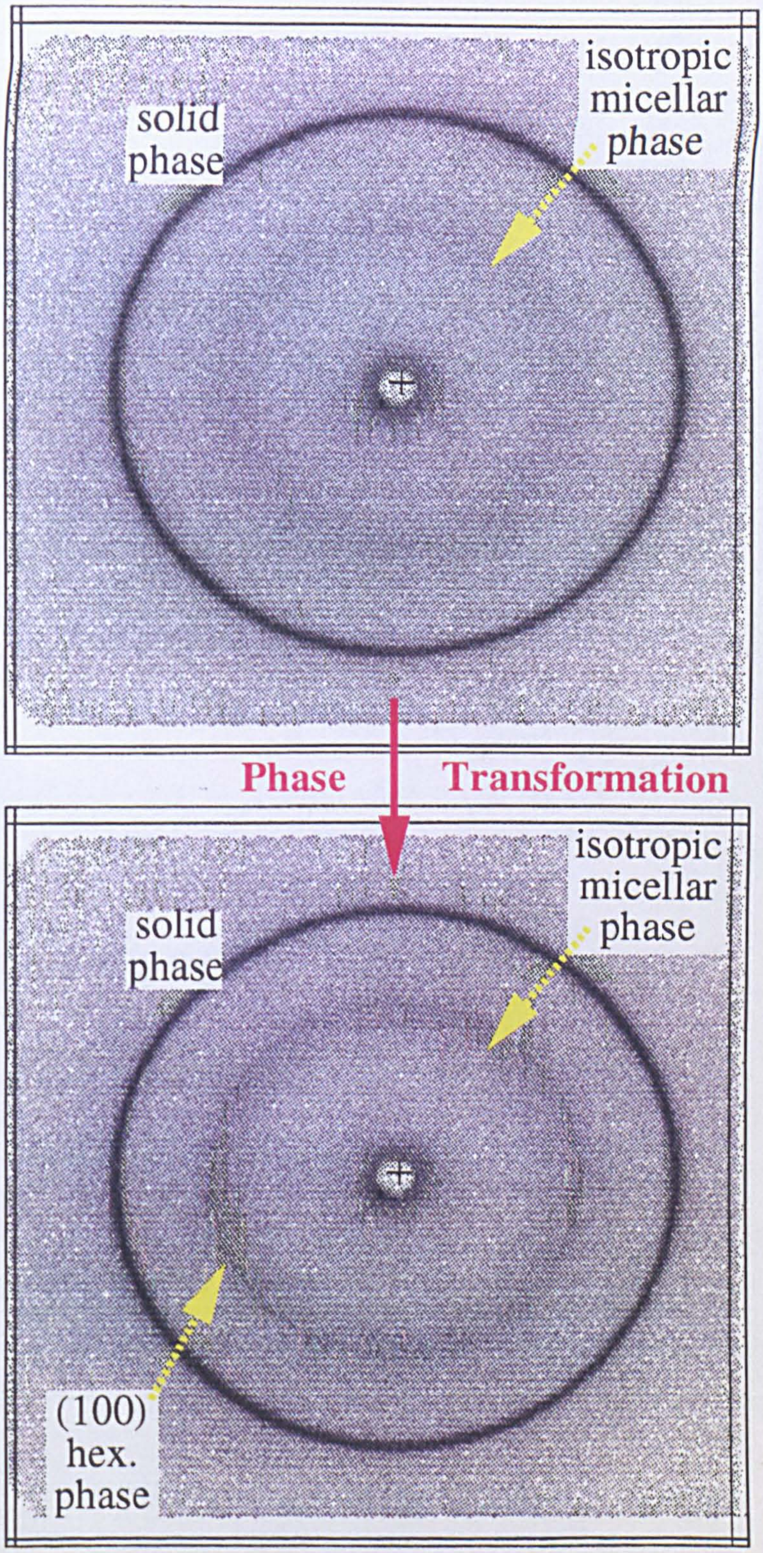

Figure 7.7 2–D SAXS data illustrating the transformation from the isotropic micellar phase to the hexagonal liquid crystalline phase on dissolution of a 40% NaP sample. The peak for the hexagonal phase can be seen to appear at the outside of the diffuse ring and not in the centre of it

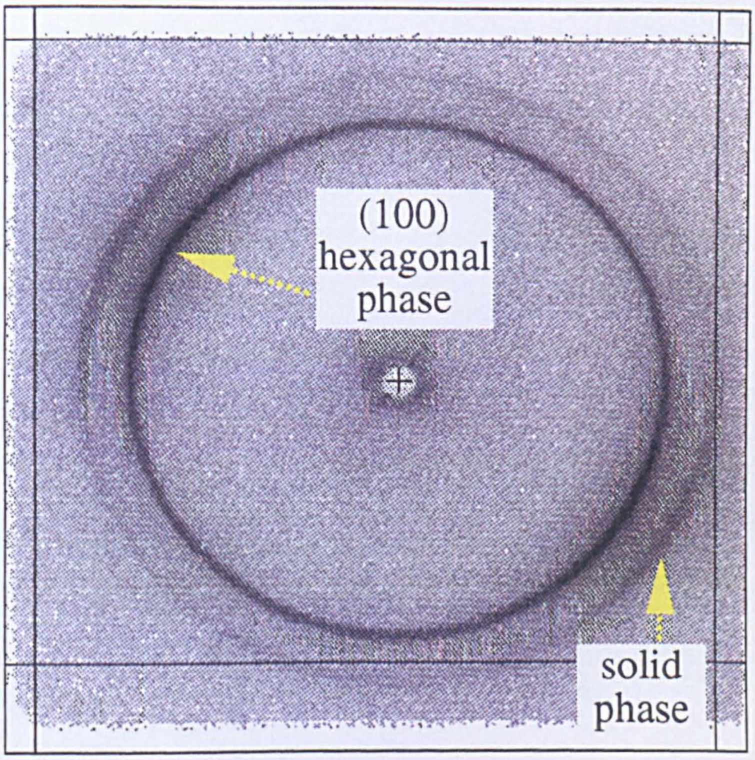

Figure 7.8 2–D SAXS data showing how the texture in the diffraction ring for the solid phase is passed on to the diffraction ring for the hexagonal phase on heating (top figure) and vice versa on cooling (botttom figure)

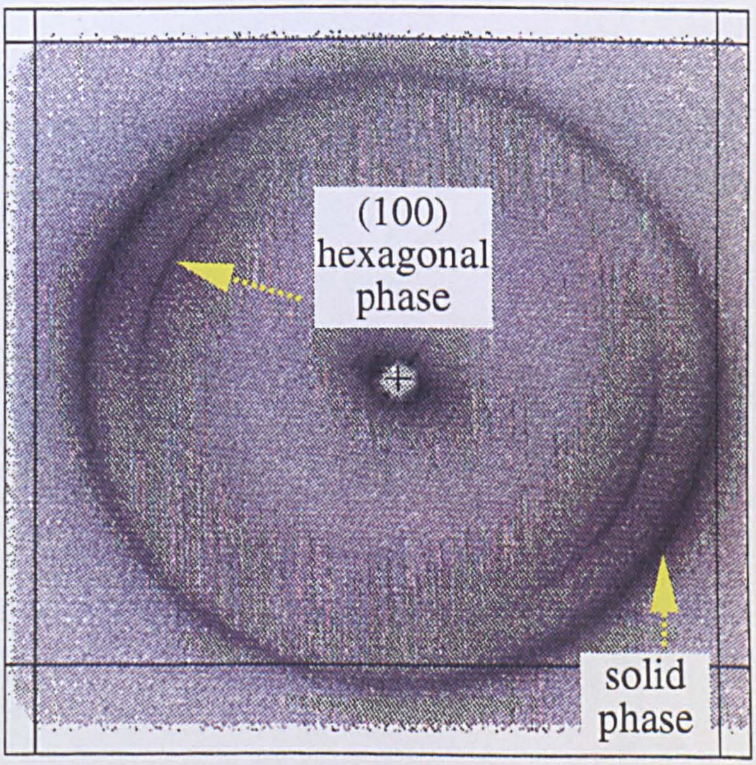

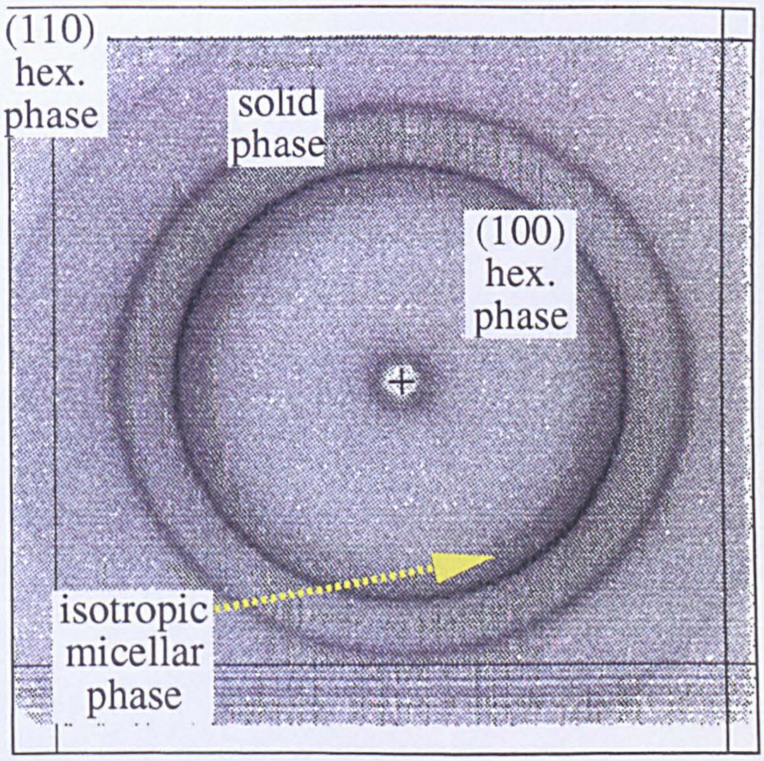

Figure 7.9 The top figure shows 2–D SAXS data, illustrating the transformation from the hexagonal phase through the isotropic micellar phase to the solid phase. The bottom figure shows the integrated 1–D pattern. The transformation process shown here is for a 70% NaM:NaP=1:3 sample

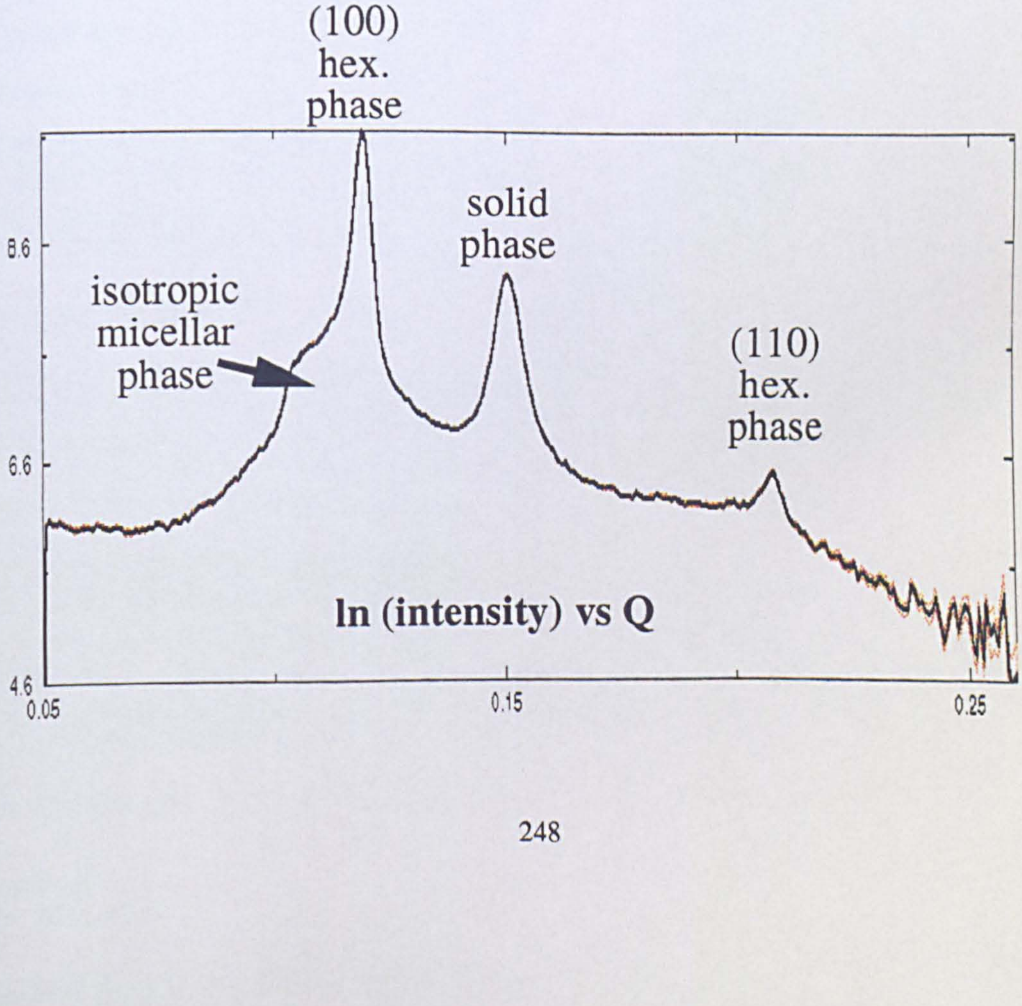

isotropic micellar phase. From this they concluded that the spheres transformed to cylindrical micelles before the transition to the hexagonal phase. This however is not consistent with the results presented here. From figures 7.7 and 7.9 it can be seen that the sharp peak is formed at the outer edge of the diffuse ring. As this part of the broad peak ring corresponds to the spherical micelles which are closest together, this indicates that the gap between these spheres has fallen below a critical distance so that the spheres have to transform to cylinders as these can pack more closely together. For this reason and for simplicity so that their size can be estimated, the micelles of the isotropic micellar solution are assumed here to remain spherical until the moment that the phase transformation to the hexagonal phase occurs.

The radius of the micelles forming the isotropic micellar solution and the water gap between them was estimated in the following way, based on the surfactant concentration given by the transition concentration and on the assumption that the micelles are spherical:

The observed d-spacing, *d*, equals :

$$d = 2r + d_w \tag{7.3}$$

(see figure 7.10), where r is the radius of a sphere and d_w is the water gap between adjacent spheres. Along an arbitrary length l, there are l/d spheres, therefore in an arbitrary volume l^3, the number of spheres is given by $(l/d)^3$. The volume of one sphere equals $\frac{4}{3}\pi r^3$. Therefore the fraction of the total volume that is taken up by the surfactant molecules as spherical micelles, ϕ_S ,is given by:

$$\phi_S = \frac{(\frac{l}{d})^3 \frac{4}{3}\pi r^3}{l^3} = \frac{4}{3}\frac{\pi r^3}{d^3} \tag{7.4}$$

Since the volume fraction surfactant (see section 7.2) and the d-spacing are known, the radius of a micelle can be calculated from re-writing equation 7.4:

$$r^3 = \frac{3\phi d^3}{4\pi} \tag{7.5}$$

Subsequently the size of the water gap between adjacent spheres can be found from equation 7.3. The number of molecules per spherical micelle, N, can be calculated from the radius of the sphere and the density of the hydrocarbon phase as follows:

$$N = \frac{4}{3}\pi r^3 \rho_h \frac{N_A}{MW} \tag{7.6}$$

where N_A is Avogadro's number and MW is the molecular weight of the hydrocarbon chain (r in m and ρ_h in g/m^3).

Using the above equations the diameters of the spheres and the number of molecules per micelle have been calculated at the transition from the isotropic micellar solution to the hexagonal phase. The concentrations at which this phase transition occurred have been taken from Madelmont and Perron (for NaL [5,6], for NaM [7] and for NaP [8]); this was taken to correspond to the moment at which the peak for the hexagonal phase first appeared (superimposed on the diffuse peak for the isotropic micellar phase). The diameters of the spheres and the number of molecules per micelle are given in table 7.7.

surfactant	**transition concentration**		**spherical micelles**			**hexagonal phase**	
	wt %	ϕ	d_{sphere}	d_w	N	d_{cyl}	d_w
NaL	0.36	0.48	39.13	1.15	85	32.59	12.20
NaM	0.28	0.37	44.11	5.49	105	35.39	20.14
NaP	0.23	0.30	54.77	11.27	178	41.98	31.17
NaL:NaM=							
3:1	0.34	0.45	no data	no data	no data	no data	no data
1:1	0.32	0.42	42.12	3.08	98	34.44	15.94
1:3	0.30	0.40	43.36	4.24	103	35.50	18.24
NaL:NaP=							
3:1	0.33	0.44	41.37	2.57	93	33.58	14.79
1:1	0.30	0.39	44.33	4.38	107	36.26	18.70
1:3	0.26	0.34	46.90	7.27	119	37.17	23.55
NaM:NaP							
3:1	0.27	0.35	49.01	6.84	140	38.57	23.18
1:1	0.26	0.34	51.08	7.92	154	40.20	25.47
1:3	0.24	0.31	53.03	9.96	167	41.35	29.09

Table 7.7 Transition between spherical micelles and hexagonally packed cylinders (transition concentrations in weight % from Madelmont and Perron [5-8])

From this table it is clear that at the moment when the transitions takes place, the water gap between the spheres, the diameter of the spheres and therefore the number of molecules per spherical micelle, increase with increasing chainlength. The values for these parameters for the mixed surfactant systems are intermediate to the ones for the single surfactant systems. The value for the water gap for NaL seems very small (1.15Å). This is might be due to inaccuracies in the transition concentration used, or it could be an indication that the micelles do change shape before the hexagonal phase is formed.

The radius of the surfactant cylinders that form the hexagonal phase were calculated from the d-spacings and the surfactant concentration in the following way: (Luzzati [9]): as there is one whole cylinder per unit cell ($4 \times \frac{1}{4} = 1$, see figure 7.10), the area taken up by surfactant molecules in the two-dimensional unit cell equals the circular area taken up by the end of one cylinder (with radius r_{cyl}), which is equal to the surfactant volume fraction multiplied by the area of the two-dimensional unit cell:

$$\pi r_{cyl}^2 = \phi_S \times (area\ unit\ cell) \qquad (7.7)$$

The area of the two-dimensional unit cell is equal to $\frac{1}{2}a^2\sqrt{3}$, where a is the cell parameter (which is the distance between the axes of the cylinders, see figure 7.10). From equation 7.7 the radius of the cylinders can be calculated when the cell parameter a and the volume fraction surfactant are known. From this the thickness of the water gap between two adjacent cylinders, d_w, can be calculated since:

$$a = 2r_{cyl} + d_w \qquad (7.8)$$

(see figure 7.10). The values thus calculated for the diameters of the surfactant cylinders and the water gap between them at the transition from the isotropic solution to the hexagonal phase are given in table 7.7. From this table it is clear that at the transition from the isotropic micellar to the hexagonal phase, the diameter of the cylinders of the hexagonal phase and the water gaps between them increase with increasing surfactant chainlength. The diameters calculated here compare well with values previously found by Luzzati *et al.* [1]. This table further illustrates that at the transition concentration the spheres have come very close together, whereas after

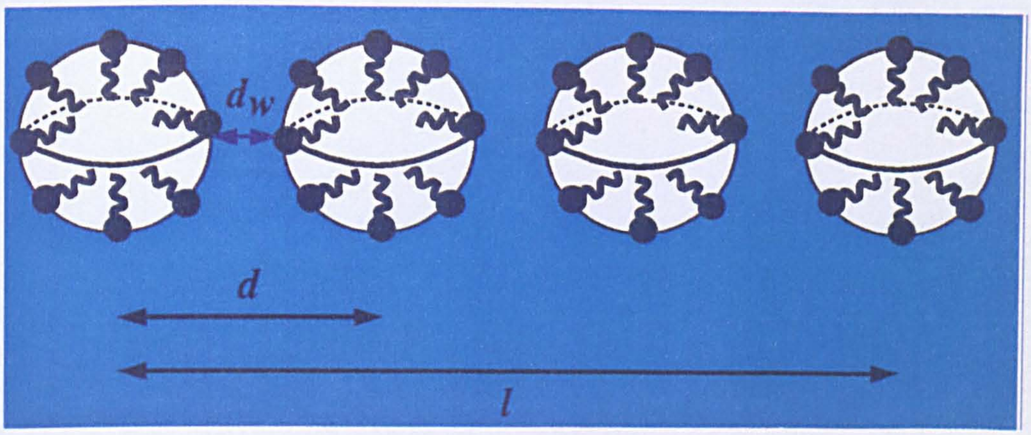

Along an arbitrary length *l*, there are *l/d* spherical micelles

$d=2r+d_w$

🟦 = water

● = soap molecule

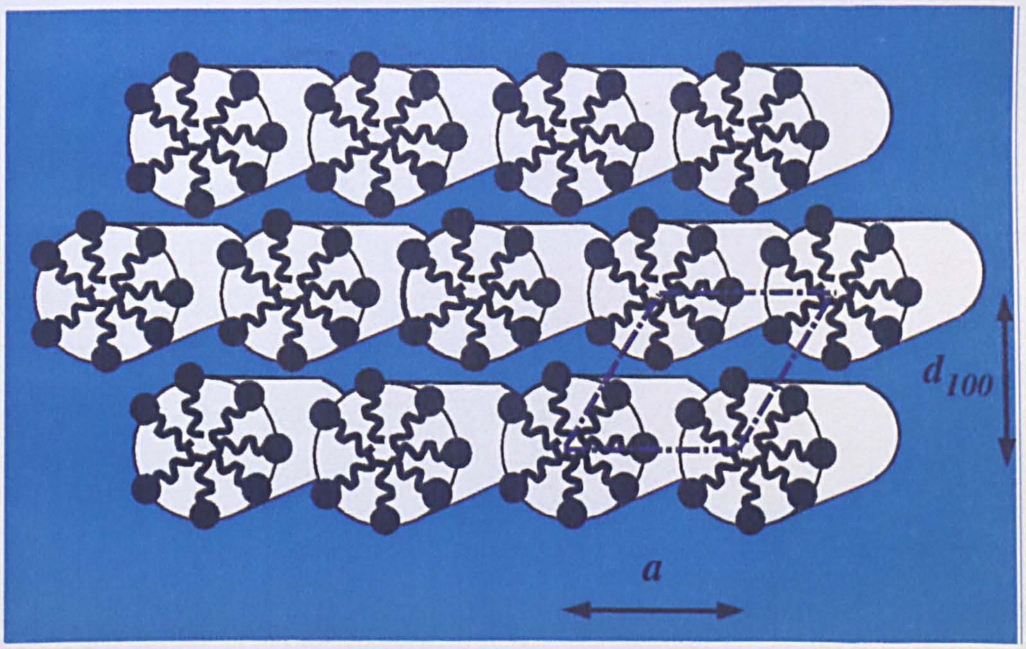

Area two dimensional unit cell=*a* sqrt(3/4)
There is one whole cylinder per unit cell (4x1/4=1)

$a=2r_{cyl}+d_w$

Figure 7.10 Showing the structural parameters for spherical micelles and for the hexagonal phase

transformation to a cylindrical shape there is a large space between the structural units again.

7.4.2 Crystallisation from the hexagonal liquid crystalline phase

In figure 7.11 some representative examples are shown of the crystallisation process from the normal hexagonal liquid crystalline phase during cooling of the sample. The reverse process takes place to that which was described for heating of the sample. The peaks for the hexagonal phase shift to larger d-spacing and become weaker as the coagel peak grows in intensity. The crystallising solid depletes the solution so that the surfactant cylinders of the hexagonal phase become further apart, which explains the shift in the d-spacings for the hexagonal peaks. Sometimes this shift was less pronounced, as can be seen from a comparison of the two graphs shown in figure 7.11. When the concentration had dropped below the transition concentration, the cylinders break up so that the isotropic micellar phase is formed (see figure 7.9)

7.5 Dissolution and crystallisation of 70wt% surfactant systems

Single and mixed surfactant samples were prepared containing 70wt% surfactant and 30wt% water (see table 7.1), in order to investigate the influence of surfactant chainlength and the mixing of chainlengths on the phase transformation processes that take place during the formation of the lamellar liquid crystalline phase (section 7.5.1) and during crystallisation from this phase (section 7.5.2). Evidence for epitaxial growth relations between all ordered phases is given in section 7.6. With some samples crash cool experiments were carried out. The results for this are given in section 7.7.

7.5.1 Formation of the lamellar phase from a coagel

Most 70% surfactant samples exhibited identical phase behaviour for the formation of the lamellar liquid crystalline phase from a coagel during heating of the sample.

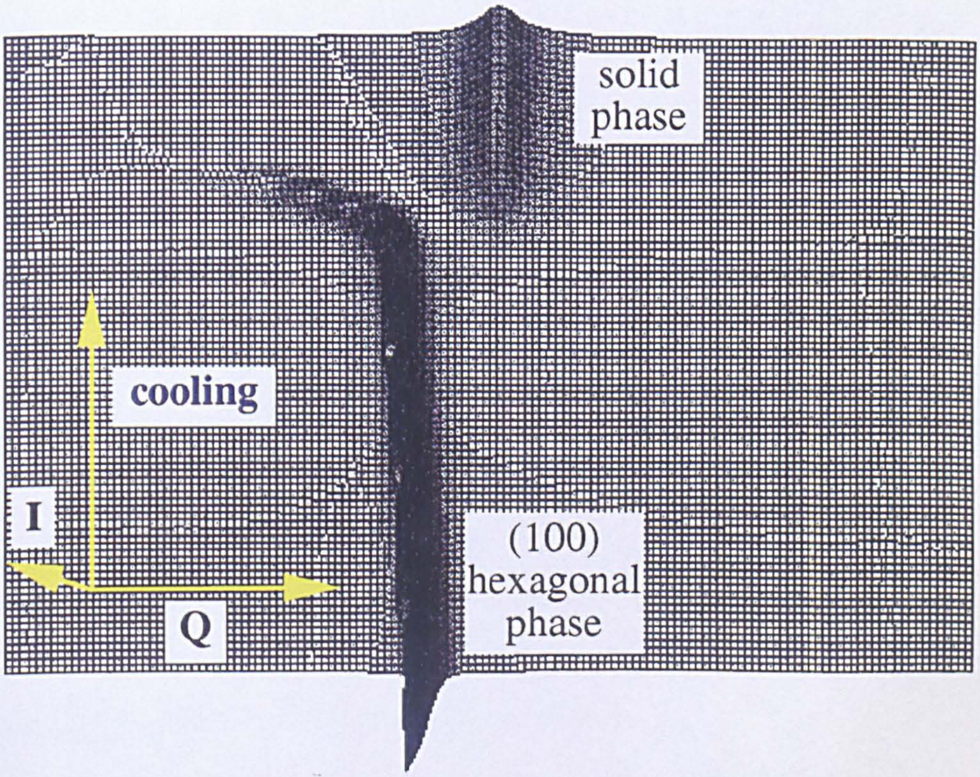

Figure 7.11 Changes in the integrated SAXS patterns due to surfactant crystallisation from the hexagonal phase during cooling. The top figure illustrates this for a NaM:NaP=1:1 1:1 40% soap sample, the bottom one for a NaL:NaP=1:3 40% soap sample

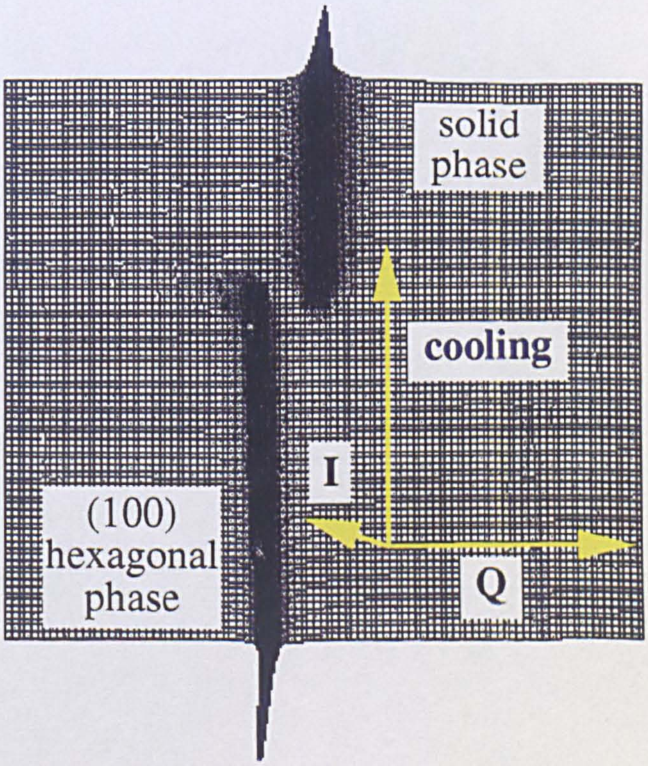

All samples were found to form at least two phases intermediate in composition between the hexagonal and the lamellar liquid crystalline phase. Some typical examples of this are shown in figures 7.12-7.14. These phases are discussed in sections 7.5.1.1-5. Results that indicated the formation of additional phases for some samples are given in section 7.8.

The first processes that occurred during heating were identical to those taking place for the 40% surfactant samples: as the solid dissolved, the concentration of the solution increased, so that first an isotropic micellar solution was formed in coexistence with the solid phase, which subsequently transformed to hexagonally packed cylinders in coexistence with the solid phase. From figures 7.12-7.14 it can be seen that as the sample was heated up further, so that more soap dissolved, two phases formed in between the hexagonal and the lamellar liquid crystalline phases. This is consistent with the results of Madelmont and Perron [6,7 and 10] and Rendall *et al.* [11] who observed two intermediate phases for NaL.

In the following sections (sections 7.5.1.1-7.5.1.5) the different phases and the phase transformations between them are discussed, in the order that they occurred on heating of the sample, starting with the phase transformation from the hexagonal phase to the first intermediate phase, as the transformation process from the isotropic micellar phase to the hexagonal phase has already been discussed in section 7.4.

7.5.1.1 The transformation from the hexagonal to the first intermediate phase

On heating the 70% samples through the hexagonal phase, more of the surfactant that was still in the solid phase dissolved, making the solution more concentrated. As a result of this the peak for the hexagonal phase can be seen to shift to a smaller d-spacing in figures 7.12 and 7.14, as was observed in section 7.4. At one point the next phase boundary was crossed and a phase transformation occurred. For almost all the 70% surfactant samples this resulted in a phase transformation to a phase that will be called here the first intermediate phase. Some samples however were found to

Figure 7.12 The changes in the integrated SAXS patterns due to the phase transformations taking place during heating of a coagel sample (NaL:NaP=3:1 70%soap). The figure reveals the existence of two phases intermediate in composition between the hexagonal and the lamellar liquid crystalline phase

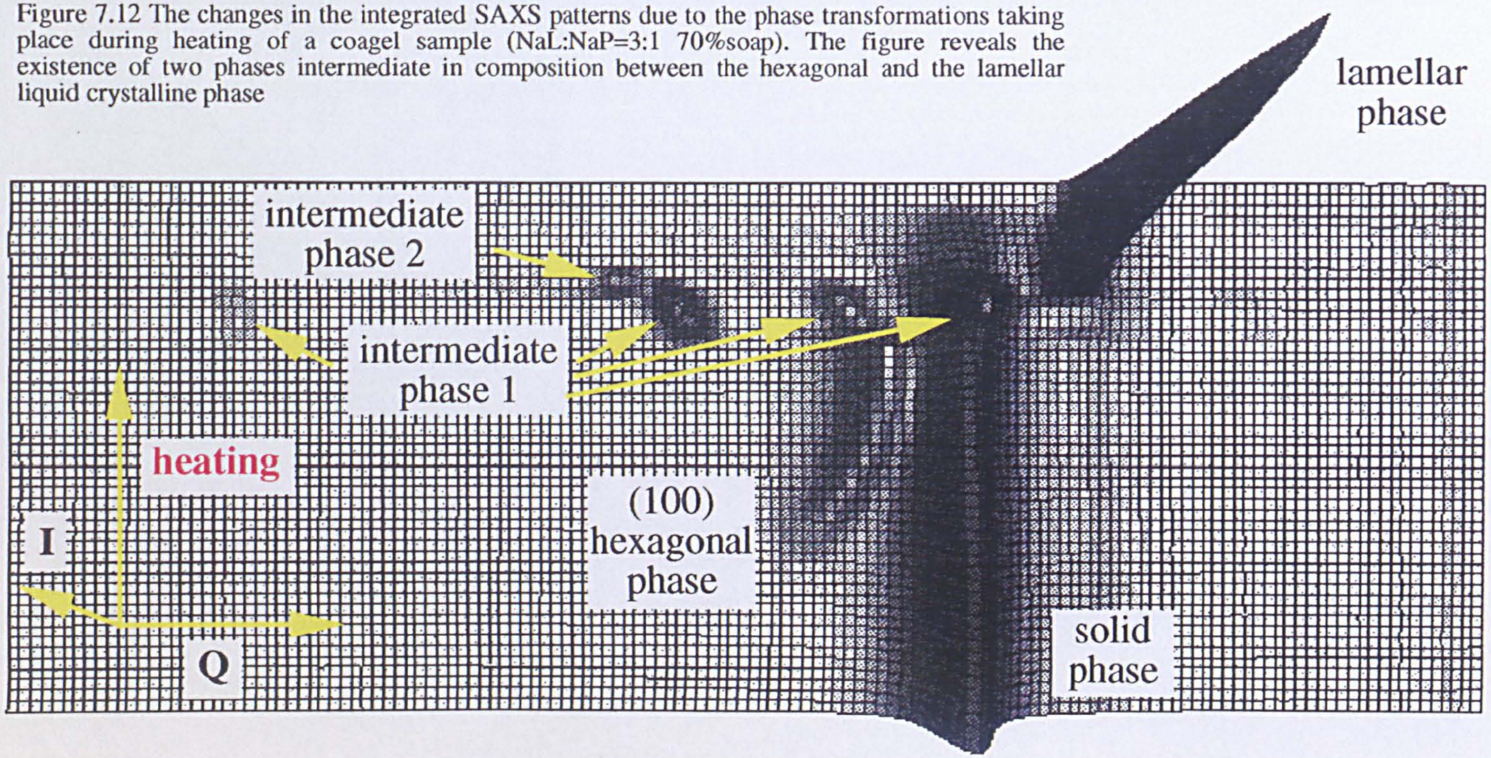

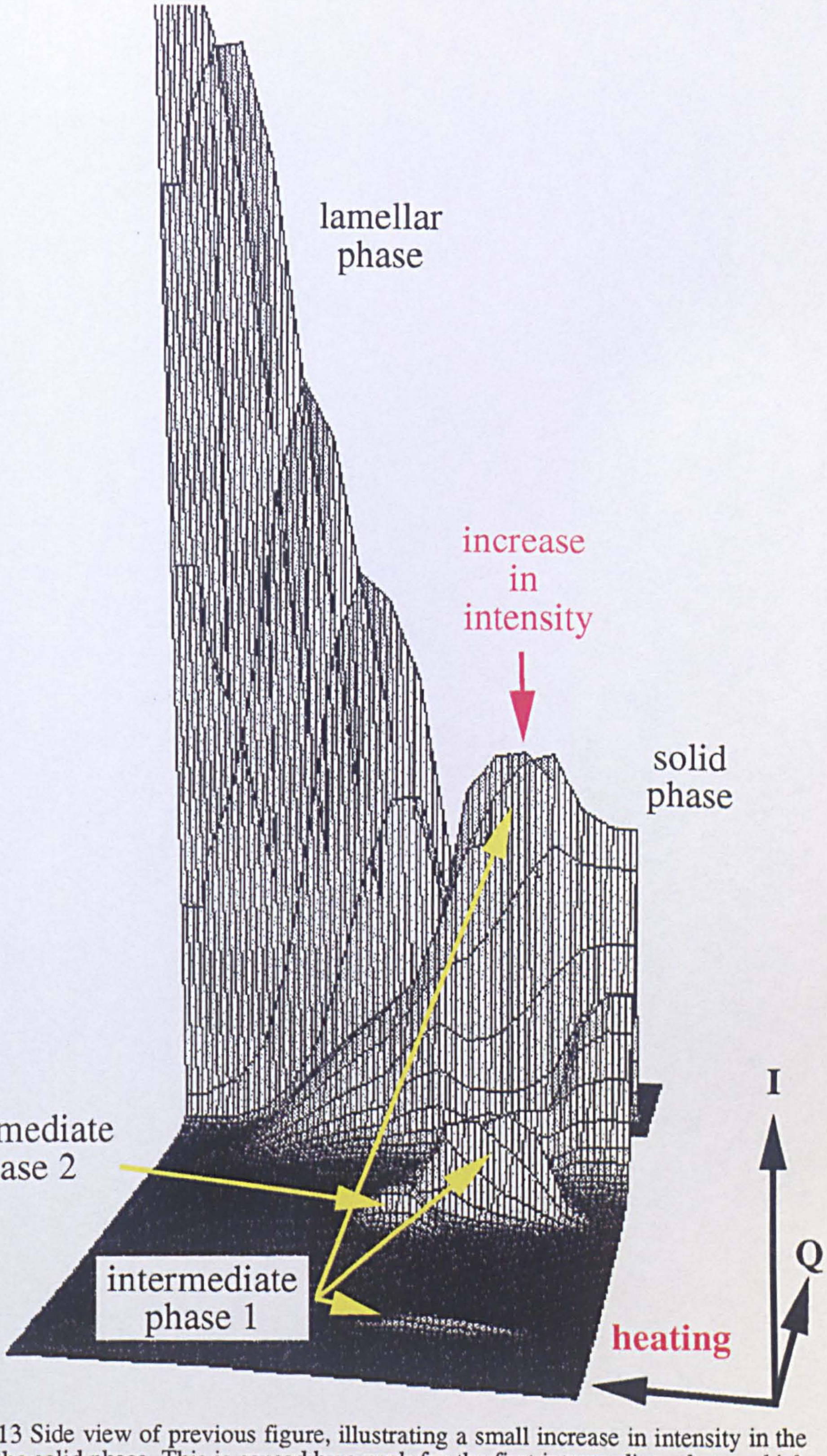

Figure 7.13 Side view of previous figure, illustrating a small increase in intensity in the peak for the solid phase. This is caused by a peak for the first intermediate phase, which coincides with the peak for the solid phase

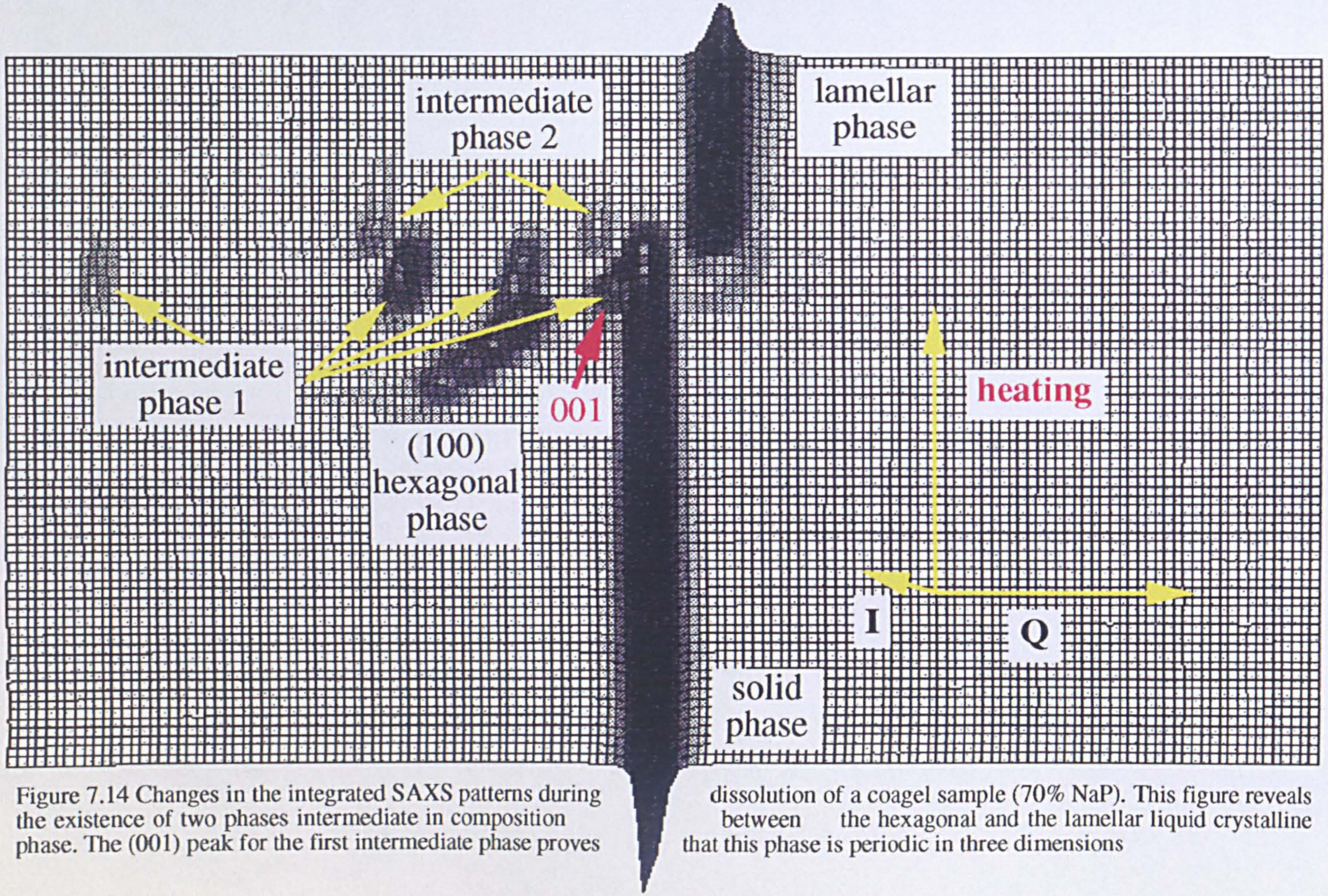

Figure 7.14 Changes in the integrated SAXS patterns during dissolution of a coagel sample (70% NaP). This figure reveals the existence of two phases intermediate in composition between the hexagonal and the lamellar liquid crystalline phase. The (001) peak for the first intermediate phase proves that this phase is periodic in three dimensions

form a phase between the hexagonal phase and this first intermediate phase; this is shown in section 7.8.

The transition concentrations for the transition between the hexagonal and the first intermediate phase for NaM and NaP have been taken as the values that were found by Husson *et al.* [12] for the transition between the deformed hexagonal and the complex hexagonal phase. From a comparison of the X-ray data given by Husson *et al.* [12] with the data presented here, it is clear that the phase which they called the complex hexagonal phase, is the same phase as what is called here the first intermediate phase. It is therefore correct to use these transition concentrations. For NaL however, using static X-ray diffraction measurements, Husson *et al.* [12] did not find any intermediate phases. The value found by Madelmont and Perron [7] for NaM (using DTA studies) for the transition between the hexagonal and the first intermediate phase is identical to the one reported by Husson *et al.* [12] for the transition between the deformed hexagonal and the complex hexagonal phase. Therefore the assumption is made here that the first intermediate phase observed by Madelmont and Perron is the same as the first intermediate phase presented here. Therefore the transition concentration that was found by Madelmont and Perron [5, 6] has been taken here for the calculations for NaL. In addition, this value seems to fit in with the trend of an increase in transition concentration with shorter chainlength. Again for mixed surfactant systems no literature data exist for transition concentrations, therefore for these systems the values for the transition concentrations have been interpolated by taking weighted averages of the values for the single surfactant systems.

From these transition concentrations the diameter of the surfactant cylinders that make up the hexagonal phase have been calculated, see table 7.8, using the same method as before (section 7.4). Again it can be seen that at the moment when the transition occurs, a surfactant with a longer chainlength results in a larger diameter of the cylinders and also in a larger water gap between the cylinders. In addition, the mixed systems still show intermediate values for d_{cyl} and d_w. From comparing table

7.7 and table 7.8 it can be seen that as the concentration of the soap increases, the thickness of the water layer between the cylinders is reduced. At one point the cylinders become too close together and a transformation occurs to the first intermediate phase. The thickness of the water layer is about 4-8Å which is about the same as it was for spherical micelles. This indicates that this is a critical distance of the entities to come together.

7.5.1.2 The structure of the first intermediate phase

The intermediate phase that formed first by most samples on heating, after the normal hexagonal phase, typically showed about 3 or 4 peaks of the type (*h*00) and (*hk*0) that indexed for a two-dimensional hexagonal structure. The spectra obtained for this phase seem to be identical to the one published by Husson *et al.* [12]. For the spectra presented here however, more peaks were observed in some cases, that indexed as the (001), (101) peak. Often the (001) peak was not observed as a separate peak (as is shown in figure 7.14), but coincided with the peak for the solid phase. This was noted however by an increase in intensity of this peak. An example of this effect is shown in figure 7.13. If no other peak would coincide with the peak for the solid phase, then the intensity of this peak would be expected to decrease continuously as more solid dissolves. However the intensity of this peak first decreases and then increases when the first intermediate phase is formed. The (001) peak of the first intermediate phase is thus easily overlooked. The same is true for the (101) peak, which could easily be mistaken for the (001) peak of the lamellar liquid crystalline phase, as this peak would appear at approximately the same position. It is possible that for these reasons Luzzati *et al.* [1] and Husson *et al.* [12] did not notice the above mentioned peaks, which are related to the c-axis of this intermediate phase. Since they therefore only observed peaks of the type (*h*00) or (*hk*0) they proposed the model of the complex hexagonal phase with two-dimensional periodicity rather than a structure with three-dimensional periodicity.

However, the diffraction peaks observed here, indicate a different type of structure with a three- rather than a two-dimensional periodicity, based on a hexagonal lattice. A hexagonal mesh phase or bicontinuous phase would therefore be a likely structure for this phase. These structures cannot be distinguished from the positions of the d-spacings alone and therefore the likelihood of a number of models was assessed on the basis of the consistency of the model with the surfactant volume fraction.

The first model to be tried here for the first intermediate phase was a hexagonal mesh structure, consisting of alternating water layers and surfactant bilayers, where each surfactant bilayer is made up of rods formed by surfactant molecules. These rods are linked together three at each junction, to form hexagonally shaped holes that are filled with water. As the d-spacings index for a hexagonal lattice, there is one water hole per unit cell and these holes in the surfactant layers are lined up with the holes in adjacent surfactant layers. Four parameters are needed to describe this geometry: the thickness of a surfactant layer d_s, the thickness of a water layer d_w, the width w of a surfactant rod and the size of a water hole x (defined here as the distance between two parallel sides of the hexagonally shaped hole). On the basis of the cell parameters two equations can be written down (see figure 7.15):

$$a = w + x \tag{7.9}$$

and

$$c = d_s + d_w \tag{7.10}$$

On the basis of the geometry and the volume fraction surfactant ϕ_s, a third equation can be derived relating the cell parameters to the parameters describing the structure:

$$\phi_s = \frac{\frac{1}{2}\sqrt{3}a^2c - V_{water\ layer} - V_{hole}}{\frac{1}{2}\sqrt{3}a^2c} \tag{7.11}$$

where

$$V_{water\ layer} = \frac{1}{2}\sqrt{3}a^2 d_w \tag{7.12}$$

is the volume of a water layer in the unit cell and

$$V_{hole} = \frac{1}{2}\sqrt{3}x^2 d_s \tag{7.13}$$

is the volume of water present in one hole in a surfactant layer. Equation 7.11 states that the surfactant volume fraction must be equal to the total volume in the unit cell taken up by surfactant (which is equal to the total volume of the unit cell minus the volume taken up by water) divided by the total volume of the unit cell. A system of three equations (7.9-11) with four unknown parameters (the parameters describing the geometry: w, x, d_s and d_w) cannot be solved, therefore an assumption had to be made in order to eliminate one of the parameters. For this reason initially the assumption was made that a surfactant rod would have a square cross-section, *i.e.*

$$w=d_s \tag{7.14}$$

In this way one of the parameters is eliminated from the equations and a system of three equations with three unknown parameters results. Combination of equations 7.9-14 leads to:

$$d_s^3 - 2d_s^2 a + a^2 c\phi_s = 0 \tag{7.15}$$

It was attempted to solve this equation for d_s, using the cell parameters and the volume fractions calculated for this phase and the transition concentrations from Husson *et al.* [12] and Madelmont and Perron [5, 6]. However, this did not lead to realistic solutions. It was not possible to accommodate in this structure the amount of surfactant required by the volume fraction. The reverse structure where the cylinders are made up of the water molecules and the holes are filled with the surfactant molecules would fit the data but seems unlikely as this does not seem to be a logical step in the overall transformation process from the hexagonal to the lamellar phase.

The proposed model thus had to be modified. Therefore, instead of assuming a square cross-section of the surfactant rods (equation 7.14), the assumption was made that the surfactant rods would have a rectangular cross-section so that a larger volume could be filled with surfactant as the water holes become smaller in this way. Since equation 7.14 is not valid anymore another simplification had to be made in order to eliminate one parameter from the equations. The assumption was therefore made that the thickness of the surfactant layers would be equal to the thickness of the surfactant layers in the lamellar phase. For all the samples this parameter was therefore first calculated for the lamellar phase (see section 7.5.1.5). When the thickness of the surfactant layer, d_s, is known then w, d_w and x can be calculated from equations 7.9-11. However, even using this model with surfactant rods with a rectangular cross-section, the amount of surfactant required by the surfactant volume fraction could still not be fitted into the structure.

For this reason the model was further modified. If instead of unconnected surfactant layers it is presumed that these layers are connected at the corners of the hexagons, then a higher volume fraction surfactant can be fitted into the unit cell. For simplicity the junctions between the rectangular rods in the same surfactant layer were assumed here to have a triangular shape. The surfactant columns connecting adjacent surfactant layers were therefore taken to have a triangular cross-section. The length of a side of the equilateral triangle is then equal to the width of a surfactant rod, w, see figure 7.15. In this way no extra unknown parameters are needed to describe the geometry of the connections between the surfactant layers. Equations 7.9-11 and 7.13 remain the same but equation 7.12 needs to be modified, as the connecting columns reduce the volume per unit cell available for water in the water layer. Equation 7.12 therefore becomes:

$$V_{water\ layer} = \tfrac{1}{2}\sqrt{3}a^2 d_w - V_{columns} \qquad (7.16)$$

where $V_{columns}$ is the volume of 2 columns of triangular cross-section present in the unit cell, connecting two adjacent surfactant layers and is given by:

$$V_{columns} = \tfrac{1}{4}\sqrt{3}w^2 d_w \qquad (7.17)$$

Substitution of equations 7.9, 7.10, 7.13, 7.16 and 7.17 into equation 7.11 and re-arranging results in:

$$w^2(d_s - \tfrac{1}{2}d_w) - 2wad_s + a^2 c\phi_s = 0 \qquad (7.18)$$

The cell parameters a and c were calculated from the X-ray diffraction data, ϕ_s was calculated from the weight percentage surfactant given by the transition concentration, d_s was assumed to be the same as in the lamellar phase so that d_w could be calculated from equation 7.10. Therefore w could be calculated from equation 7.18 (where w is limited by the following constraints: $0<w<a$). After w was known, the distance across a water hole, x, was calculated from equation 7.9 and the

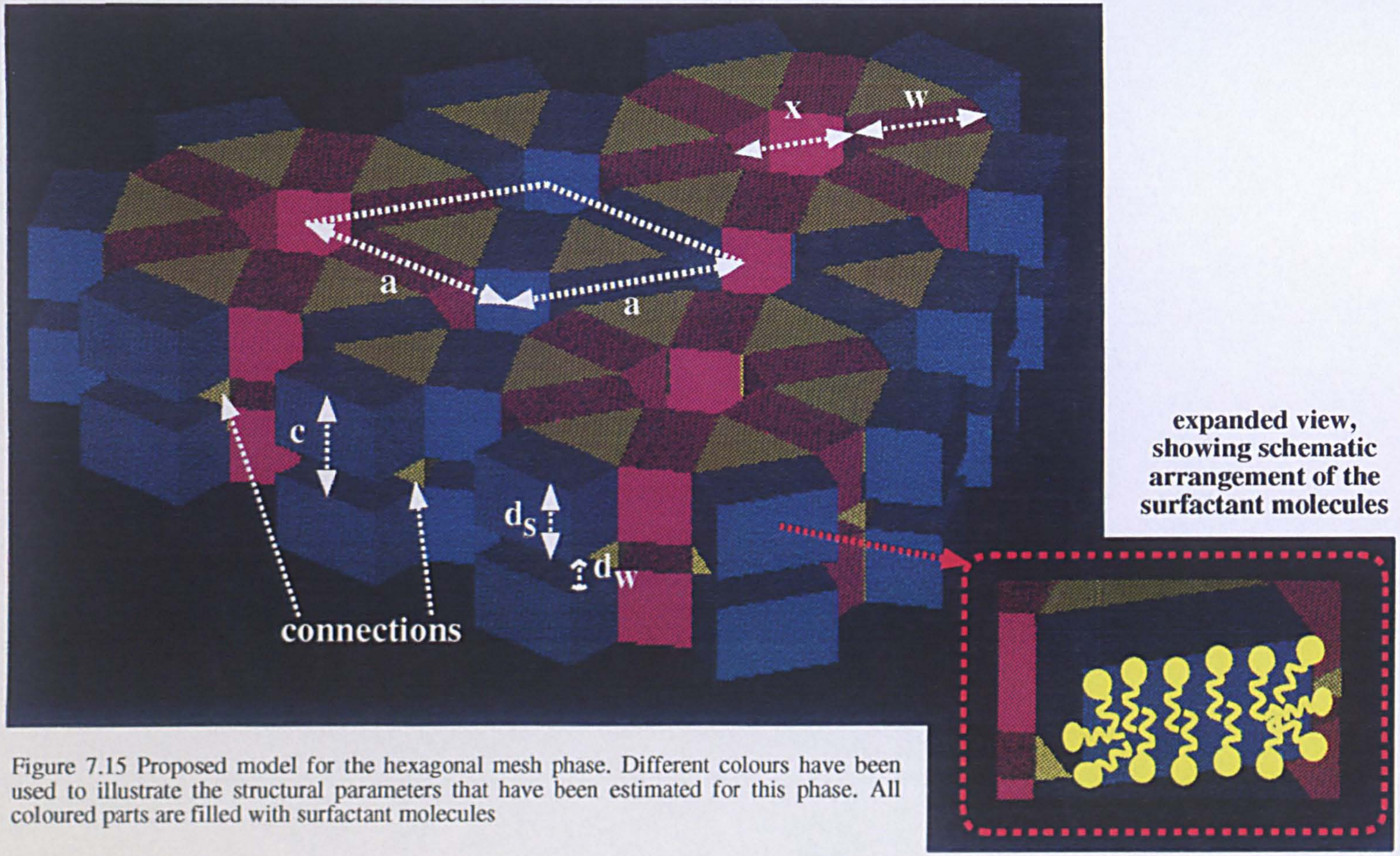
x
w
a
a
c
ds
dw
connections
expanded view,
showing schematic
arrangement of the
surfactant molecules

Figure 7.15 Proposed model for the hexagonal mesh phase. Different colours have been used to illustrate the structural parameters that have been estimated for this phase. All coloured parts are filled with surfactant molecules

surfactant	**transition concentration**		**hexagonal phase**		**hexagonal mesh phase**							
	wt%	ϕ_s	d_{cyl}	d_w	a	c	d_s	d_w	w	x	V_{hole} x10^3Å^3	$V_{columns}$ x10^3Å^3
NaL	0.56	0.75	39.19	4.00	85.62	34.29	24.44	9.85	64.37	21.25	9.56	17.7
NaM	0.55	0.72	41.84	5.00	96.14	37.63	27.25	10.38	66.30	29.84	21.0	19.8
NaP	0.52	0.68	48.54	7.71	113.36	43.94	28.56	15.38	79.85	33.51	27.8	42.5
NaL:NaM=												
3:1	0.56	0.74	40.81	4.26	82.45	34.52	25.38	9.14	58.52	23.93	12.6	13.6
1:1	0.56	0.74	40.76	4.31	94.24	36.53	25.71	10.82	70.17	24.07	12.9	23.1
1:3	0.55	0.73	40.82	4.82	94.85	33.60	27.39	6.21	58.42	36.43	31.5	9.18
NaL:NaP=												
3:1	0.55	0.73	38.71	4.48	88.47	35.65	25.14	10.51	64.24	24.23	12.8	18.8
1:1	0.54	0.71	40.90	5.31	98.05	38.79	25.81	12.98	72.22	25.83	14.9	29.3
1:3	0.53	0.69	42.86	6.18	98.05	39.52	26.91	12.61	67.43	30.62	21.8	24.8
NaM:NaP												
3:1	0.54	0.71	43.02	5.68	100.77	37.85	27.14	10.71	68.67	32.10	24.2	21.9
1:1	0.54	0.71	44.45	5.93	103.65	39.40	27.38	12.02	73.03	30.62	22.2	27.8
1:3	0.53	0.69	45.53	6.66	106.69	40.28	27.92	12.36	72.04	34.65	29.0	27.8

Table 7.8 Transition between hexagonally packed cylinders and the hexagonal mesh phase, all distances are in Å (transition concentrations in weight % from Husson *et al.* [12] and Madelmont and Perron [5, 6])

volume taken up by the triangular columns and the volume of the hexagonal water hole were calculated from equations 7.17 and 7.13 respectively.

The values for d_s, d_w, w, x, $V_{columns}$ and V_{hole} thus calculated are given in table 7.8, together with the cell parameters calculated from the d-spacings on the basis of a hexagonal unit cell. This table shows that all the structural parameters increase with surfactant chainlength. The distance across a hexagonal hole, x, is smaller than the width of a surfactant rod, w.

In order to be able to compare the theoretical X-ray spectrum of the proposed model, with the experimental one, a much simplified model was build with the molecular modelling program *Cerius2*. To simulate the surfactant layers, a model was built of layers of benzene rings, packed on a hexagonal lattice (see figure 7.16). The benzene rings simulated the hexagonally shaped holes in the surfactant layers as it would be too complicated to built a structure of rods made up of individual surfactant molecules. With *Cerius2* the X-ray diffraction pattern of this structure was simulated. Despite the simplicity of the used model, the predicted diffraction pattern fitted the experimental data remarkably well. By changing the cell parameters of the model, it could be scaled to fit the observed diffraction peaks. An example is shown in figure 7.17, where the cell parameters have been scaled to the ones found for NaP. It can be seen that by using the correctly scaled cell parameters, even the intensities of the peaks of the predicted spectrum compare very well with the intensities for the observed diffraction peaks.

7.5.1.3 The transformation from the second intermediate phase to the lamellar phase

From figures 7.12-7.14 it can be seen that as the sample was heated up through the first intermediate phase and more soap dissolved, a transition took place to a phase that will be called here the second intermediate phase. This phase only seemed to exist over a very narrow concentration range. Initially, as this phase was formed it coexisted with the first intermediate phase and later, as more soap had dissolved,

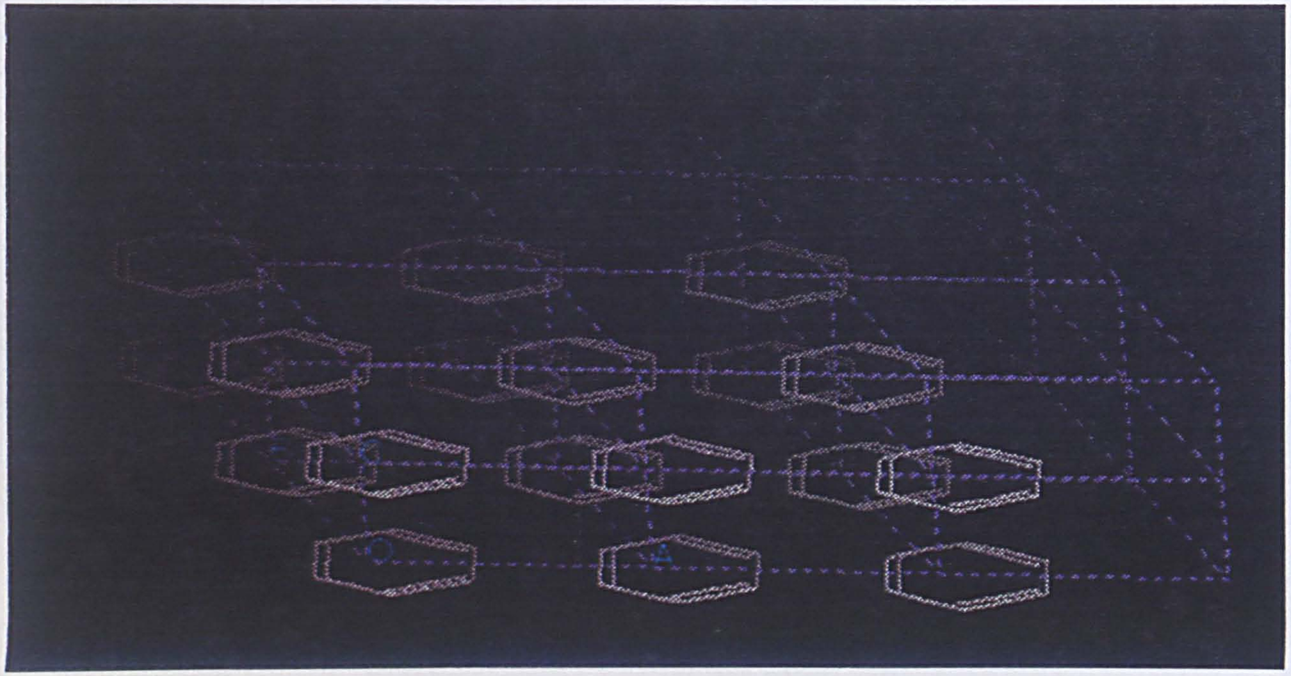

Figure 7.16 Model used for simulating the X–ray diffraction pattern of the hexagonal mesh phase. The hexagonally shaped water holes are simulated by benzene rings packed on a hexagonal lattice

Figure 7.17 Comparison of predicted spectrum for the hexagonal mesh phase with experimental data for a 70% NaP sample

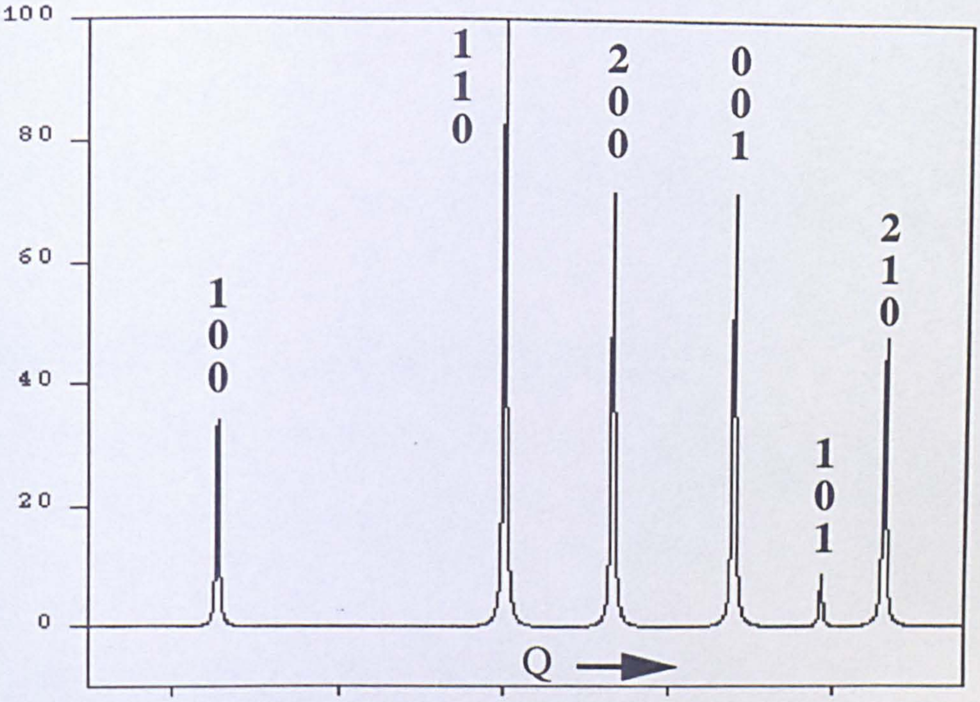

XRD–spectrum predicted with Cerius2

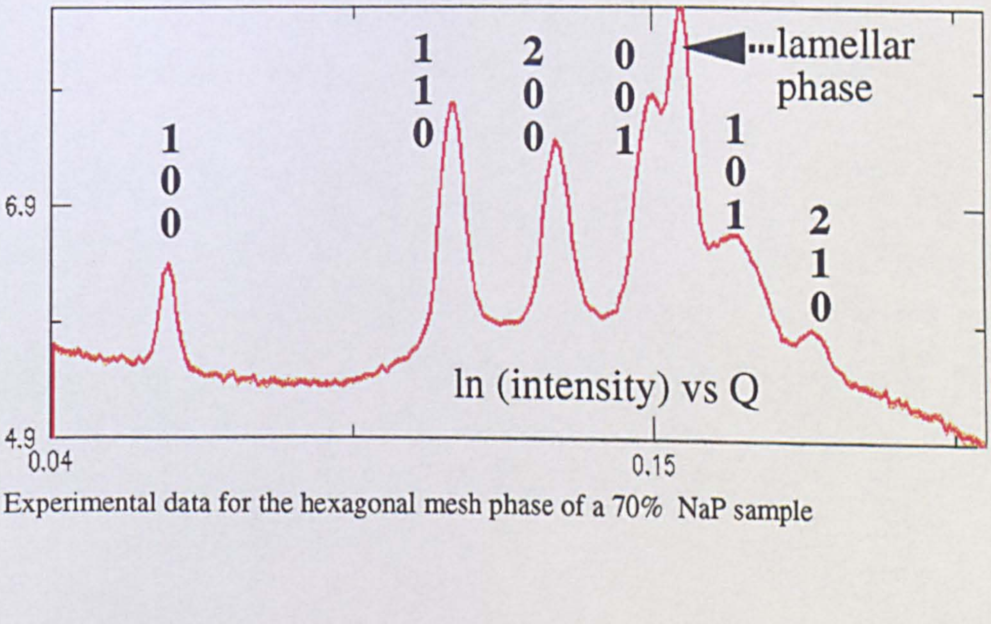

Experimental data for the hexagonal mesh phase of a 70% NaP sample there was a small region in which it coexisted with the lamellar phase. The transition from the first to the second intermediate phase seemed to take place continuously and so did the transition from the second intermediate phase to the lamellar phase. As the exact concentration where the transition occurs from the first to the second intermediate phase is not known, the parameters describing the structure of this phase have been calculated at the point where this phase transforms to the lamellar phase. The assumption is thus made that the concentrations given in literature where the lamellar phase region starts would be where the transition occurs between the second intermediate phase observed here and the lamellar phase. These transition concentrations have been taken from Madelmont and Perron [5-8, 10].

7.5.1.4 The structure of the second intermediate phase

The second intermediate phase for all samples gave rise to two diffraction peaks in the SAXS range covered by the detector, with a d-spacings ratio of 0.76. The fact that this ratio was identical for all the samples, was consistent with same phase being formed for all sample compositions. However, the two peaks could not be indexed for a hexagonal, cubic or lamellar structure. For SDS (a very similar surfactant, see chapter 3) a body-centred tetragonal mesh phase has been observed to exist over a very narrow concentration range as the last intermediate phase to form before the lamellar phase (Kékicheff and Cabane [13]). For SDS this phase showed two strong peaks (the (101) and the (200) peak) that also had a d-spacings ratio of 0.76. A third strong peak was also observed. This third peak was not observed in the data presented here, but would occur at the same position as the (001) peak for the lamellar phase. The peaks for SDS were found using synchrotron radiation and a counting time of 13 hours. Since the counting time used here was only 90 seconds it is not surprising that no other peaks were observed. A body-centred tetragonal mesh structure thus seems a likely structure for the second intermediate phase and the two observed peaks were thus indexed as the (101) and the (200) peak respectively. With this, the cell parameters for all surfactant samples were calculated from the observed peaks using the equation for a tetragonal lattice given in chapter 2. The cell parameters obtained in this way are given in table 7.9.

A model was tested and modified for the second intermediate phase. A tetragonal body-centred mesh phase was modelled based upon a structure consisting of a layered structure of alternating surfactant bilayers and water layers, where each surfactant bilayer is made up of surfactant rods linked together, four at each junction, thus forming square water filled holes (see figure 7.18). As the lattice is body-centred, the holes in a surfactant layer are not lined-up with the holes in adjacent surfactant layers, but alternate in position. The holes in one layer thus coincide in position with junctions of surfactant rods in the adjacent layers. As for the hexagonal mesh phase three equations can be derived, relating the unit cell parameters to the parameters that describe the geometry of this phase. The cell parameter, *a*, is equal to the sum of the width of a surfactant rod, *w*, and the length of the side of a hole, *x* (see figure 7.18):

$$a = w + x \tag{7.19}$$

Since the structure is based on a body-centred lattice there are two whole water holes per unit cell ($(8\times\frac{1}{8})+1=2$) and the c-axis is made up of the thickness of two surfactant and two water layers (see figure 7.18), therefore:

$$c = 2d_s + 2d_w \tag{7.20}$$

Analogue to equation 7.11, a third equation can be derived on the basis of the geometry of the structure and the surfactant volume fraction ϕ_s, relating the cell parameters to the parameters describing the structure:

$$\phi_s = \frac{a^2c - 2V_{water\ layer} - 2V_{hole}}{a^2c} \tag{7.21}$$

where

$$V_{water\ layer} = a^2 d_w \tag{7.22}$$

is the volume of a water layer in the unit cell and

$$V_{hole} = x^2 d_s \tag{7.23}$$

is the volume of water present in one hole in a surfactant layer. Equation 7.21 states that the surfactant volume fraction must be equal to the total volume of the unit cell taken up by surfactant (which is equal to the total volume of the unit cell minus the volume taken up by water) divided by the total volume of the unit cell. As for the

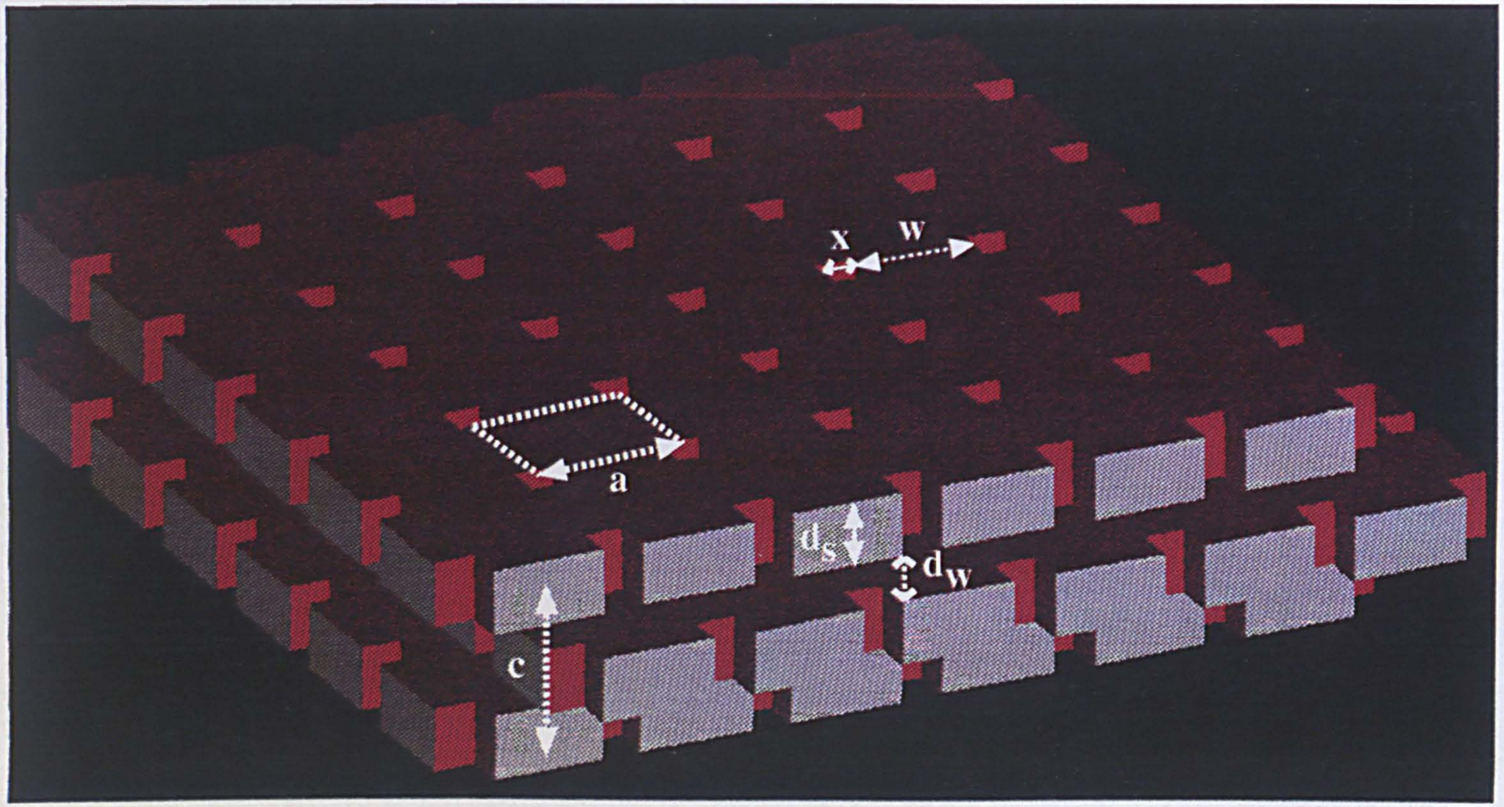

Figure 7.18 The proposed model for the tetragonal mesh phase, consisting of alternating surfactant bilayers and water layers. There are square water holes in the surfactant layers which are ordered on a body–centred tetragonal lattice

hexagonal mesh phase this is a system of three equations (7.19-21) with four unknown parameters (d_s, d_w, w and x) that therefore cannot be solved. Again, in order to eliminate one parameter from the equations, initially the assumption was made that the surfactant rods would have a square cross-section, *i.e.*

$$w=d_s \tag{7.24}$$

Combination of equations 7.19-24 then leads to:

$$2{d_s}^3 - 4{d_s}^2 a + a^2 c\phi_s = 0 \tag{7.25}$$

With this equation d_s can be calculated from the cell parameters and the surfactant volume fraction. However no realistic values for d_s were found this way. As for the hexagonal mesh phase it was not possible to accommodate the amount of surfactant, that was required by the surfactant volume fraction, into a tetragonal mesh structure made up of rods with a square cross-section.

For this reason the model for the tetragonal mesh phase was modified in the following way: in order to fit a larger volume surfactant into the unit cell, the surfactant rods were presumed to have a rectangular cross-section instead of a square one, as was done for the hexagonal mesh phase, so that equation 7.24 is no longer valid. In this way the water holes in the surfactant layers become smaller, thus allowing more surfactant to be fitted into the structure. However, in order to be able to solve equations 7.19-21, one parameter needs to be eliminated. Since equation 7.24 is no longer valid, another simplification had to be made in order to eliminate one parameter from the equations. As for the hexagonal mesh phase, the assumption was therefore made that the thickness of the surfactant layers would be equal to the thickness of the surfactant layers in the lamellar phase (see section 7.5.1.5). Combination of equations 7.19-23 and re-arranging results in:

$$2w^2 d_s - 4wad_s + a^2 c\phi_s = 0 \tag{7.26}$$

Using the calculated cell parameters, the surfactant volume fraction calculated from the transition concentration (from Madelmont and Perron [5-8, 10]) and the values for d_s calculated for the lamellar phase, the value of w was found with this equation (where w is limited by the following constraints: $0<w<a$). The other parameters d_w, x and V_{hole} were subsequently calculated from equations 7.19-20 and 7.23.

These structural parameters thus calculated are given in table 7.9. A comparison between these values and the ones determined for the first intermediate phase, shows that the width of the surfactant rods has remained practically the same, but the size of the water holes has become much smaller than in the first intermediate phase. The thickness of the water layers has decreased as well.

7.5.1.5 The lamellar phase

For all single and mixed surfactant samples the lamellar phase resulted in one strong diffraction ring in the SAXS range covered by the detector. During the formation of the lamellar phase this peak shifted to smaller d-spacing. Since this phase simply consists of alternating surfactant bilayers and water layers, the repeat distance *d* is given by:

$$d = d_s + d_w \tag{7.27}$$

The thickness of the surfactant layer, d_s, is equal to the percentage of the repeat distance *d* given by the surfactant volume fraction (Luzzati [9]):

$$d_s = \phi_s d \tag{7.28}$$

The thickness of the water layers was subsequently calculated from equation (7.27). Values for d_s and d_w calculated in this way are given in table 7.9. These values were calculated using the volume fractions at the lower concentration limit of the lamellar phase region (taken from Madelmont and Perron [5-8, 10]). These values are taken here to correspond to the concentration where the second intermediate phase transforms to the lamellar phase. From table 7.9 it can be seen that d_s increases with chainlength. The values for d_s have been used for the calculations of the structural parameters of the first and second intermediate phases.

7.5.2 Crystallisation from the lamellar liquid crystalline phase

In figures 7.19 and 7.20 some typical examples are shown of the changes that occurred in the integrated SAXS patterns, caused by phase transformations taking place during crystallisation of soap from the lamellar phase (70% surfactant samples). From this it is clear that not all the solid material in the coagel was crystallised from the lamellar liquid crystalline phase. Instead, the reverse processes

surfactant	**transition concentration**		**tetragonal mesh phase**						**lamellar phase**	
	wt%	ϕ_s	a	c	d_w	w	x	V_{hole} x10^3Å^3	d_s	d_w
NaL	0.59	0.79	68.02	57.56	4.34	50.06	17.96	7.883	24.44	6.63
NaM	0.59	0.78	78.06	67.55	6.53	63.83	14.23	5.518	27.25	7.85
NaP	0.56	0.73	88.50	77.21	10.05	78.31	10.19	2.966	28.56	10.71
NaL:NaM=										
3:1	0.59	0.78	71.80	62.73	5.99	58.16	13.64	4.722	25.38	7.01
1:1	0.59	0.78	74.80	64.18	6.38	62.64	12.16	3.802	25.71	7.19
1:3	0.59	0.78	no	data					27.39	7.73
NaL:NaP=										
3:1	0.58	0.77	72.02	62.58	6.15	57.32	14.70	5.433	25.14	7.58
1:1	0.58	0.76	no	data					25.81	8.15
1:3	0.57	0.75	82.42	71.34	8.76	76.11	6.31	1.072	26.91	9.20
NaM:NaP										
3:1	0.58	0.76	79.54	69.56	7.64	66.70	12.84	4.475	27.14	8.56
1:1	0.58	0.76	82.78	71.64	8.44	76.52	6.26	1.073	27.38	8.73
1:3	0.57	0.74	85.72	74.20	9.18	74.65	11.07	3.422	27.92	9.70

Table 7.9 Transition between tetragonal mesh phase and lamellar phase, all distances are in Å (transition concentrations in weight % from Madelmont and Perron [5-8, 10]). The thickness of the surfactant layers was taken to be the same as in the lamellar phase

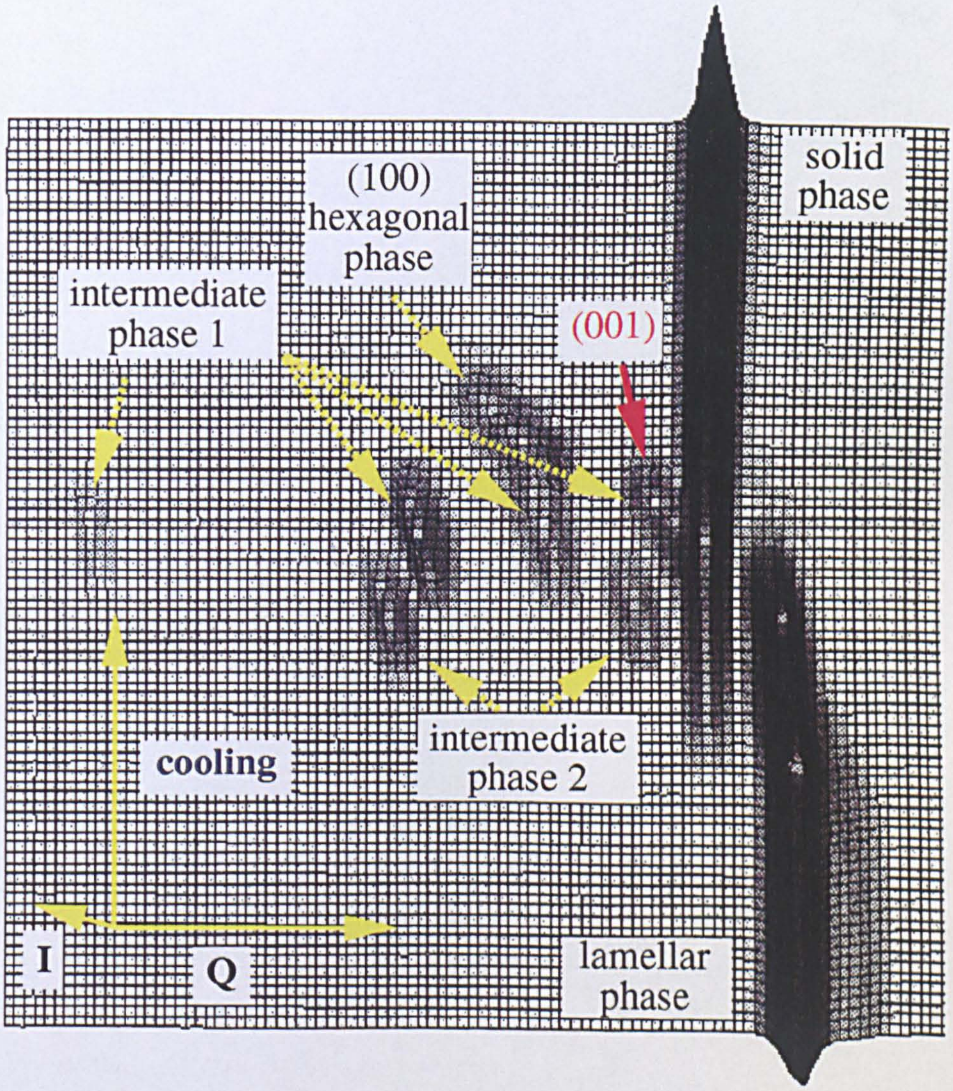

Figure 7.19 Changes in the integrated SAXS patterns, caused by the phase transformations occurring during crystallisation from the lamellar liquid crystalline phase for a 70% NaP sample. In this case the (001) peak for the first intermediate phase is clearly visible, which demonstrates this phase to be periodic in three dimensions

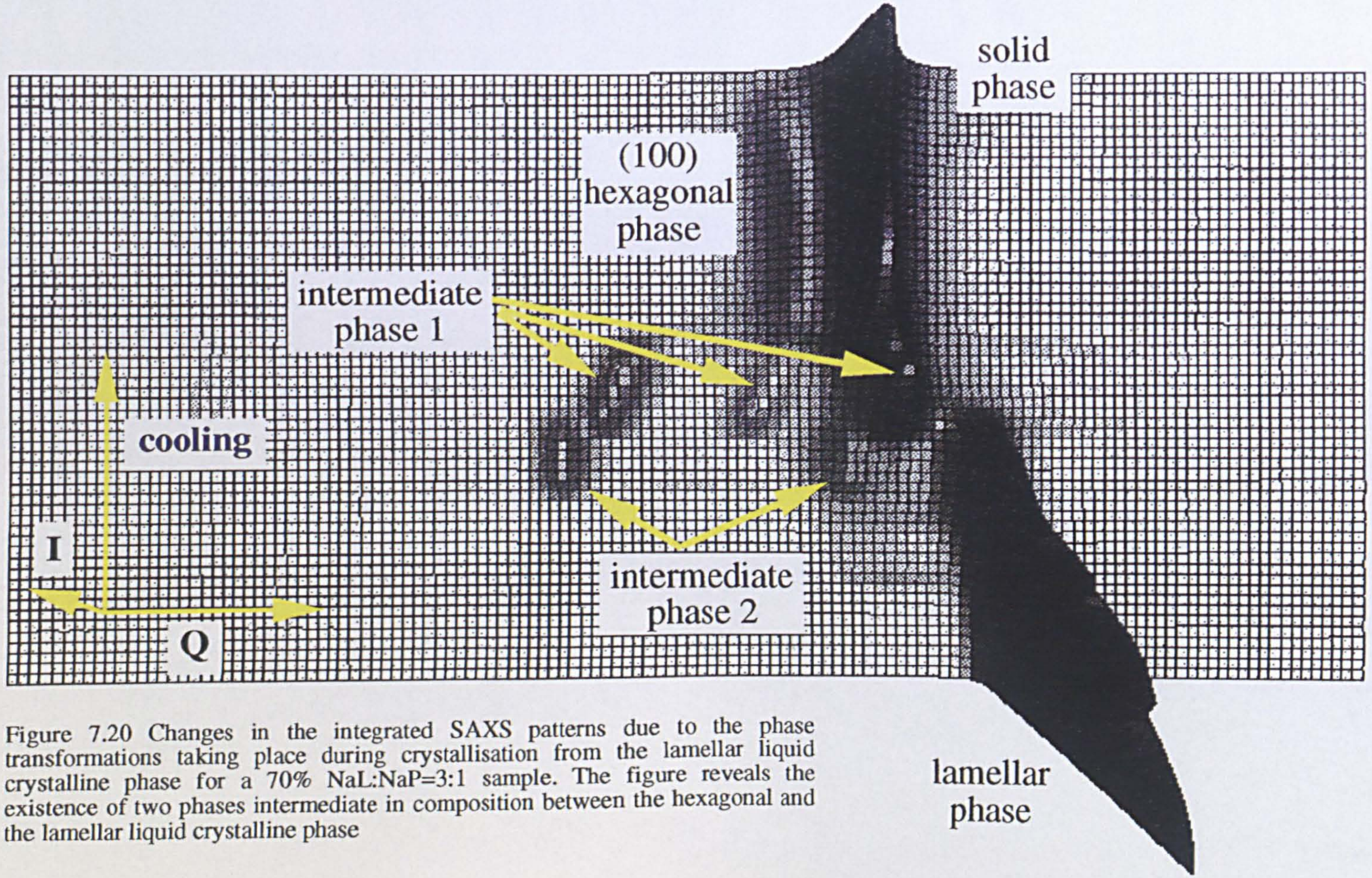

Figure 7.20 Changes in the integrated SAXS patterns due to the phase transformations taking place during crystallisation from the lamellar liquid crystalline phase for a 70% NaL:NaP=3:1 sample. The figure reveals the existence of two phases intermediate in composition between the hexagonal and the lamellar liquid crystalline phase

occurred that took place during dissolution of the sample whilst heating. On cooling the sample from the lamellar liquid crystalline phase, some surfactant started to crystallise; because of this the aqueous region of the sample was effectively diluted so that the second intermediate phase (the tetragonal mesh phase) was formed. For all samples studied this phase was longer present during the cooling process than during the heating process. For some samples this phase was not observed at all during heating, only during cooling.

On cooling through the tetragonal mesh phase, more surfactant crystallised, further depleting the aqueous regions of the sample, thus causing the system to shift further through the phase diagram. In total this led to the following phase sequence: the lamellar phase, the second intermediate phase (thought to be a body-centred tetragonal mesh phase), the first intermediate phase (thought to be a hexagonal mesh phase), the normal hexagonal phase and finally the isotropic micellar phase, until at the end of the experiment all surfactant had crystallised.

7.6 Texture revealing epitaxial growth

In some cases texture in the diffraction rings was observed, due to preferred orientation of the soap particles inside the capillaries. For those samples it was found that all ordered phases showed preferred orientation and that the texture in the diffraction rings of all these phases was related in a specific way. An example is shown in figure 7.21. A 70% NaM:NaP=1:3 sample for which the solid phase showed preferred orientation has been transformed by heating to the lamellar liquid crystalline phase. In figure 7.21a the diffraction ring for the lamellar liquid crystalline phase can be seen to exhibit two brighter arcs. During cooling of this phase some soap started to crystallise. Figure 7.21b reveals the diffraction ring for the solid phase to show the same orientation as the lamellar phase. Due to the crystallisation of soap, the sample becomes diluted so that a phase boundary is crossed and the tetragonal mesh phase is formed. The (101) ring of this phase shows four regions of higher intensity, which form the corners of a rectangle (figure 7.21c). As more soap crystallised, the system shifted further through the phase diagram so that the hexagonal mesh phase was formed. The (*h*00) and (*hk*0) diffraction rings for this phase can clearly be seen to show the exact opposite orientation of the ring for the solid phase (figure 7.21d). When after the hexagonal mesh phase the normal hexagonal phase formed, the (100) ring for this phase exhibited the same orientation as the ring for the solid phase (figure 7.21e), as had been observed for the 40% soap samples (see figure 7.8). When all soap was crystallised, the diffraction ring for the solid phase showed texture which was identical to the texture of the lamellar liquid crystalline phase it was crystallised from. This reveals that the orientation of the lamellar liquid crystalline phase has been passed on through all the other phases to the solid phase. For the cases in which preferred orientation was present in a sample, the orientation effects in the diffraction rings were always totally reversible on repeated cooling and heating of the sample. These effects indicate epitaxial growth between all the ordered phases. That this is the case and that the orientation of each phase was not induced by the geometry of the capillary can be seen from a comparison between figures 7.21d and 7.22. By coincidence the crystallites in the 70% NaL:NaP=1:3 sample happened to be orientated the exact opposite way as the sample shown in figure 7.21. Although the diffraction rings are therefore orientated the opposite way round as in figure 7.21, the orientation of the diffraction rings for the different phases relative to each other has remained identical. The ring for the solid phase shows the same orientation as the one for the lamellar phase, the orientation in the (*h*00) and (*hk*0) rings for the hexagonal mesh phase are oriented exactly opposite to this and the (101) ring for the tetragonal mesh phase shows again shows four brighter arcs. In addition figure 7.22 shows that the (001) ring for the hexagonal mesh phase has the same orientation as the diffraction ring for the lamellar phase and the one for the solid phase. By comparing figure 7.21 and 7.22 it is thus clear that the orientation in the samples is indeed passed on from one phase to the next and is not induced by the confinement of the capillary. The texture effects have thus revealed epitaxial relations to exist between the solid state and all liquid crystalline phases. These are explained in detail in the discussion section 7.10.3.2.

On station X12B at Brookhaven National Laboratory all experiments were carried out using the X-ray cell where the sample was held inside a capillary (see chapter 4).

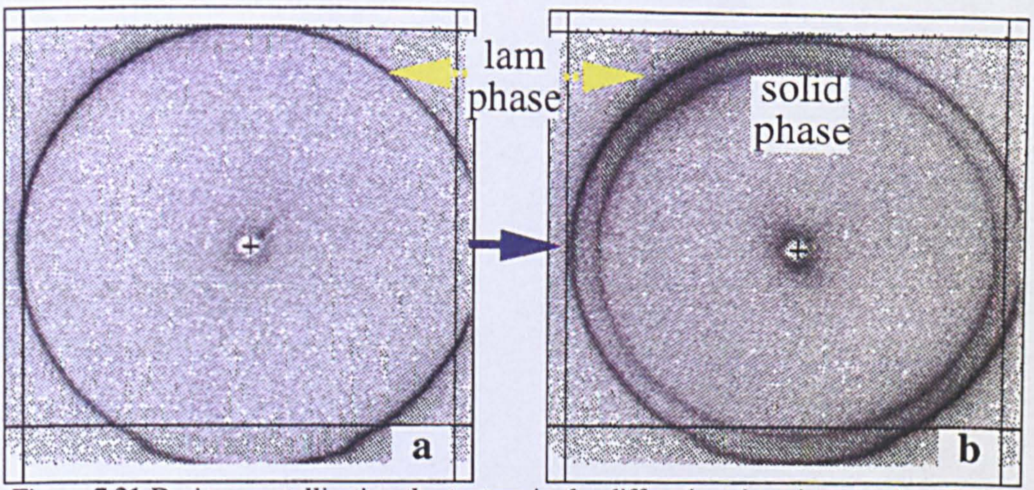

Figure 7.21 During crystallisation the texture in the diffraction rings is passed on from one phase to the next, demonstrating epitaxial relations between all ordered phases (liquid crystalline and solid state), see text for further explanation. The X–ray patterns shown are for a 70% NaM:NaP=1:3 sample

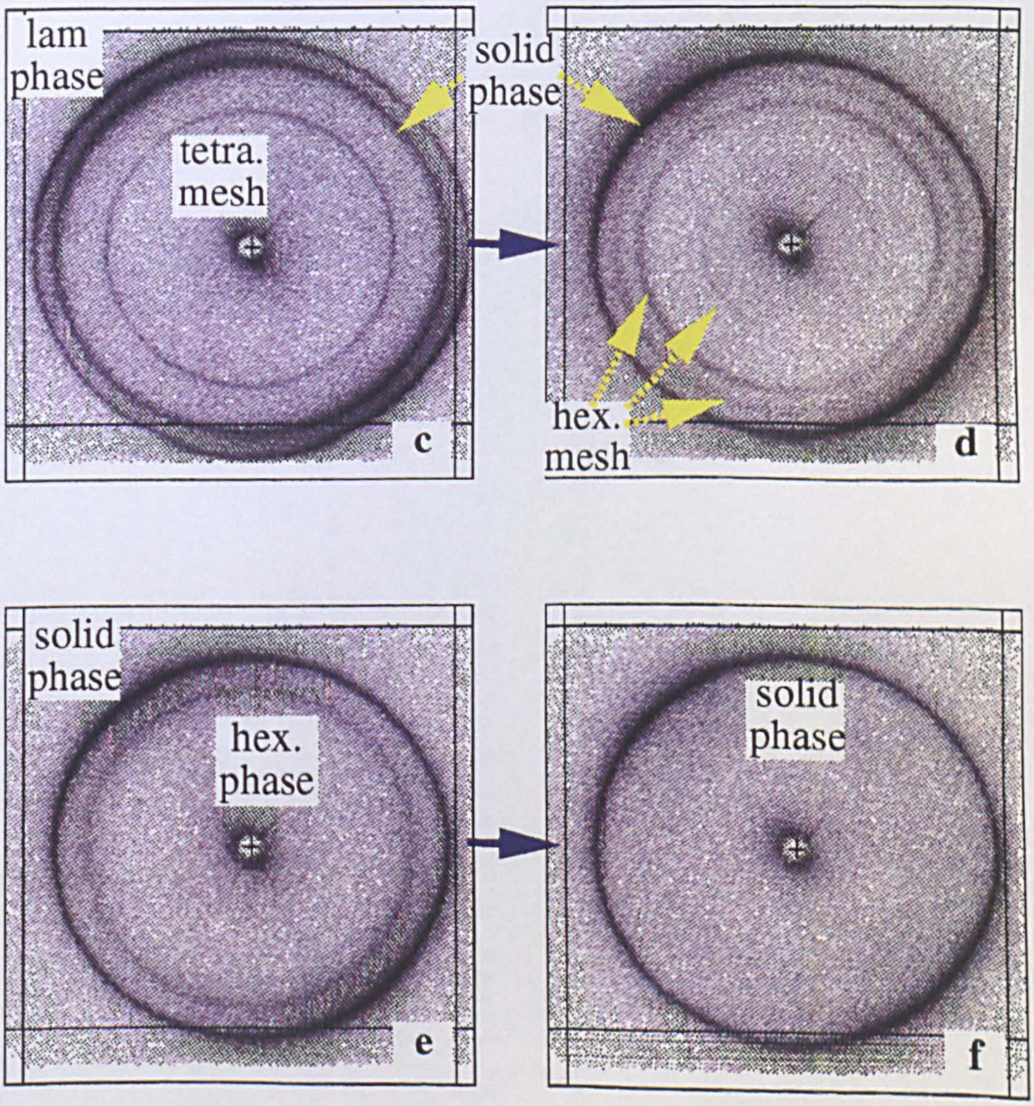

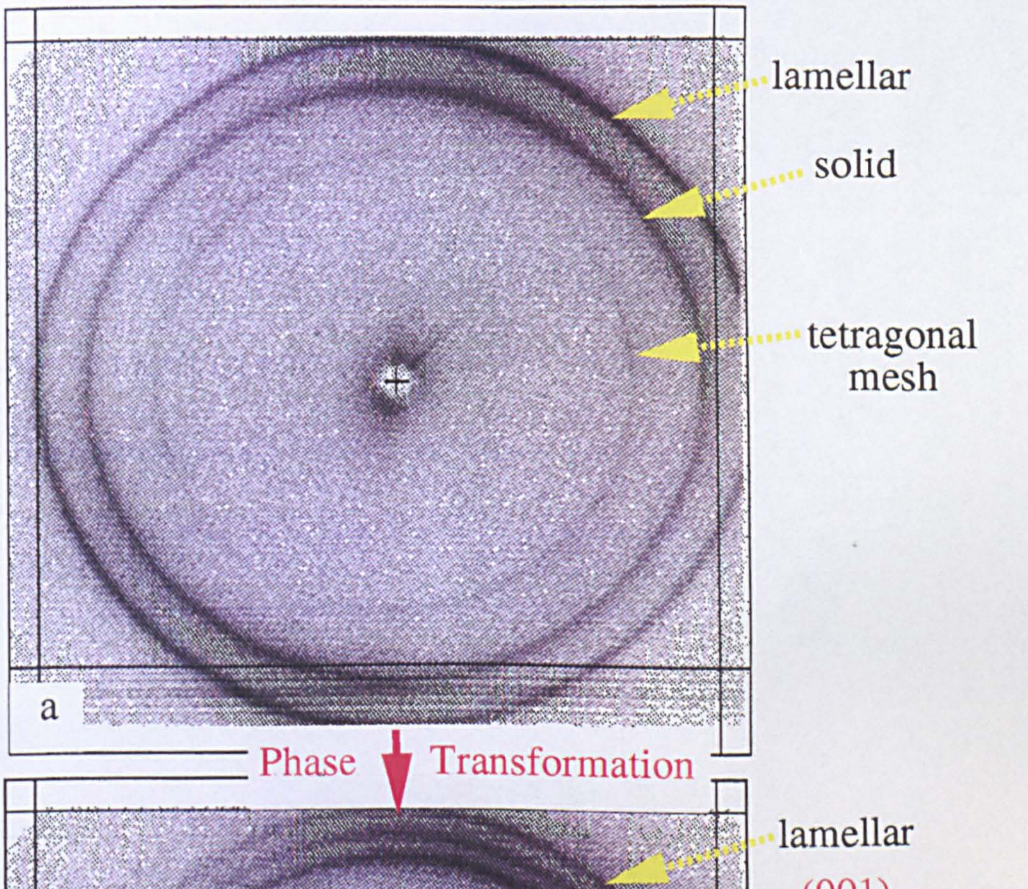

Figure 7.22 Transformation from the tetragonal mesh phase to the hexagonal mesh phase for a 70% NaL:NaP=1:3 sample. In (b) the (001) ring for the hexagonal mesh phase can clearly be seen to have the opposite orientation of the (*h*00) and (*hk*0) rings. The four regions of higher intensity from the tetragonal phase can still be seen in the bottom figure on the inside of the (110) ring for the hexagonal mesh phase

Instead of using this cell, on station 16.1 at Daresbury Laboratory the X-ray cell with the mica windows (see chapter 4) was used. With this cell a diffraction pattern was recorded of the hexagonal mesh phase of a NaM sample. This diffraction pattern shows six-fold symmetry in the (*h*00) and the (*hk*0) rings and a weak (001) ring, see figure 7.23. In this X-ray cell the surfactant layers of the hexagonal mesh phase would be expected to orient themselves parallel to the mica windows. The water holes (and the c-axis of this structure) are thus perpendicular to the windows, so that six fold symmetry would be expected in the (*h*00) and the (*hk*0) rings. The observed diffraction pattern is therefore consistent with the proposed model for the hexagonal mesh phase. A comparison of the two fold symmetry in the (*h*00) and the (*hk*0) diffraction rings for this phase when the X-ray cell with the capillaries was used and the six fold symmetry observed for the same phase when the X-ray cell with the mica windows was used, shows that it is possible to induce orientation of the sample by confinement between two parallel container walls.

7.7 Crash cool experiments

T-jump experiments were carried out by connecting the X-ray cell (where the sample is held inside a capillary) to the arrangement of valves described in chapter 4, in order to study the influence of cooling rate on the phase transformations taking place during crystallisation from the lamellar liquid crystalline phase. With this set-up it was possible to cool the samples from 80°C to 20°C in approximately 1 minute. An example of such an experiment is shown in figure 7.24. After crash cooling the samples they were "crash heated" by switching over the valves, so that the processes occurring during rapid dissolution could be investigated. The following 70% soap samples were studied: NaP, NaL:NaP=1:3, NaM:NaP=1:3. On crash cooling the samples, the tetragonal mesh phase was observed in almost all cases. The hexagonal mesh phase was only observed in some cases and the normal hexagonal phase was not observed at all during crash cooling. However, this phase was observed some times on "crash heating". The hexagonal mesh phase was observed on all cases during crash heating, in contrast to the tetragonal mesh phase, which was never observed. These effects are explained in the discussion (section 7.10.3.4).

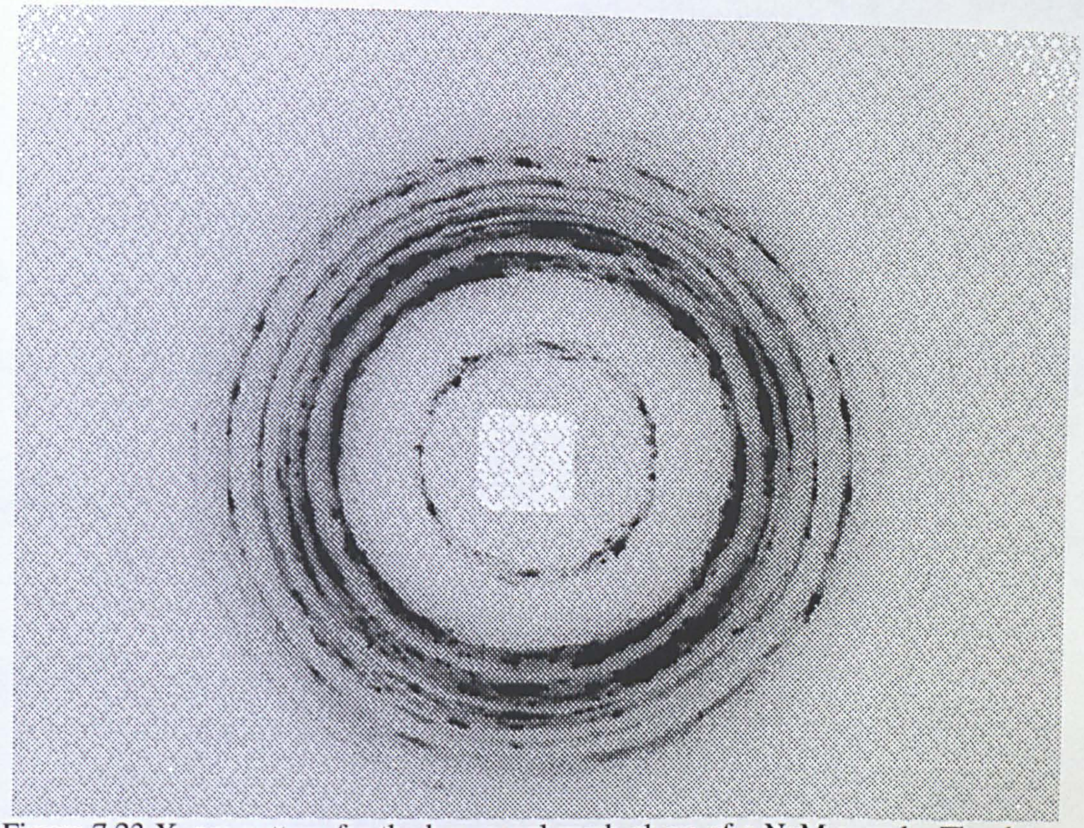

Figure 7.23 X–ray pattern for the hexagonal mesh phase of a NaM sample. The data were collected with an image plate at Daresbury Laboratory. Six fold symmetry can be seen in the (*h*00) and (*hk*0) diffraction rings. The bottom figure shows the integrated pattern

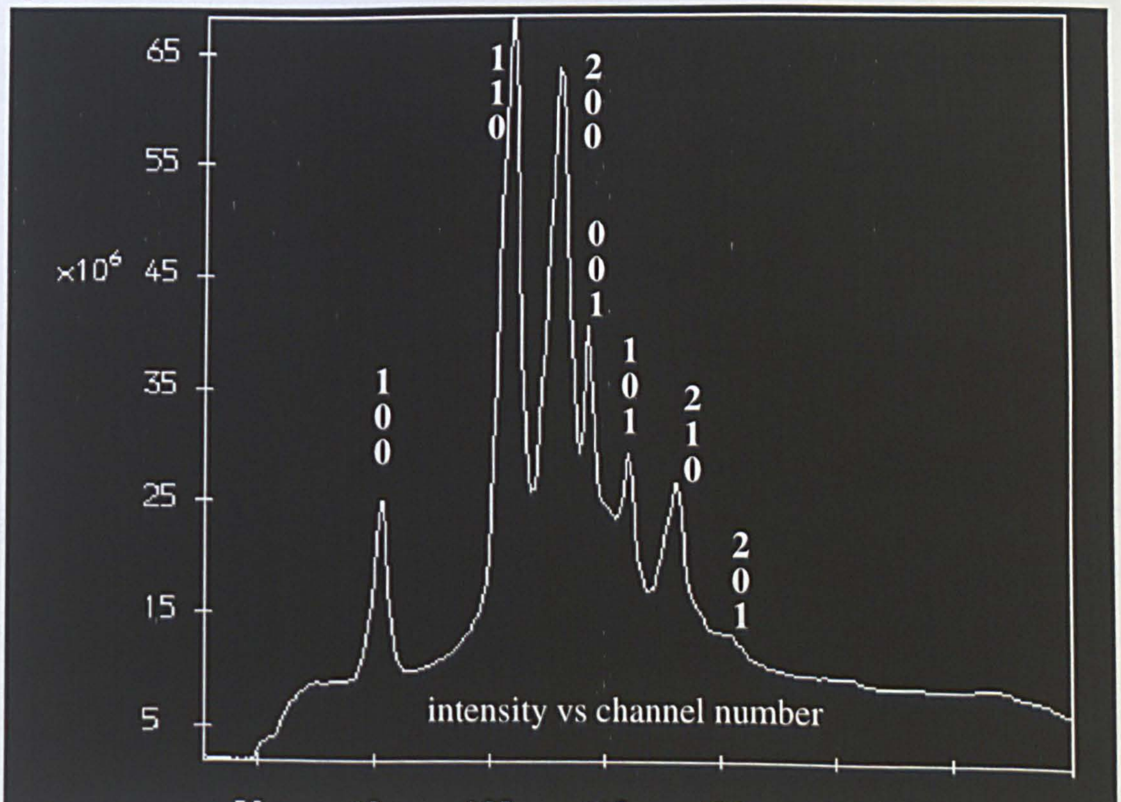

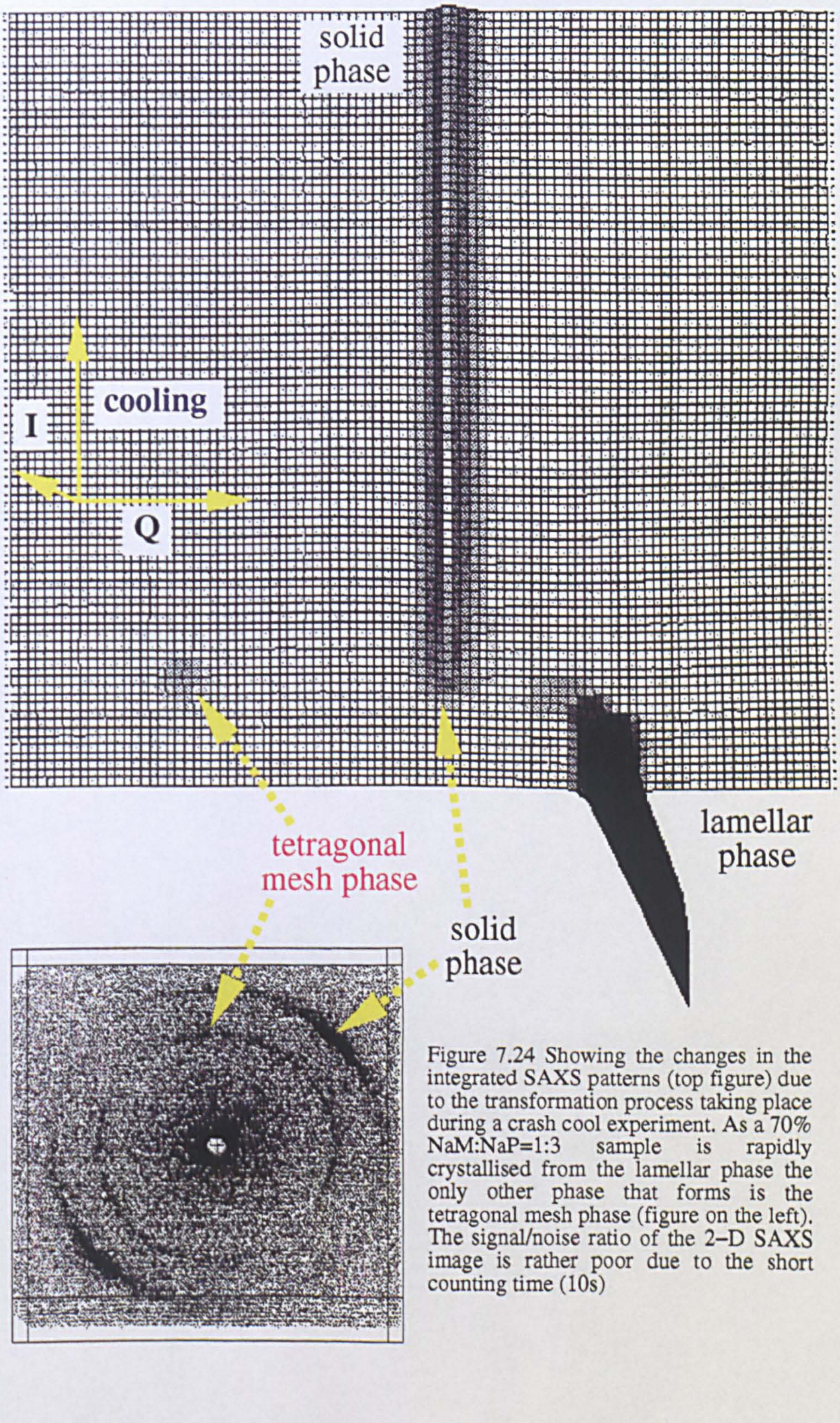

Figure 7.24 Showing the changes in the integrated SAXS patterns (top figure) due to the transformation process taking place during a crash cool experiment. As a 70% NaM:NaP=1:3 sample is rapidly crystallised from the lamellar phase the only other phase that forms is the tetragonal mesh phase (figure on the left). The signal/noise ratio of the 2–D SAXS image is rather poor due to the short counting time (10s)

7.8 Samples exhibiting additional phases

Apart from the phases that have been discussed so far, two other phases have been observed. One of these phases formed in between the hexagonal mesh phase and the normal hexagonal phase. This phase gave rise to one to two peaks in the angular range covered by the detector, some examples are shown in figures 7.25 and 7.26. Sometimes for this phase only one peak was seen because the second one coincided with the peak for the solid phase. In those cases the intensity of the peak for the solid phase could be seen to increase as is shown in figure 7.25. The peak that did not coincide with the peak for the solid phase exhibited the same orientation effects as the normal hexagonal phase. Based on a comparison with other surfactant systems (see chapter 3) the most likely structure for a phase at this position in the phase diagram, would be a deformed hexagonal phase, *i.e.* the cross-section of the cylinders in the hexagonal phase has deformed to become probably elliptical and the packing of the cylinders has changed to a different lattice type. The specific lattice for this could not be determined from the two observed peaks.

Another phase that was observed for some samples gave rise to a weak diffuse peak at low angle (in the range of 65-80Å), see figure 7.27. Literature on other surfactant systems (see chapter 3) indicates that this peak could be caused by a defected lamellar phase, *i.e.* a lamellar phase with water holes at irregular positions in the surfactant layers. However, in some cases the diffuse peak was also observed at room temperature, when all soap was in the solid phase. Whether the peak had been present at high temperature (in conjunction with the peak for the lamellar phase) or at room temperature (in conjunction with the peak for the solid phase), the diffuse peak always disappeared when the sample passed through the intermediate phases either on cooling or on heating.

Table 7.10 shows an overview of the samples that formed a phase additional to the ones that have been discussed in the previous sections. This table shows that the deformed hexagonal phase was not formed by single surfactants, only by mixtures of NaL-NaM and mixtures of NaM-NaP. The NaL-NaP mixtures did not form this

Figure 7.25 The figure reveals the existence of a phase in between the normal hexagonal phase and the hexagonal mesh phase, during dissolution of a 70% NaM:NaP=3:1 sample. Before disappearing the peak for the solid phase can be seen to increase twice in intensity. The first time is due to coincidence with a peak for what is thought to be a deformed hexagonal phase. The second increase is caused by coincidence with the (001) peak for the first intermediate phase

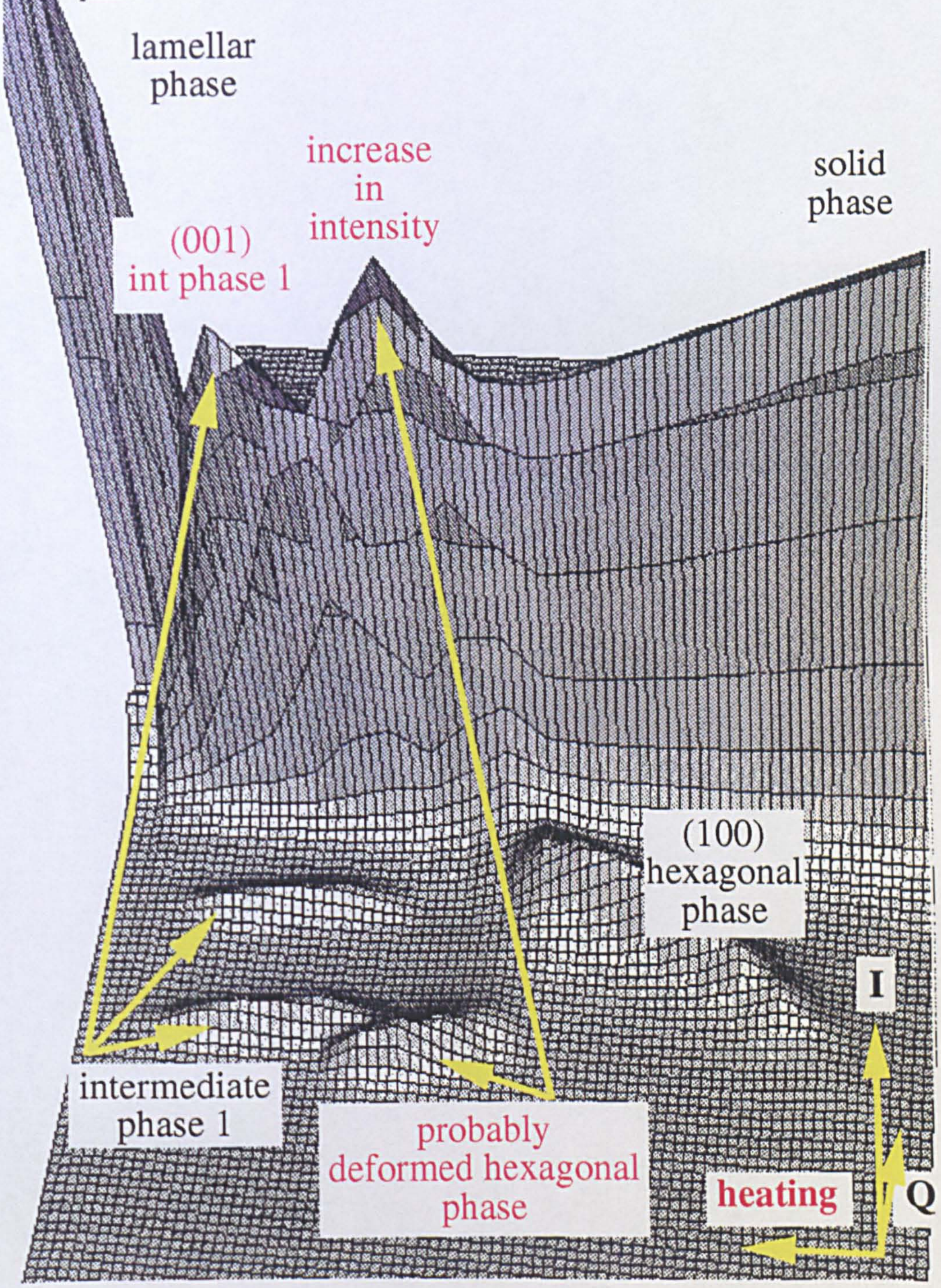

Figure 7.26 Showing the processes that take place on cooling the same sample as in the previous figure. It can be seen that the tetragonal mesh phase is formed on cooling, which was not the case during heating (compare with previous figure).

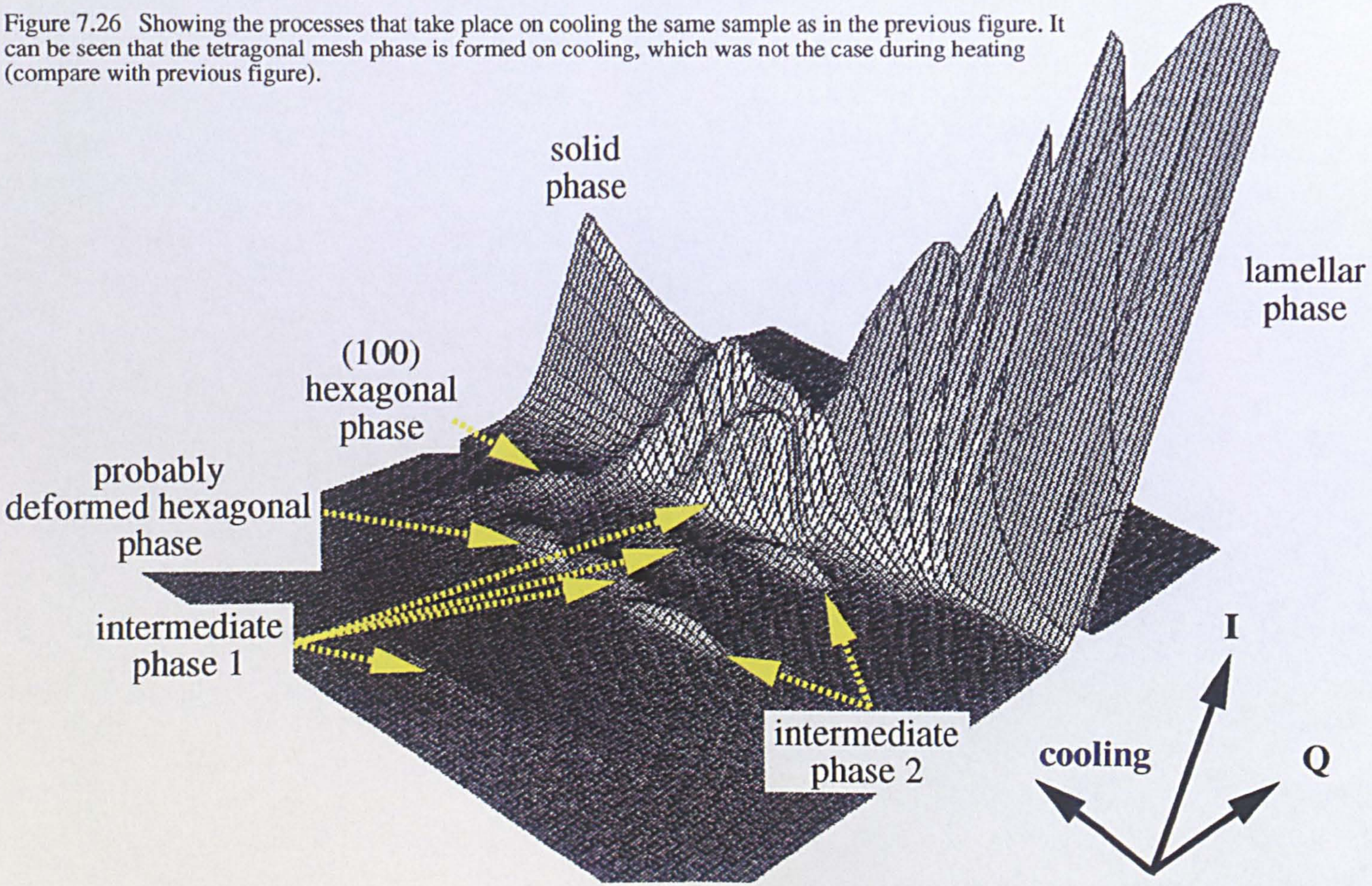

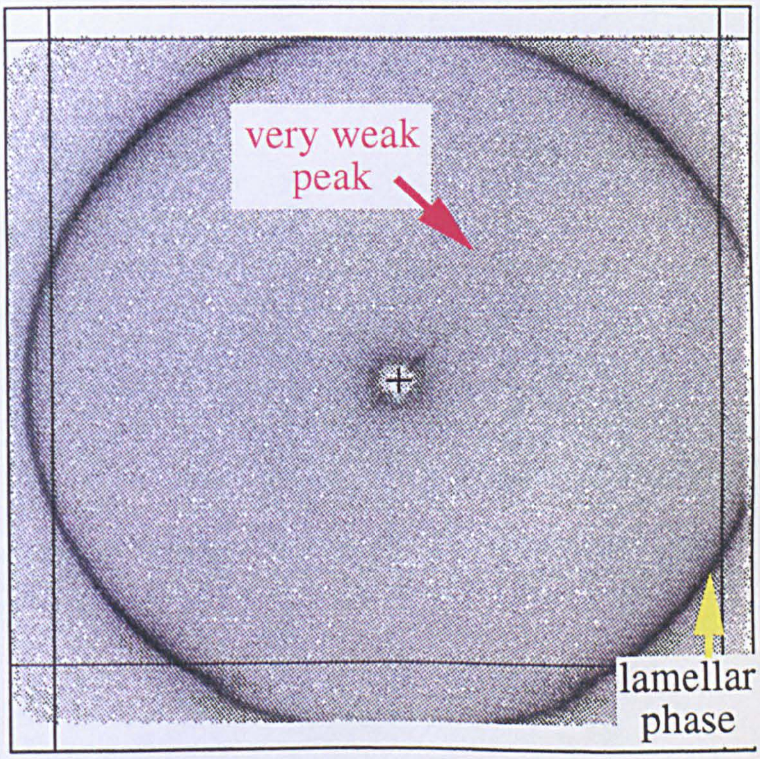
very weak peak
lamellar phase

Figure 7.27 Diffraction pattern for a 70% NaM:NaP=3:1 sample. A very weak diffraction ring appears close to the beam centre during cooling from the lamellar liquid crystalline phase

phase. The diffuse peak at low angle was also only observed for mixed surfactant systems.

sample	**diffuse peak at low angle**	**deformed hexagonal**
NaL	no	no
NaM	no	no
NaP	no	no
NaL:NaM=		
3:1	yes	yes
1:1	yes	only on cooling
1:3	yes	no
NaL:NaP=		
3:1	yes	no
1:1	no	no
1:3	no	no
NaM:NaP		
3:1	yes	yes
1:1	no	yes
1:3	no	yes

Table 7.24 Samples that exhibited additional phases

7.9 Micellar behaviour of samples containing ethanol

At elevated temperatures different scattering characteristics were observed for the surfactant samples containing ethanol from the surfactant samples for which the solvent was pure water. For the samples for which the solvent was an ethanol-water mixture a very weak diffuse peak appeared when all the soap had dissolved, see figures 7.28 and 7.29. The difference however between this peak and the diffuse peak observed for the isotropic micellar solutions was that this peak occurred at much smaller d-spacing. It was found that the d-spacing was dependent on the amount of ethanol in the sample: the more ethanol the smaller the d-spacing, see table 7.11. For the sample of which the solvent contained 80wt% ethanol this diffuse peak was extremely weak. The sample of which the solvent solely consisted of ethanol did not exhibit this peak at all.

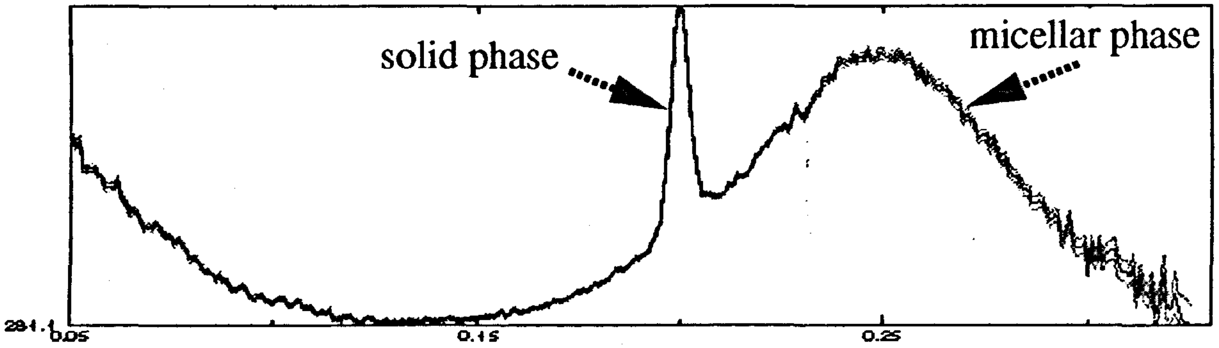

Figure 7.28 As a 30% NaL sample of which the solvent contains 60% ethanol is heated, the solid dissolves and micelles are formed. The broad peak for the micellar phase is at a smaller d–spacing than it would have been if the sample had not contained any ethanol

Figure 7.29 .Crystallisation of a 30% NaL sample from an ethanol–water mixture (solvent containing 10% ethanol and 90% water). A diffuse diffraction ring is observed when all soap is dissolved (inset).

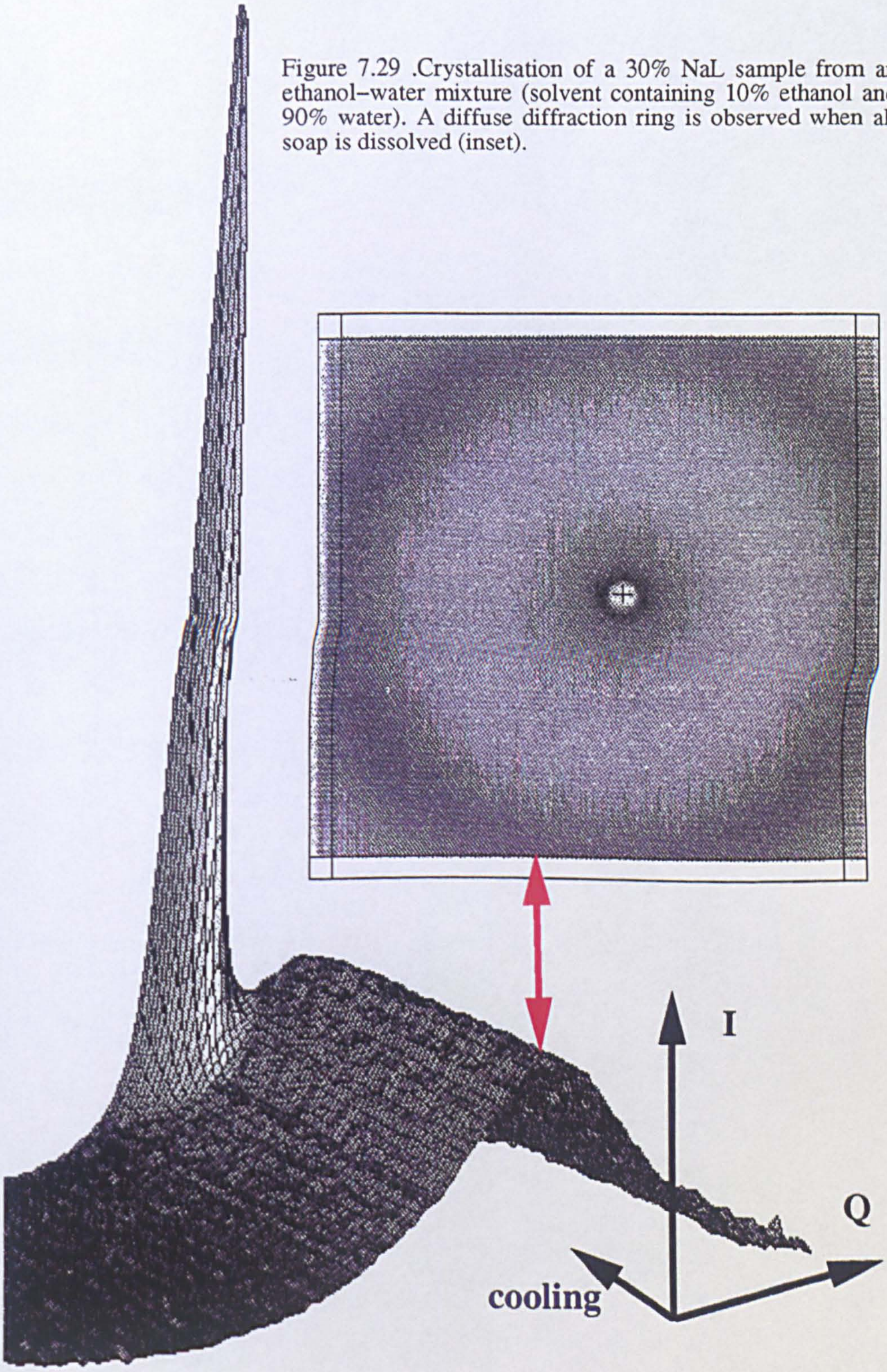

NaL	% ethanol in solvent	% water in solvent	observed d-spacings
30%	10	90	26.4-27.7
30%	60	40	24.8-25.0
30%	70	30	23.7-24.2
20%	80	20	23.0-23.8
10%	100	0	-

Table 7.11 The d-spacings for diffuse ring that appeared when all solid was dissolved

7.10 Discussion

In the previous sections results have been presented on the processes taking place during dissolution and crystallisation of single and mixed surfactant systems. In this section the main points of these results are discussed in more detail.

7.10.1 Coagels

7.10.1.1 Single surfactant coagels

All single surfactant coagels crystallised from water showed one diffraction peak in the range covered by the SAXS 2-D detector. It was found that these observed d-spacings increased linearly with chainlength. This observed linear relationship between chainlength and d-spacing indicates that all the studied single sodium soaps have similar structures. With this relation the angle of tilt of the molecules in the unit cell was calculated to be approximately 83°. This is very different from the angle of tilt for the B form of KP (a very similar surfactant) for which the tilt angle is 52° (Dumbleton and Lomer [3]). The B form is anhydrous though which could contribute to the difference in tilt angle with the sodium soaps. The large angle of tilt for the sodium soaps indicates a close structural resemblance with their structures and that of a lamellar liquid crystalline phase.

7.10.1.2 Mixed surfactant coagels

The diffraction patterns of all mixed coagel systems studied here, all showed only one peak. This provided no evidence for phase separation between the individual homologues, implying that all systems formed solid solutions. This was not previously known. No SAXS data was found that could be directly correlated to the effect observed during the nucleation experiments, where the turbidity increased and decreased in a two step process (see chapter 6). The same samples were used as during the nucleation experiments and since they were subjected to the same cooling and heating cycles as during the nucleation experiments, the only experimental condition that was different was the degree of agitation. During the nucleation experiments the samples were continuously stirred, during the *in-situ* X-ray diffraction experiments the samples were stagnant. The results thus seem to indicate that at a sufficiently high stirring rate, segregation occurs of the two surfactants in the mixture. This is not fully unexpected since the growth rate of the particles is slow. Therefore if the sample is stagnant de-solvation of the molecules is hard and growth may be diffusion limited. However, when the sample is stirred this will make desolvation easier so that the growth process might become surface integration controlled. In the latter case the purifying nature of the crystallisation process will be more efficient, causing rejection of the impurities (the other homologues) at the surface of the growing crystalline particles, so that phase separation occurs.

It was found that all observed d-spacings for the mixtures are larger than the calculated spacings based on weighted averages of the observed d-spacings for the single surfactant coagels. The mixtures where the difference in chainlength was two CH_2 groups (the NaL-NaM and NaM-NaP mixtures) all show the same linear correlation between average chainlength and d-spacing. These d-spacings are larger than the calculated spacings based on weighted averages of the observed d-spacings for the single surfactant systems. An exception to this was the NaM:NaP=3:1 mixture. The observed d-spacing for this sample *did* seem to fit in with the trend between chainlength and observed d-spacing for the single surfactant samples. This might be caused by experimental uncertainty. However, it could also be an indication that the structure of the NaM:NaP=3:1 sample is different from the structures of the

NaL-NaM and the other NaM-NaP mixtures. It is remarkable in this respect that the NaM:NaP=3:1 sample was the only mixture with a chainlength difference of two CH_2 groups that *did* exhibit phase separation during the nucleation experiments (see chapter 6). It is possible that at this ratio of NaM and NaP a denser solid solution can be formed than at other compositions. This solid solution may then be more difficult to nucleate than the ones that are less efficiently packed, which could lead to phase separation in the stirred samples during the nucleation experiments.

The NaL-NaP mixtures, where the chainlength difference is four CH_2 groups, show even larger d-spacings than the NaL-NaM and the NaM-NaP mixtures, where this difference is two CH_2 groups. This means that the surfactant molecules are less efficiently packed together in a mixed structure than when there is only one chainlength present (apart from the NaM:NaP=3:1 sample). In addition, it shows that in general the larger the difference in chainlength of the two surfactants in the mixture, the less efficient the molecules can be packed together. It also means that the crystal lattice of a single surfactant sample is likely to become distorted by the presence of low concentrations of surfactants with a different chainlength. This demonstrates the need for high purity material for structure determination and for surfactant products which demand high lattice perfection.

7.10.1.3 Solid soap crystallised from ethanol-water mixtures

The cooling rate used during crystallisation was found not to affect the d-spacing for the solid soap. Different diffraction characteristics for solid soap were found however for two of the samples crystallised from ethanol-water mixtures. Of the samples studied these were the ones containing most ethanol: one contained no added water (since ethanol is hygroscopic it always contains some water), for the other the solvent consisted of 80% ethanol and 20% water. The latter sample showed only one diffraction ring before heating and three diffraction rings after it had been re-crystallised by heating and subsequent cooling. This indicates that the sample had changed at room temperature over a period of time. After this re-crystallisation it showed the same diffraction characteristics as the sample crystallised from ethanol without added water. It is possible that from the ethanol-water mixtures above a certain ethanol concentration an anhydrous form is crystallised instead of a hydrate. The change in the diffraction pattern of the sample of which the solvent consisted of 80% ethanol and 20% water may then be caused by a slow hydration of the sample. This could be the cause of some of the inconsistencies in surfactant literature discussed in chapter 3 (*e.g.* Ferguson [14]).

7.10.2 The 20 and 40wt% surfactant samples

7.10.2.1 The isotropic micellar phase

The shift in the peaks to a smaller d-spacing on heating for the isotropic micellar solution and the hexagonal phase can be explained by the fact that as the sample is heated up more soap dissolves, so that the solution becomes more concentrated. Therefore there will be more spherical micelles, respectively surfactant cylinders, that are thus coming closer together. This also explains the reverse process, the shift of these peaks to larger d-spacing on cooling: as the sample is cooled some soap starts to crystallise, thus depleting the solution. Because of this, the surfactant cylinders or spherical micelles become further apart, resulting in a larger d-spacing.

At the transition between the isotropic micellar solution and the hexagonal liquid crystalline phase the (100) peak for the hexagonal phase for all the samples appeared at a smaller d-spacing than the one for the micellar solution. This is in contradiction with Reiss-Husson and Luzzati [4], who found that for sodium soaps the (100) peak for the hexagonal phase coincided with the centre of the peak for the isotropic micellar phase. The results presented here however, indicate that the spheres which are closest together first transform into cylinders. The number of molecules in the micelles was calculated at the transition from the isotropic micellar phase to the hexagonal phase. These calculations were based on the assumption that the micelles remained spherical until the creation of the hexagonal phase and show that the number of molecules per micelle increases with chainlength.

7.10.2.2 The hexagonal phase

The results indicate that there is an increase in the diameter of the surfactant cylinders making up the hexagonal as the sample is heated up through the hexagonal phase and thus more soap dissolves. Luzzati *et al.* [15] however found that the diameter of the cylinders is independent of the surfactant concentration. Although all calculations presented here are based on transition concentrations taken from literature where it is stated that those values may not be accurate, it is unlikely that the diameter of the cylinders would remain constant as the system becomes more concentrated. This can be understood in the following way: as the soap concentration increases, the distance between the surfactant cylinders becomes smaller, therefore the sodium ions approach the head groups closer than at lower concentration. This causes a reduction in the repulsion between the head groups, thus allowing for a smaller curvature of the surfactant-water interface. Effectively this means that the diameter of the cylinders increases.

7.10.3 The transformation process between the lamellar and the solid phase

The transformation process between the hexagonal and lamellar liquid crystalline phase has been elucidated for the surfactant systems studied. For most samples two phases were found to exist, intermediate in composition between the hexagonal and the lamellar liquid crystalline phase. These intermediate phases did not only form for single surfactants but were also observed for all the mixed systems studied, *i.e.* this represents a generic process for surfactant crystallisation from the lamellar liquid crystalline phase. No data on intermediate phases for mixed surfactant systems have been published before. These phases are very difficult to study as they only occur over very narrow concentration ranges. They can therefore easily be missed without the use of *in-situ* experiments. If only static experiments had been performed, small increases in intensities in a certain peak due to coincidence with other peaks would not have been noticed. By using the slow heating/cooling cycles, peaks for the different phases are easily differentiated. In addition, studying the phase diagram of mixed surfactant systems with the standard microscope penetration technique would be very difficult. In this technique a small amount of solid surfactant is placed between a microscope slide and cover slip, where it is slowly hydrated by putting some water around it. However if the sample is just a physical mixture of two surfactants then the most soluble component will dissolve first. Information obtained on the phase diagram of mixed surfactant systems from experiments carried out in that way must be treated with caution.

The high viscosity of phases observed by Rendall *et al.* [11] can be explained by the proposed structures for the mesh phases: the viscosity of the hexagonal mesh phase is likely to be high because of the connections between the surfactant layers. In the proposed model for the tetragonal mesh phase there are no connections between the surfactant layers. The point where the surfactant rods in the layers are connected to form the water holes are in reality (as opposed to the simplified model presented here) likely to be thicker than the rest of the rods. Therefore flow of this phase would cause these junctions to move over one another and coincide with junctions from adjacent layers. This would cause a high viscosity of this phase as was already suggested by Kékicheff and Tiddy [16]. In this way the macroscopic behaviour of the liquid crystalline phases of surfactants can be explained by an improved understanding of the microstructure of these materials

7.10.3.1 Assumptions made in the proposed models

Models have been proposed here for the intermediate phases, as a hexagonal and tetragonal mesh phase. These models have been optimised using the surfactant volume fraction as a constraint, in order to ensure that the proposed structures would accommodate the required volume fraction surfactant. The initial models where rods of uniform thickness (with a square cross-section) were used had to be modified as these models could not accommodate the required volume fraction of surfactant in the rods forming the surfactant layers. The inverse structures where the cylinders are made up of the water molecules and the holes are filled with the surfactant molecules would fit the data but seem unlikely as these inverse structures do not seem to be a logical step in the overall transformation process from the hexagonal to the lamellar phase. Therefore the models were *modified and a rectangular* cross-section of the rods was presumed.

In reality the structures are likely to have a much smoother geometry, with rounded edges. The rods are more likely to have an elliptical than a rectangular cross-section as they are squashed between the layers. It is only for simplicity that the surfactant rods were assumed here to have a rectangular cross-section. Nevertheless, the models used here are likely to give a good indication of how the geometry of the phases changes with concentration and chainlength. Another simplification made here was that the surfactant layer thickness was presumed to be the same in both the intermediate phases as in the lamellar phase. This assumption had to be made in order to eliminate one parameter from the equations so that the other structural parameters could be calculated.

All structural calculations for all the phases (isotropic micellar, hexagonal, hexagonal mesh, tetragonal mesh and lamellar phase) are based on volume fractions, which were calculated from transition concentrations, taken from literature. These may not always have been determined with a very high accuracy. Although these values might therefore not be absolutely precise, the calculated results do show sensible trends of the structural parameters with increasing chainlength and concentration. Since no data were available for the mixed surfactant systems, for these samples the transition concentrations have been taken as weighted averages of the concentrations of the single surfactant systems. This seemed a reasonable approximation as these concentrations for the single surfactant did not seem to depend very strongly on chainlength.

7.10.3.1.1 The hexagonal mesh phase

Evidence for the hexagonal mesh phase is based on a number of arguments: the main argument is the fact that the d-spacings for this phase can be indexed for a three- rather than a two-dimensional hexagonal structure as Luzzati e*t al.* [1] and Husson *et al.* [12] proposed. Calculations based on the volume fraction and a simplified geometry of the system indicate that the layers are connected with surfactant columns. The reason that Luzzati *et al.* [1] and Husson *et al.* [12] proposed a model with two- rather than three-dimensional periodicity is probably that they overlooked two peaks related to the c-axis of the structure. These peaks for the hexagonal mesh phase are easily overlooked, as the (001) peak in the SAXS pattern often coincides with the (001) peak for the coagel and the (101) peak is easily mistaken for the (001) peak for the lamellar phase, as this peak occurred at approximately the same position. This emphasises the necessity of time-resolved *in-situ* crystallisation studies rather than the use of static experiments. In time-resolved experiments unexpected increases in peak intensity are much easier to notice.

Another argument in favour of the hexagonal mesh structure and against the complex hexagonal structure proposed by Luzzati *et al.* [1] and Husson *et al.* [12] is the different curvature on the in- and outside of the cylinders for the complex hexagonal phase, as was pointed out by Tiddy [17] and Leigh *et al.* [18]. This would mean that the surfactant head groups are closer together on the inside than on the outside of the cylinders, which is unlikely as the electrostatic interactions on the inside of the cylinders would be unfavourable. Molecular modelling using the program *Cerius2* also showed the proposed model to fit well with the experimental data. More evidence for the structure as a hexagonal mesh phase (and against a complex hexagonal structure) was provided by the observed texture in the diffraction rings. This is explained in section 7.10.3.2.

7.10.3.1.2 The tetragonal mesh phase

Evidence for the tetragonal mesh phase is less strong than the evidence for the hexagonal mesh phase, as only two peaks were observed for this phase. The fact that the d-spacings ratio of these peaks was the same for all single and mixed surfactant systems indicates that this is the same phase for all samples. It is then very likely that this phase is a body-centred tetragonal mesh phase since this d-spacings ratio is identical to the ratio of two of the strong peaks found for the body-centred tetragonal mesh phase of SDS, a very similar surfactant (see chapter 3). This would also make the phase sequence of the sodium soaps studied here very similar to the phase sequence found for SDS. In addition the two observed peaks do not index for a lamellar, hexagonal or cubic structure. In addition, Rendall *et al.* [11] noticed that this phase showed birefringence, which means that it cannot be cubic. This phase is difficult to prepare experimentally, since it only forms over a very narrow concentration range. In addition, one of the two observed peaks often coincided with the peak for the solid phase or for the lamellar phase. This again stresses the need for time-resolved *in-situ* studies, since else such changes in the diffraction patterns are easily overlooked.

The tetragonal mesh phase was always observed on cooling but not always on heating of the samples. This indicates that the tetragonal mesh phase is easier nucleated from the lamellar phase than from the hexagonal mesh phase, which is confirmed by the results from the crash cool experiments: although the lamellar phase was cooled extremely rapidly, the tetragonal mesh phase was still observed. This suggests very close structural similarities between the tetragonal mesh phase and the lamellar phase, which is consistent with the proposed structures. For the tetragonal mesh phase to form from the lamellar phase, the only change in the structure is that water holes have to be created in the surfactant layers. When the tetragonal mesh phase is formed from the hexagonal mesh phase however, not only does a re-organisation have to take place of the water holes, but in addition connections between the surfactant layers have to be broken. It is probable that this process will take longer than just the creation of water holes in the surfactant layers of the lamellar phase.

The observed difference in phase behaviour during cooling and heating also indicates that the formation of the hexagonal mesh phase from the lamellar phase is more difficult than the other way around. This is consistent with the suggested model of the hexagonal mesh phase in which connections exist between the surfactant layers. This means that when this phase is created these connections have to form at regular positions. This is likely to take more time than to disrupt the connections which takes place during the transformation from the hexagonal mesh phase to the lamellar phase.

The kinetics of the formation of the hexagonal mesh phase from the lamellar phase are therefore likely to be slower than for the reverse process. This means, that on cooling the tetragonal mesh phase would have more time to form. The observed difference in phase behaviour on cooling and heating of the samples can thus be explained from a structural understanding of the phases involved in the transformation process. This provides a good indication for the proposed structures to be correct. The lack of connections between the surfactant layers in the tetragonal mesh phase could mean that the correlations between the water holes in these layers are easier lost than if they were connected. If because of this the structure is less perfectly formed this could be an additional reason why only two diffraction peaks were observed.

The values of the d-spacings for the tetragonal mesh phase are close to values found by Luzzati *et al.* [19] and Husson *et al.* [12] for rectangular phases in saturated potassium soaps. However, the ratio of those d-spacings are all slightly different for the various surfactants, whereas here the same ratio was observed for all samples studied. The ratios given by Luzzati *et al.* [19] range from 0.71 to 0.83 for different saturated and unsaturated potassium soaps. This is very close to the ratio found here which is approximately 0.76. However, the rectangular phases were found by Luzzati *et al.* [19] at lower concentration than the phase which they called the complex hexagonal phase. For the rectangular phases Luzzati *et al.* [19] proposed a primitive two-dimensional rectangular structure. If the second intermediate phase observed here would be based on a primitive rather than on a centred lattice then (in comparison with data from Luzzati *et al.* [19]) the two observed peaks would be the (100) and the (010) peak. The (110) peak is not observed but Husson *et al.* [12] did not observe this peak either for their rectangular phases, and showed that the intensity of this peak would theoretically be extremely low. Higher order peaks like *e.g.* (200) and (020) would be just outside the range of the detector for the experimental data presented here. The possibility that the second intermediate phase observed has the same structure as the rectangular phases observed by Luzzati *et al.* [19] can thus not be excluded. A two-dimensional structure of surfactant blocks of indefinite length does not seem to fit in with the overall phase sequence however. In addition, the phase transition from the hexagonal mesh phase to the tetragonal mesh took place gradually and so did the subsequent transition from the tetragonal mesh phase to the lamellar phase. This seems consistent with the models presented here and not with the model of the rectangular phases. In addition to this, Eins [20] concluded the lattice of the phase observed by Luzzati et *al.* [19] to be two-dimensional face centred rather than primitive on the basis of electron microscopy results. For these reasons the model of the tetragonal mesh phase proposed here seems a much more likelier candidate. It is possible that Luzzati's rectangular phases were tetragonal mesh phases as well. An additional argument is that the observed texture in the diffraction rings is consistent with the model proposed here (see section 7.10.3.2).

7.10.3.1.3 Comparison of the size of the water holes in the mesh phases

The volume calculated for the water holes in the tetragonal mesh structure is smaller than the volume calculated for the water holes in the hexagonal mesh phase. This indicates a rational trend; the holes in the surfactant layers become smaller as the surfactant concentration is increased. The holes are largest in the hexagonal mesh phase, decrease in size in the tetragonal mesh phase and disappear when the lamellar phase is formed. Another reason for the holes to be smaller in the tetragonal phase than in the hexagonal mesh phase is that in the tetragonal mesh structure proposed here there are no connections between adjacent surfactant layers, therefore all the surfactant molecules have to be packed into the surfactant layers; this reduces the size of the water holes.

It is possible that in the tetragonal mesh phase the holes are not extended through the layers but are just dimples in curved surfaces. For simplicity of the calculations the surfactant rods have been assumed here to have a rectangular cross-section. As was pointed out before an elliptical cross-section would be more likely. If the rods have an elliptical cross-section than they might be so close together that they actually touch at the centre of the holes, in which case dimples are created rather than holes extended through the layers.

An alternative model for the tetragonal mesh phase could be proposed in which adjacent layers in the tetragonal mesh phase are connected, like in the hexagonal mesh phase. If that assumption is made, then the calculated volume of the holes would become larger, since in that case some of the surfactant would have to make up these connections, thus decreasing the width of the surfactant rods in the surfactant layers and thereby increasing the size of the water holes. However, in the previous sections arguments have been given which indicate that the structure of the tetragonal mesh phase is very similar to the structure of the lamellar phase, which has no connections between adjacent layers. It therefore seems a good assumption that the layers in the tetragonal phase are not be connected either. From the two observed peaks for this phase it is not possible to obtain conclusive evidence on whether the layers are connected or not.

7.10.3.1.4 The deformed hexagonal phase and the defected lamellar phase

For some samples additional phases were found which only exhibited one or two diffraction peaks. As this is very little information to identify an unknown phase, structures for these phases could only be proposed on the basis of a comparison with literature data on similar surfactant systems. The two most likely models for these phases are discussed below.

- *The deformed hexagonal phase*

The phase which was found to exist between the normal hexagonal phase and the hexagonal mesh phase is likely to be a deformed hexagonal phase. This phase was formed by NaL-NaM and the NaM-NaP mixtures. Since it was not formed by the NaL-NaP mixtures nor by the single surfactant samples, the results indicate that for the formation of this phase a mixture of chainlengths is required, with a difference in chainlength of two CH_2 groups. Although the exact structure of this phase is not known, it is possible that with such mixtures its curvature is easiest accomplished. The rods forming the deformed hexagonal phase are thought to have an elliptical cross-section. It seems plausible that this is easier accomplished when different chainlengths are present in the sample.

- *The defected lamellar phase*

Some samples exhibited a phase that only caused one very weak diffuse diffraction ring at low angle. Similar diffraction rings for other surfactant systems have been interpreted to be caused by defects, in the form of uncorrelated water holes or dimples in the lamellar phase, (see chapter 3). This phase has therefore been called a defected lamellar phase or a random mesh phase. Here however, this diffraction ring was sometimes observed at room temperature when all soap was presumed to be in the solid phase. This could indicate that defects similar to the ones for a defected lamellar phase can exist in the solid state as well. This is possible as the structure of the solid phase is likely to be similar to the structure of the lamellar phase (especially since the large tilt angle, 83°, indicates that the surfactant molecules are almost perpendicular to the layers). Another explanation would be that the diffuse peak was caused by a different phase that can coexist both with the lamellar and with the solid phase. This is very unlikely however because it would imply that this unidentified phase could exist over a very wide temperature and concentration range.

7.10.3.2 Epitaxial relations during the overall transformation process

Preferred orientation effects in the diffraction rings have revealed epitaxial growth relations between the solid phase and all liquid crystalline phases. The orientation observed in the diffraction rings for *e.g.* the solid phase was not always the same. The orientation in the diffraction rings of the solid phase relative to the orientation in the diffraction rings for the other phases however was always identical. This means that the orientation of the phases was not induced by the confinement of the capillaries but was caused by epitaxy as is explained below. The confinement of the capillaries could in principle lead to the same effects: a phase transition from an ordered phase to another ordered phase could in principle take place through a disordered state. If the new phase was forced to orient itself because of the confinement of the capillary then it would also appear that expitaxial relations exist between the two ordered phases. Here this is not the case however, because different orientations have been found in the starting material and in all cases the relative orientation in the diffraction rings for the next phase would be exactly the same. A certain orientation was thus passed on from one phase to the next. The observed orientation effects confirm the proposed models for the intermediate phases. This is explained in detail below.

7.10.3.2.1 Orientation of the hexagonal phase

The capillaries were filled by dipping them into the samples at elevated temperatures, where the samples exist as liquid crystals. The soaps thus crystallised inside the capillaries. In some cases this caused preferred orientation of the soap crystallites. This resulted in two more intense arcs in the (001) diffraction ring for the solid phase, corresponding to the (001) and $(00\bar{1})$ points in reciprocal space. These points are smeared out to form arcs since the orientation of the surfactant layers is not perfect. As the surfactant sample is heated from a coagel at room temperature, some of the solid will dissolve so that the concentration of the solution between the solid soap particles in the coagel increases. When the c.m.c. is exceeded spherical micelles are formed; as the concentration is increased further these come very close together until at some point they transform into cylinders. By transforming into cylinders space between the entities is created. The cylinders however are confined to narrow spaces between the solid particles. They are therefore forced to grow parallel to the soap layers of the solid phase. This is similar to the well known situation where the cylinders of the hexagonal phase orient parallel to container walls, such as a microscope slide and cover slip. Within the planes defined by the solid soap particles, called here the *xy*-planes, the cylinders have directional freedom. No orientational freedom is present however perpendicular to the *xy*-plane (see figure 7.30) due to the solid soap particles.

If the cylinders of the hexagonal phase were viewed end-on, this would result in diffraction spots or arcs in the (100) ring, corresponding with the following points in reciprocal space: (010), (100), $(1\bar{1}0)$, $(0\bar{1}0)$, $(\bar{1}00)$, and $(\bar{1}10)$. Due to the orientational freedom in the *xy*-plane, the orientation effects average out to result in only two arcs, corresponding to the (100) and the $(\bar{1}00)$ points in reciprocal space. Since these lattice planes in real space are parallel to the (001) planes of the solid phase, the two arcs of the hexagonal phase have the same orientation as the arcs in

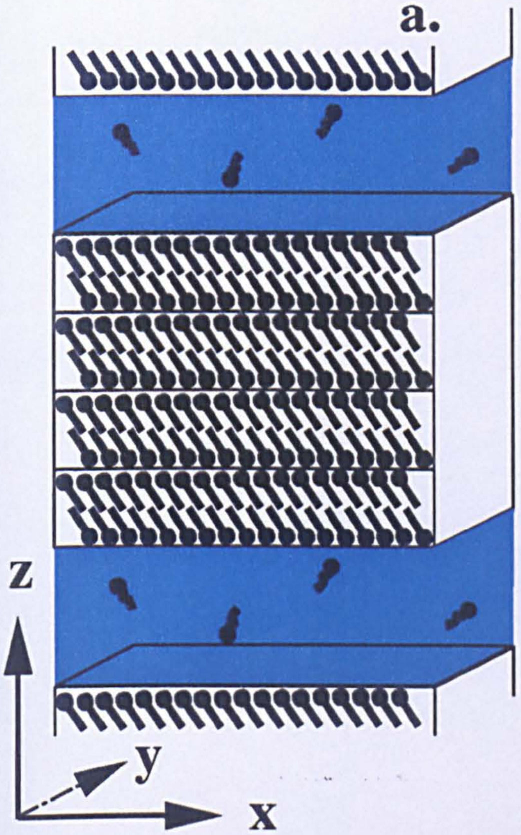

Figure 7.30 Showing how the orientation of the ordered phases is retained during the transformation processes that occur on heating of a coagel sample. The reverse processes take place during crystallisation on cooling.

The figure shows the phases that are formed in the aqueous part of the coagel, in coexistence with the remaining solid phase.

In (a) the coagel is shown before heating. The sample consists of solid soap particles with water trapped between these particles. There are some surfactant monomers present in the water.

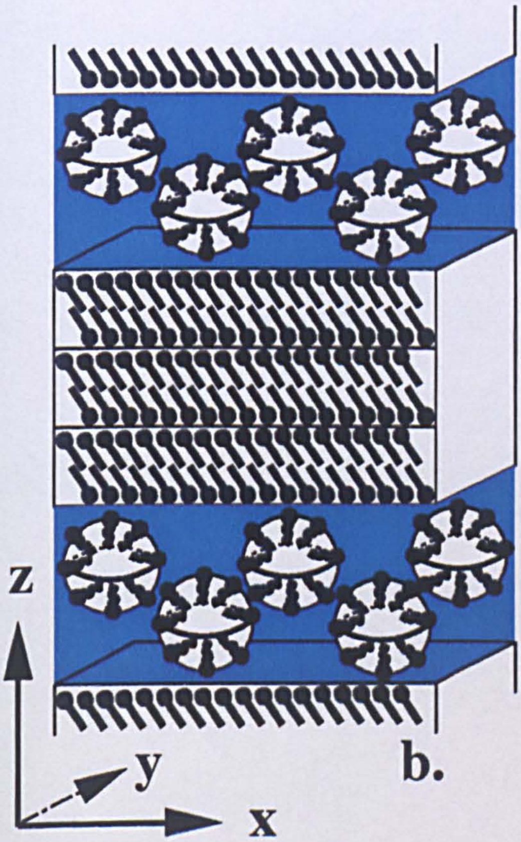

When the temperature of the sample is increased, some solid dissolves. When the c.m.c. is exceeded, micelles form (b). When the water gap between the micelles becomes too small a phase tranformation occurs to the hexagonal phase (see (c), next page).

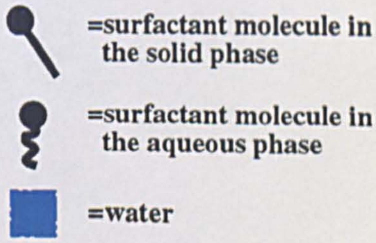
=surfactant molecule in the solid phase
=surfactant molecule in the aqueous phase
=water

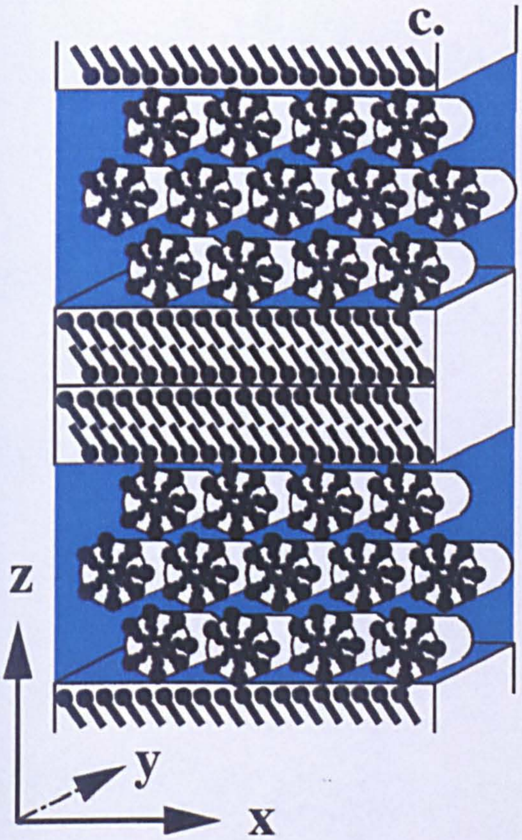

When the hexagonal phase (c) is formed, the cylinders are confined to narrow spaces in between the solid particles. They will therefore lie in the xy–plane.

On further heating more surfactant dissolves, the cylinders get closer together until at one point the hexagonal mesh phase (d) is formed.

In (e) a top–view (xy–plane) is shown of one of the surfactant layers of this mesh phase. The part in this figure that is enclosed by the broken lines (—·—·—) corresponds to the part of a surfactant layer of the mesh phase that is visible in (d).

The water holes are perpendicular to these layers and are lined–up with the holes in adjacent layers. These surfactant layers of the mesh phase have the same orientation as the original surfactant layers in the solid phase.

When through further heating of the sample the concentration of the aqueous phase is increased beyond a certain limit, the hexagonal mesh phase transforms to the tetragonal mesh phase, see (f) on the next page.

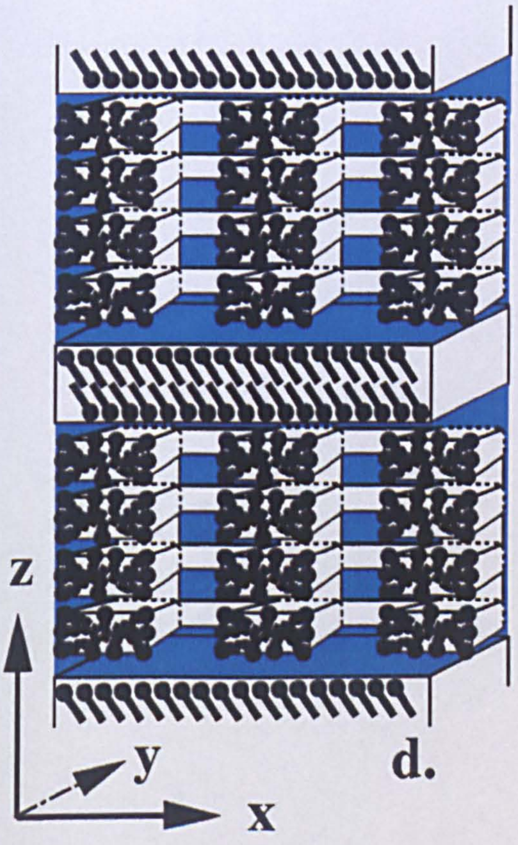

Top–view (xy–plane) of hexagonal mesh phase

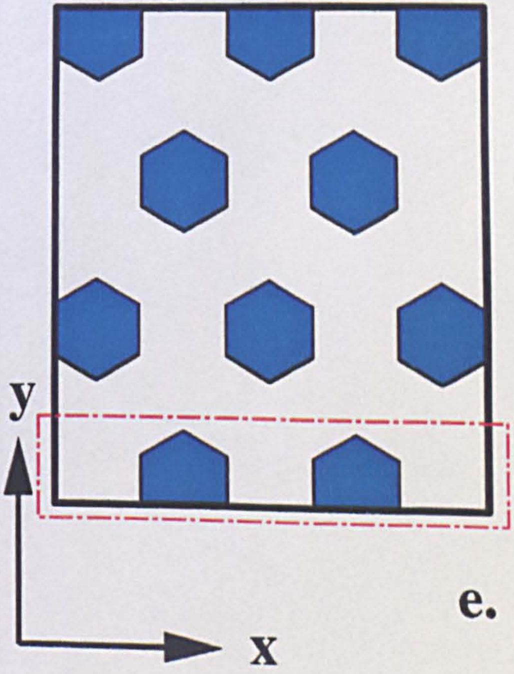

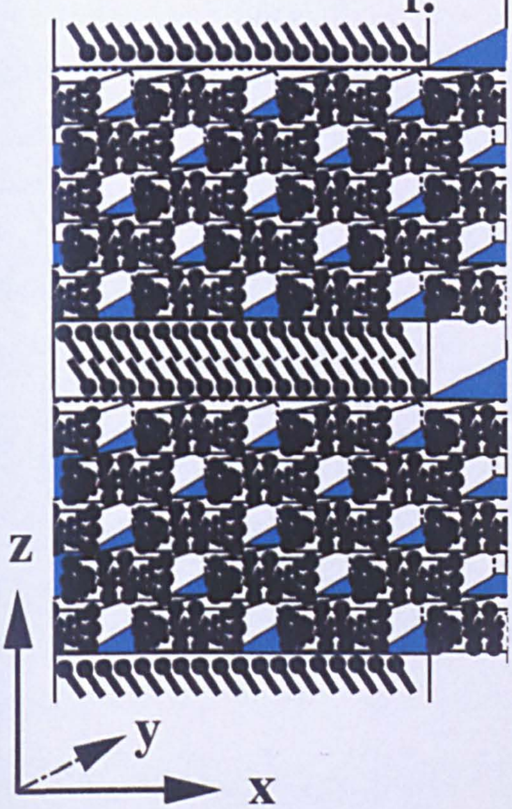

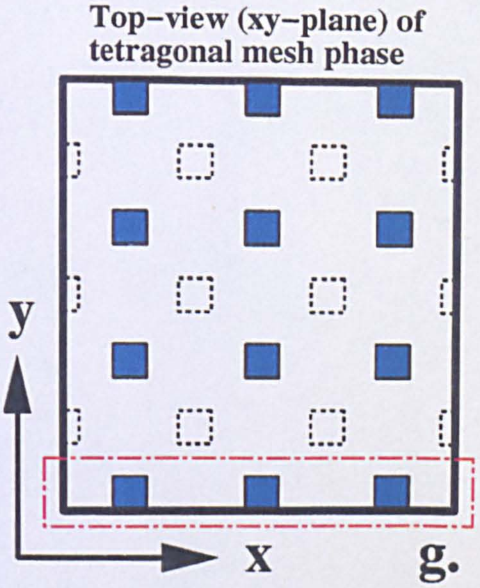

In (f) a 3D–view of the tetragonal mesh phase is shown. In (g) a top–view (xy–plane) of one of the surfactant layers of this mesh phase is shown. The part in this figure that is enclosed by the broken lines (—·—·—) corresponds to the part of a surfactant layer of the mesh phase that is visible in (f).

The water holes are perpendicular to these layers but are not lined–up with the holes in adjacent layers. The water holes in the layer underneath the one that is shown in (g) are represented in this figure by squares with broken lines (⬚).

The orientation of the surfactant layers of the mesh phase is the same as that of the surfactant crystallites in the original solid phase. Therefore when on a further increase of the temperature of the sample the concentration of the aqueous phase is further increased and the lamellar phase (h) is formed, the surfactant layers of this phase will have the same orientation as the surfactant layers in the original solid phase. The original orientation of the surfactant crystallites in the solid phase has thus been preserved throughout all the ordered phases.

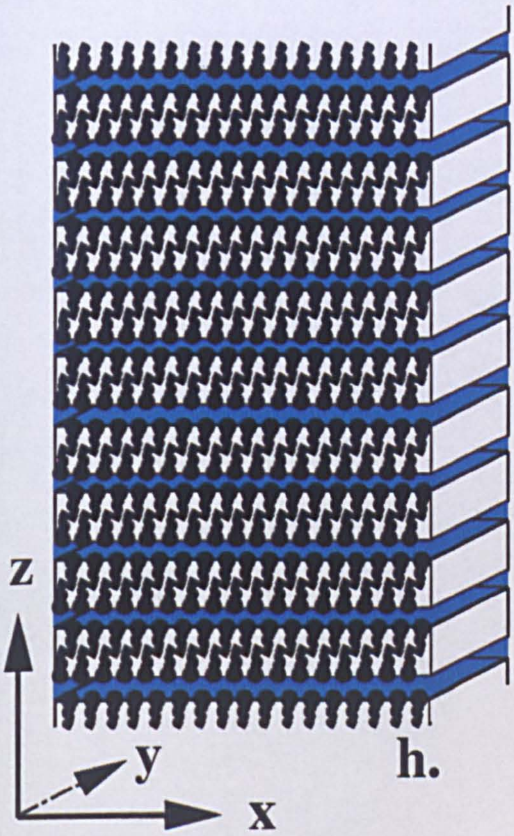

the diffraction ring for the solid phase. The results for the 40% samples have shown that even when all solid soap is fully dissolved the preferred orientation of the cylinders remains due to the high viscosity of the hexagonal phase. In that way, as the soap was crystallised on cooling, the solid phase regained its original orientation. Repeated heating and cooling experiments have shown that this process is absolutely reversible.

7.10.3.2.2 The deformed hexagonal phase

For some samples the next phase that formed after further heating was thought to be a deformed hexagonal phase. No clear texture was observed in the diffraction rings for this phase. It would however be expected that the ribbons remain parallel to the (001) planes of the solid phase. The rods are thought to have an elliptical cross-section. The shorter axis of this ellipse is likely to be perpendicular to the (001) planes of the solid phase as the rods are squashed between these layers. Since the peaks for this phase were not indexed it is not known what texture to expect for the deformed hexagonal phase.

7.10.3.2.3 The hexagonal mesh phase

When the solution becomes more concentrated the structure has to change in order to accommodate the increased surfactant volume fraction in solution. The next phase to form after either the hexagonal or the deformed hexagonal phase was the hexagonal mesh phase. An experiment with the X-ray cell with the two parallel mica windows showed a diffraction pattern with six-fold symmetry. Layered structures are known to align parallel to surfaces in a confined space, *e.g.* between a microscope slide and cover slip. The observed orientation effects are thus consistent with the proposed model: the hexagonal mesh structure is viewed along the c-axis, the layers are oriented parallel to the mica windows so that the water holes are being viewed end-on. This is also consistent with a weak (001) peak. The six-fold symmetry in the (100) diffraction ring corresponds to the following points in reciprocal space: (010), (100), $(1\bar{1}0)$, $(0\bar{1}0)$, $(\bar{1}00)$, and $(\bar{1}10)$. The six-fold symmetry is not perfect because even if the layers are aligned parallel to the mica windows, there can still exist ordered regions in the sample where the unit cell is rotated around the c-axis with respect to other ordered regions. The fact that the diffraction pattern is so spotty however indicates that the same ordering extends over large distances. The observed texture is also evidence against the model of the complex hexagonal phase which was proposed by Luzzati *et al.* [1] and Husson *et al.* [12]. If this phase was made up of cylinders than it would be improbable for these to orient perpendicular to the mica windows.

The orientation effects that were observed using the X-ray cell with the capillaries can be explained in the following way: the surfactant layers of the hexagonal mesh phase are parallel to the layers in the solid phase and parallel to the cylinders of the hexagonal phase. Orientational freedom is only possible in the *xy*-plane, by rotation around the c-axis. The orientation of the (001) ring would be expected to be the same as for the (001) peak of the solid phase (and the (100) ring for the hexagonal phase). This is consistent with experimental evidence (see figure 7.22). All (*h*00) and (*hk*0) lattice planes are thus perpendicular to the surfactant layers. Therefore the orientation of the two regions of highest intensity in the (100) diffraction ring, (corresponding to the (100) and $(\bar{1}00)$ points in reciprocal space) is the opposite of the observed orientation for the (001) ring of the solid phase and the (100) ring of the hexagonal phase. The observed texture effects in the diffraction rings for the hexagonal mesh phase are therefore consistent with the proposed structure. In addition, the effects indicate expitaxial growth of the surfactant layers in the hexagonal mesh phase either from the hexagonal or the deformed hexagonal phase, by connecting the rods which are already ordered in layers. As the diameter of the cylinders increases due to an increasing surfactant concentration (and because of this probably become slightly squashed so that their cross-section is likely to become elliptical), connections are formed between them, so that surfactant layers with water holes are created. These holes are thus perpendicular to the layers and this is reflected by the opposite orientation effects in the diffraction rings. This model of the transformation process from the hexagonal phase to the hexagonal mesh phase also suggests it to be likely that connections between the surfactant layers exist, since the surfactant cylinders are approaching each other from all sides. Therefore there would be no reason why they would only form connections in the *xy*-plane and not in the direction of the c-axis of the hexagonal mesh structure.

For SDS Leigh *et al.* [18] observed during microscopy studies a phase of which the cylinders aligned perpendicular to the microscope slide. During X-ray diffraction studies they found a deformed hexagonal phase. It is not likely however that the rods of the deformed hexagonal phase would exhibit the observed orientation. It is more probable that during their microscopy studies they observed a hexagonal mesh phase (later found for SDS by [13]) and during the X-ray diffraction they observed a deformed hexagonal phase.

7.10.3.2.4 The tetragonal mesh phase

Although the evidence for the tetragonal mesh phase is less strong than for the hexagonal mesh phase, it does appear to be a likely structure in the overall phase transformation process. As the surfactant sample is heated through the hexagonal mesh phase more soap dissolves, which causes the structure to change. It is likely that the water holes become smaller as the system becomes more concentrated. A body-centred tetragonal mesh is then a plausible structure, especially since this structure has also been reported for SDS at this position in the phase diagram (Kékicheff and Cabane [13]). The surfactant layers are likely to retain the orientation they had in the hexagonal mesh phase. The connections between the layers are disrupted and the water holes become ordered on a body-centred tetragonal lattice instead of a hexagonal lattice. If the inner diffraction ring corresponds to the (101) peak than this ring is expected to exhibit four regions of higher intensity at the corners of a rectangle, corresponding to the (101), $(\bar{1}01)$, $(\bar{1}0\bar{1})$, and $(10\bar{1})$ points in reciprocal space. This is consistent with the observed texture (see figures 7.21c and 7.22).

7.10.3.2.5 The lamellar phase

When the sample was heated further, the last solid dissolved so that the concentration was further increased and the lamellar phase was formed. Although this phase is only periodic in one-dimension, this direction is chosen here to correspond with the c-axis, analogue to the mesh phases where the c-axis is perpendicular to the surfactant layers. The two brighter arcs in what is thus called here the (001) ring (corresponding to the (001) and the $(00\overline{1})$ points in reciprocal space) for this phase always had the same orientation as the two brighter arcs in the (001) ring for the solid phase. This shows that the original orientation of the soap in the solid phase was passed on to the lamellar phase, through the hexagonal, deformed hexagonal, hexagonal mesh and tetragonal mesh phase. This indicates very simple epitaxial relations between the tetragonal mesh phase and the lamellar phase. The orientation of the surfactant layers is retained, all that changes is that the water holes are reduced in size until they disappear. It is possible that in certain cases some of the water holes persisted into the lamellar phase, but the correlations between them were lost so that a defected lamellar phase was formed.

7.10.3.3 Generic model for the structural transformation processes between the lamellar and the solid phase

From the previous section it is clear that the results presented here show that the transformation processes that occur *during dissolution* and crystallisation are generic for the surfactant systems studied. The overall transformation process from coagel to lamellar phase and *vice versa* does not depend on chainlength or composition, all single and mixed surfactant systems studied here showed the same phase behaviour. The only difference that has been found is that only for the mixtures with a chainlength difference of two CH_2 groups a deformed hexagonal phase was observed in between the normal hexagonal and the hexagonal mesh phase. It is however possible that all samples would form this phase during slower cooling or heating rates. The fact that all structures for all the surfactant mixtures resulted in d-spacings intermediate in position to those of the two surfactants present in the mixture means that in all the mixtures the two different surfactants are completely mixed in all the observed phases (solid, isotropic micellar, hexagonal, deformed hexagonal, hexagonal mesh, tetragonal mesh and lamellar phase).

The phase sequence found here seems rational, as the structure of every phase resembles in some way the structure of the previous phase and as it is almost identical to the phase sequence previously found for SDS (see chapter 3), a very similar surfactant. Evidence for the phase sequence presented here however, is not only based on the structures of the individual phases but also on the transformations that occur between them. These transformations were elucidated by preferred orientation effects in the diffraction rings, showing epitaxial relations between all the ordered phases.

During crystallisation from the lamellar phase the reverse processes take place that were described in the previous section: as the sample is cooled from the lamellar phase, some soap starts to crystallise, thus depleting the solution. In this way the system shifts slowly through the phase diagram: after the lamellar phase the tetragonal mesh phase is formed and then hexagonal mesh phase, all in coexistence with the solid phase. When the crystallising soap has depleted the solution beyond a certain limit, the surfactant layers of the hexagonal mesh phase break up into rods, so that either the deformed or the normal hexagonal phase is created. These rods still have the same orientation as the layers of the lamellar phase as they are trapped between the layers of the mesh phase and also between the formed solid soap. As more surfactant crystallises the solution in between the solid regions becomes more dilute so that the diameter of the cylinders decreases and they become further apart. At one point the correlations between the cylinders is lost and as they break up the isotropic micellar phase is formed.

The overall process described here explains how a coagel is formed on crystallisation from the lamellar phase: during crystallisation the remaining solution becomes entrapped between the solid particles, so that a heterogeneous dispersion of solid soap and water is formed. It also explains how the original structural orientation is retained during all the phase transitions. The structure of each phase acts as a template for the next one. Evidence for this has been given by preferred orientation effects in the diffraction rings. These remained the same after repeated heating and cooling of the samples. This shows the epitaxial relations described in these sections to be totally reversible. In this way the overall transformation process during the formation of a coagel by crystallisation from the lamellar phase can be explained in small, logical steps. The proposed models of the intermediate phases fit in very well with this structural transformation process.

7.10.3.4 Phase transformations during rapid cooling

Crash cool experiments revealed that during rapid crystallisation of the solid phase from the lamellar liquid crystalline phase the hexagonal phase did not form. Since the system passed through the concentration regime where the hexagonal phase is thermodynamically stable, an explanation for this must be sought in kinetic effects. The structural explanation given below attempts to relate the geometry of the various phases to the kinetics of their formation under non-equilibrium conditions, on a dynamical basis.

In the lamellar phase, there are water layers separating the surfactant layers. During rapid crystallisation this water has to be squeezed out from between these layers as quickly as possible, in order to form the structure of the solid phase. As these surfactant layers extend over large distances, the fastest way to squeeze out the water is by the formation of holes in the layers (see figure 7.31). The surfactant layers in the solid phase are thicker than in the lamellar phase, this means that in going from the lamellar phase to the solid phase the layers expand as the hydrocarbon chains straighten. This effect also acts to press out the water between the forming solid phase and the migrating surfactant layers of the lamellar phase. Effectively this water then rapidly dilutes the remaining aqueous regions, inducing the system to shift through the phase diagram. Two explanations can be given for the fact that the tetragonal mesh phase was always observed to form during the crash cool experiments:

1. the tetragonal mesh phase is probably easily nucleated from the lamellar phase, as these two liquid crystalline phase have a very similar structure
2. the architecture of the tetragonal mesh phase can serve as a means for the water to escape from between the solid layers and the layers of the liquid crystalline phase, which are either moving rapidly toward the solid layers or are expanding as they are crystallising themselves (see figure 7.31)

Experiments have shown that during crash cooling of the sample the hexagonal mesh phase sometimes formed, but the hexagonal phase is never formed. This means that the kinetics of nucleation for these phases are slow. This can be understood on the basis of the differences between the structures between the phases. The differences in structure between the lamellar phase and the tetragonal mesh phase are very small, the differences between the tetragonal and the hexagonal mesh phase are larger and the differences between the hexagonal mesh phase and the hexagonal phase are the largest. In addition, the structure of the solid phase is likely to show similarities with the layered structures of the lamellar and the intermediate phases. It is therefore possible that the solid phase is nucleated so rapidly from these structures, that its nucleation rate exceeds the nucleation rate of the hexagonal phase from the hexagonal mesh phase.

It is also possible that the hexagonal phase did not form since by the time the solution had reached the right concentration regime for the hexagonal phase, the temperature had dropped below the value where the hexagonal phase normally forms. Effectively the system thus consisted of a mixture of solid phase and undercooled lamellar and mesh phases. Since the hexagonal phase was not formed during crash cooling, all solid was either crystallised from the lamellar phase or from the mesh phases. No deviations of the d-spacings for the solid phases were found however compared to the d-spacings for the solid soap that had been crystallised at a slower rate.

From the above arguments it seems likely that no matter how fast a sample is cooled from the lamellar phase the intermediate phases will still form, due to the structural similarities and since they provide the most efficient means of the system to drain out

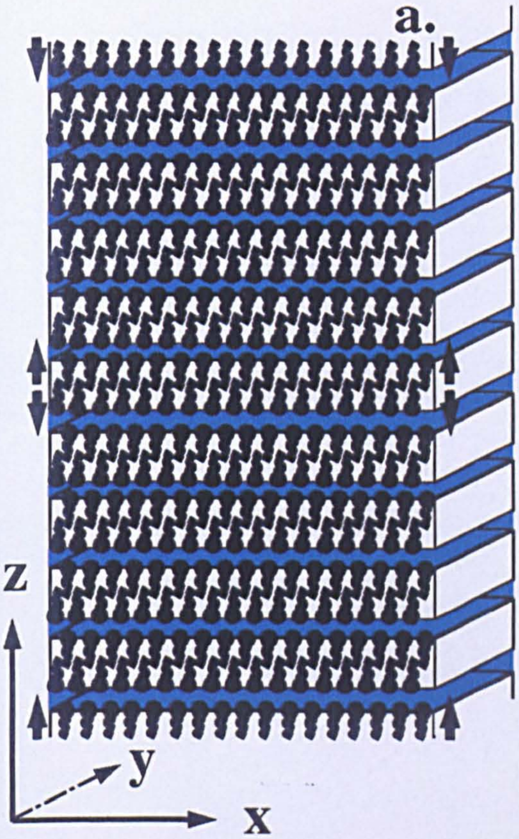

Figure 7.31 Shows the proposed mechanism for the transformation process that takes place during the formation of the coagel on crystallisation from the lamellar liquid crystalline phase, during a crash cool experiment.

In (a) the lamellar liquid crystalline phase is shown, at the onset of rapid cooling. The sample consists of bilayers of surfactant molecules, alternated with water layers. As the sample is cooled, supersaturation is induced and nucleation will occur. In (a) this is depicted by the arrows, which indicate that those surfactant layers are about to expand and change to the solid phase.

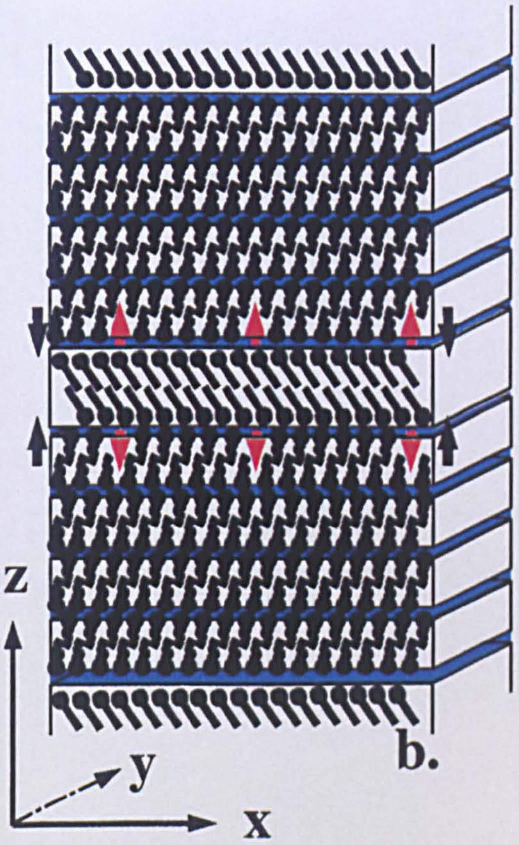

In (b) these layers have crystallised. Crystal growth will now take place. This means that surfactant molecules from the lamellar phase will now move towards the formed solid, as is indicated in (b) by solid arrows. For this the water needs to escape from between the solid layer and the migrating surfactant molecules of the lamellar phase. This is visualised in (b) by the red arrows. Effectively this water then dilutes the remaining aqueous phase so that a phase transformation occurs to the tetragonal mesh phase, see (c), next page.

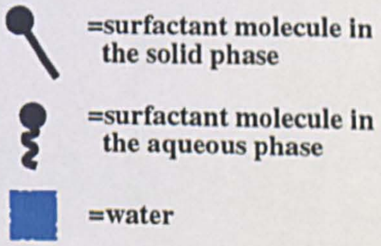
=surfactant molecule in the solid phase
=surfactant molecule in the aqueous phase
=water

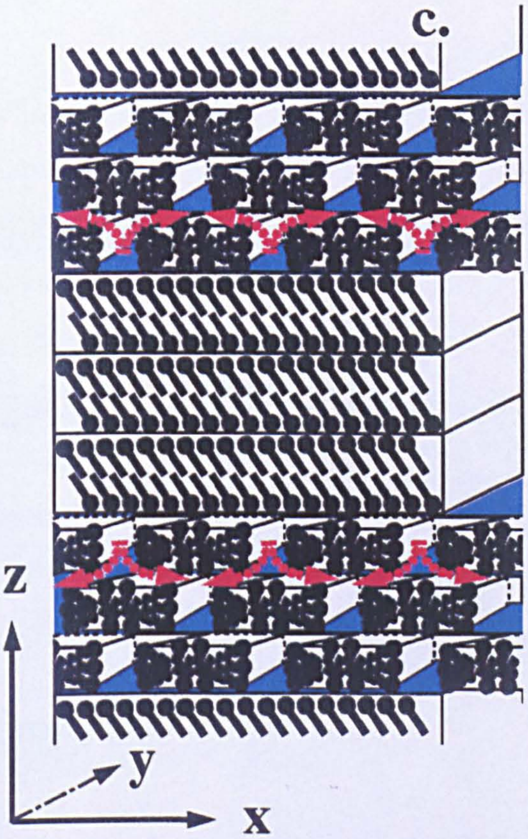

In (c) the tetragonal mesh phase is shown. This phase is always formed, even when the sample is cooled very rapidly from the lamellar phase. Possible explanations for this are:

1. The tetragonal mesh phase is probably easily nucleated from the lamellar phase, as these two liquid crystalline phases have a very similar structure. The tetragonal mesh phase is therefore easily formed.
2. In addition the architecture of the tetragonal mesh phase can serve as a means for the water to escape from between the solid particles and the layers of the liquid crystalline phase, as is indicated by the red arrows.

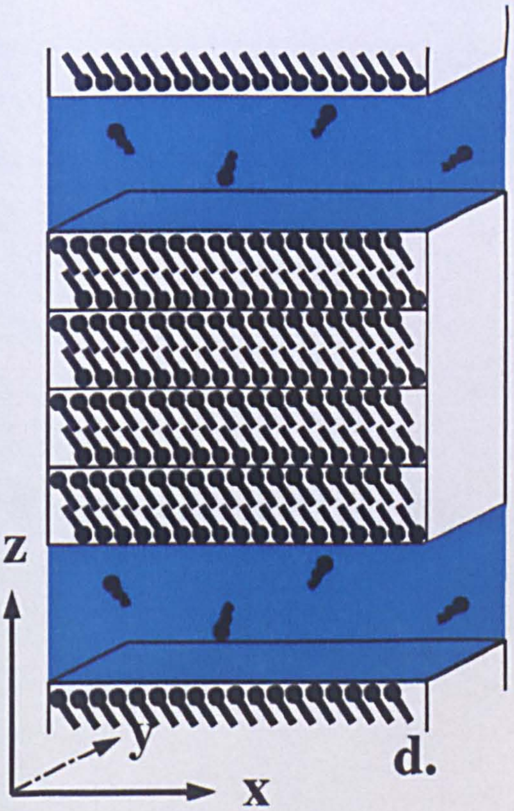

Since the hexagonal phase is not always formed during crash cooling, it is possible to by-pass this phase and crystallise all solid either from the lamellar phase or from one of the mesh phases (d).

the water from between the surfactant layers, which it needs to do in order to crystallise.

The structure of the sodium soaps studied here is likely to be similar to the known structure of KP. This structure shows a close resemblance with a lamellar liquid crystalline phase (see chapter 3). Therefore if soap could be crystallised at a slow rate from the lamellar phase without forming any other phases, this material would be expected to have a higher degree of crystallinity than material crystallised from the hexagonal phase, because the lamellar phase provides a structural template for the solid phase to grow from. This epitaxial growth relation was confirmed by the observed orientation effects in the diffraction rings. The data presented here however revealed that when a surfactant is crystallised from a 70% lamellar sample little material actually crystallises from the lamellar phase, since as soon as the solid starts to crystallise the system goes through several phase transformations, even if the sample is cooled very rapidly (which is not a good way to obtain good crystalline material anyway). This is a good example of Ostwald's step rule: although the structure of the solid phase is likely to be closely related to that of the lamellar phase, during crystallisation first the intermediate phases and then the hexagonal and the isotropic micellar phase are formed which are structurally very different from the solid phase. Although each mesophase shows a close structural resemblance to the previous one, after all the phase transformations a structure results (the isotropic micellar phase), which shows very little structural resemblance with the solid phase. The irony is that the structure of the starting phase (the lamellar phase) is probably closely related to that of the solid phase, but through all the phase transformations this structural template is progressively lost. It has been shown here that surfactant mixtures of different chainlengths form solid solutions, this is also likely to cause the material to be of a poor crystallinity. The crystal lattice of a single surfactant would become distorted by low concentrations of surfactant homologues. Therefore the need exists for soaps of high purity for structure determination. Knowledge of the solid state structures of soaps could lead to a better understanding of the physical properties of these materials, *e.g.* explain the differences in solubility of the different polymorphs.

7.10.4 Micellar phase behaviour of samples containing ethanol

The samples containing ethanol showed different phase behaviour from the aqueous samples. The diffuse ring that appeared when the sample was heated and the solid soap dissolved was at smaller d-spacing than the diffuse ring for the aqueous samples. A possible explanation for this is that the ethanol is incorporated into the surfactant micelles. By increasing the hydrocarbon volume and reducing the repulsions between the head groups, the ethanol molecules allow a smaller curvature and thus larger radius of the micelles. The micelles are thus closer together than they were for the aqueous samples and thus give rise to a smaller d-spacing. This is consistent with the observed decrease in d-spacing with increasing ethanol concentration. Due to a lack of water the 100% ethanol sample cannot form micelles, which explains why no diffuse ring was observed for this sample.

7.11 Conclusions

7.11.1 Mixed structures

None of the surfactant mixtures was found to segregate into its components, mixed structures were found to exist in all phases: in the lamellar phase, the intermediate phases, the hexagonal phase, the isotropic micellar solution and in the solid phase as solid solutions. The phase segregation which was indicated by the two step increase and decrease in the turbidity curves (see chapter 6) was not found to occur during the *in-situ* X-ray diffraction studies. This indicates that this phenomenon may be dependent on the degree of agitation of the sample. The sole observed difference between the single and the mixed surfactants was that only the mixtures with a chainlength difference of two CH_2 groups formed what is probably a deformed hexagonal phase.

7.11.2 Coagels

For the solid phase present in the coagels the following was found:

1. Single surfactants crystallised from aqueous solutions

a) d-spacings are not dependent on the concentration of the solution the sample was crystallised from.

b) The observed d-spacings are also independent of the cooling rate used during crystallisation, *i.e.* the cooling rate was not found to affect the crystal structure of the resulting solid material.

c) There is a linear relationship between d-spacing and chainlength, which implies that the sodium soaps studied here have similar crystal structures.

d) An estimation was made of the angle of tilt of the molecules in the unit cell. This showed this angle to be larger than the angle of tilt in the B form of KP. The large angle of tilt suggests that the structure of the sodium soaps is very similar to that of a lamellar liquid crystal.

2. Mixed surfactants crystallised from aqueous solutions

   a) All investigated sample compositions formed solid solutions; on crystallisation only one X-ray diffraction peak was observed.

   b) Almost all mixtures with a difference in chainlength of two CH_2 groups (the NaL-NaM and the NaM-NaP mixtures) showed a linear relationship between d-spacing and chainlength. The NaM:NaP=3:1 sample was the only exception to this. The results indicate that this sample forms a denser solid solution than the other mixtures This may explain why it was the only mixed sample with a chainlength difference of two CH_2 groups that exhibited phase separation during the stirred nucleation experiments.

   c) For the mixtures with a difference in chainlength of four CH_2 groups (the NaL-NaP mixtures) a linear relation was found between observed d-spacing and chainlength, different from the one for the samples with a chainlength difference of two CH_2 groups.

   d) Apart from the NaM:NaP=3:1 sample, all observed d-spacings for the other mixtures were found to be larger than the weighted averages of the d-spacings of the two surfactants present in the mixtures. In general, the larger the difference in chainlength, the larger the d-spacing for the mixture becomes. This indicates that the molecules become less efficiently packed together as the difference in chainlength between them increases.

e) In some cases the diffraction peak for the mixture was observed to shift slightly to larger d-spacing on heating and to smaller d-spacing on cooling. Since this was found to occur both for single surfactants and for surfactant mixtures, this was probably caused by thermal expansion and contraction of the crystal lattice.

3. Solid surfactant crystallised from ethanol-water mixtures
   a) Of the samples that were crystallised from ethanol-water mixtures the only ones that exhibited different diffraction characteristics from the rest of the samples (crystallised from aqueous solutions or ethanol-water mixtures) were the ones with the highest ethanol content. This indicates that when the ethanol content of the solvent is high enough, anhydrous soap is crystallised instead of a hydrate.
   b) A difference in diffraction pattern before and after re-crystallisation was observed for the sample crystallised from a solvent mixture containing 80% ethanol and 20% water. This could be an indication that the sample slowly hydrates at room temperature.

7.11.3 The aqueous mesophases

1. Sizes were estimated of the spherical micelles in the isotropic micellar phase and of the cylinders of the hexagonal phase. The diameter of these cylinders was found to increase with increasing surfactant concentration.

2. The following phases were found to exist intermediate in concentration between the hexagonal and the lamellar liquid crystalline phase:

   a) Deformed hexagonal phase

   The mixed surfactant samples with a chainlength difference of two CH_2 groups were found to form a phase which is probably a deformed hexagonal phase. This phase is thought to be formed by a deformation of the lattice of the hexagonal phase, whereby the cross-section of the cylinders becomes elliptical. It is plausible that this elliptical cross-section is easier achieved with a surfactant mixture of two different chainlengths.

b) Hexagonal mesh phase

The following model was proposed for this intermediate phase: a hexagonal mesh phase consisting of alternating surfactant and water layers. There are hexagonally shaped holes filled with water in the surfactant layers. These holes are lined up with the holes in adjacent surfactant layers. Adjacent surfactant layers are connected with columns consisting of surfactant molecules.

c) Tetragonal mesh phase

The following model was proposed for this intermediate phase: a tetragonal mesh phase consisting of alternating surfactant and water layers. There are square water holes in the surfactant layers. The lattice is body-centred which means that the holes are not lined-up with the holes in adjacent surfactant layers. There are no connections between adjacent surfactant layers.

d) The defected lamellar or random mesh phase

Some samples exhibited a diffuse diffraction ring at low angle which indicates the presence of a defected lamellar phase.

3. Crash cool experiments revealed that even on very rapid cooling at least one of the intermediate phases was still formed. This has been explained on the basis of structural similarities between the lamellar phase and the tetragonal mesh phase. In addition the architecture of the intermediate phases provides an efficient means of the system to squeeze out the water from between the surfactant layers.

4. The surfactant solutions containing ethanol showed a different micellar behaviour from the aqueous surfactant samples. The value of the d-spacing for the isotropic micellar phase was found to decrease with increasing ethanol content. This indicates that the ethanol is incorporated into the micelles. Because of the higher hydrocarbon content and the reduced head group repulsions, the micelles can achieve a smaller curvature and therefore a larger size.

7.11.4 Generic process

The overall process that occurs during the transformation process from the coagel to the lamellar phase and *vice versa* appeared to be the same for all surfactant samples studied. This process consists of a number of rational steps, the structure of each phase acts as a template for the formation of the next phase. These epitaxial growth relations were revealed by texture in the diffraction rings and were found to be totally reversible on repeated heating and cooling.

7.12 Recommendations for future work

- The use of synchrotron radiation in combination with slow cooling and heating of the samples has proved to be very successful for *in-situ* studies of phase transitions. Now that the scattering characteristics of the intermediate phases of the sodium soaps have been established it would be of commercial interest to investigate real soap systems using the same technique.

- The effect of chainlength, head group and counter ion on the liquid crystalline phases formed during crystallisation could be further studied in order to investigate the generics of the phase behaviour observed here.

- In order to calculate the parameters describing the structures of the various phases with more precision, the phase boundaries need to be established with higher accuracy. This could be accomplished by careful preparation of samples of different concentrations and subsequent phase determination by means of X-ray diffraction.

- In order to verify the proposed structures of the intermediate phases, it should be attempted to obtain more diffraction peaks for these phases. This could be achieved by varying the sample to detector distance at a temperature where the intermediate phases are thermodynamically stable. Longer counting times could then be used which may reveal the existence of weak peaks. In addition it could be attempted to induce texture in the diffraction rings by orienting the samples by shearing.

- Some phases might not have been observed because of slow kinetics of formation although they are thermodynamically stable under certain conditions. For this reason experiments could be performed using slower cooling and heating rates.

- In chapter 5 it was shown that very low levels of impurities had a dramatic effect on the structure of the solid phase of fatty acids. Soaps could be made of the purified material in order to investigate the effects of the presence of low levels of other homologues on the crystallisation process of soaps.

- Applications should be sought for the newly found structures of the intermediate phases. With supra-molecular templating techniques for instance it may be possible to exploit the structures of these phases for molecular sieve applications.

7.13 References used in this chapter

1. Luzzati V, Mustacchi H and Skoulios A, *Discussions of the Faraday Society* **25**, 43 (1958)
2. Timmermans J, *Physico-chemical constants of pure organic compounds*, Elsevier Publishing company (1965)
3. Dumbleton JH and Lomer TR, *Acta Cryst* **19**, 301 (1965)
4. Reiss-Husson F and Luzzati V, *Journal of Physical Chemistry* **68**, 3504 (1964)
5. Madelmont C and Perron R, *Bulletin de la Société Chimique de France* **12**, 3263 (1973)
6. Madelmont C and Perron R, *Bulletin de la Société Chimique de France* **3-4**, 425 (1973)
7. Madelmont C and Perron R, *Bulletin de la Société Chimique de France* **9-10**, 1795 (1974)
8. Madelmont C and Perron R, *Colloid and Polymer Science* 254, 581 (1976)

9. Luzzati V, *Biological Membranes, Physical fact and function*, edited by Dennis Chapmann, Academic Press, London and New York (1968)

10. Madelmont C and Perron R, *Bulletin de la Société Chimique de France*, **9-10 pt 1**, page 1799-1805 (1974)

11. Rendall K, Tiddy GJT and Trevethan MA, *J Chem Soc Faraday Trans 1*, **79**, 637-649 (1983)

12. Husson F, Mustacchi H and Luzzati V, *Acta Crystallographica* **13**, 668 (1960)

13. Kékicheff P and Cabane B, *J Physique* **48**, 1571-1583 (1987)

14. Ferguson RH, *Oil and Soap* **21**, 6 (1944)

15. Luzzati V, Mustacchi H and Skoulios A, *Nature* **180**, 600 (1957)

16. Kékicheff P and Tiddy GJT, *Journal of Physical Chemistry* **93**, 2520 (1989)

17. Tiddy GJT, *Physical Reports* **57**, pages 1-46 (1980)

18. Leigh ID, McDonald MP, Wood RM, Tiddy GJT and Trevethan MA, *J Chem Soc, Faraday Trans 1*, **77**, 2867 (1981)

19. Luzzati V, Mustacchi H and Skoulios AE, Husson F, *Acta Crystallographica* **13**, 660, (1960)

20. Eins S, *Molecular Cystals and Liquid Crystals* **11**, 119 (1970)

Chapter 8

Conclusions

Chapter 8 Conclusions

8.1 Introduction

In the first part of this chapter (section 8.2) the main conclusions from the previous chapters have been collected, in order to provide an integrated picture and to put the individual results from the different chapters in a wider perspective. This train of thought is continued in section 8.3. where recommendations for further work are given based on these conclusions.

8.2 Overall conclusions from this work

In chapter 1 it was emphasised that although the chemistry of soap manufacture is very old, operation of the process is still largely empirical and pragmatic due to the lack of a detailed understanding of the many physical changes that take place during soap production. During process operations such as spray drying where the soap is crystallised from a lamellar liquid crystalline phase, milling and plodding, structural phase transitions occur that are not fully understood (see chapter 3). In chapter 3 it was demonstrated that surfactants have the ability to form many different phases, depending on temperature, composition and sample history. Since the fats used consist of a blend of many sources, the composition of the raw material used in soap manufacture is far from constant. For these reasons an investigation was undertaken to assess the effect of mixing surfactant homologues on their nucleation and crystallisation behaviour.

A zone refiner was modified to be made suitable for operation over long periods of time, thus enabling successful purification of fatty acids. For lauric and myristic acid it was demonstrated through a combined use of GC, DSC and XRD techniques that above a certain purity level, a phase transition takes place in the solid state from the C (or α) form to the A super (or γ) form. Even very low levels of impurities can inhibit this phase transformation. This was explained by demonstrating the major molecular re-arrangement that has to take place in the solid state for this transition to occur. The purified material was found to have a higher melting point and a larger metastable zone width than the unpurified material. This illustrates that in some cases it can be easier to assess the purity of a substance by monitoring one of its properties rather than by analytical means. Values for the segregation coefficients of a number of impurities were calculated, using the equations for the ultimate distribution. All values were found to be very close to unity, which was to be expected on the basis of the close similarities between the molecules of the host material and the impurities.

The kinetics of nucleation during crystallisation from the isotropic micellar phase were studied of single and mixed aqueous surfactant systems of NaL, NaM and NaP. For the single surfactants, the saturation temperature was found to increase with increasing chainlength and concentration. The enthalpy and entropy of dissolution also increased with increasing chainlength. The metastable zone width and the apparent order of nucleation appeared to decrease with increasing concentration and chainlength although there were deviations to this. For some of the mixed samples (all the NaL/NaP mixtures as well as the NaM:NaP=3:1 mixture), the crystallisation and subsequent dissolution process appeared to take place in a two step process. This indicates that one of the surfactants of the mixture crystallised first, followed by the other one. *In-situ* X-ray diffraction experiments on the same samples however, revealed that all mixed samples crystallised as solid solutions. Since identical cooling and heating rates were used during the X-ray diffraction measurements as during the nucleation experiments, the only experimental parameter that was different between these two experimental techniques was the rate of stirring. It was therefore postulated that a certain degree of agitation of the samples during crystallisation can in some cases result in segregation of the two surfactants present in the mixture. It is thinkable that for stagnant samples the growth mechanism is diffusion limited, where desolvation is difficult. Stirring of the samples may aid desolvation and reduce the diffusion layer, leading to a more efficient rejection of impurities (other surfactant homologues) at the crystal surface. This thus leads to phase separation of the two surfactants present in the mixture. The reason that this occurred for the NaM:NaP=3:1 sample was thought to be the denser molecular packing of this sample in comparison with the other mixtures, as was indicated by the X-ray diffraction measurements. This may make this structure more difficult to be nucleated so that phase separation can take place. The occurrence of phase separation for the NaL-NaP mixtures was explained by the fact that the chainlength difference between the two components of this mixture is larger than that for the other mixtures. This could make the formation of a solid solution more difficult.

The above explanation seems consistent with the observation that when during the nucleation experiments crystallisation and dissolution did not occur by a two step process, the metastable zone width for the mixtures appeared to be larger than for the single surfactant samples. This indicates that mixed structures are more difficult to nucleate than single phase systems. An alternative explanation for the larger metastable zone widths might be a higher stability of micelles consisting of a mixture of chainlengths than of micelles which are made up of molecules of uniform chainlength. This could be due to molecular crowding effects near the core of the micelles.

In addition to the "slow cool" experiments, "crash cool" experiments were carried out in order to measure the induction time as a function of supersaturation. From these data the size of the critical nucleus was estimated assuming a cylindrical shape of the nucleus. Although care must be taken in the interpretation of the results of these measurements, since only two single surfactants and one surfactant mixture were studied, the following trend was found: at the same supersaturation, more molecules are required to form a critical nucleus for the smaller chainlength surfactant than for the larger one. This can be understood in terms of size dependent attractive forces between the molecules, which stabilise the critical nucleus.

High intensity synchrotron radiation was used for *in-situ* X-ray diffraction studies of the crystallisation process of surfactants from three different concentration regimes: the isotropic micellar phase, the hexagonal and the lamellar liquid crystalline phase. Single and mixed surfactant systems were studied in order to investigate the effect of mixing chainlengths on the liquid crystalline and solid state phase behaviour. In addition, the effect of mother liquor on the resulting solid state structure was studied by crystallising NaL from various ethanol-water mixtures.

For all aqueous samples at least two phases were found to exist at compositions intermediate in concentration between the hexagonal and lamellar liquid crystalline phases. Orientation effects in the diffraction rings aided in the determination of the structures of these phases and revealed epitaxial relations between all ordered phases (liquid crystalline and solid state). This led to the following model of the overall process taking place during crystallisation from the lamellar liquid crystalline phase: the lamellar phase consists of alternating surfactant bilayers and water layers. In some cases the data indicated the existence of a defected lamellar phase. As the sample is cooled from a normal or defected lamellar phase, supersaturation is induced and some soap crystallises, the remaining liquid crystalline phase thus becomes depleted of surfactant so that the system starts to shift through the phase diagram. This results in the formation of water holes in the surfactant layers of the lamellar phase, so that first a body-centred tetragonal and then a hexagonal mesh phase is formed. As the sample is cooled further, more surfactant crystallises, so that the liquid crystalline phase region effectively becomes more diluted. At one point this causes the surfactant layers of the hexagonal mesh phase to break up into rods. For the mixtures with a chainlength difference of two CH_2 groups this was found to result in the formation of the deformed hexagonal phase, which subsequently transformed to the normal hexagonal phase on further cooling (and thus further dilution of the liquid crystalline phase region). The other aqueous samples were found to directly form the normal hexagonal phase after the hexagonal mesh phase. After further cooling of the sample the rods break up into spheres, which when the concentration drops below the c.m.c. disintegrate into surfactant monomers. The original orientation of the surfactant layers in the lamellar phase is passed on from one phase to the next; each phase acts as a template for the subsequent one, even after repeated heating and cooling. The overall phase transformation process during crystallisation from a lamellar liquid crystalline phase thus takes place through a sequence of rational steps, the order of which appears to be generic for the systems studied and in addition is consistent with the phase sequences known from literature for other surfactant systems.

For aqueous samples that were crash cooled, it was found that the tetragonal mesh phase was always formed whereas the hexagonal phase was not. This was explained in terms of close structural similarities between the lamellar phase and the tetragonal mesh phase. An additional argument given was that the architecture of the mesh phases is very suitable for efficient drainage of the water from between the surfactant layers during rapid crystallisation.

During the X-ray diffraction experiments segregation of the two surfactants present in the mixtures was not found to occur for any of the phases (solid state or mesophases), irrespective of sample composition. No indication was found that the concentration regime the sample was crystallised from and the cooling rate used during crystallisation affected the resultant solid state structure of the product. For the single surfactant samples in the solid state, a linear relation was found to exist between the observed d-spacing and the number of carbon atoms in the hydrocarbon chain. From the slope of this line an estimation was made of the angle of tilt. The calculated value for this suggests that the solid state structure of the sodium soaps is closely related to the structure of the lamellar liquid crystalline phase. All surfactant mixtures were found to form solid solutions. The d-spacings of these samples however indicated that the molecular packing becomes less efficient with increasing difference in chainlength of the two components of the mixture. The NaM:NaP=3:1 sample was an exception to this. The results indicated that at this composition a more dense structure was formed than for the other solid solutions.

Of the samples that were crystallised from ethanol-water mixtures only the ones with the highest ethanol content showed different diffraction characteristics in the solid state. This could indicate that when the ethanol content of the solvent is high enough, anhydrous soap is crystallised instead of the expected hydrated forms. A difference between the X-ray pattern of the sample for which the solvent contained 80% ethanol and 20% water before and after re-crystallisation indicates that the structure of the sample had slowly changed at room temperature. It is likely that this change involves a hydration of the sample. In addition to this, all samples containing ethanol exhibited X-ray diffraction characteristics for the isotropic micellar phase which were different from the ones exhibited by the aqueous samples. The observed smaller d-spacings for the samples containing ethanol indicate that the ethanol is incorporated into the micelles. It thus increases the hydrocarbon volume and reduces the head group repulsions. Therefore the micelles can achieve a smaller curvature which corresponds to a larger size.

In combining the results from all the previous chapters it appears that the solid state structure of sodium soaps can be affected by a number of factors: the degree of sample agitation during crystallisation, the influence of solvent and slow hydration with time, and the formation of solid solutions. The dramatic effect even very small quantities of impurities in the form of close homologues can have on solid state structures was stressed by the results of chapter 5. A combination of the above effects might explain some of the inconsistencies in surfactant literature discussed in chapter 3 (*e.g.* Ferguson [1]).

8.3 Future perspective

Based on the conclusions given in the first part of this chapter, in this second part some recommendations for further work in this area of research are provided.

- For a more detailed structural understanding of the spontaneous phase transformation from the C to the A super form of lauric and myristic acid, it should be investigated which fatty acid homologues inhibit this transition. As it has been shown that soaps form solid solutions with close homologues a clear need exists for using highly pure material for the determination of their solid state structures. The best way to obtain this material would be to convert the purified fatty acids to the corresponding soaps by the experimental procedure described in chapter 4. With soaps prepared this way the effect of close homologues on the nucleation and crystallisation process and physical properties of soaps could be assessed.

- It would be in the interest of commercial soap manufacture to determine the effect of stirring rate on the two step increase and decrease in turbidity observed during the nucleation studies. Two ways appear obvious for investigating this:
  1. by varying the stirring rate during the nucleation experiments
  2. by *in-situ* X-ray diffraction studies of samples that are crystallised under stirred conditions.

The latter experiments could be undertaken with the use of a recently developed temperature controlled cone and plate shear stress cell for *in-situ* X-ray measurements (van Gelder *et al.* [2]). This should be combined with *in-situ* crystallisation studies from liquid crystalline phases under the influence of shear stress, in order to investigate the effect of stirring on the phase diagram and to simulate more realistic processing conditions. These experiments could result in valuable information for surfactant industry.

- The use of *in-situ* X-ray diffraction experiments has proved to be a very powerful technique for real-time studies of the phase transformations occurring during crystallisation processes. The advantages of this technique over the use of static experiments or the standard microscopy hydration technique has been demonstrated in chapter 7. It should however be attempted to obtain more diffraction peaks on the intermediate phases in order to assess the correctness of the proposed structures. This could be done through the use of static XRD experiments with longer counting times and by varying the sample to detector distance. Vital information could also be obtained from orientation effects in the diffraction rings, by inducing alignment of the samples under the influence of shear stress.

- Now that more insight into the phase diagrams of single sodium soaps and aqueous mixtures of two sodium soaps has been obtained and the diffraction characteristics of the aqueous phases of these systems have been identified, *in-situ* X-ray diffraction experiments should be carried out on real soap systems during the different stages of soap manufacture. In addition, nucleation studies and *in-situ* X-ray diffraction studies could be undertaken of surfactants with different chainlength, head groups and counter ions, in order to investigate the generics of the results presented in this thesis.

The findings of this thesis do not have to remain limited to applications in the surfactant industry alone. The fascinating variety of self-assembling structures evoke the imagination to envisage a myriad of applications. The isotropic micellar phase for instance has found applications in chromatography techniques (Khaledi [3]) and emulsion polymerisation. The use of liquid crystals in the creation of particles through supra-molecular templating has initiated the development of a new class of materials for which the properties can be tailored by adjusting the sizes of the aggregates of the template used. This technique has been successfully applied to the formation of organic and inorganic particles of tuneable sizes from hexagonal, cubic, lamellar and reversed hexagonal phases (*e.g.* Smith *et al.* [4] for organic systems and Sayari and Lui [5] for inorganic systems). By applying supra-molecular templating techniques to the mesh phases described in chapter 7, for example molecular sieves could be created, where the size of the pores in the end product could be manipulated by varying the chainlength of the surfactant that is used as a template.

Thus, through the use of self-assembling systems (such as isotropic micellar systems and liquid crystalline phases) in supra-molecular templating, a variety of products with superior properties could be envisaged. However, the ultimate application of liquid crystals has been realised a long time ago with the creation of life: analogues to lamellar, cubic and reversed hexagonal liquid crystalline structures have been reported to serve vital functions in biological systems, see figure 8.1. Cubic phases have been found in living organisms (Larsson [7]). Phase transitions between liquid crystals can serve as model systems for processes occurring between biological

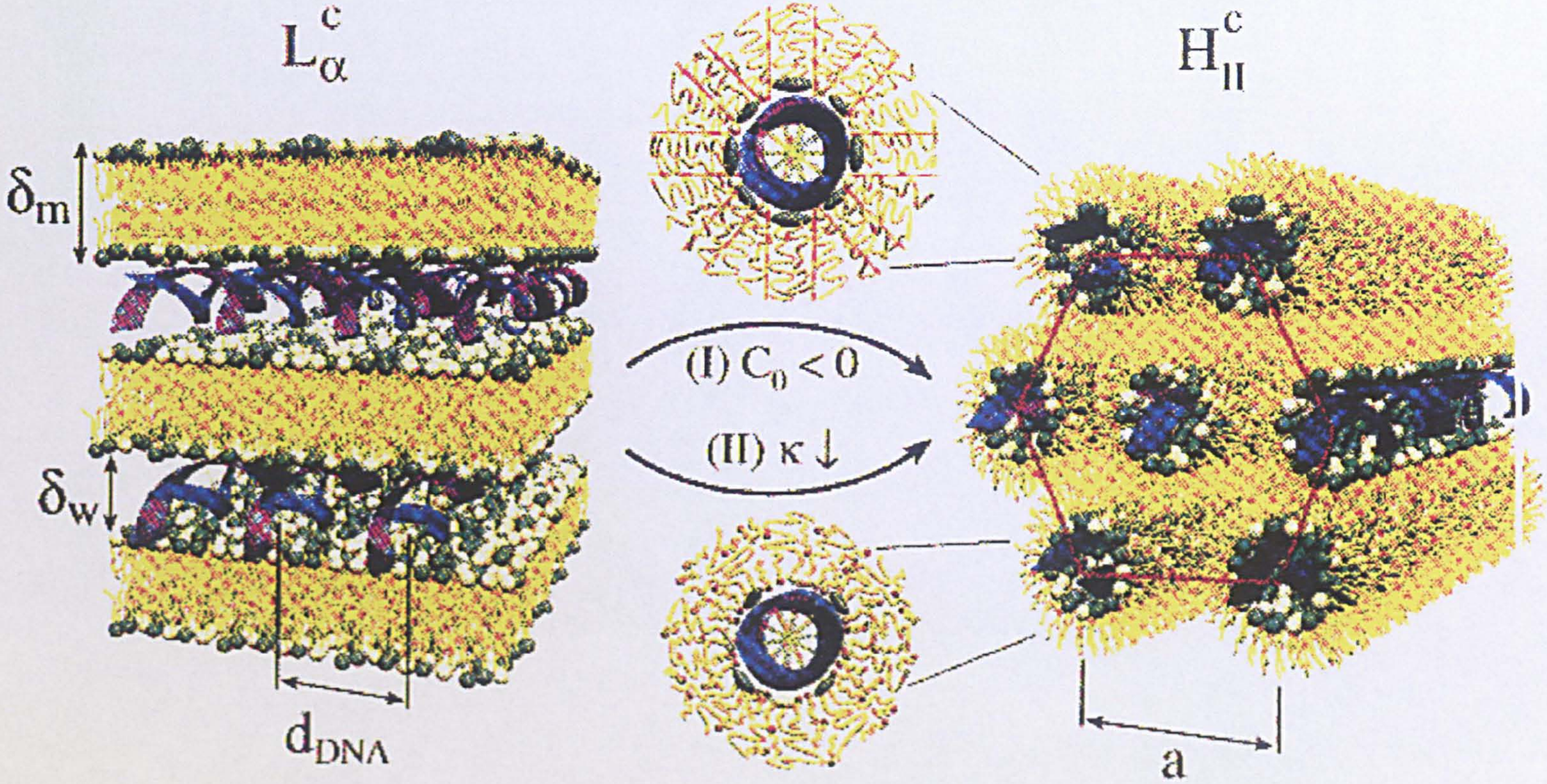
L_α^c
H_{II}^c
δ_m
δ_w
d_{DNA}
(I) $C_0 < 0$
(II) κ ↓
a

Figure 8.1 Showing a phase transition from the lamellar to the reversed hexagonal phase occurring in a liposome–DNA system. This illustrates the diversity of materials that have the ability to form liquid crystalline structures (from Koltover *et al.* [6])

membranes. Therefore a better understanding of liquid crystals and their phase transitions could result in an improved understanding of life itself.

8.4 References used in this chapter

1. Ferguson RH, *Oil and Soap* **21**, 6 (1944)
2. van Gelder RNMR, Hodgson N, Roberts KJ, Rossi A, Wells M, Polgreen M, *Crystallisation and Polymorphism in Cocoa Butter Fat: In-Situ Studies Using Synchrotron Radiation X-Ray Diffraction*, in *Crystal Growth of Organic Materials, American Chemical Society Conference Proceedings Series*, edited by Myerson AS, Green DA and Meenan P, pages 209-215 (1996)
3. Khaledi MG, *Journal of Chromatography* **A 780**, 3 (1997)
4. Smith RC, Fischer WM and Gin DL, *Journal of the American Chemical Society* **119**, 4092 (1997)
5. Sayari A and Lui P, *Microporous Materials* **12**, 149 (1997)
6. Koltover I, Salditt T, Rädler JO and Cyrus RS, *Science* **281**, 78 (1998)
7. Larsson K, *Journal of Physical Chemistry* **93**, 7304 (1989)

Appendix A

Calculation of the available area per polar head group

Appendix A Calculation of the available area per polar head group

A1 Introduction

The available area per polar head group, a, must not be confused with the actual physical area per polar head group, which is independent of the aggregate structure. The available area per polar head group is a measure for the "crowdedness" of the head groups at the hydrocarbon-water interface. This makes it an important parameter in assessing the likelihood of a proposed liquid crystalline structure, as it decreases with increasing surfactant concentration. If the calculated available area per polar head group of a proposed structure does not fit in with this trend, the proposed structure is likely to be wrong. Head group repulsions arising from electrostatic, solvation and steric effects act to increase the area per polar head group. The hydrocarbon/water repulsion acts to reduce the area per polar head group.

In order to evaluate the available area per polar head group, first the molecular volume of the hydrocarbon chain, $v_{molecular}$ has to be known, which can be obtained from the density, ρ of the corresponding alkane, since the hydrocarbon chains are assumed to be in a liquid state comparable to liquid alkanes:

$$\rho = \frac{MW}{v_{molecular} \times N_A} \qquad \text{(A1)}$$

where MW is the molecular weight, $v_{molecular}$ is the molecular volume and N_A is Avogadro's number (6.0×10^{23}). In the following sections it is explained how to calculate the area per polar head group for spherical, cylindrical and lamellar aggregates, when the size of the aggregate has been obtained from X-ray diffraction measurements.

A2 Spheres with radius r_{sphere}:

The interfacial area/volume ratio of a sphere is given by:

$$\frac{\text{interfacial area}}{\text{volume}} = \frac{4\pi r_{sphere}^{2}}{\frac{4}{3}\pi r_{sphere}^{3}} = \frac{3}{r_{sphere}} \tag{A2}$$

The total interfacial area is equal to the product of the interfacial area available per polar head group, a, and the number of soap molecules, N_{soap}. The total volume occupied by the hydrocarbon chains of the soap molecules is equal to the product of the molecular volume of a hydrocarbon chain and the number of soap molecules, therefore:

$$\frac{\text{interfacial area}}{\text{volume}} = \frac{a \times N_{soap}}{v_{molecular} \times N_{soap}} = \frac{a}{v_{molecular}} \tag{A3}$$

Combination of equations A2 and A3 leads to the following expression for the available area per polar head group, a:

$$a = \frac{3v_{molecular}}{r_{sphere}} \tag{A4}$$

A3 Cylinders with radius r_{cyl} and length l

Analogue to the spherical aggregates, the equation for cylinders becomes:

$$\frac{\text{interfacial area}}{\text{volume}} = \frac{a}{v_{molecular}} = \frac{2\pi r_{cyl} l}{\pi r_{cyl}^{2} l} \Rightarrow a = \frac{2v_{molecular}}{r_{cyl}} \tag{A5}$$

A4 Surfactant lamellae with thickness d_s

Considering that a surfactant bilayer, with thickness d_s, has an interface with the aqueous region on both sides of the bilayer, the equation for the available area per head group becomes:

$$\frac{\text{interfacial area}}{\text{volume}} = \frac{a}{v_{molecular}} = \frac{2 \times (\mathit{area\ of\ a\ layer})}{d_s \times (\mathit{area\ of\ a\ layer})} \tag{A6}$$

Therefore:

$$a = \frac{2v_{molecular}}{d_s} \tag{A7}$$

A5 A comparison between the different aggregate structures

As can be seen from equations A4, A5 and A7, as the aggregate size increases, the available area per polar head group decreases. If it is assumed that the diameter of the micelles (or the thickness of the bilayers) cannot be larger than twice the length of an all trans hydrocarbon chain, this leads to a minimum in the available area per polar head group, for a certain chainlength. In order to further reduce the available area per polar head group, a phase transition to a differently shaped aggregate will occur when the available area per polar head group falls below the minimum value, because the surfactant cannot achieve a smaller area per head group in a specific aggregate shape. It is possible to theoretically calculate the minimum area per polar head group for a certain aggregate shape. For this the volume of the hydrocarbon chain can be calculated from the volume of a CH_3 group (which is about 54Å^3) and the volume of the CH_2 groups (each of which is about 27Å^3). When the all trans chainlength, l_{chain} is known, the theoretical minimum available area per head group of the different aggregates is given by (*e.g.* Bleasdale and Tiddy [1]):

- spheres

$$a_{\min} = 3\frac{v_{molecular}}{l_{chain}} \tag{A8}$$

- cylinders

$$a_{\min} = 2\frac{v_{molecular}}{l_{chain}} \tag{A9}$$

- lamellae

$$a_{\min} = \frac{2v_{molecular}}{2l_{chain}} = \frac{v_{molecular}}{l_{chain}} \tag{A10}$$

A comparison of these three equations illustrates the decrease in area per polar head group in the sequence spheres, cylinders and layers. A further decrease can be achieved by changing to reversed cylinders and reversed spheres. Within a particular phase, on increasing the surfactant concentration the area per polar head group decreases until it has reached the packing limit and then a phase transition occurs. Equations A8-10 also demonstrate that the available area per polar head group does not alter significantly with chainlength because both the molecular volume and the chainlength are roughly linearly dependent on the carbon number (Bleasdale and Tiddy [1])

A6 References used in this appendix

1. Bleasdale TA and Tiddy GJT, *The structure, dynamics and equilibrium properties of colloidal systems*, edited by Bloor DM and Wyn-Jones E, Kluwer Academic Publishers (1990)